INFORMATION TO USERS

This manuscript has been reproduced from the microfilm master. UMI films the text directly from the original or copy submitted. Thus, some thesis and dissertation copies are in typewriter face, while others may be from any type of computer printer.

The quality of this reproduction is dependent upon the quality of the copy submitted. Broken or indistinct print, colored or poor quality illustrations and photographs, print bleedthrough, substandard margins, and improper alignment can adversely affect reproduction.

In the unlikely event that the author did not send UMI a complete manuscript and there are missing pages, these will be noted. Also, if unauthorized copyright material had to be removed, a note will indicate the deletion.

Oversize materials (e.g., maps, drawings, charts) are reproduced by sectioning the original, beginning at the upper left-hand corner and continuing from left to right in equal sections with small overlaps.

ProQuest Information and Learning
300 North Zeeb Road, Ann Arbor, MI 48106-1346 USA
800-521-0600

DISSERTATION

ELASTIC AND VISCOELASTIC CHARACTERIZATION OF TRANSVERSELY ISOTROPIC COMPOSITE LAMINAE

Submitted by

José Daniel Diniz Melo

Department of Mechanical Engineering

In partial fulfillment of the requirements

for the Degree of Doctor of Philosophy

Colorado State University

Fort Collins, Colorado

Summer, 2002

UMI Number: 3064008

UMI Microform 3064008

ProQuest Information and Learning Company
300 North Zeeb Road
P.O. Box 1346
Ann Arbor, MI 48106-1346

COLORADO STATE UNIVERSITY

June 10, 2002

WE HEREBY RECOMMEND THAT THE DISSERTATION PREPARED UNDER OUR SUPERVISION BY JOSÉ DANIEL DINIZ MELO ENTITLED "ELASTIC AND VISCOELASTIC CHARACTERIZATION OF TRANSVERSELY ISOTROPIC COMPOSITE LAMINAE" BE ACCEPTED AS FULFILLING IN PART REQUIREMENTS FOR THE DEGREE OF DOCTOR OF PHILOSOPHY.

Committee on Graduate Work

Dr. P. R. Heyliger, Civil Engineering.

Dr. M. L. Peterson, Mechanical Engineering.

Dr. F. W. Smith, Mechanical Engineering.

Dr. D. W. Radford, Advisor, Mechanical Engineering.

Dr. A. T. Kirkpatrick, Department Head, Mechanical Engineering.

ABSTRACT OF DISSERTATION

ELASTIC AND VISCOELASTIC CHARACTERIZATION OF TRANSVERSELY ISOTROPIC COMPOSITE LAMINAE

With the advent of "designed damping" in composite materials, and modern computer design tools, accurate three-dimensional material properties information is critically important. Further, design of advanced composite structures often requires knowledge of material properties over a range of temperatures. Conventional testing approaches for the determination of material properties present difficulties related to specimen preparation, fixturing and test apparatus. Consequently, engineers frequently make use of micromechanics generated properties. Unfortunately, micromechanics approaches do not usually account for manufacturing and temperature variations, which affect material properties. This research focuses on developing approaches to allow experimental characterization of elastic and viscoelastic properties of fiber reinforced composite laminae, over a range of temperatures. In addition to investigating the temperature dependence of the three-dimensional material properties, for the viscoelastic characterization, the effect of loading frequency is also addressed.

A technique for the determination of the three-dimensional elastic coefficients of transversely isotropic laminae is developed, using a combination of laminate coefficient of thermal expansion (CTE) measurements and two elastic properties measured from a standard tensile test. The CTE measurements are conducted in a laboratory thermo mechanical analyzer (TMA), using samples of simple geometry. PEEK/IM7 laminae are used to verify this approach and the computed room temperature elastic properties are in good agreement with quoted elastic material properties measured by standard techniques.

Viscoelastic material characterization is essential to designs that incorporate specified levels of damping, and to understand processing problems. This work also presents an approach to determine the three-dimensional viscoelastic properties of transversely isotropic fiber reinforced materials. The minimum number of independent coefficients for three-dimensional viscoelastic characterization of transversely isotropic laminae is investigated and a reduced set of material coefficients, that specify the constitutive relationships, is proposed. The experimental approach developed is based only on flexural measurements allowing complete characterization using a dynamic mechanical analyzer (DMA). To verify the approach, viscoelastic properties of PEEK/IM7 laminae and laminates are determined over ranges of temperature and frequency.

The mechanics relations and experimental techniques developed in this work provide means for measuring the elastic and viscoelastic properties of fiber reinforced composites, and constitute a valuable contribution to the understanding of temperature and frequency dependence of these mechanical properties.

José Daniel Diniz Melo
Department of Mechanical Engineering
Colorado State University
Fort Collins, CO 80523
Summer 2002

ACKNOWLEDGEMENTS

I would like to express my sincerest gratitude to all the committee members for their constructive criticism which was crucial to the final result of this work: Dr. Donald Radford, Dr. Fred Smith, Dr. Paul Heyliger, from Colorado State University, and Dr. Michael Peterson from the University of Maine. Special thanks to my advisor, Dr. Radford, for his support and words of encouragement. It has been a great pleasure to work with Dr. Radford for the past four years from whom I learned a lot in the field of composite materials.

I am also indebted to the many people who provided assistance during the course of the experiments. Special mention to Dr. John Suwardie, from Rheometric Scientific Inc., who performed many of the dynamic mechanical analysis and was always willing to help. To David Leach from Cytec Fiberite Inc. who donated the PEEK/IM7 prepreg material. To Shenghong Fu, for conducting some of the experimental measurements of coefficient of thermal expansion in laminates. To Anish Senan for his interest and willingness in helping to perform some of the DMA tests. To Luke Goldenstein who gave invaluable help with TMA testing, tool manufacturing and specimen preparation.

I am grateful to CAPES foundation – Brazil, for providing the fellowship support throughout the four years of this Ph.D. program. Finally, I wish to acknowledge the support of my family - wife, sons, parents, brother and sisters, and relatives - during my long journey as a student. Special gratitude to my father, Antonio Mello (*in memoriam*) and my sister, Ana Cristina (*in memoriam*), who were very proud of my academic accomplishments and for always giving me incentive to pursue a higher education degree.

To my sons:

Marcelo and Artur

Table of Contents

List of Tables

List of Figures

1

Introduction

The design of modern structures often requires material capabilities, which are difficult to obtain with traditional materials. Such design requirements may include a combination of low-density, high-strength, high-stiffness, high damping, chemical resistance, thermal-shock resistance and many others. Unlike traditional materials, properties of composite materials can be tailored to meet the design criteria and therefore can offer a unique design solution. Due to these unique characteristics, composite materials are now well established in applications including aerospace structures, automotive parts, marine structures, and sporting goods such as tennis rackets, golf clubs, skis and snowboards (Figure 1.1). Moreover, in many structural applications where an improvement in specific stiffness and in damping characteristics can be beneficial, advanced composite materials are an appealing option as a substitute for conventional materials [1,2]. In this case, besides providing superior properties, the weight savings can be considerable (Figure 1.2). For aircraft construction, besides the advantages listed, composite structures allow the incorporation of more complex curved surfaces and considerably simplify the assembly process, reducing the number of parts, joints, seams, and rivets, thus improving aerodynamic efficiency (Figure 1.3).

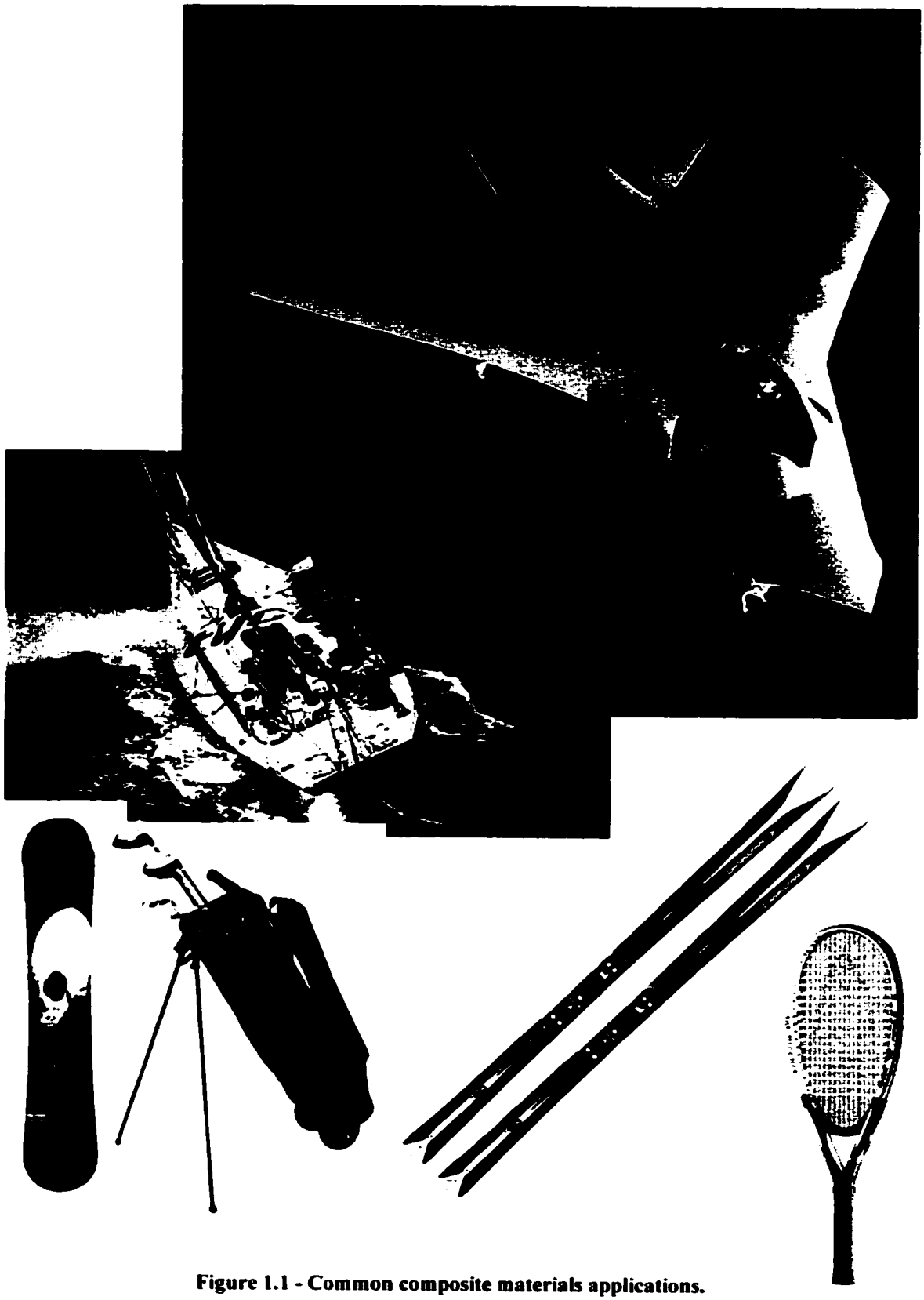

Figure 1.1 - Common composite materials applications.

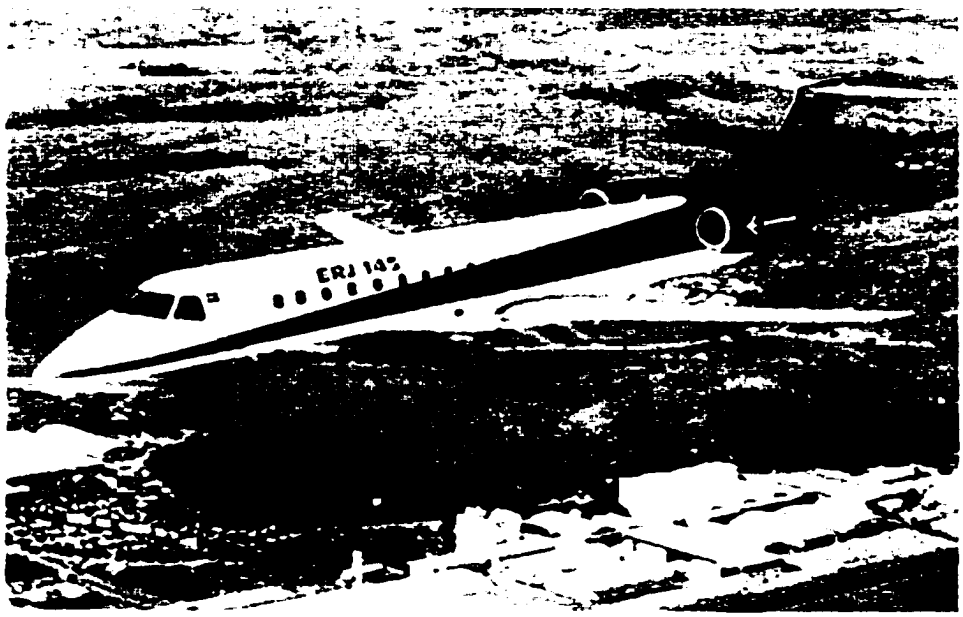

Figure 1.2 - Composite parts of the Embraer ERJ 145 are 15% lighter [3].

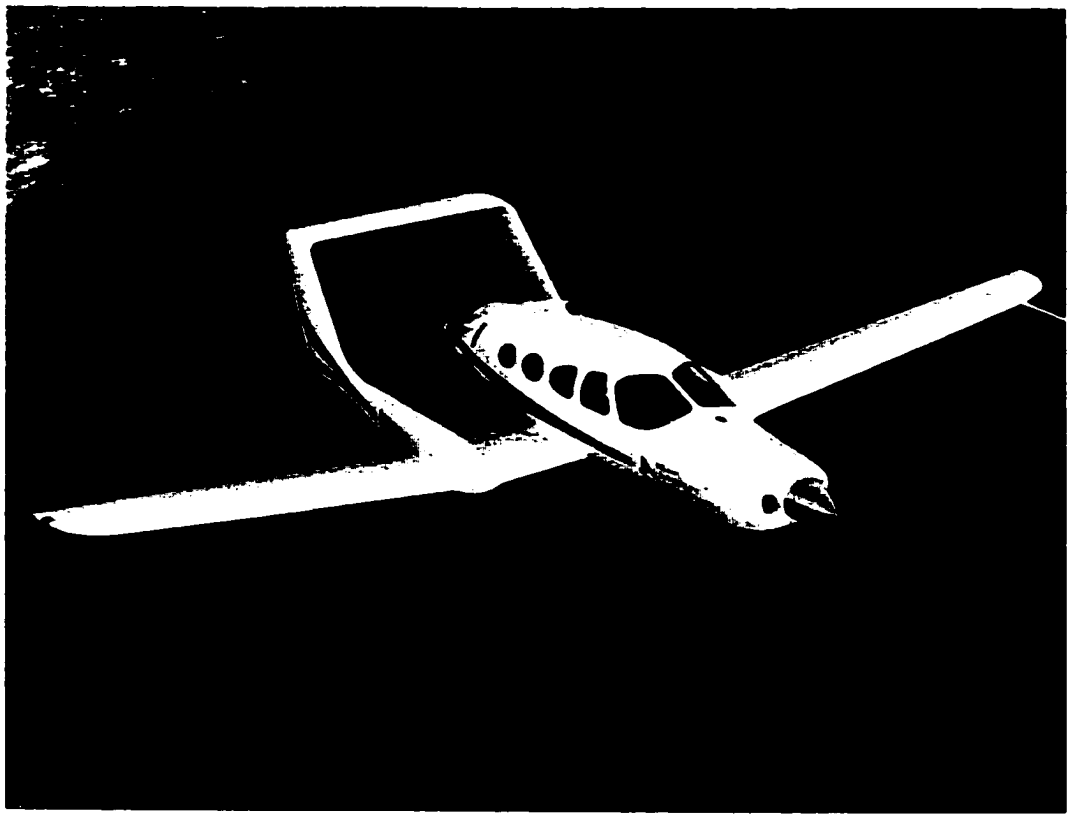

Figure 1.3 - Adam CarbonAero with all carbon composite structure.
(Adam Aircraft Industries, Englewood, CO)

Historically, much of the development in advanced composite materials has been related to aerospace structures because of the high-performance combination of material properties demanded in this type of application and the great importance of weight savings. For the design of many of these structures, knowledge of the material properties over a range of temperatures is essential. For instance, the program initiated by NASA to develop a Mach 2.4 high-speed commercial airplane (Figure 1.4), requires materials that perform not only at room temperature, but also at 177°C, for a period of 60,000 hours[4]. Also, materials for missile applications must meet performance requirements where the temperature profiles may include operating at temperatures near 0°C for short-term and then, at temperatures around 450°C due to the supersonic aerodynamic heating [5]. Therefore, for optimal design and analysis it becomes indispensable to determine the actual material properties over the range of operational temperatures.

Figure 1.4 - High Speed Civil Transport (HSCT) [6].

Information regarding frequency dependence of material properties is also fundamental for many designs. In the case of tires, which are constructed of transversely isotropic, fiber reinforced belts, frequency dependence is a critical parameter for the determination of performance [7]. Frequency affects the vibration performance of polymers and, thus, of polymeric composite parts. Hence, designs, where knowledge of the viscoelastic properties is critical, may require determination of the material response over the frequency range of actual use. Further, understanding the material frequency dependency is very important for the development of predictive methods such as time-temperature superposition.

1.1 Elastic Characterization

Engineering elastic properties of composite materials are fundamental to the analysis and design of structures. Unidirectional fiber reinforced composite laminae are generally considered transversely isotropic materials and, as such, they are defined as having five independent elastic parameters. While the in-plane properties are relatively easily, and accurately, measured using mechanical tests, the measurement of the properties in the through-thickness direction, involves more complicated techniques, apparatus and specimen preparation [8,9,10,11].

Of the five independent elastic parameters of transversely isotropic laminae, the two tensile modulus, E_1 and E_2, and the in-plane Poisson's ratio, ν_{12}, can be determined according to ASTM standard test method D 3039/D 3039M-00 [8]. A constant rectangular cross-section coupon is used in this test, which simplifies the specimen preparation

process. Strain gages or extensometers can be used to indicate strain. If Poisson's ratio is to be determined, the specimen needs to be instrumented to measure strain in both longitudinal and lateral directions, simultaneously. Overall, the test is relatively simple and does not require any special fixturing.

Three experimental procedures for measuring shear properties of composites laminae have been adopted as ASTM standards [9,10,11]. The standards are: D 3518/D 3518M-94, D 4255/D 4255M-83, and D 5379/D 5379M-98. The simplest method [9], ASTM D 3518/D 3518M-94, uses a ±45° balanced, symmetric, laminate specimen, which is tested in tension, in accordance to a standard tensile test method [8]. The test coupon, of constant rectangular cross-section, is of simple manufacture. Extensometers or strain gages are used for the strain measurements. The main limitation of this test is that only in-plane shear properties are determined. Further, the gage section is not in a state of pure shear, as an in-plane stress component normal to the fibers is also present. Although this effect is minimized in internal plies by the fiber reinforcement of the neighboring plies, it can be a concern in surface plies, which are constrained by only one neighboring ply.

Another standard, ASTM D 4255/D 4255M-83, for measuring shear properties of composites [10], presents two separate methods (Figure 1.5). Method A, uses a fixture consisting of two pairs of rails, which are fastened to the specimen and loaded in tension. Method B, makes use of a fixture consisting of three pairs of rails, which are fastened to the specimen and loaded in tension or compression. In both cases, the uniaxial loading applied to the fixture produces in-plane shear loads on the specimens' edge. Strain gages are mounted in the specimen, at 45° to the specimen's longitudinal axis (Figure 1.5).

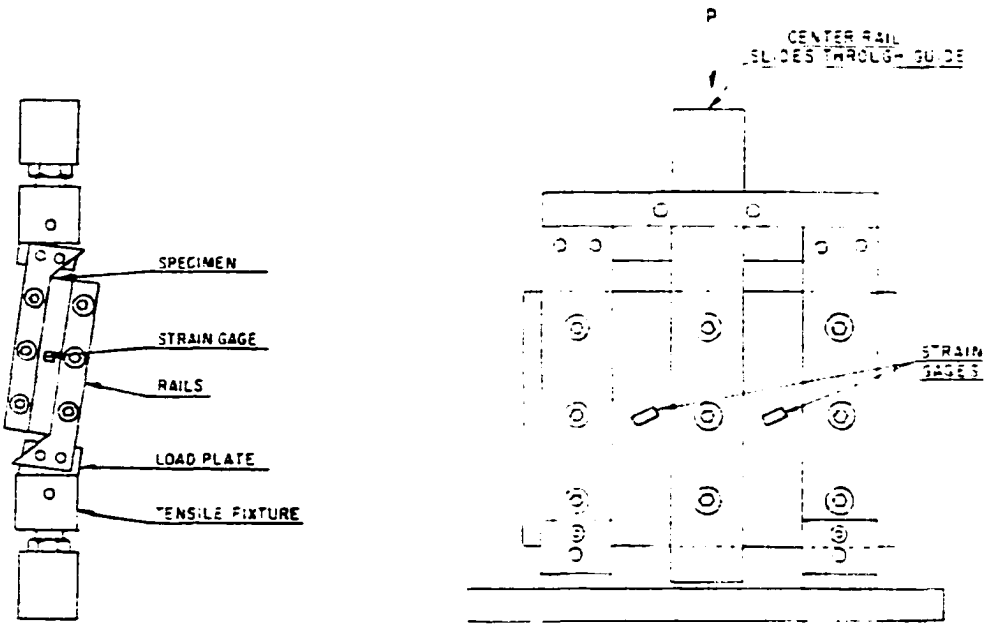

Method A. Method B.

Figure 1.5 - Rail shear test fixtures (ASTM D 4255).

As in the $[\pm 45]_s$ laminate tensile test method, the rail shear test can only produce in-plane shear properties. However, in this case, the specimen size required is larger than in other shear tests, which can be a disadvantage for costly materials. Another important limitation of the rail shear test is that the measured modulus can be affected by the sample dimensions and constraints. Moreover, a previous study has indicated low reproducibility of the measured properties [10]. Therefore, the technique is described as a standard guide, not as a standard method.

Of all the standardized procedures, only one, ASTM D 5379/D 5379M-98, allows the determination of the interlaminar shear modulus, G_{23}, of composites. The method [11], commonly referred to in the literature as Iosipescu shear test, uses a rectangular flat strip coupon with V-notches, symmetrically located at the mid-length (Figure 1.6). The

purpose of the notches is to make the shear strain more uniform along the loading direction. Either in-plane or out-of-plane shear can be evaluated, depending upon the lamination orientation with respect to the loading axis (Figure 1.6). The method requires the use of special fixturing (Figure 1.7), which was adapted from a test fixture first originally developed for use with metals [12,13,14,15,16]. Strain gages are required, to measure the shear response of the material. They must be placed at ±45° to the loading axis, in the mid-length of the specimen (Figure 1.8).

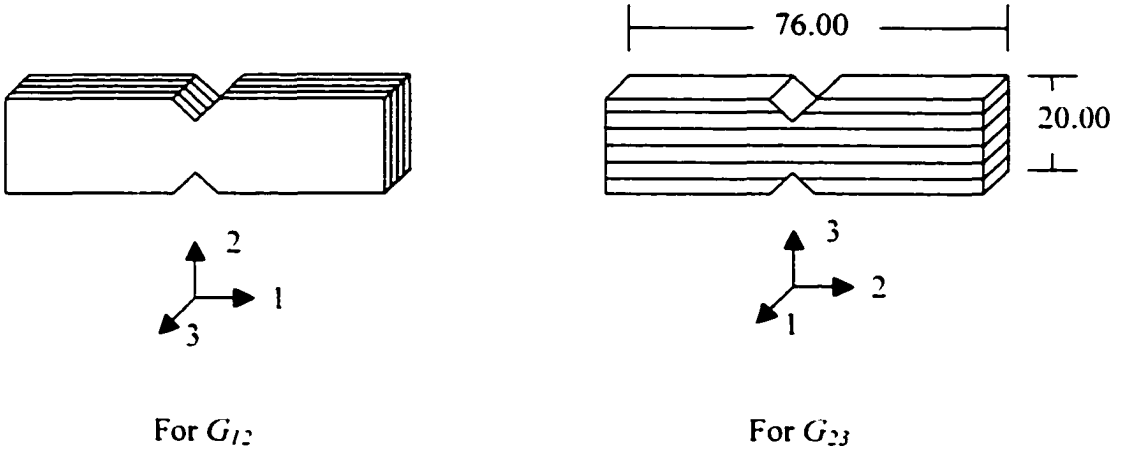

For G_{12} For G_{23}

Figure 1.6 - V-notched beam test specimen with local coordinate axis (ASTM D 5379). (1 represents the fiber direction, 2 the transverse direction and 3 the through-thickness direction)

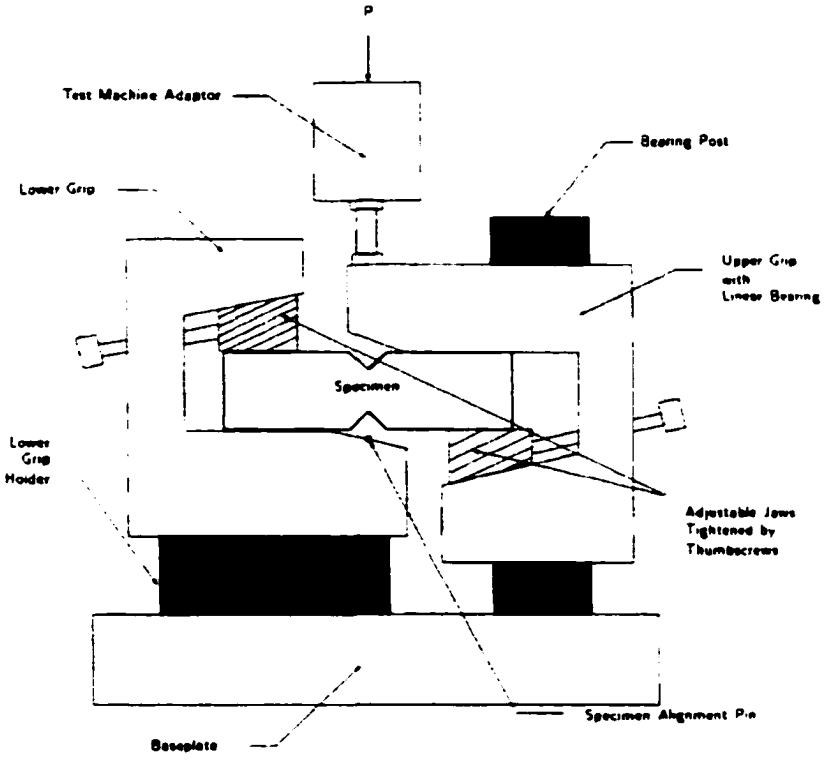

Figure 1.7 - V-notched beam test fixture (ASTM D 5379).

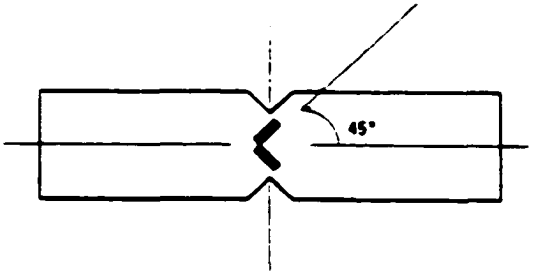

Figure 1.8 - Strain gage locations for the V-notched beam test (ASTM D 5379).

One of the limitations of this test method is that twisting of the specimen can occur during the test, due to load eccentricity, which may significantly affect the measured modulus. Also, damage induced during coupon machining is often a cause of data

scatter. Thus, specimen preparation in this type of test is critical, yet not simple. The notch dimensions (angle, depth and radius) are dependent upon the degree of material orthotropy. Therefore, the optimal notch dimensions, based on a given material, are not necessarily the best for all materials. The single geometry, currently recommended by the standard, intends to minimize the complexity of specimen preparation.

According to Figure 1.6, the required laminate thickness for the determination of the shear modulus, G_{23}, is 20.00mm. In order to achieve the required thickness, the standard recommends the laminate to be cured to the final required thickness, or built from bonded pre-cured laminates of smaller thickness [11]. However, measurements in laminates manufactured by either of the procedures listed, may not be a good representation of thinner structures. Therefore, if actual layer properties are to be determined, a different approach needs to be applied.

Besides the standardized methods, other mechanical testing approaches, based on bending beam tests and torsion tests, to determine through-thickness shear properties, have also been considered in the past [17,18,19]. Nevertheless, as a consequence of the difficulties and limitations of the determination of the through-thickness elastic properties, they are most often excluded from experimental investigations [20].

In recent years, advances in engineering software development have significantly influenced structural design and analysis procedures. Increasingly, engineers are using Finite Element Analysis (FEA) as an important engineering design tool, aiming for designs that are more efficient, safe and cost-effective. Moreover, with the complete integration of Finite Element Analysis (FEA) codes and Computer Aided Design (CAD) software packages, which is now available for most commercial programs, the

application of these techniques is becoming even more appealing. The use of FEA in the design of composite structures can be very advantageous, especially when designing structures with complex geometries. However, knowledge of 3-Dimensional material properties may be necessary. Therefore, the determination of three-dimensional elastic properties is of utmost importance, to take advantage of the capabilities of these advanced design tools.

Micromechanics-based approaches that relate composite properties to constituent material properties are commonly used to predict laminate elastic properties[21,22,23]. This methodology is based on the properties of the fiber and matrix and fiber volume fraction. Unfortunately, most micromechanics approaches do not account for temperature changes and manufacturing variations, which can affect the elastic properties of laminates. Even the details of the form of the interaction between the constituent materials can be affected by temperature change, yet are generally not accounted for in micromechanics models. Moreover, these techniques depend on the precise knowledge of the constituent material properties, *i.e.*, fiber and matrix, which are often difficult to obtain.

Relationships between mechanical properties and thermal expansion coefficients of composites have also been described in the literature [24,25,26]. Based on this concept, in the present research, relationships are developed to enable the determination of the 3-D elastic properties of transversely isotropic, fiber-reinforced laminae, using a combination of tensile tests and CTE measurements in laminates. As it is shown in Chapter 5, the technique also allows the elastic characterization over a range of temperatures.

1.2 Viscoelastic Characterization

Many structural designs are based on elastic material properties. only. This is normally the case of design of structures subjected only to static loads. Yet. most materials show viscoelastic behavior. Polymers are known to display viscoelastic behavior and. therefore. polymer matrix composite materials may also present a considerable viscoelastic behavior. Viscoelastic materials exhibit both elastic and damping characteristics. Damping is a material property. related to the dissipation of energy during dynamic deformation. essential for the design and analysis of many advanced structures especially when vibration and noise control are critical. In fact. some structures require specified levels of damping as a major design criterion. This is the case. for example. for structures where dynamic stability and positioning accuracy are important design requirements (Figure 1.9). Damping is also a parameter significant to fatigue life and impact resistance [27]. Further. it may be that tailorable damping becomes an enabling technology in the advancement of important consumer applications such as faster. higher storage density computer hard drives. Therefore. in the case of tailored damping. information about the elastic properties is very important. but not sufficient. Dynamic characterization of the material becomes necessary. However. due to the difficulties involved with experimental measurement of accurate viscoelastic properties of transversely isotropic materials. many of the properties are estimated from experience rather than determined.

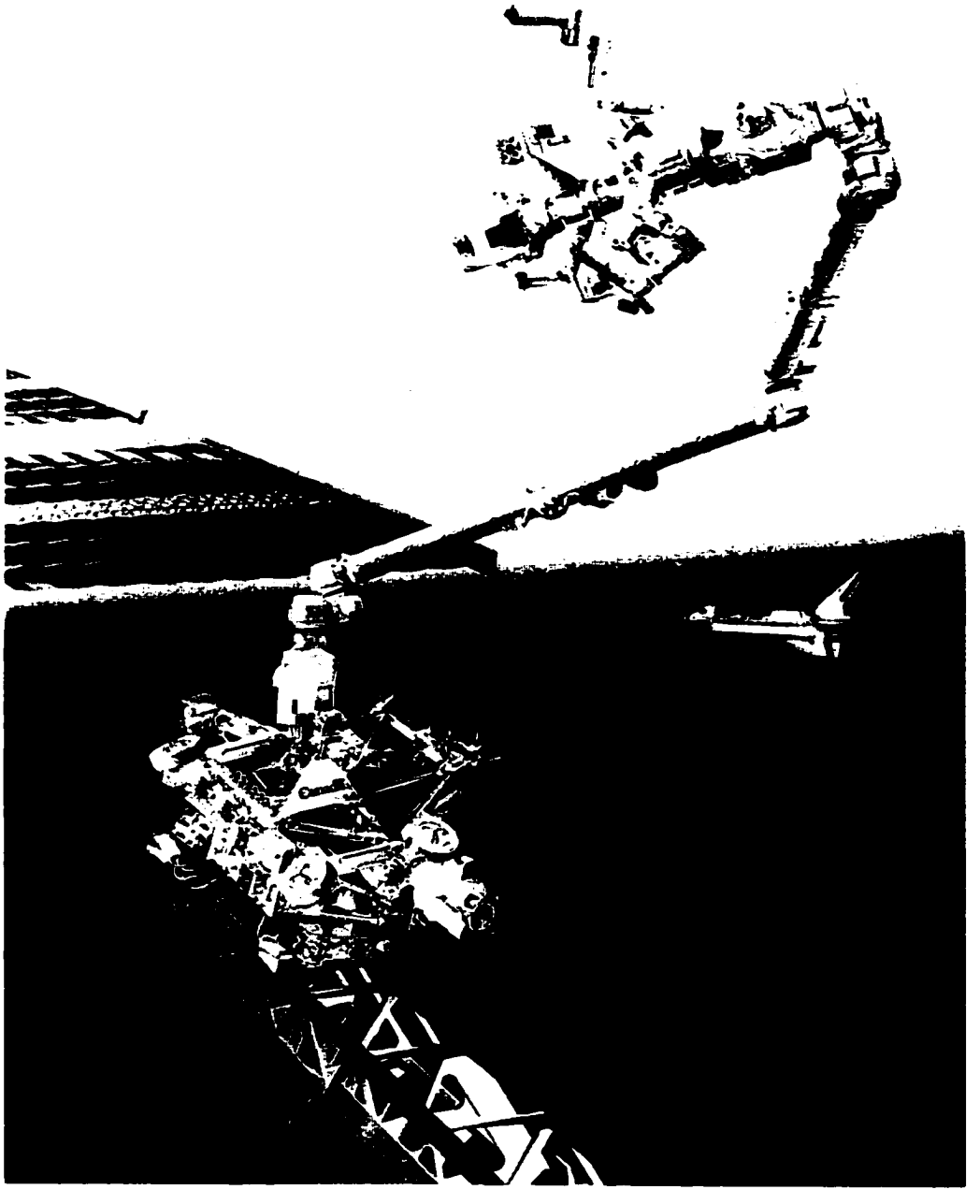

Figure 1.9 - Space Station Remote Manipulator System – SSRMS, (Canadarm2).

Consists of PEEK/IM7 booms designed for construction, maintenance and repair of the Space Station [28].

Variations in damping can also be potentially used as a way to understand processing related problems and to monitor structural damage [29,30,31,32]. Fatigue damage in fiber reinforced composite structures is, in general, the result of a complicated interaction between different damage mechanisms, which may involve matrix cracking, fiber breakage, fiber/matrix debonding, delamination, or a complex combination of these [33,34]. Thus, a mechanistic solution for the prediction of damage may get very cumbersome for practical purposes. A different, and perhaps more realistic, approach is to evaluate damage by monitoring changes in material properties, such as damping.

As in the study of the elastic properties, micromechanics models to generate viscoelastic properties have also been investigated. In a previous research program, focused on generating reliable material properties for the implementation of mechanics models, a micromechanics methodology for the prediction of damping properties of composites was developed [35]. However, the fiber and matrix properties need to be determined if the model is to be accurately tested and applied. Furthermore, in micromechanics based models, it is difficult to incorporate the effects of temperature and frequency in the viscoelastic properties. This is due to the fact that the temperature will affect not only the constituent materials properties but also the fiber/matrix interface, which plays an important role in the mechanical behavior of the material [36,37,38]. Therefore, a different approach is necessary to incorporate these effects.

Valid dynamic mechanical properties for composite materials are difficult to obtain experimentally [39]. Free and forced vibration test methods and also wave propagation experiments have been used to determine the dynamic properties of composites. Ultrasonic non-destructive testing is a recognized tool for defect monitoring of composite

materials and has also been applied in elastic and viscoelastic characterization [40,41,42,43,44]. In general, ultrasonic methods for the measurement of mechanical properties involve wave pulse transmission or resonance measurements, such as resonant ultrasound spectroscopy (RUS) [45]. The RUS method uses resonance frequencies to determine the elastic modulus components [45]. Typically, the sample is suspended between the transmitter and receiver transducers and the excitation frequency is swept to determine the resonance frequencies, which are then related to the elastic properties.

In ultrasonic transmission approaches, the specimen is either immersed in a fluid [44,46] or in direct contact with the transducer [47]. A limitation of the direct contact technique is that it usually requires a fairly thick sample (3 to 5 cm), and also requires cutting the testing sample at different angles [48]. In the past, one important drawback of the immersion technique, especially for in-service inspections, was the need to immerse the material in a liquid, usually water or oil [44,46]. However, modern transducer technology has allowed significant reduction in signal noise and air-coupled ultrasonics are now successfully applied for the viscoelastic characterization of composite materials [49,50,51].

In the transmission method, an acoustic pulse is generated by a transducer and travels through the material, without change in shape, to a receiving transducer. The elastic modulus components are related to the ultrasonic wave velocities, measured in different directions, which are determined by the distance traveled and the respective time-of-flight. Also, there is a transmission loss as the wave propagates through the material and the attenuation is related to the material viscoelasticity [43,52]. Therefore, by measuring the attenuation, the loss modulus components, which are associated to material damping, can be determined [43,48]. The attenuation of an ultrasonic beam transmitted

through the laminate is measured by pulse-echo mode or by through-transmission mode. The pulse-echo mode is of special interest in composite structures for it allows single-sided inspection.

Ultrasonics testing is now a rather common method for non-destructive evaluation of polymers and composite materials. However, for material characterization, ultrasonics methods are not as common in commercial use as mechanical testing methods. One of the most common approaches is the impulse-frequency response method, which has been used for the characterization of composite beams and plates [53,54,55,56,57,58,62]. This method has been reported as fast and relatively simple [39,59], compared to other approaches. The viscoelastic properties are normally determined by measuring the storage modulus and the loss factor (tan δ). ASTM standards such as D 4065-95, D 5023-99, D 5026-95a, provide means for determining the dynamic mechanical properties of plastics and composites, through application of various vibration test techniques and testing apparatus.

Due to the high stiffness of the fiber-reinforced composites, flexural and torsional modes are the most often employed vibration techniques. The storage modulus is normally obtained by measurements of a specimen's natural frequency. For example, in flexural vibration tests, the frequency equation using Bernoulli-Euler beam theory is given by [39]:

$$f_n = \frac{(\lambda_n)^2}{2\pi L^2}\left(\frac{EI}{\rho A}\right)^{\frac{1}{2}}$$

where:

λ_n is the eigenvalue for the n^{th} vibration mode
L is the beam length
E is the storage modulus
I is the moment of inertia of the beam cross section.
ρ is the mass density of the beam
A is the cross sectional area of the beam

The loss factor has been generally determined based upon amplitude decay or half-power bandwidth [62,64]. The loss factor ($\eta = \tan \delta$) is related to the logarithmic decrement, Δ, by (Appendix 1) [60,62].

$$\eta = \frac{\Delta}{\pi}$$

For the half-power bandwidth method, the loss factor is defined as [61,64].

$$\eta = \frac{\Delta f_n}{f_n}$$

where:

Δf_n is the half-power bandwidth
f_n is the n^{th} natural frequency

Generally, flexure and torsion vibration tests are required for the determination of the in-plane viscoelastic properties, and two different testing apparatus are needed [62,63]. Moreover, different testing setups have been used between diverse authors [32,61,62,63,64,65,66,67,68,69,70,71,72], which may lead to differences in damping measurements. Friction at the supports, aerodynamic drag, transducer attachments, are some factors that may affect the dynamic measurements and result in incorrect data [39]. Because of the possible influence of the experimental technique and apparatus used in the measured properties, it is important to develop a procedure, which uses standard laboratory

equipment. Further, the testing apparatus used must offer accurate temperature control if measurements are carried out over a temperature range.

Viscoelastic material characterization through sinusoidal excitation has been employed with universal testing machines such as MTS [61] and also with standard Dynamic Mechanical Analysis (DMA) equipment [65,73,74,75]. Further investigation concerning the use of standard equipment, such as DMA, may lead to more consistent material characterization. Commercial DMA equipment offer very accurate temperature control and allow fast material characterization over a wide range of temperature. However, the torsional dynamic test, typically used for the determination of the shear properties, is normally not available in this type of equipment. Although torsional dynamic mechanical analyzers do exist [7], they are not as common and also, they are specific for torsion tests, thus requiring additional equipment for the flexure tests. Therefore, with the test mode limited to flexure, although specimens with specific stacking sequences and fiber orientations have been studied, no attempt has been made to separate the material independent parameters.

1.3 Goals of Research

The present research focuses on the development of techniques for three-dimensional elastic and viscoelastic characterization of transversely isotropic laminae, which enable the study of the properties of fiber reinforced composite materials over a range of temperatures and frequencies, using standard laboratory thermo mechanical analysis equipment. The establishment of theoretical mechanics relationships necessary to define

the experimental procedures for both elastic and viscoelastic characterization is an essential precursor to this goal.

Specifically, this work will:

- Generate an approach to experimentally determine elastic properties of a transversely isotropic lamina from coefficient of thermal expansion measurements in sub-scale laminates, performed in a TMA (Thermo Mechanical Analyzer). The temperature dependence of the coefficients of thermal expansion (CTE's), and thus of the elastic properties, will also be evaluated in this stage.
- Generate an approach, making use of DMA (Dynamic Mechanical Analyzer) measured parameters in unidirectional sub-scale bend beam specimens, that will enable prediction of the viscoelastic material properties for a transversely isotropic, fiber reinforced material. The temperature and frequency dependence of the viscoelastic performance will also be experimentally studied in this stage.
- Apply existing approaches to generate predicted laminate behavior from layer properties measured by the newly generated technique, and perform DMA measurements on corresponding laminates for verification of both lamina properties prediction and laminate model capabilities, over a range of temperature and frequency.

The projected contributions of this work will be:

- The development of a new method to experimentally determine the five independent elastic parameters of a transversely isotropic lamina, over a range

of temperatures, from TMA measured laminate coefficients of thermal expansion.

- The development of a new method for three-dimensional viscoelastic characterization of a transversely isotropic material, based on DMA measurements of sub-scale bend beam specimens, over a range of temperature and frequency.
- A verification of the ability of published approaches for computing laminate viscoelastic properties to accurately scale from measured lamina properties to laminate properties, over a range of temperature and frequency.
- A discussion of the changing damping with temperature and frequency, as these relate to the measured viscoelastic properties and how the accuracy of model predictions of laminate damping is affected.

The following chapter is devoted to a literature review on four important topics: the techniques of Thermo Mechanical Analysis (TMA) and Dynamic Mechanical Analysis (DMA), a discussion about microstructure-related mechanical properties of polymeric materials, and simplified linear viscoelastic models. In Chapter 3, a review on mechanics of anisotropic materials is presented, which includes elasticity and viscoelasticity equations, tensor transformation, contracted notation, and classical laminate theory equations. Chapter 4 presents the method developed in this work to calculate the three-dimensional elastic properties of transversely isotropic laminae, based on tensile tests and CTE measurements in laminates. Then, in Chapter 5, the experimental determination of the elastic properties for PEEK/IM7, using the proposed method, is

performed at room temperature and also over a range of temperatures. Subsequently, a method is presented in Chapter 6 to determine the three-dimensional viscoelastic properties of transversely isotropic laminae. Also, two approaches published in literature, for calculating laminate viscoelastic behavior from laminae properties, are reviewed and compared. In Chapter 7, the experimental characterization of PEEK/IM7 unidirectional lamina and cross-ply laminates are carried out over temperature and frequency ranges. Further, laminate properties, measured at different temperatures and frequencies, are compared with predictions, based on laminae properties, according to the two laminate models published in literature, for verification of both lamina properties prediction and laminate model capabilities, over a range of temperature and frequency. In Chapter 8, some recommendations for future research are presented. Finally, Chapter 9 presents the conclusions.

2

Thermo Mechanical Analysis, Dynamic Mechanical Analysis, Mechanical Properties of Polymers, and Linear Viscoelastic Behavior

In this chapter, a literature review in the techniques of Themo Mechanical Analysis and Dynamic Mechanical Analysis and their advantages for the investigation of material viscoelastic properties are presented. Following is a discussion about mechanical properties of polymeric materials and how they relate to molecular microstructure and environmental changes. Finally, background information on simplified linear viscoelastic models is introduced.

2.1 Thermo Mechanical Analysis

Thermo Mechanical Analysis (TMA) is a technique by which dimensional changes of a material sample are monitored as a function of temperature or time, under a controlled atmosphere, while the sample may be subjected to an additional mechanical load. A variety of measurement modes are available with TMA equipment including

tension. compression. bending and penetration modes. allowing analysis of solids. powders. fibers and thin film samples. A number of mechanical properties can be determined by this technique including strength. elastic modulus. yield stress. and creep/stress relaxation behavior. However. TMA instruments are most commonly used for the determination of coefficient of thermal expansion and transition temperatures of materials. e.g. glass transition temperature. Thermo Mechanical Analysis (TMA) method is used for characterization of a variety of materials including polymers. ceramics. metals and composites. Modern commercial TMA equipment normally allow measurements over a temperature range of -150°C to 1500°C. Typical TMA collected data for the determination of the material coefficient of thermal expansion is presented in Figure 2.1.

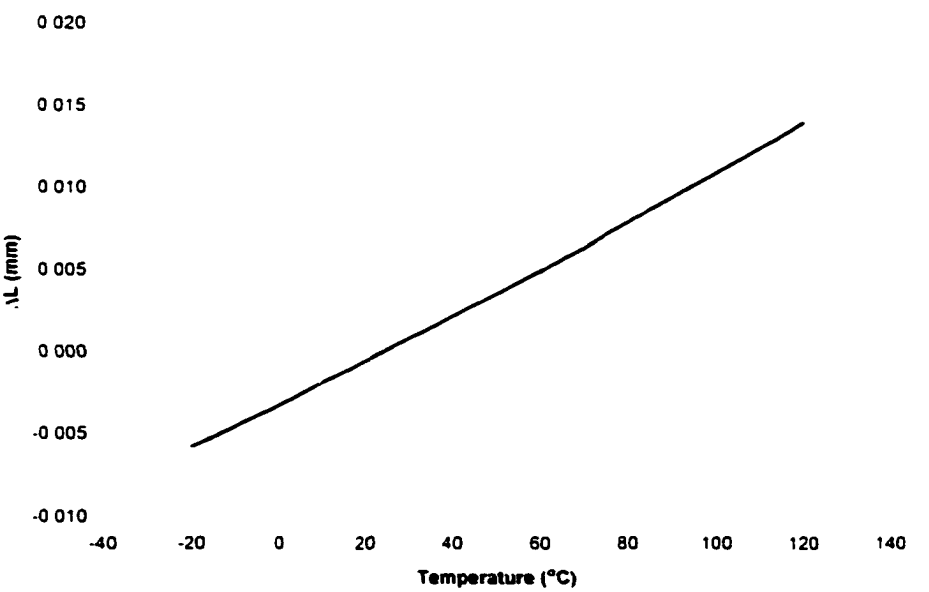

Figure 2.1 - Typical TMA collected data.

In this research. thermo mechanical analysis equipment is applied to measure coefficients of thermal expansion of fiber reinforced laminated samples. over a range of

temperatures. For the purposes of this work, a dilatometer could be used in place of the TMA, as only a static preload was used for testing and no load measurement capability is necessary. The measured CTE's, are used for the determination of the material elastic properties, according to the approach developed.

2.2 Dynamic Mechanical Analysis

Dynamic Mechanical Analysis (DMA), also referred to as Dynamic Mechanical Thermal Analysis (DMTA), is an experimental technique, which analyzes the material's response to an applied dynamic excitation. DMA is a widely accepted research technique in the polymer industry for the determination of material's properties such as viscosity, modulus and damping, providing important information about cure of thermoset resins and the aging of thermoplastics [7].

In recent times this methodology has gained interest as a tool for investigating mechanical properties of composite materials [65,73,74,75,76]. DMA has also been described as an important tool to study viscoelastic properties in prepreg processing operations [77] and to provide an understanding of the aging process of fiber reinforced composites [78]. The method provides fast and reliable results using a very small amount of material, which can, in many cases, be taken directly from the part. In addition, DMA testing equipment allows precise temperature and atmosphere control. The small sample size used contributes to a uniform temperature distribution throughout the specimen, which is difficult to achieve with large dimensions. Measurements are most often carried out under air or an inert gas (e.g. nitrogen). Modern DMA equipment have also capabilities

to analyze materials while immersed in liquids [79]. This procedure allows investigating the effect of chemicals in the material mechanical properties.

In a typical DMA analysis, a periodic force or displacement is applied to a specimen and the resulting displacement or force is measured. When a material displays a viscoelastic nature, the applied excitation and the measured response are out-of-phase, as shown in Figure 2.2.

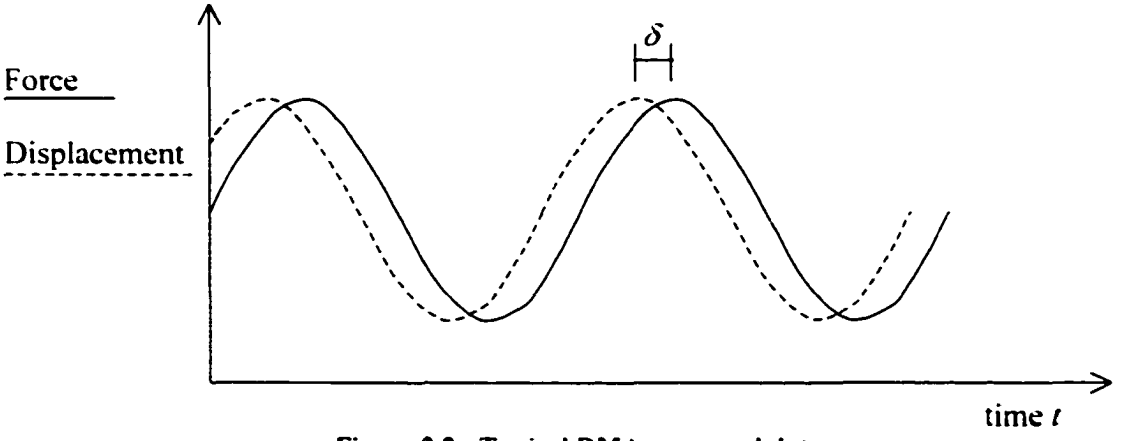

Figure 2.2 - Typical DMA measured data.

The stress can be decomposed into two components: one in-phase with the strain and the other 90° out-of-phase with the strain. Dividing the stress components by the correspondent strain component, two components of moduli can be obtained: an in-phase component (storage modulus or dynamic modulus) and an out-of-phase component (loss modulus). The storage modulus component (real), or dynamic modulus, is related to the material elastic modulus while the loss modulus component (imaginary) is related to the viscous behavior. The resultant of the two components is referred to as the complex modulus, E^* (Figure 2.3). For a purely elastic material the stress is in-phase with the strain and for a purely viscous material the stress is 90° out-of-phase.

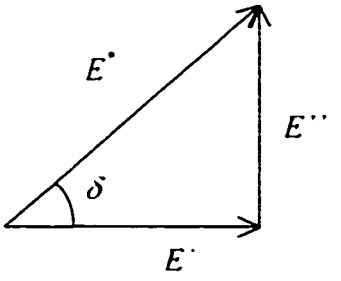

Figure 2.3 - Representation of complex modulus components.

Where:

E^* = complex modulus
E' = storage modulus
E'' = loss modulus

And,

$$E^* = E' + iE''$$
$$E^* = E'(1 + i\tan\delta) \qquad (2.1)$$

DMA is a very useful tool for investigating material properties related to temperature and/or frequency. In a DMA, the material properties are measured each time an excitation cycle is applied. Hence, if the temperature is varied at a small rate compared to the cycling rate, such that the change in temperature within one cycle is not significant, the material properties can be recorded as related to temperature. Commercial DMA testing equipment normally offers built-in software to directly calculate the complex modulus over a temperature range. Typical DMA temperature-scan analyzed data are presented in Figure 2.4.

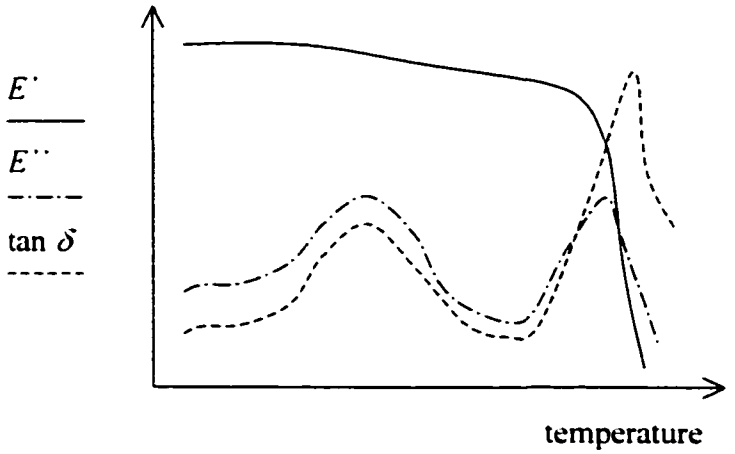

Figure 2.4 - DMA measured properties related to temperature.

A similar approach can be used to study changes in material properties with the excitation frequency (Figure 2.5). In this case, the rate of frequency change needs to be small compared to the cycling frequency.

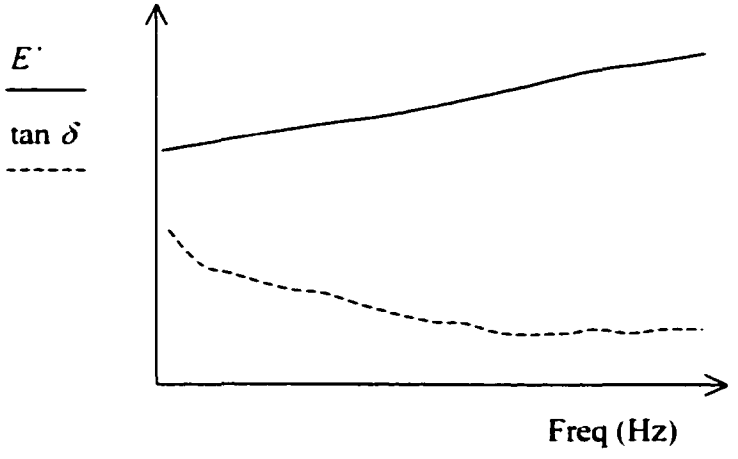

Figure 2.5 - Frequency dependence of viscoelastic properties.

DMA's can be programmed to perform temperature and/or frequency scan, allowing a fast and reliable material characterization. Then, the measured material properties can potentially be used in conjunction with the principle of time-temperature-superposition [80] to predict long-term material behavior. In contrast, if traditional mechanical test approaches are used, the determination of material properties across a temperature or frequency range can become very time-consuming.

When using DMA for material characterization, it is important to notice that the properties measured may not be the same as in more traditional experimental approaches. For example, the modulus, which is often referred to in engineering applications as the Young's modulus, represents the slope of a stress-strain curve with the material being deformed at a constant rate. In contrast, the dynamic modulus determined by DMA is normally based on the peak stress and peak strain, for the material response to a sine wave. Moreover, DMA measured material properties will depend on frequency of measurement, which must always be specified in any reported data, for comparison purposes with other techniques (see Figure 2.6).

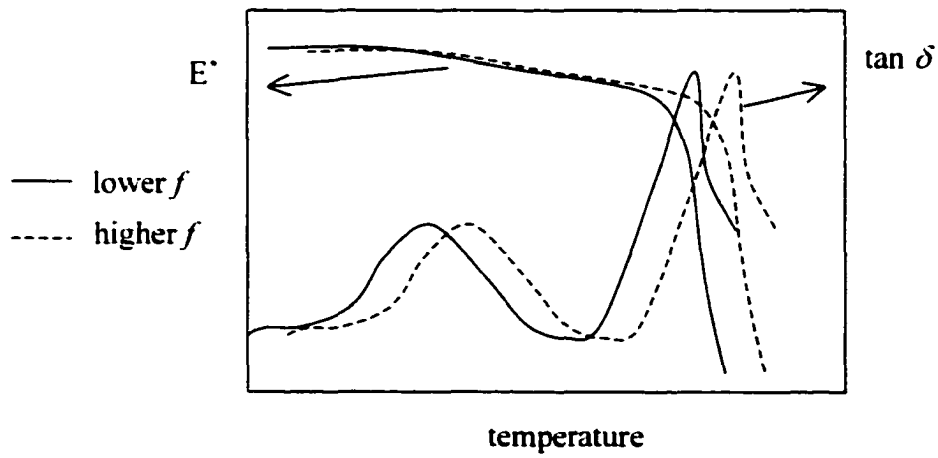

Figure 2.6 - Frequency dependency of a DMA temperature scan.

DMA equipment offers different testing geometries. Common DMA geometries include: tension, compression, simple shear, and bending. The choice of the testing geometry is normally dictated by the type of information desired and also by the stiffness of the material being tested. For fiber-reinforced materials, the bending mode is the most used geometry due to the high stiffness, which severely limits the strain in tensile mode evaluations.

In this research, DMA equipment is used for the viscoelastic characterization of fiber reinforced laminae. The small specimen size required by this equipment can be very advantageous, especially when the material to be tested is very expensive, which is the case of many composites. Also, the accurate temperature control allows studying of temperature effects on material properties, as required by many applications of composite materials. Finally, by using standard laboratory equipment for material characterization, more consistency is expected for data collected by different researchers.

2.3 Mechanical Properties of Polymers

Traditional design approaches of structural components are usually based on engineering properties such as elastic modulus and strength. In many cases, these properties are obtained directly from literature, instead of being experimentally measured, and applied in the design with an appropriate safety factor. This procedure has been well accepted and employed, especially in designs with metals. However, the same approach may not be adequate when designing with polymers. Mechanical properties of polymers are highly sensitive to variations in formulation, temperature, humidity, rate of loading, etc. Although metals are also affected by some of the factors listed above, they are less

sensitive to the variations and the changes in mechanical behavior are usually well documented and, therefore, can be included in the design, with no need to perform additional tests.

Many engineering materials are considered either elastic of viscous. In an ideal elastic material, the applied stress is proportional to the strain and independent of the strain rate (Hooke's law). Conversely, for ideally viscous materials the applied stress is proportional to the rate of strain and independent of the strain magnitude (Newton's relationship). Polymers will exhibit elastic and viscous responses simultaneously. Materials with such behavior are referred to as viscoelastic. Thus, for viscoelastic materials, the stress is a function of both strain and strain rate. This is especially important in designs involving dynamic loads.

The viscoelastic behavior of materials can be observed by creep and relaxation experiments. In creep experiments, a specified constant stress is applied to a structural member and the increasing strain is measured as a function of time. On the other hand, in relaxation experiments a given constant deformation is imposed and the stress reduction is observed as a function of time.

As viscoelastic materials, polymers are significantly affected by temperature and rate of applied load. The effects of temperature on modulus and damping of polymers are most often studied through Dynamic Mechanical Analysis (DMA). In general, the modulus decreases with an increase in temperature. This behavior is more pronounced in the glass transition, T_g, region, where the material changes from glassy to rubbery, and where a considerable drop in modulus is observed when the temperature of the polymeric material is increased. The reduction in modulus also is followed by a reduction in

strength and a considerable increase in strain to failure. In thermosets, the T_g may even be above the decomposition temperature, and this temperature dependence of mechanical properties is typically less significant [7]. The loading rate produces an effect opposite to temperature. At high frequencies, the molecules have less time to respond and material response is glassy [81]. Thus, an increase in loading rate increases the measured modulus while reducing the strain to failure and toughness.

Other environmental factors may also have an important effect on the material's behavior. Moisture is known to reduce stiffness and increase damping in polymers and polymer composites [39,73,82,83]. Normally, the increase in damping is more pronounced than the decrease in modulus, as a result of moisture increase. Also, short fiber reinforced composites are shown to be more affected by moisture than continuous fiber composites [39].

2.3.1 Structure-Properties Relationships in Polymers

A very broad variety of stress-strain behavior can be observed in polymers. While some thermoplastic polymers may have a high toughness, some thermosets may have a limited amount of plastic deformation with a more brittle behavior (Figure 2.7).

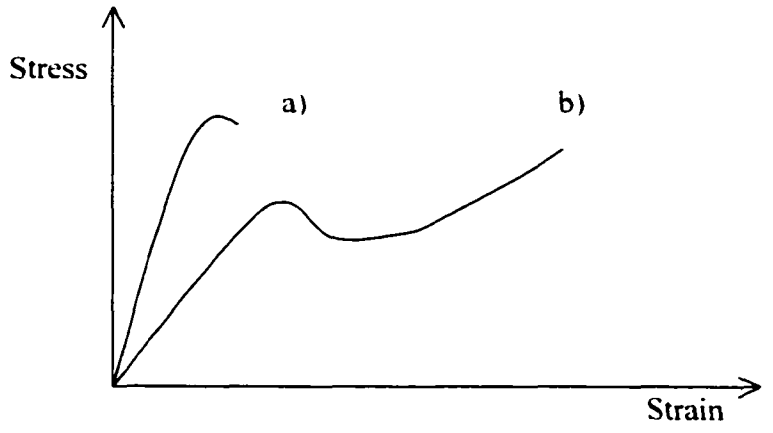

a) High modulus, low toughness; b) Low modulus, high toughness.

Figure 2.7 - Stress-strain behavior of polymers.

The stress-strain behavior of polymers is highly dependent on the molecular structure. Parameters such as molecular weight, degree of crystallinity, and cross-linking are known to influence the polymer mechanical properties. When a solid polymer is stressed, the flexible, thread-like, long molecular chains will move with respect to one another (Figure 2.8), straightening out the kinked and coiled portions, stretching and rotating the molecular bonds [84]. These molecular rearrangements occur in various molecular and time scales. Local-scale (kinks) rearrangements are rapid, while large-scale motions are very slow [80,85]. The deformation mechanism may include chain slippage, where segments of the molecular chains slide past one another. This response involves energy dissipation and generates material damping [86]. The so-called crankshaft model (Figure 2.9) is found very useful to describe the movements of the various segments of the molecules [7].

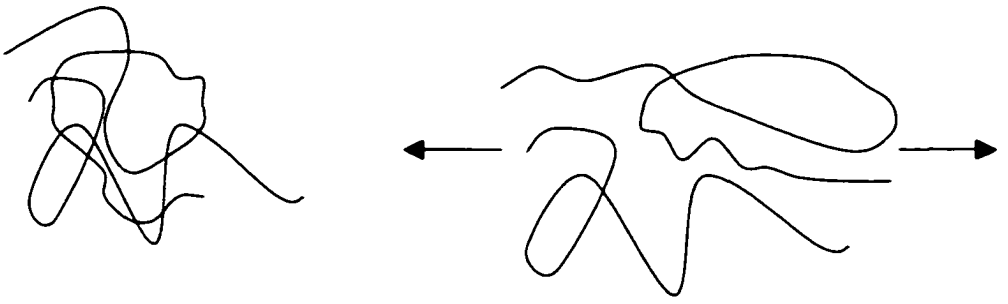

a)unstressed state b) stressed state

Figure 2.8 - Molecular rearrangements during polymer deformation.

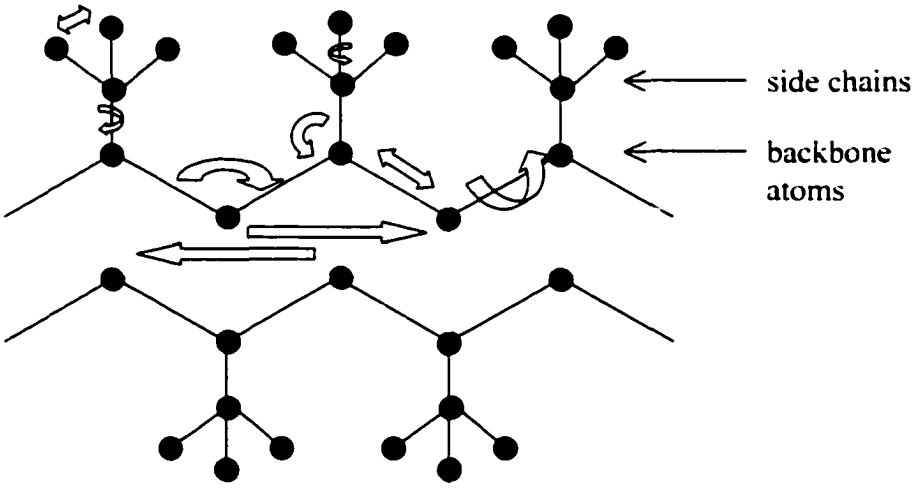

Figure 2.9 - Crankshaft model for molecular rearrangements.

Both damping and stiffness are affected by the degree of crystallinity since, in crystalline arrangements, the molecular chains are closer to one another in a crystal, which strengthen the intermolecular bonds and restrain the movement of adjacent molecules. Thus, in crystalline polymers, the modulus and yield point will increase as

the degree of crystallinity increases [7]. The trade-off in this case is that the material will become more brittle with a decrease in the elongation to failure.

The degree of cross-linking also affects both elastic stiffness and damping [73]. Molecular cross-linking hinders the slippage between molecules. In this case, stressed molecules will be allowed to slip pass relatively to one another in the regions between cross-links, but once these regions are stretched, no more slippage will be allowed. Thus, the strain to failure of thermosets is, normally, much smaller than in thermoplastics due to the cross-links. Cross-linked polymers show a very particular behavior in a creep test with a horizontal equilibrium region since the cross-links do not allow flow [7]. Similar effect is caused by the increase of the molecular weight since the longer chains will also increase the degree of entanglement, which behaves like temporary cross-links.

2.3.2 Temperature Transitions in Polymers

The concept of free volume, v_f, is often used to explain the temperature transitions in polymers. The free volume is defined as the difference between the volume of the polymer mass and the volume occupied by the polymer molecules. Thus, the free volume represents the void space that is available for the molecules to move. As the free volume increases, the mobility of the various segments of the molecules also increases resulting in lower modulus [7].

At very low temperatures, the molecules are packed together in the solid polymer, with a small free volume. As the temperature increases, the material expands, increasing the free volume, and allowing very small localized motions of backbone atoms and side

chains. This transition is called gamma transition, T_γ, and it is detected in a DMA temperature-scan as a slight drop in the storage modulus and a small peak in *tan* δ [7].

As the temperature continues to increase, the material undergoes a beta transition, T_β, where localized movement of small groups of backbone atoms and large motion of the side chains are allowed. This large side chains movement has been related to polymer toughness [87,88]. Studies with high-impact and low-impact nylon 6/6 have shown that, at the T_β, the high-impact polymer exhibits a larger area under the *tan* δ curve [7]. Other investigations have also related the beta transition with vibration damping [89]. However, although the beta transition may be often associated to toughness, it has been shown that it may not be necessarily an indicator of toughness [90].

With further increase in temperature, the material undergoes an alpha transition, where large segments of the molecular chains are allowed to move [7]. This alpha transition is referred to as the glass transition temperature, T_g, as the material changes its mechanical response from glassy to rubbery, in this stage. The glass transition temperature is a very important material property, where significant changes in physical and mechanical properties occur, and therefore, it becomes an essential design parameter. The T_g may represent the upper use temperature of the material for applications where stiffness and strength are required, while it can also be the lower limit for use in for some rubbers.

The relaxations observed at the T_g and sub-T_g transitions (T_γ and T_β), occur only in the amorphous regions of the polymer. Hence, a completely crystalline polymer does not present a T_g, or the sub-T_g transitions. For semi-crystalline polymers, although the crystals remain rigid at the T_g, the amorphous regions are affected, thus changing the

modulus and damping. Amorphous polymers are rigid at temperatures under the T_g and fluid-like above the T_g, as a result of the decrease in viscosity with increase in temperature. If the amorphous polymer is also cross-linked, a rubbery behavior is observed above the T_g, since the cross-links prevent slippage between molecular chains.

If the temperature is increased further, above the T_g, the material ultimately reaches the melting temperature, T_m, where the free volume reached allows the molecular chains to slide past each other. At the T_m , the material flows, as a result of significant chain slippage. Polymers with higher molecular weights require larger free volume for the chain movements and, consequently, melt at higher temperatures. For cured thermosets, the chain slippage is prevented by the cross-links and thus, the material does not melt. Instead, the high temperature may cause thermal degradation.

For the determination of the transition temperatures, DMA is much more sensitive than other thermal analysis techniques such as Differential Scanning Calorimetry (DSC) or Differential Thermal Analysis (DTA). In a DMA temperature scan, the T_g is the temperature at which the damping has a peak and the modulus decreases substantially. Figure 2.10 shows the features observed in a DMA temperature scan of a semi-crystalline polymer.

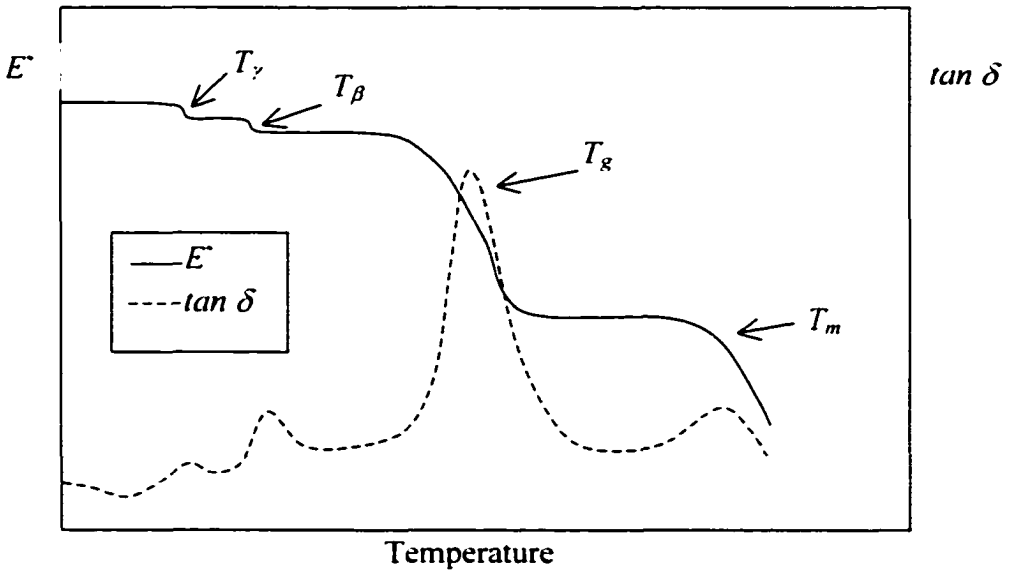

Figure 2.10- Transition in storage modulus and damping for a semi-crystalline polymer. [91]

As it was shown in this section, the polymer properties are very dependent on loading and environmental conditions. The temperature transitions experienced by polymers will directly affect the properties of polymeric matrix composites. Therefore, determining the behavior of composites over the range of service temperature is essential. DMA's have been successfully used to study the temperature effects in polymers, and thus, may offer great potential in the characterization of polymeric composite materials. In this research, the temperature effects on the mechanical properties of PEEK/IM7 will be investigated.

2.4 Linear Viscoelastic Behavior

For a general viscoelastic material subjected to a series of incremental strains, the modulus at a given time is a function of time and strain history. However, if the material presents a linear viscoelastic behavior, then the modulus is a function of time only. The

Boltzmann principle states that: for a linear viscoelastic material subjected to a series of incremental strains, the total stress induced is simply the sum of all the incremental stresses [92]. Each stress increment is based on the modulus, which is a function of the time of application of the strain increment, but not a function of the strain history.

The Boltzmann principle can be expressed by

$$\sigma(t) = \int_{-\infty}^{t} C(t-\tau)d\varepsilon(\tau) \tag{2.2}$$

or

$$\varepsilon(t) = \int_{-\infty}^{t} S(t-\tau)d\sigma(\tau) \tag{2.3}$$

where:

$C(t-\tau)$ = stress relaxation function;

$S(t-\tau)$ = creep function.

For a material with a constant rate of strain, which starts a time t = 0,

$$\begin{aligned} \sigma(t) &= \int_{0}^{t} C(t-\tau)\frac{d\varepsilon(\tau)}{d\tau}d\tau \\ \sigma(t) &= R\int_{0}^{t} C(t-\tau)d\tau \end{aligned} \tag{2.4}$$

A new variable of integration u can be defined as,

$$u = t - \tau \quad \therefore \quad du = -d\tau$$

thus,

$$\sigma(t) = -R\int_{t}^{0} C(u)du$$
$$\sigma(t) = R\int_{0}^{t} C(u)du \qquad (2.5)$$

Differentiating both sides of the equation with respect to t (see Appendix 2).

$$\frac{\sigma(t)}{dt} = C(t)R \qquad (2.6)$$

Therefore, the slope of the stress-strain curve is a function of time and the curve is non-linear even though the linear viscoelastic behavior (Figure 2.11).

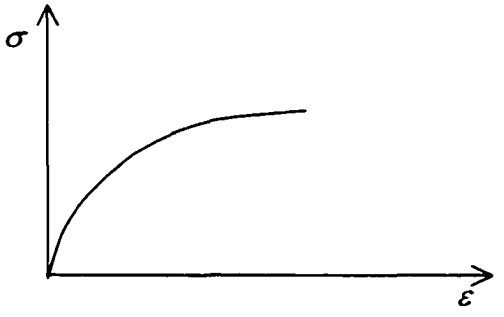

Figure 2.11 - Stress-strain curve for a linearly viscoelastic material.

From one stress-strain curve, it is not possible to distinguish if the material is linearly viscoelastic. It is necessary to perform a series of creep tests at different stress levels or a series of relaxation tests at different strain levels [93]. In the linear viscoelastic region, the creep and the relaxation functions are independent of stress or strain. The Boltzmann superposition principle can be applied to estimate the linear viscoelastic region. According to the superposition principle, the effect of stresses may be added in the linear

region. Thus, in a series of creep tests performed at different stress levels, the stress is proportional to the strain, at a given time, in the linear region. In this case, the ratio of stress to strain is a function of time alone, not of the stress amplitude. Figure 2.12 shows a linear viscoelastic behavior up to an applied stress of 2.0 MPa.

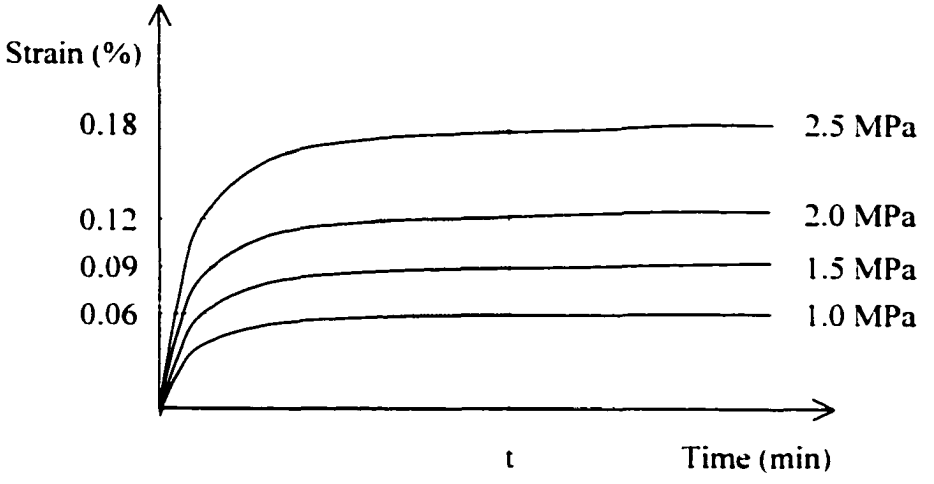

Figure 2.12 - Series of creep tests to determine linear viscoelastic behavior.

Linear viscoelastic behavior can be observed in polymeric materials under small stresses [80]. This behavior is often idealized as a combination of springs, to represent purely elastic or Hookean behavior, and dashpots to represent purely viscous or Newtonian behavior[80,91,92]. One-dimensional problems are often used as a tool to help understanding linear viscoelastic behavior. In this case, the combination of elements - spring and dashpot – are arranged in series and in parallel. The simplest models are the Voigt model and the Maxwell model (Figure 2.13).

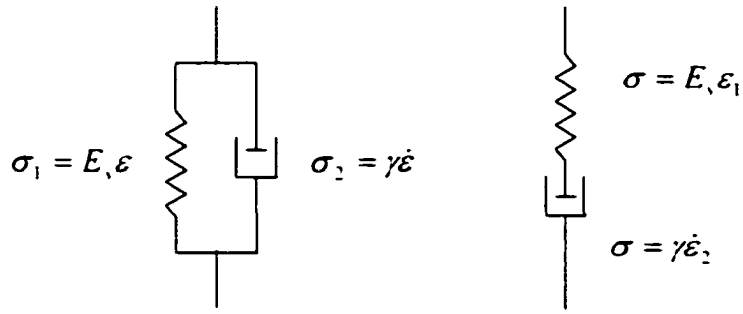

a)Voigt model b)Maxwell model

Figure 2.13 - Simplified one-dimensional viscoelastic models.

2.4.1 Voigt Model

The Voigt model is represented by a parallel combination of an elastic element and a viscous element. The total stress in this arrangement is given by the sum of the element contributions. Thus,

$$\begin{aligned} \sigma &= \sigma_1 + \sigma_2 \\ \sigma &= E_1\varepsilon + \gamma\dot{\varepsilon} \end{aligned} \tag{2.7}$$

$$\sigma = E_1\left(\varepsilon + \lambda\dot{\varepsilon}\right) \tag{2.8}$$

where: $\lambda = \frac{\gamma}{E_1}$, is the ratio between the viscous and the elastic responses.

For a harmonically excited element, the stress and strain are written in complex form as

$$\varepsilon^* = \varepsilon^0 e^{i\omega t} \tag{2.9}$$

$$\sigma^* = \sigma^0 e^{i(\omega t + \delta)} \tag{2.10}$$

Thus.

$$\sigma^* = E_1\left(\varepsilon^* + \lambda\dot{\varepsilon}^*\right) \tag{2.11}$$

$$\sigma^* = E_1\left(\varepsilon^* + i\omega\lambda\varepsilon^*\right) \tag{2.12}$$

and.

$$E^* = \frac{\sigma^*}{\varepsilon^*} \tag{2.13}$$

Hence.

$$E^* = E_1\left(1 + i\omega\lambda\right) \tag{2.14}$$

and.

$$E^* = E' + iE'' \tag{2.15}$$

where.

$$E' = E_1 \tag{2.16}$$

$$E'' = E_1\omega\lambda \tag{2.17}$$

Therefore.

$$\tan\delta = \frac{E''}{E'} = \omega\lambda \tag{2.18}$$

Hence, for the Voigt model, tan δ is proportional to the oscillating frequency.

2.4.2 Maxwell Model

In this model, the spring and dashpot are arranged in series. Hence, the total strain is the sum of the elemental strains. The strain rate for the spring element is given by,

$$\dot{\varepsilon}_1 = \frac{\dot{\sigma}}{E_1} \tag{2.19}$$

and, the total strain rate is

$$\dot{\varepsilon} = \dot{\varepsilon}_1 + \dot{\varepsilon}_2 \tag{2.20}$$

Hence,

$$\dot{\varepsilon} = \frac{\dot{\sigma}}{E_1} + \frac{\sigma}{\gamma} \tag{2.21}$$

$$\dot{\sigma} = E_1\dot{\varepsilon} - \frac{1}{\lambda}\sigma \tag{2.22}$$

For a harmonically exited element,

$$\varepsilon^* = \varepsilon^0 e^{i\omega t} \tag{2.23}$$

$$\sigma^* = \sigma^0 e^{i(\omega t+\delta)} \tag{2.24}$$

Thus.

$$\dot{\sigma}^{*} = E_{\infty}\dot{\varepsilon}^{*} - \frac{1}{\lambda}\sigma^{*} \tag{2.25}$$

$$i\omega\sigma^{*} = E_{\infty}i\omega\varepsilon^{*} - \frac{1}{\lambda}\sigma^{*} \tag{2.26}$$

$$E^{*} = \frac{\sigma^{*}}{\varepsilon^{*}} = E_{\infty}\left(\frac{\omega^{2}\lambda^{2} + i\omega\lambda}{1+\omega^{2}\lambda^{2}}\right) \tag{2.27}$$

Thus.

$$E' = E_{\infty}\omega^{2}\lambda^{2}\left(1+\omega^{2}\lambda^{2}\right)^{-1} \tag{2.28}$$

$$E'' = E_{\infty}\omega\lambda\left(1+\omega^{2}\lambda^{2}\right)^{-1} \tag{2.29}$$

$$\tan\delta = \frac{E''}{E'} = \frac{1}{\omega\lambda} \tag{2.30}$$

Hence, for the Maxwell model, *tan* δ is inversely proportional to the frequency.

It is important to emphasize that, although the simplistic theoretical models introduced – Voigt and Maxwell - are important for the basic understanding of the viscoelastic phenomena, they do not represent the behavior of real materials. Figure 2.14 shows measurements of *tan* δ for polyethylene compared with the predicted values based on the Voigt and Maxwell models [94]. For the predicted values, it was assumed $\lambda = 1$. It is very clear that none of the models could predict the behavior of polyethylene.

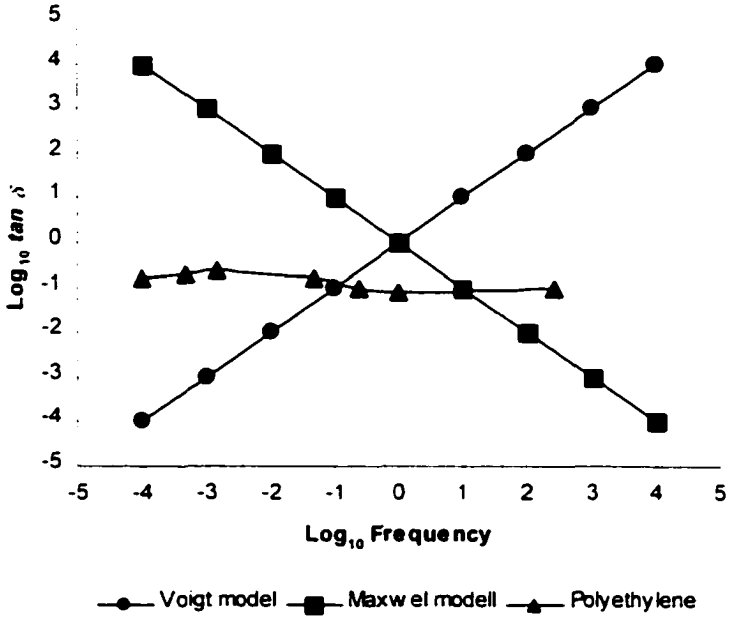

Figure 2.14 - Log_{10} *tan* δ vs. log_{10} frequency for polyethylene. [94]

More complex combinations of linear springs and viscous dampers can be investigated in an attempt to model to viscoelastic behavior of a given polymeric material. However, it would be very complicated to derive a model capable of describing the behavior of all polymers, and at the same time, including effects such as loading frequency and environmental changes. Furthermore, the complexity of the problem can increase considerably when, instead of a polymer, the properties of a composite are needed. In this case, the models need to include not only the properties of the constituent materials, fiber and matrix, but also the interface. Therefore, the approach taken in the present research allows effects, such as frequency, on properties of composites, to be investigated by experimentally measuring the properties, instead of attempting to predict.

3

Mechanics of Anisotropic Materials

In this chapter a review on elasticity and viscoelasticity equations for anisotropic materials is introduced. Also, the classical laminate plate theory is presented.

3.1 Elasticity Equations for Anisotropic Materials

For a general elastic-linear anisotropic material, strain and stress tensors are related as follows:

$$\begin{aligned} \varepsilon_{ij} &= S_{ijkl}\sigma_{kl} \\ \sigma_{ij} &= C_{ijkl}\varepsilon_{kl} \end{aligned} \tag{3.1}$$

where: σ_{ij} is the stress;

ε_{ij} is the strain;

S_{ijkl} is the elastic compliance tensor;

C_{ijkl} is the elastic stiffness tensor.

Stress and strain are second rank tensors (9 components) while stiffness and compliance are fourth rank tensors (81 components). Due to symmetry of the stress and

strain tensors. from the nine components of the stress or strain tensor only six are independent.

From the symmetry of the stress tensor.

$$\sigma_{ij} = \sigma_{ji} \tag{3.2}$$

Hence.

$$\begin{aligned} C_{ijkl}\varepsilon_{kl} &= C_{jikl}\varepsilon_{kl} \\ C_{ijkl} &= C_{jikl} \end{aligned} \tag{3.3}$$

Thus. the stiffness tensor is symmetric with respect to subscripts *ij*. There is also symmetry between subscripts *ij* and *kl*. The symmetry follows from the consideration of strain energy. The strain energy for an elastic-linear body can be written as:

$$W = \int_0^{\varepsilon_{pq}} \sigma_{ij}\, d\varepsilon_{ij} = \int_0^{\varepsilon_{pq}} C_{ijkl}\varepsilon_{kl}\, d\varepsilon_{ij} \tag{3.4}$$

The strain energy must be independent of the path taken by ε_{ij}. from 0 to ε_{pq}. This implies.

$$W = \int dW \tag{3.5}$$

or.

$$dW = C_{ijkl}\varepsilon_{kl}\, d\varepsilon_{ij} = \frac{\partial W}{\partial \varepsilon_{ij}} d\varepsilon_{ij} \tag{3.6}$$

Since $d\varepsilon_{ij}$ is arbitrary.

$$C_{ijkl}\varepsilon_{kl} = \frac{\partial W}{\partial \varepsilon_{ij}} = \sigma_{ij} \tag{3.7}$$

Differentiating the previous equation with respect to ε_{kl} gives

$$C_{ijkl} = \frac{\partial^2 W}{\partial \varepsilon_{kl}\partial \varepsilon_{ij}} \tag{3.8}$$

The double differentiations are interchangeable, thus,

$$C_{ijkl} = C_{klij} \tag{3.9}$$

Therefore, two symmetry conditions were proven so far (eqs (3.3)and (3.9)). These two symmetry conditions imply another symmetry condition,

$$C_{ijkl} = C_{klij} = C_{lkij} = C_{ijlk} \tag{3.10}$$

or,

$$C_{ijkl} = C_{ijlk} \tag{3.11}$$

In summary, the three symmetry conditions of the elastic stiffness tensor (eqs (3.3), (3.9) and (3.11)) are:

$$C_{ijkl} = C_{jikl}\ ,\ C_{ijkl} = C_{ijlk}\ ,\ C_{ijkl} = C_{klij} \tag{3.12}$$

Similar arguments are used to justify that elastic compliances also present the same symmetry conditions. The symmetry conditions for the compliances are:

$$S_{ijkl} = S_{jikl} \; . \; S_{ijkl} = S_{ijlk} \; . \; S_{ijkl} = S_{klij} \tag{3.13}$$

As a result of the symmetry conditions, the number of independent components of the compliance or stiffness tensors is reduced from 81 to 21. Using the symmetries, the strain energy per unit volume of material (eq. (3.5)) can be re-written as,

$$W = \int \frac{1}{2}(C_{ijkl} + C_{klij})\varepsilon_{kl} d\varepsilon_{ij}$$

$$W = \frac{1}{2}\int (C_{ijkl}\varepsilon_{kl} d\varepsilon_{ij} + C_{klij}\varepsilon_{kl} d\varepsilon_{ij})$$

$$W = \frac{1}{2}\int (C_{ijkl}\varepsilon_{kl} d\varepsilon_{ij} + C_{ijkl}\varepsilon_{ij} d\varepsilon_{kl})$$

$$W = \frac{1}{2}\int d(C_{ijkl}\varepsilon_{ij}\varepsilon_{kl})$$

$$W = \frac{1}{2}C_{ijkl}\varepsilon_{ij}\varepsilon_{kl}$$

Therefore,

$$W = \frac{1}{2}C_{ijkl}\varepsilon_{ij}\varepsilon_{kl} = \frac{1}{2}\sigma_{ij}\varepsilon_{ij} = \frac{1}{2}S_{ijkl}\sigma_{ij}\sigma_{kl} \tag{3.14}$$

3.1.1 Contracted Notation

Stress-strain relations are often written using a contracted notation as,

$$\begin{aligned} \varepsilon_\alpha &= S_{\alpha\beta}\sigma_\beta \\ \sigma_\alpha &= C_{\alpha\beta}\varepsilon_\beta \end{aligned} \tag{3.15}$$

The subscripts are changed according to the following rule:

- *ij* is replaced by the subscript *i* if $i = j$:
- *ij* is replaced by a subscript given by 9-*i*-*j*, if $i \neq j$.

Note: This notation (eq. (3.15)) is also referred to as engineering notation, while the previous (eq. (3.1)) is called tensor notation.

In the stress-strain law using contracted notation, $\{\sigma\}$ and $\{\varepsilon\}$ are 6x1 column matrices and $[S]$ and $[C]$ are 6x6 symmetric matrices given by:

$$\{\sigma\} = \begin{Bmatrix} \sigma_{11} \\ \sigma_{22} \\ \sigma_{33} \\ \sigma_{23} \\ \sigma_{13} \\ \sigma_{12} \end{Bmatrix} = \begin{Bmatrix} \sigma_1 \\ \sigma_2 \\ \sigma_3 \\ \sigma_4 \\ \sigma_5 \\ \sigma_6 \end{Bmatrix} \qquad \{\varepsilon\} = \begin{Bmatrix} \varepsilon_{11} \\ \varepsilon_{22} \\ \varepsilon_{33} \\ 2\varepsilon_{23} \\ 2\varepsilon_{13} \\ 2\varepsilon_{12} \end{Bmatrix} = \begin{Bmatrix} \varepsilon_1 \\ \varepsilon_2 \\ \varepsilon_3 \\ \varepsilon_4 \\ \varepsilon_5 \\ \varepsilon_6 \end{Bmatrix} \tag{3.16}$$

and

$$[S] = \begin{bmatrix} S_{11} & S_{12} & S_{13} & S_{14} & S_{15} & S_{16} \\ & S_{22} & S_{23} & S_{24} & S_{25} & S_{26} \\ & & S_{33} & S_{34} & S_{35} & S_{36} \\ & & & S_{44} & S_{45} & S_{46} \\ & & & & S_{55} & S_{56} \\ Sym. & & & & & S_{66} \end{bmatrix} \tag{3.17}$$

And also,

$$[C]=\begin{bmatrix} C_{11} & C_{12} & C_{13} & C_{14} & C_{15} & C_{16} \\ & C_{22} & C_{23} & C_{24} & C_{25} & C_{26} \\ & & C_{33} & C_{34} & C_{35} & C_{36} \\ & & & C_{44} & C_{45} & C_{46} \\ & & & & C_{55} & C_{56} \\ Sym. & & & & & C_{66} \end{bmatrix} \tag{3.18}$$

The transformation between S_{ijkl} and $S_{\alpha\beta}$ and between C_{ijkl} and $C_{\alpha\beta}$ is as follows:

- $S_{\alpha\beta} = S_{ijkl}$, if both $\alpha\beta \leq 3$,
- $S_{\alpha\beta} = 2S_{ijkl}$, if either α or $\beta \leq 3$,
- $S_{\alpha\beta} = 4S_{ijkl}$, if both $\alpha\beta > 3$.

and

- $C_{\alpha\beta} = C_{ijkl}$

The number of independent constants (21) can be further reduced if the material holds any type of symmetry.

3.1.2 Tensor Transformations and Material Symmetry

Under an orthogonal transformation (rigid body rotation or reflection) the tensor components in the "new" (primed) coordinate system is related to the components in the "old" (unprimed) coordinate system as follows:

$$\begin{aligned} x_{i'} &= \Omega_{i'i} x_i \\ \sigma_{i'j'} &= \Omega_{i'i}\Omega_{j'j}\sigma_{ij} \\ C_{i'j'k'l'} &= \Omega_{i'i}\Omega_{j'j}\Omega_{k'k}\Omega_{l'l}C_{ijkl} \end{aligned} \tag{3.19}$$

If Ω is a proper orthogonal matrix ($\Omega^{-1} = \Omega^T$ & $|\Omega| = 1$) the transformation represents a rigid body rotation about an axis. The components Ω_{ij} are the direction cosines of the angles between the axes of the "new" and the "old" coordinate system. For instance, a rotation about the x_3 axis, from the unprimed to the primed coordinate system (Figure 3.1), is represented by:

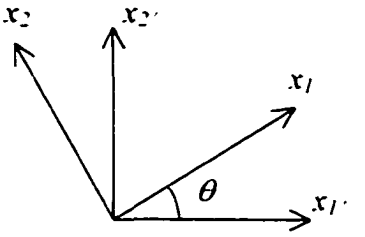

Figure 3.1 - Rigid-body rotation about x_3-axis.

$$\Omega_{ij'}(\theta) = \begin{bmatrix} \cos\theta & -\sin\theta & 0 \\ \sin\theta & \cos\theta & 0 \\ 0 & 0 & 1 \end{bmatrix} \tag{3.20}$$

The orthogonal transformation is a reflection if Ω is an improper orthogonal matrix ($\Omega^{-1} = \Omega^T$ & $|\Omega| = -1$). In this case Ω is given by

$$\Omega = I - 2\vec{n}\vec{n}^T \tag{3.21}$$

where $\vec{n}$ is a unit vector normal to the reflection plane, and

$$\Omega\vec{n} = -\vec{n}$$

For instance, if the symmetry plane contains the x_3-axis and it's unit normal vector makes an angle θ with the x_1 axis (Figure 3.2), then

$$\vec{n}^{T} = \{\cos\theta, \sin\theta, 0\}$$

$$\Omega(\theta) = \begin{bmatrix} -\cos 2\theta & -\sin 2\theta & 0 \\ -\sin 2\theta & \cos 2\theta & 0 \\ 0 & 0 & 1 \end{bmatrix} \tag{3.22}$$

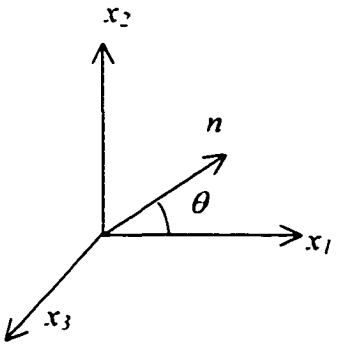

Figure 3.2 - Symmetry plane containing x_3-axis and with unit normal $\vec{n}$.

For $\theta = 0$, $\Omega(0)$ represents a reflection about the plane (x_2, x_3).

Orthotropic materials hold three mutually perpendicular planes of symmetry. Thus, the three coordinate planes are the symmetry planes and the following components must vanish to satisfy the symmetry conditions:[95]

$$C_{14} = C_{15} = C_{16} = C_{24} = C_{25} = C_{26} = C_{34} = C_{35} = C_{36} = C_{45} = C_{46} = C_{56} = 0$$

Similar conditions are applied for the compliance components.

Therefore, the stiffness and compliance matrices in contracted form for an orthotropic material become.

$$[S]=\begin{bmatrix} S_{11} & S_{12} & S_{13} & 0 & 0 & 0 \\ & S_{22} & S_{23} & 0 & 0 & 0 \\ & & S_{33} & 0 & 0 & 0 \\ & & & S_{44} & 0 & 0 \\ & & & & S_{55} & 0 \\ Sym. & & & & & S_{66} \end{bmatrix} \tag{3.23}$$

$$[C]=\begin{bmatrix} C_{11} & C_{12} & C_{13} & 0 & 0 & 0 \\ & C_{22} & C_{23} & 0 & 0 & 0 \\ & & C_{33} & 0 & 0 & 0 \\ & & & C_{44} & 0 & 0 \\ & & & & C_{55} & 0 \\ Sym. & & & & & C_{66} \end{bmatrix} \tag{3.24}$$

Hence, if the material is orthotropic, the number of independent elastic constants is reduced to 9.

If, after a reflection, $C_{ijkl} = C_{ijkl}$ is satisfied for any θ in the range $-\pi/2 \le \theta \le \pi/2$ (Figure 3.2), then the material is called transversely isotropic and x_3 is the axis of symmetry, which means that (x_1, x_2) is the plane of isotropy.

For a transversely isotropic material, the number of independent constants is reduced to 5. If, for example, (x_2, x_3) coincides with the plane of isotropy (x_1 is the axis of symmetry), Figure 3.3,then

$$[S]=\begin{bmatrix} S_{11} & S_{12} & S_{12} & 0 & 0 & 0 \\ & S_{22} & S_{23} & 0 & 0 & 0 \\ & & S_{22} & 0 & 0 & 0 \\ & & & S_{44} & 0 & 0 \\ & & & & S_{66} & 0 \\ Sym. & & & & & S_{66} \end{bmatrix} \tag{3.25}$$

$$[C]=\begin{bmatrix} C_{11} & C_{12} & C_{12} & 0 & 0 & 0 \\ & C_{22} & C_{23} & 0 & 0 & 0 \\ & & C_{22} & 0 & 0 & 0 \\ & & & C_{44} & 0 & 0 \\ & & & & C_{66} & 0 \\ Sym. & & & & & C_{66} \end{bmatrix} \tag{3.26}$$

where:

$$C_{44} = \frac{1}{2}(C_{22} - C_{23}) \tag{3.27}$$
$$S_{44} = 2(S_{22} - S_{23})$$

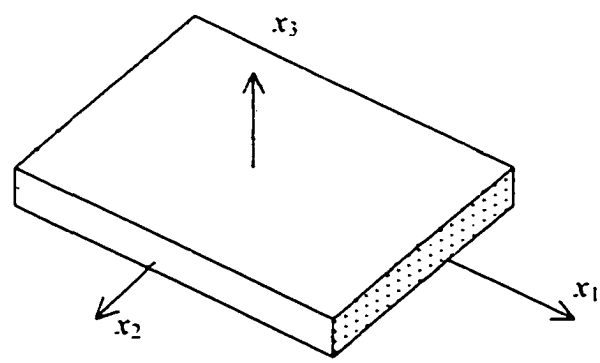

Figure 3.3 - Unidirectional lamina with local coordinates (transversely isotropic).

Stiffness and compliance coefficients may be expressed in terms of the engineering constants. For an orthotropic material the compliance matrix is.

$$[S]=\begin{bmatrix} \frac{1}{E_1} & \frac{-\nu_{21}}{E_2} & \frac{-\nu_{31}}{E_3} & 0 & 0 & 0 \\ & \frac{1}{E_2} & \frac{-\nu_{32}}{E_3} & 0 & 0 & 0 \\ & & \frac{1}{E_3} & 0 & 0 & 0 \\ & & & \frac{1}{G_{23}} & 0 & 0 \\ & & & & \frac{1}{G_{13}} & 0 \\ Sym. & & & & & \frac{1}{G_{12}} \end{bmatrix} \tag{3.28}$$

where:

E_i, are the Young's moduli in directions i.

G_{ij} are the shear moduli in the plane (x_i, x_j).

ν_{ij} are the Poisson's ratios, which describes the strain in x_j direction for an applied stress in the x_i direction ($\nu_{ij} = -\varepsilon_j/\varepsilon_i$).

Due to the symmetry of the compliance matrix,

$$\frac{\nu_{21}}{E_2} = \frac{\nu_{12}}{E_1}, \quad \frac{\nu_{32}}{E_3} = \frac{\nu_{23}}{E_2}, \quad \frac{\nu_{31}}{E_3} = \frac{\nu_{13}}{E_1}$$

or

$$E_i \nu_{ji} = E_j \nu_{ij} \quad \text{(no sum on } i,j) \tag{3.29}$$

The inverse of the compliance matrix gives the stiffness matrix. Thus, for an orthotropic material, the components of the stiffness matrix are,

$$
\begin{aligned}
C_{11} &= \frac{E_1(1-\nu_{23}\nu_{32})}{\Delta} \\
C_{22} &= \frac{E_2(1-\nu_{31}\nu_{13})}{\Delta} \\
C_{33} &= \frac{E_3(1-\nu_{12}\nu_{21})}{\Delta} \\
C_{12} &= \frac{E_2(\nu_{12}+\nu_{13}\nu_{32})}{\Delta} = \frac{E_1(\nu_{21}+\nu_{23}\nu_{31})}{\Delta} \\
C_{13} &= \frac{E_3(\nu_{13}+\nu_{12}\nu_{23})}{\Delta} = \frac{E_1(\nu_{31}+\nu_{32}\nu_{21})}{\Delta} \\
C_{23} &= \frac{E_3(\nu_{23}+\nu_{21}\nu_{13})}{\Delta} = \frac{E_2(\nu_{32}+\nu_{31}\nu_{12})}{\Delta} \\
C_{44} &= G_{23}, \quad C_{55} = G_{13}, \quad C_{66} = G_{12},
\end{aligned}
\tag{3.30}
$$

where:

$$
\Delta = \begin{vmatrix} 1 & -\nu_{12} & -\nu_{13} \\ -\nu_{21} & 1 & -\nu_{23} \\ -\nu_{31} & -\nu_{32} & 1 \end{vmatrix} = 1-\nu_{12}\nu_{21}-\nu_{23}\nu_{32}-\nu_{31}\nu_{13}-2\nu_{12}\nu_{23}\nu_{31} \tag{3.31}
$$

For a transversely isotropic material where (x_2, x_3) is the plane of isotropy, the following relations must hold:

$$
\begin{aligned}
&E_2 = E_3, \quad G_{13} = G_{12} \\
&\nu_{12} = \nu_{13}, \quad \nu_{21} = \nu_{31}, \quad \nu_{23} = \nu_{32} \\
&G_{23} = \frac{E_2}{2(1+\nu_{23})} = \frac{E_3}{2(1+\nu_{32})}
\end{aligned}
\tag{3.32}
$$

In this case, the compliance matrix becomes,

$$[S]=\begin{bmatrix} \frac{1}{E_1} & \frac{-\nu_{21}}{E_2} & \frac{-\nu_{21}}{E_2} & 0 & 0 & 0 \\ & \frac{1}{E_2} & \frac{-\nu_{32}}{E_2} & 0 & 0 & 0 \\ & & \frac{1}{E_2} & 0 & 0 & 0 \\ & & & \frac{1}{G_{23}} & 0 & 0 \\ & & & & \frac{1}{G_{12}} & 0 \\ Sym. & & & & & \frac{1}{G_{12}} \end{bmatrix} \tag{3.33}$$

3.1.3 Transformation of the Contracted Compliance and Stiffness Matrices

Compliances and stiffnesses in contracted matrix form do not transform like a tensor. Therefore, the tensor transformation law presented cannot be applied for them. In this case, a new transformation law for the components in contracted notation $C'_{\alpha\beta}$ and $S_{\alpha\beta}$ must be derived.

The transformation of stress and strain tensor components is given by (see eq. (3.19)).

$$\sigma_{ij'} = \Omega_{i'i}\Omega_{j'j}\sigma_{ij} \tag{3.34}$$

$$\varepsilon_{ij'} = \Omega_{i'i}\Omega_{j'j}\varepsilon_{ij} \tag{3.35}$$

This stress transformation (eq. (3.34)) can be expressed in matrix form as

$$[\sigma_{ij'}] = [\Omega][\sigma_{ij}][\Omega]^t \tag{3.36}$$

Thus, for a rotation about the x_3-axis, which transforms the unprimed coordinate system to the primed coordinate system (Figure 3.1).

$$\begin{bmatrix} \sigma_{1'1'} & \sigma_{1'2'} & \sigma_{1'3'} \\ \sigma_{1'2'} & \sigma_{2'2'} & \sigma_{2'3'} \\ \sigma_{1'3'} & \sigma_{2'3'} & \sigma_{3'3'} \end{bmatrix} = \begin{bmatrix} \cos\theta & -\sin\theta & 0 \\ \sin\theta & \cos\theta & 0 \\ 0 & 0 & 1 \end{bmatrix} \begin{bmatrix} \sigma_{11} & \sigma_{12} & \sigma_{13} \\ \sigma_{12} & \sigma_{22} & \sigma_{23} \\ \sigma_{13} & \sigma_{23} & \sigma_{33} \end{bmatrix} \begin{bmatrix} \cos\theta & \sin\theta & 0 \\ -\sin\theta & \cos\theta & 0 \\ 0 & 0 & 1 \end{bmatrix} \tag{3.37}$$

Carrying out the matrix multiplication, gives

$$\begin{Bmatrix} \sigma_{1'1'} \\ \sigma_{2'2'} \\ \sigma_{3'3'} \\ \sigma_{2'3'} \\ \sigma_{1'3'} \\ \sigma_{1'2'} \end{Bmatrix} = \begin{bmatrix} \cos^2\theta & \sin^2\theta & 0 & 0 & 0 & -2\cos\theta\sin\theta \\ \sin^2\theta & \cos^2\theta & 0 & 0 & 0 & 2\cos\theta\sin\theta \\ 0 & 0 & 1 & 0 & 0 & 0 \\ 0 & 0 & 0 & \cos\theta & \sin\theta & 0 \\ 0 & 0 & 0 & -\sin\theta & \cos\theta & 0 \\ \cos\theta\sin\theta & -\cos\theta\sin\theta & 0 & 0 & 0 & \cos^2\theta - \sin^2\theta \end{bmatrix} \begin{Bmatrix} \sigma_{11} \\ \sigma_{22} \\ \sigma_{33} \\ \sigma_{23} \\ \sigma_{13} \\ \sigma_{12} \end{Bmatrix} \tag{3.38}$$

Using the contracted notation (eq.(3.16)),

$$\begin{Bmatrix} \sigma_{1'} \\ \sigma_{2'} \\ \sigma_{3'} \\ \sigma_{4'} \\ \sigma_{5'} \\ \sigma_{6'} \end{Bmatrix} = \begin{bmatrix} \cos^2\theta & \sin^2\theta & 0 & 0 & 0 & -2\cos\theta\sin\theta \\ \sin^2\theta & \cos^2\theta & 0 & 0 & 0 & 2\cos\theta\sin\theta \\ 0 & 0 & 1 & 0 & 0 & 0 \\ 0 & 0 & 0 & \cos\theta & \sin\theta & 0 \\ 0 & 0 & 0 & -\sin\theta & \cos\theta & 0 \\ \cos\theta\sin\theta & -\cos\theta\sin\theta & 0 & 0 & 0 & \cos^2\theta - \sin^2\theta \end{bmatrix} \begin{Bmatrix} \sigma_1 \\ \sigma_2 \\ \sigma_3 \\ \sigma_4 \\ \sigma_5 \\ \sigma_6 \end{Bmatrix} \tag{3.39}$$

The inverse relationship is given by

$$\begin{Bmatrix}\sigma_1\\ \sigma_2\\ \sigma_3\\ \sigma_4\\ \sigma_5\\ \sigma_6\end{Bmatrix}=\begin{bmatrix}\cos^2\theta & \sin^2\theta & 0 & 0 & 0 & 2\cos\theta\sin\theta\\ \sin^2\theta & \cos^2\theta & 0 & 0 & 0 & -2\cos\theta\sin\theta\\ 0 & 0 & 1 & 0 & 0 & 0\\ 0 & 0 & 0 & \cos\theta & -\sin\theta & 0\\ 0 & 0 & 0 & \sin\theta & \cos\theta & 0\\ -\cos\theta\sin\theta & \cos\theta\sin\theta & 0 & 0 & 0 & \cos^2\theta-\sin^2\theta\end{bmatrix}\begin{Bmatrix}\sigma_{1'}\\ \sigma_{2'}\\ \sigma_{3'}\\ \sigma_{4'}\\ \sigma_{5'}\\ \sigma_{6'}\end{Bmatrix} \tag{3.40}$$

Therefore,

$$\{\sigma\}_a=[R]\{\sigma\}_{a'} \tag{3.41}$$

and

$$\{\sigma\}_{a'}=[R]^{-1}\{\sigma\}_a \tag{3.42}$$

where:

$$[R]=\begin{bmatrix}\cos^2\theta & \sin^2\theta & 0 & 0 & 0 & 2\cos\theta\sin\theta\\ \sin^2\theta & \cos^2\theta & 0 & 0 & 0 & -2\cos\theta\sin\theta\\ 0 & 0 & 1 & 0 & 0 & 0\\ 0 & 0 & 0 & \cos\theta & -\sin\theta & 0\\ 0 & 0 & 0 & \sin\theta & \cos\theta & 0\\ -\cos\theta\sin\theta & \cos\theta\sin\theta & 0 & 0 & 0 & \cos^2\theta-\sin^2\theta\end{bmatrix} \tag{3.43}$$

and

$$[R]^{-1}=\begin{bmatrix} \cos^2\theta & \sin^2\theta & 0 & 0 & 0 & -2\cos\theta\sin\theta \\ \sin^2\theta & \cos^2\theta & 0 & 0 & 0 & 2\cos\theta\sin\theta \\ 0 & 0 & 1 & 0 & 0 & 0 \\ 0 & 0 & 0 & \cos\theta & \sin\theta & 0 \\ 0 & 0 & 0 & -\sin\theta & \cos\theta & 0 \\ \cos\theta\sin\theta & -\cos\theta\sin\theta & 0 & 0 & 0 & \cos^2\theta-\sin^2\theta \end{bmatrix} \tag{3.44}$$

Similarly to (eq. (3.38)), the transformation of the strain tensor components is given by,

$$\{\varepsilon\}_{x'y'}=[R]^{-1}\{\varepsilon\}_{xy}$$

or

$$\begin{Bmatrix} \varepsilon_{1'1'} \\ \varepsilon_{2'2'} \\ \varepsilon_{3'3'} \\ \varepsilon_{2'3'} \\ \varepsilon_{1'3'} \\ \varepsilon_{1'2'} \end{Bmatrix}=\begin{bmatrix} \cos^2\theta & \sin^2\theta & 0 & 0 & 0 & -2\cos\theta\sin\theta \\ \sin^2\theta & \cos^2\theta & 0 & 0 & 0 & 2\cos\theta\sin\theta \\ 0 & 0 & 1 & 0 & 0 & 0 \\ 0 & 0 & 0 & \cos\theta & \sin\theta & 0 \\ 0 & 0 & 0 & -\sin\theta & \cos\theta & 0 \\ \cos\theta\sin\theta & -\cos\theta\sin\theta & 0 & 0 & 0 & \cos^2\theta-\sin^2\theta \end{bmatrix}\begin{Bmatrix} \varepsilon_{11} \\ \varepsilon_{22} \\ \varepsilon_{33} \\ \varepsilon_{23} \\ \varepsilon_{13} \\ \varepsilon_{12} \end{Bmatrix} \tag{3.45}$$

Using the contracted notation (eq. (3.16)),

$$\begin{Bmatrix} \varepsilon_{1'} \\ \varepsilon_{2'} \\ \varepsilon_{3'} \\ \varepsilon_{4'}/2 \\ \varepsilon_{5'}/2 \\ \varepsilon_{6'}/2 \end{Bmatrix}=\begin{bmatrix} \cos^2\theta & \sin^2\theta & 0 & 0 & 0 & -2\cos\theta\sin\theta \\ \sin^2\theta & \cos^2\theta & 0 & 0 & 0 & 2\cos\theta\sin\theta \\ 0 & 0 & 1 & 0 & 0 & 0 \\ 0 & 0 & 0 & \cos\theta & \sin\theta & 0 \\ 0 & 0 & 0 & -\sin\theta & \cos\theta & 0 \\ \cos\theta\sin\theta & -\cos\theta\sin\theta & 0 & 0 & 0 & \cos^2\theta-\sin^2\theta \end{bmatrix}\begin{Bmatrix} \varepsilon_1 \\ \varepsilon_2 \\ \varepsilon_3 \\ \varepsilon_4/2 \\ \varepsilon_5/2 \\ \varepsilon_6/2 \end{Bmatrix} \tag{3.46}$$

or

$$\begin{Bmatrix} \varepsilon_{1'} \\ \varepsilon_{2'} \\ \varepsilon_{3'} \\ \varepsilon_{4'} \\ \varepsilon_{5'} \\ \varepsilon_{6'} \end{Bmatrix} = \begin{bmatrix} \cos^2\theta & \sin^2\theta & 0 & 0 & 0 & -\cos\theta\sin\theta \\ \sin^2\theta & \cos^2\theta & 0 & 0 & 0 & \cos\theta\sin\theta \\ 0 & 0 & 1 & 0 & 0 & 0 \\ 0 & 0 & 0 & \cos\theta & \sin\theta & 0 \\ 0 & 0 & 0 & -\sin\theta & \cos\theta & 0 \\ 2\cos\theta\sin\theta & -2\cos\theta\sin\theta & 0 & 0 & 0 & \cos^2\theta - \sin^2\theta \end{bmatrix} \begin{Bmatrix} \varepsilon_1 \\ \varepsilon_2 \\ \varepsilon_3 \\ \varepsilon_4 \\ \varepsilon_5 \\ \varepsilon_6 \end{Bmatrix} \tag{3.47}$$

or

$$\{\varepsilon\}_{\alpha'} = [R]^T \{\varepsilon\}_{\alpha} \tag{3.48}$$

and, therefore,

$$\{\varepsilon\}_{\alpha} = [R]^{-T} \varepsilon_{\alpha'} \tag{3.49}$$

Hence,

$$\begin{aligned} \{\varepsilon\}_{\alpha} &= [S]_{\alpha\beta} \{\sigma\}_{\beta} \\ \{\sigma\}_{\alpha} &= [C]_{\alpha\beta} \{\varepsilon\}_{\beta} \end{aligned}$$

$$\begin{aligned} [R]\{\sigma\}_{\alpha'} &= [C]_{\alpha\beta}[R]^{-T} \{\varepsilon\}_{\beta'} \\ \{\sigma\}_{\alpha'} &= [R]^{-1}[C]_{\alpha\beta}[R]^{-T} \{\varepsilon\}_{\beta'} \\ \{\sigma\}_{\alpha'} &= [C]_{\alpha'\beta'} \{\varepsilon\}_{\beta'} \end{aligned} \tag{3.50}$$

where:

$$[C]_{\alpha'\beta'} = [R]^{-1}[C]_{\alpha\beta}[R]^{-T} \tag{3.51}$$

also,

$$
\begin{aligned}
[R]^{-T}\{\varepsilon\}_{\alpha'} &= [S]_{\alpha\beta}[R]\{\sigma\}_{\beta'} \\
\{\varepsilon\}_{\alpha'} &= [R]^{T}[S]_{\alpha\beta}[R]\{\sigma\}_{\beta'} \\
\{\varepsilon\}_{\alpha'} &= [S]_{\alpha'\beta'}\{\sigma\}_{\beta'}
\end{aligned}
\tag{3.52}
$$

where:

$$
[S]_{\alpha'\beta'} = [R]^{T}[S]_{\alpha\beta}[R] \tag{3.53}
$$

3.2 Viscoelastic Characteristics of Anisotropic Bodies

In practice, most materials deviate from Hooke's Law and exhibit time-dependent mechanical properties. This behavior is referred to as viscoelasticity. In metals such as steel or aluminum, the stress-strain behavior at room temperature does not deviate much from linear elasticity. In this case the application of the linear elasticity theory is appropriate. However, metals at high temperature may show significant viscoelastic behavior. This is also the case of polymeric materials and polymer matrix composites.

The general form of the linear theory of the viscoelastic body is given by

$$
\sigma_{ij}(t) = \int_{-\infty}^{t} C_{ijkl}(t-\tau)\, d\varepsilon_{kl}(\tau) \tag{3.54}
$$

or

$$
\varepsilon_{ij}(t) = \int_{-\infty}^{t} S_{ijkl}(t-\tau)\, d\sigma_{kl}(\tau) \tag{3.55}
$$

where:

C_{ijkl} = tensor of the stress relaxation function:

S_{ijkl} = tensor of the creep function.

In a harmonically excited viscoelastic body, stresses and strains are out-of-phase (Figure 3.4). If the viscoelastic behavior of the material is linear and a sinusoidal strain is applied to the material, the out-of-phase stress will also be sinusoidal [80].

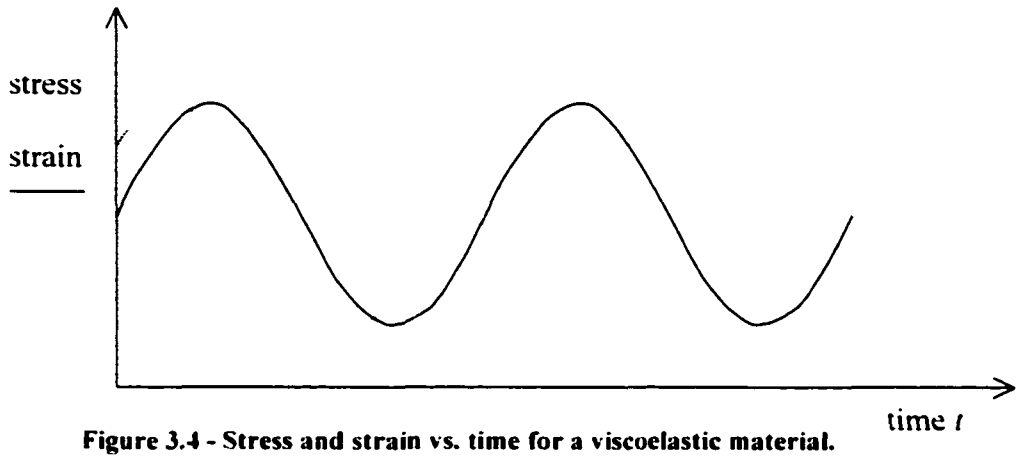

Figure 3.4 - Stress and strain vs. time for a viscoelastic material.

Consider a sinusoidal strain history with frequency, ω, and amplitude of strains, ε^{0}_{kl}. The complex strain, ε^{*}_{kl}, can be written in polar form as

$$\varepsilon^{*}_{kl}(t) = \varepsilon^{0}_{kl} e^{i\omega t} \tag{3.56}$$

Then, the equation (3.54) can be written as,

$$\begin{aligned} \sigma^{*}_{ij} &= \int_{-\infty}^{t} C_{ijkl}(t-\tau)\, d\varepsilon^{*}_{kl}(\tau) \\ \sigma^{*}_{ij} &= \int_{-\infty}^{t} C_{ijkl}(t-\tau)\frac{d\varepsilon^{*}_{kl}(\tau)}{d\tau} d\tau \\ \sigma^{*}_{ij} &= \int_{-\infty}^{t} C_{ijkl}(t-\tau) i\omega \varepsilon^{0}_{kl} e^{i\omega\tau} d\tau \end{aligned} \tag{3.57}$$

Defining $u = t - \tau \Rightarrow du = -d\tau$.

$$\begin{aligned}
\sigma_{ij}^{\bullet} &= i\omega\varepsilon_{kl}^{0}\int_{\infty}^{0} C_{ijkl}(u)e^{i\omega(t-u)}(-du) \\
\sigma_{ij}^{\bullet} &= i\omega\varepsilon_{kl}^{0}e^{i\omega t}\int_{0}^{\infty} C_{ijkl}(u)e^{-i\omega u}du \\
\sigma_{ij}^{\bullet} &= i\omega\varepsilon_{kl}^{\bullet}\int_{0}^{\infty} C_{ijkl}(u)(\cos\omega u - i\sin\omega u)du
\end{aligned} \tag{3.58}$$

or

$$\sigma_{ij}^{\bullet} = C^{\bullet}_{ijkl}\varepsilon_{kl}^{\bullet} \tag{3.59}$$

The complex moduli $C^{\bullet}_{ijkl}$ have real and imaginary components

$$\begin{aligned}
C^{\bullet}_{ijkl} &= i\omega\int_{0}^{\infty} C_{ijkl}(u)(\cos\omega u - i\sin\omega u)du \\
C^{\bullet}_{ijkl} &= \omega\int_{0}^{\infty} C_{ijkl}(u)\sin\omega u du + i\omega\int_{0}^{\infty} C_{ijkl}(u)\cos\omega u du \\
C^{\bullet}_{ijkl} &= C''_{ijkl} + iC'''_{ijkl}
\end{aligned} \tag{3.60}$$

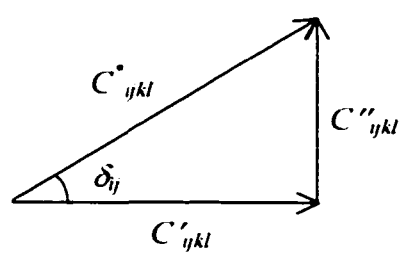

Figure 3.5 - Complex modulus components.

where:

$$C'_{ijkl}(\omega) = \omega \int_0^{\infty} C_{ijkl}(u) \sin \omega u du$$
$$C''_{ijkl}(\omega) = \omega \int_0^{\infty} C_{ijkl}(u) \cos \omega u du \tag{3.61}$$

Inverse Fourier transform can be used to obtain the tensor of creep function from the complex moduli functions (see Appendix 3):

$$C_{ijkl}(t) = \frac{2}{\pi} \int_0^{\infty} \frac{C'_{ijkl}(\omega)}{\omega} \sin \omega t d\omega \tag{3.62}$$

or

$$C_{ijkl}(t) = \frac{2}{\pi} \int_0^{\infty} \frac{C''_{ijkl}(\omega)}{\omega} \cos \omega t d\omega \tag{3.63}$$

For a dynamic mechanical experiment with sinusoidally varying stress and strain (Figure 3.4), and the strain given by equation (3.56), the equation for the complex stress can be represented in the form

$$\sigma^*_{ij} = \sigma^0_{ij} e^{i(\omega t + \delta_{ij})} \tag{3.64}$$

where:

σ^0_{ij} = amplitude of stress.

ω = angular frequency.

δ_{ij} = phase angle.

Thus.

$$\begin{aligned}
\sigma_{ij}^{*} &= \sigma_{ij}^{0}[\cos(\omega t + \delta_{ij}) + i\sin(\omega t + \delta_{ij})] \\
\sigma_{ij}^{*} &= \sigma_{ij}^{0}[(\cos\omega t\cos\delta_{ij} - \sin\omega t\sin\delta_{ij}) + i(\sin\omega t\cos\delta_{ij} + \sin\delta_{ij}\cos\omega t)] \\
\sigma_{ij}^{*} &= \sigma_{ij}^{0}\cos\delta_{ij}\cos\omega t - \sigma_{ij}^{0}\sin\delta_{ij}\sin\omega t + i(\sigma_{ij}^{0}\cos\delta_{ij}\sin\omega t + \sigma_{ij}^{0}\sin\delta_{ij}\cos\omega t)
\end{aligned} \tag{3.65}$$

or

$$\begin{aligned}
\sigma_{ij}^{*} &= (C'_{ijkl} + iC''_{ijkl})\varepsilon_{kl}^{0}e^{i\omega t} \\
\sigma_{ij}^{*} &= (C'_{ijkl} + iC''_{ijkl})\varepsilon_{kl}^{0}(\cos\omega t + i\sin\omega t) \\
\sigma_{ij}^{*} &= C'_{ijkl}\varepsilon_{kl}^{0}\cos\omega t - C''_{ijkl}\varepsilon_{kl}^{0}\sin\omega t + i(C'_{ijkl}\varepsilon_{kl}^{0}\sin\omega t + C''_{ijkl}\varepsilon_{kl}^{0}\cos\omega t)
\end{aligned} \tag{3.66}$$

Comparing equations (3.65) and (3.66). It can be concluded that

$$C'_{ijkl}\varepsilon_{kl}^{0} = \sigma_{ij}^{0}\cos\delta_{ij} \tag{3.67}$$

and

$$C''_{ijkl}\varepsilon_{kl}^{0} = \sigma_{ij}^{0}\sin\delta_{ij} \tag{3.68}$$

where:

$$\sigma_{ij}^{0} = \sqrt{(C'_{ijkl}\varepsilon_{kl}^{0})^{2} + (C''_{ijkl}\varepsilon_{kl}^{0})^{2}} \tag{3.69}$$

The result of out-of-phase stresses and strains is the formation of a hysteresis loop on the stress-strain diagram (Figure 3.6). The area of the hysteresis loop defines the energy lost in a unit volume of the body. The shaded triangular area represents the elastic potential energy. Dividing the lost energy by the amplitude of the elastic potential energy. gives the Specific Damping Capacity (SDC).

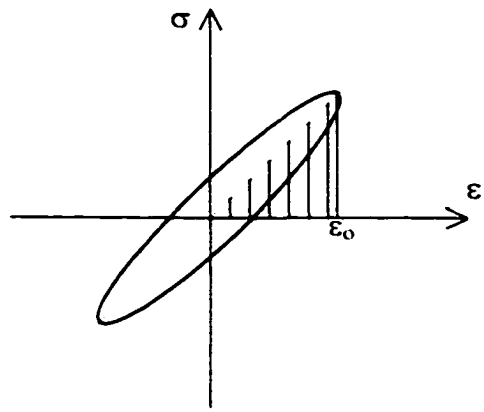

Figure 3.6 - Stress-strain for a linearly viscoelastic material under sinusoidal loading.

The specific damping capacity is defined as the ratio between the energy lost and the amplitude value of the elastic potential energy, in a given loading cycle [35,61,63,96].

$$\psi = \frac{\Delta W}{W} \tag{3.70}$$

The specific damping capacity may depend upon the exciting frequency, the temperature, amplitude of vibrations, and possibly other factors.

The energy loss in a load cycle is the area of the hysteresis loop, or

$$\begin{aligned} \Delta W &= \oint \sigma_{ij} d\varepsilon_{ij} \\ \Delta W &= \oint \mathrm{Re}\,\sigma^{*}_{ij} d(\mathrm{Re}\,\varepsilon^{*}_{ij}) \end{aligned} \tag{3.71}$$

where, from equation (3.56),

$$\mathrm{Re}\,\varepsilon^{*}_{ij} = \varepsilon^{0}_{ij} \cos\omega t \tag{3.72}$$

and, from equation (3.66),

$$\mathrm{Re}\,\sigma^{*}_{ij} = \varepsilon^{0}_{kl}(C'_{ijkl} \cos\omega t - C''_{ijkl} \sin\omega t) \tag{3.73}$$

Therefore.

$$\Delta W = \int_0^{2\pi/\omega} \varepsilon_{kl}^{0}(C'_{ijkl}\cos\omega t - C''_{ijkl}\sin\omega t)\frac{d(\varepsilon_{ij}^{0}\cos\omega t)}{dt}dt$$

$$\Delta W = \int_0^{2\pi/\omega} \varepsilon_{kl}^{0}(C'_{ijkl}\cos\omega t - C''_{ijkl}\sin\omega t)\varepsilon_{ij}^{0}\omega(-\sin\omega t)dt$$

$$\Delta W = \int_0^{2\pi/\omega} \omega(C''_{ijkl}\sin^2\omega t - \frac{1}{2}C'_{ijkl}\sin 2\omega t)\varepsilon_{ij}^{0}\varepsilon_{kl}^{0}dt \qquad (3.74)$$

$$\Delta W = \varepsilon_{ij}^{0}\varepsilon_{kl}^{0}\omega\left[C''_{ijkl}\left(\frac{\omega t - \cos\omega t\sin\omega t}{2\omega}\right) - \frac{C'_{ijkl}}{2}\left(\frac{-\cos 2\omega t}{2\omega}\right)\right]_0^{2\pi/\omega}$$

$$\Delta W = \varepsilon_{ij}^{0}\varepsilon_{kl}^{0}\omega C''_{ijkl}\frac{\pi}{\omega}$$

Thus.

$$\Delta W = \pi C''_{ijkl}\varepsilon_{ij}^{0}\varepsilon_{kl}^{0} \qquad (3.75)$$

Similarly, the energy losses in the unit volume of a body corresponding to one cycle can be given as a function of the complex compliances.

Hence.

$$\Delta W = \pi S''_{ijkl}\sigma_{ij}^{0}\sigma_{kl}^{0} \qquad (3.76)$$

where:

$$S^{*}_{ijkl} = S'_{ijkl} - iS''_{ijkl} \qquad (3.77)$$

and

$$S'_{ijkl}(\omega) = \omega \int_0^{\infty} S_{ijkl}(u) \sin \omega u du$$
$$S''_{ijkl}(\omega) = -\omega \int_0^{\infty} S_{ijkl}(u) \cos \omega u du \tag{3.78}$$

After defining the equation for the energy loss, (3.75) or (3.76), the dependence of the specific damping capacity, ψ, on amplitude of vibrations can be studied. The specific elastic energy for an anisotropic body was already defined as (equation (3.14)).

$$W = \frac{1}{2} C_{ijkl} \varepsilon_{ij} \varepsilon_{kl} = \frac{1}{2} S_{ijkl} \sigma_{ij} \sigma_{kl} \tag{3.79}$$

Thus, a proportional change in the amplitude of stress (or strain) components

$$\sigma'_{ij} = \mu \sigma_{ij} \tag{3.80}$$

will change the elastic energy as

$$W' = \mu^2 W \tag{3.81}$$

where, μ is a constant of proportionality.

Similarly, from equations (3.75) and (3.76), a proportional change in the amplitude of stress (or strain) components changes the energy loss as,

$$\Delta W' = \mu^2 \Delta W \tag{3.82}$$

Substitution of equations (3.81) and (3.82) into equation (3.70), gives,

$$\psi = \frac{\Delta W}{W} = \frac{\Delta W'}{W'} \tag{3.83}$$

Therefore, equation (3.83) implies that the specific damping capacity, ψ, does not depend on the amplitude of stress or strain. This statement is confirmed experimentally for small stress (strain) amplitudes [60,97,98].

3.3 Laminate Theories - Classical Laminate Equations

The Classical Laminated Plate Theory (CLT) is the simplest of the laminate theories and adequately describes the kinematics behavior of laminates with side-to-thickness ratio above 40.

Laminate theories are normally defined by assuming a displacement field. CLT is based on Kirchhoff hypothesis: Straight lines normal to the mid-surface before deformation remain straight, normal to the mid-surface and unchanged in length, after deformation.

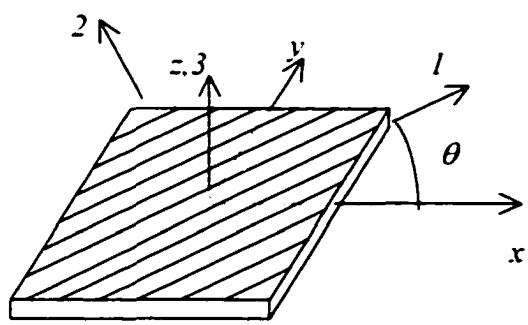

Figure 3.7 - Laminate coordinate axis (x,y,z) and material coordinate axis (1,2,3).

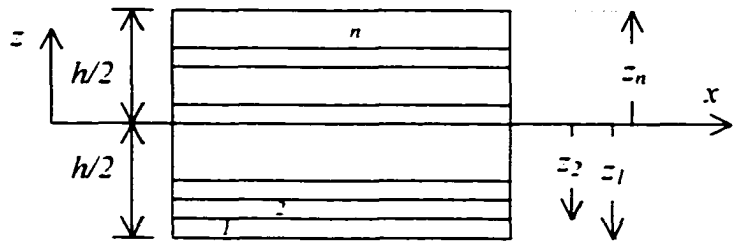

Figure 3.8 – Layer numbering convention in a laminate.

3.3.1 Kinematics

The assumed displacement field for CLT is:

$$\begin{aligned} u(x,y,z,t) &= u_0(x,y,t) - z\frac{\partial w_0}{\partial x} \\ v(x,y,z,t) &= v_0(x,y,t) - z\frac{\partial w_0}{\partial y} \\ w(x,y,z,t) &= w_0(x,y,t) \end{aligned} \tag{3.84}$$

where: u, v, w are the displacements along x, y, and z coordinates, respectively;

u_0, v_0, w_0 are the mid-plane displacements along x, y, and z coordinates, respectively.

z is the distance from the midsurface, as shown in Figure 3.8.

The Green-Lagrange strain tensor $\vec{E}$ is given in terms of the displacement gradients as:[99]

$$\vec{E} = \frac{1}{2}\left[\nabla\vec{u} + (\nabla\vec{u})^T + \nabla\vec{u}\cdot(\nabla\vec{u})^T\right] \tag{3.85}$$

In rectangular Cartesian form, the tensor components are,

$$E_{ij} = \frac{1}{2}\left[\frac{\partial u_i}{\partial X_j} + \frac{\partial u_j}{\partial X_i} + \frac{\partial u_k}{\partial X_i}\frac{\partial u_k}{\partial X_j}\right] \tag{3.86}$$

Where: (u_1, u_2, u_3) are the displacement components:

(X_1, X_2, X_3) are the reference coordinates.

If the displacement gradients $|u_{i,j}|$ are very small, their squares and products can be neglected. Then, with the small strain assumption, the infinitesimal strain tensor components reduce to:

$$\varepsilon_{ij} = \frac{1}{2}\left(\frac{\partial u_i}{\partial X_j} + \frac{\partial u_j}{\partial X_i}\right) \tag{3.87}$$

Furthermore, the small strain assumption also implies that the deformed and undeformed shapes have same geometry.

$$\varepsilon_{ij} = \frac{1}{2}\left(\frac{\partial u_i}{\partial x_j} + \frac{\partial u_j}{\partial x_i}\right) \tag{3.88}$$

Where: (x_1, x_2, x_3) are the current (deformed) coordinates.

Thus, with the assumed displacement field for CLT (equation (3.84)), the tensor strains are

$$
\begin{aligned}
\varepsilon_{xx} &= \frac{\partial u_0}{\partial x} - z\frac{\partial^2 w_0}{\partial x^2} \\
\varepsilon_{yy} &= \frac{\partial v_0}{\partial y} - z\frac{\partial^2 w_0}{\partial y^2} \\
\varepsilon_{xy} &= \frac{1}{2}\left(\frac{\partial u_0}{\partial y} + \frac{\partial v_0}{\partial x}\right) - z\frac{\partial^2 w_0}{\partial x \partial y} \\
\varepsilon_{xz} &= \frac{1}{2}\left(-\frac{\partial w_0}{\partial x} + \frac{\partial w_0}{\partial x}\right) = 0 \\
\varepsilon_{yz} &= \frac{1}{2}\left(-\frac{\partial w_0}{\partial y} + \frac{\partial w_0}{\partial y}\right) = 0 \\
\varepsilon_{zz} &= 0
\end{aligned}
\tag{3.89}
$$

Hence, using the engineering contracted notation, the non-zero strains in CLT, have the form:

$$
\begin{Bmatrix} \varepsilon_x \\ \varepsilon_y \\ \gamma_{xy} \end{Bmatrix} = \begin{Bmatrix} \varepsilon_x^0 \\ \varepsilon_y^0 \\ \gamma_{xy}^0 \end{Bmatrix} + z\begin{Bmatrix} \kappa_x^0 \\ \kappa_y^0 \\ \kappa_{xy}^0 \end{Bmatrix} \tag{3.90}
$$

where:

$$
\begin{Bmatrix} \varepsilon_x^0 \\ \varepsilon_y^0 \\ \gamma_{xy}^0 \end{Bmatrix} = \begin{Bmatrix} \dfrac{\partial u_0}{\partial x} \\ \dfrac{\partial v_0}{\partial y} \\ \dfrac{\partial u_0}{\partial y} + \dfrac{\partial v_0}{\partial x} \end{Bmatrix}, \qquad \begin{Bmatrix} \kappa_x^0 \\ \kappa_y^0 \\ \kappa_{xy}^0 \end{Bmatrix} = \begin{Bmatrix} -\dfrac{\partial^2 w_0}{\partial x^2} \\ -\dfrac{\partial^2 w_0}{\partial y^2} \\ -2\dfrac{\partial^2 w_0}{\partial x \partial y} \end{Bmatrix} \tag{3.91}
$$

where: ε^0_x, ε^0_y, and γ^0_{xy}, are the mid-plane strains;

κ^0_x, κ^0_y, and κ^0_{xy}, are the curvatures.

3.3.2 Constitutive Relations for a Lamina (linear elasticity)

In the classical laminate theory, the three components of the out-of-plane strains are zero (equation (3.89)), as a direct result of the assumed displacement field (equation (3.84)). In reality, these strains are small, but not zero.

If the plate is very thin, although the out-of-plane stresses are not zero, they are very small compared to the in-plane stresses and can be neglected. Therefore, the plate can be assumed to be in a state of plane stress. Under plane stress, the strain-stress relation for each lamina is written in material coordinate system as

$$\begin{Bmatrix} \varepsilon_1 \\ \varepsilon_2 \\ \varepsilon_6 \end{Bmatrix} = \begin{bmatrix} S_{11} & S_{12} & 0 \\ S_{12} & S_{22} & 0 \\ 0 & 0 & S_{66} \end{bmatrix} \begin{Bmatrix} \sigma_1 \\ \sigma_2 \\ \sigma_6 \end{Bmatrix} \tag{3.92}$$

Then, the stress-strain relation can be written as

$$\begin{Bmatrix} \sigma_1 \\ \sigma_2 \\ \sigma_6 \end{Bmatrix} = \begin{bmatrix} Q_{11} & Q_{12} & 0 \\ Q_{12} & Q_{22} & 0 \\ 0 & 0 & Q_{66} \end{bmatrix} \begin{Bmatrix} \varepsilon_1 \\ \varepsilon_2 \\ \varepsilon_6 \end{Bmatrix} \tag{3.93}$$

Where:$[Q] = [S]^{-1}$, is the reduced stiffness matrix.

In the laminate coordinate system, the relations are

$$\begin{Bmatrix} \varepsilon_x \\ \varepsilon_y \\ \gamma_{xy} \end{Bmatrix} = \begin{bmatrix} \bar{S}_{11} & \bar{S}_{12} & \bar{S}_{16} \\ \bar{S}_{12} & \bar{S}_{22} & \bar{S}_{26} \\ \bar{S}_{16} & \bar{S}_{26} & \bar{S}_{66} \end{bmatrix} \begin{Bmatrix} \sigma_x \\ \sigma_y \\ \sigma_{xy} \end{Bmatrix} \tag{3.94}$$

and.

$$\begin{Bmatrix} \sigma_{x} \\ \sigma_{y} \\ \sigma_{xy} \end{Bmatrix} = \begin{bmatrix} \overline{Q}_{11} & \overline{Q}_{12} & \overline{Q}_{16} \\ \overline{Q}_{12} & \overline{Q}_{22} & \overline{Q}_{26} \\ \overline{Q}_{16} & \overline{Q}_{26} & \overline{Q}_{66} \end{bmatrix} \begin{Bmatrix} \varepsilon_{x} \\ \varepsilon_{y} \\ \varepsilon_{xy} \end{Bmatrix} \tag{3.95}$$

From equation (3.53).

$$[\overline{S}] = [R]^{T}_{3x3}[S]_{3x3}[R]_{3x3} \tag{3.96}$$

where.

$$[R]_{3x3} = \begin{bmatrix} \cos^2\theta & \sin^2\theta & 2\cos\theta\sin\theta \\ \sin^2\theta & \cos^2\theta & -2\cos\theta\sin\theta \\ -\cos\theta\sin\theta & \cos\theta\sin\theta & \cos^2\theta - \sin^2\theta \end{bmatrix} \tag{3.97}$$

Hence.

$$\begin{aligned} [\overline{Q}]_{3x3} &= [\overline{S}]^{-1}_{3x3} \\ [\overline{Q}]_{3x3} &= \left[[R]^{T}_{3x3}[S]_{3x3}[R]_{3x3}\right]^{-1} \\ [\overline{Q}]_{3x3} &= [R]^{-1}_{3x3}[S]^{-1}_{3x3}[R]^{-T}_{3x3} \end{aligned} \tag{3.98}$$

Thus. the components of the compliance matrix in laminate coordinates are:

$$\begin{aligned} \overline{S}_{11} &= S_{11}\cos^4\theta + S_{22}\sin^4\theta + (2S_{12} + S_{66})\sin^2\theta\cos^2\theta \\ \overline{S}_{12} &= (S_{11} + S_{22} - S_{66})\sin^2\theta\cos^2\theta + S_{12}(\sin^4\theta + \cos^4\theta) \\ \overline{S}_{16} &= [2S_{11}\cos^2\theta - 2S_{22}\sin^2\theta + (2S_{12} + S_{66})(\sin^2\theta - \cos^2\theta)]\sin\theta\cos\theta \\ \overline{S}_{22} &= S_{11}\sin^4\theta + S_{22}\cos^4\theta + (2S_{12} + S_{66})\sin^2\theta\cos^2\theta \\ \overline{S}_{26} &= [2S_{11}\sin^2\theta - 2S_{22}\cos^2\theta - (2S_{12} + S_{66})(\sin^2\theta - \cos^2\theta)]\sin\theta\cos\theta \\ \overline{S}_{66} &= 4(S_{11} - 2S_{12} + S_{22})\sin^2\theta\cos^2\theta + (\sin^2\theta - \cos^2\theta)^2 S_{66} \end{aligned} \tag{3.99}$$

And. for the reduced stiffness matrix in laminate coordinates. the components are:

$$
\begin{aligned}
\overline{Q}_{11} &= Q_{11}\cos^4\theta + Q_{22}\sin^4\theta + 2(Q_{12}+2Q_{66})\sin^2\theta\cos^2\theta \\
\overline{Q}_{12} &= (Q_{11}+Q_{22}-4Q_{66})\sin^2\theta\cos^2\theta + Q_{12}(\sin^4\theta+\cos^4\theta) \\
\overline{Q}_{16} &= [Q_{11}\cos^2\theta - Q_{22}\sin^2\theta + (Q_{12}+2Q_{66})(\sin^2\theta-\cos^2\theta)]\sin\theta\cos\theta \\
\overline{Q}_{22} &= Q_{11}\sin^4\theta + Q_{22}\cos^4\theta + 2(Q_{12}+2Q_{66})\sin^2\theta\cos^2\theta \\
\overline{Q}_{26} &= [Q_{11}\sin^2\theta - Q_{22}\cos^2\theta - (Q_{12}+2Q_{66})(\sin^2\theta-\cos^2\theta)]\sin\theta\cos\theta \\
\overline{Q}_{66} &= (Q_{11}-2Q_{12}+Q_{22})\sin^2\theta\cos^2\theta + Q_{66}(\sin^2\theta-\cos^2\theta)^2
\end{aligned}
\tag{3.100}
$$

The equation (3.95) can also be written as:

$$
\begin{Bmatrix} \sigma_x \\ \sigma_y \\ \sigma_{xy} \end{Bmatrix}^{(k)} = \begin{bmatrix} \overline{Q}_{11} & \overline{Q}_{12} & \overline{Q}_{16} \\ \overline{Q}_{12} & \overline{Q}_{22} & \overline{Q}_{26} \\ \overline{Q}_{16} & \overline{Q}_{26} & \overline{Q}_{66} \end{bmatrix}^{(k)} \left\{ \begin{Bmatrix} \varepsilon_x^0 \\ \varepsilon_y^0 \\ \gamma_{xy}^0 \end{Bmatrix} + z \begin{Bmatrix} \kappa_x^0 \\ \kappa_y^0 \\ \kappa_{xy}^0 \end{Bmatrix} \right\} \tag{3.101}
$$

where the superscript (k) indicates that the stresses are referred to the k^{th} layer.

The resultant forces per unit length of edge on the laminate. can be calculated by integrating the stresses through the thickness. Thus.

$$
\begin{Bmatrix} N_x \\ N_y \\ N_{xy} \end{Bmatrix} = \int_{-\frac{h}{2}}^{\frac{h}{2}} \begin{Bmatrix} \sigma_x \\ \sigma_y \\ \sigma_{xy} \end{Bmatrix} dz \tag{3.102}
$$

Although the strains are continuous through the laminate thickness. the stresses are not since the material properties are different for each layer. Thus. the integration in equation (3.102) is performed layerwise:

$$\begin{Bmatrix} N_x \\ N_y \\ N_{xy} \end{Bmatrix} = \sum_{k=1}^{n} \int_{z_{k-1}}^{z_k} \begin{Bmatrix} \sigma_x \\ \sigma_y \\ \sigma_{xy} \end{Bmatrix}^{(k)} dz \tag{3.103}$$

$$\begin{Bmatrix} N_x \\ N_y \\ N_{xy} \end{Bmatrix} = \sum_{k=1}^{n} \int_{z_{k-1}}^{z_k} \begin{bmatrix} \overline{Q}_{11} & \overline{Q}_{12} & \overline{Q}_{16} \\ \overline{Q}_{12} & \overline{Q}_{22} & \overline{Q}_{26} \\ \overline{Q}_{16} & \overline{Q}_{26} & \overline{Q}_{66} \end{bmatrix}^{(k)} \left\{ \begin{Bmatrix} \varepsilon_x^0 \\ \varepsilon_y^0 \\ \gamma_{xy}^0 \end{Bmatrix} + z \begin{Bmatrix} \kappa_x^0 \\ \kappa_y^0 \\ \kappa_{xy}^0 \end{Bmatrix} \right\} dz \tag{3.104}$$

Similarly, the moment resultants per unit length of edge on the laminate, can be calculated by:

$$\begin{Bmatrix} M_x \\ M_y \\ M_{xy} \end{Bmatrix} = \sum_{k=1}^{n} \int_{z_{k-1}}^{z_k} \begin{Bmatrix} \sigma_x \\ \sigma_y \\ \sigma_{xy} \end{Bmatrix}^{(k)} z \, dz \tag{3.105}$$

$$\begin{Bmatrix} M_x \\ M_y \\ M_{xy} \end{Bmatrix} = \sum_{k=1}^{n} \int_{z_{k-1}}^{z_k} \begin{bmatrix} \overline{Q}_{11} & \overline{Q}_{12} & \overline{Q}_{16} \\ \overline{Q}_{12} & \overline{Q}_{22} & \overline{Q}_{26} \\ \overline{Q}_{16} & \overline{Q}_{26} & \overline{Q}_{66} \end{bmatrix}^{(k)} \left\{ \begin{Bmatrix} \varepsilon_x^0 \\ \varepsilon_y^0 \\ \gamma_{xy}^0 \end{Bmatrix} + z \begin{Bmatrix} \kappa_x^0 \\ \kappa_y^0 \\ \kappa_{xy}^0 \end{Bmatrix} \right\} z \cdot dz \tag{3.106}$$

Equations (3.104) and (3.106) can be rewritten as.

$$\begin{Bmatrix} N_x \\ N_y \\ N_{xy} \end{Bmatrix} = \begin{bmatrix} A_{11} & A_{12} & A_{16} \\ A_{12} & A_{22} & A_{26} \\ A_{16} & A_{26} & A_{66} \end{bmatrix} \begin{Bmatrix} \varepsilon_x^0 \\ \varepsilon_y^0 \\ \gamma_{xy}^0 \end{Bmatrix} + \begin{bmatrix} B_{11} & B_{12} & B_{16} \\ B_{12} & B_{22} & B_{26} \\ B_{16} & B_{26} & B_{66} \end{bmatrix} \begin{Bmatrix} \kappa_x^0 \\ \kappa_y^0 \\ \kappa_{xy}^0 \end{Bmatrix} \tag{3.107}$$

$$\begin{Bmatrix} M_x \\ M_y \\ M_{xy} \end{Bmatrix} = \begin{bmatrix} B_{11} & B_{12} & B_{16} \\ B_{12} & B_{22} & B_{26} \\ B_{16} & B_{26} & B_{66} \end{bmatrix} \begin{Bmatrix} \varepsilon_x^0 \\ \varepsilon_y^0 \\ \gamma_{xy}^0 \end{Bmatrix} + \begin{bmatrix} D_{11} & D_{12} & D_{16} \\ D_{12} & D_{22} & D_{26} \\ D_{16} & D_{26} & D_{66} \end{bmatrix} \begin{Bmatrix} \kappa_x^0 \\ \kappa_y^0 \\ \kappa_{xy}^0 \end{Bmatrix} \tag{3.108}$$

where,

$$(A_{ij}, B_{ij}, D_{ij}) = \sum_{k=1}^{n} \int_{z_{k-1}}^{z_k} \overline{Q}_{ij}^{(k)} (1, z, z^2) dz$$

or,

$$A_{ij} = \sum_{k=1}^{n} \overline{Q}_{ij}^{(k)} (z_{k-1} - z_k)$$

$$B_{ij} = \frac{1}{2} \sum_{k=1}^{n} \overline{Q}_{ij}^{(k)} (z_{k-1}^2 - z_k^2)$$

$$D_{ij} = \frac{1}{3} \sum_{k=1}^{n} \overline{Q}_{ij}^{(k)} (z_{k-1}^3 - z_k^3)$$

Equations (3.107) and (3.108) can be combined as,

$$\begin{Bmatrix} \begin{Bmatrix} N_x \\ N_y \\ N_{xy} \end{Bmatrix} \\ \begin{Bmatrix} M_x \\ M_y \\ M_{xy} \end{Bmatrix} \end{Bmatrix} = \begin{bmatrix} \begin{bmatrix} A_{11} & A_{12} & A_{16} \\ A_{12} & A_{22} & A_{26} \\ A_{16} & A_{26} & A_{66} \end{bmatrix} & \begin{bmatrix} B_{11} & B_{12} & B_{16} \\ B_{12} & B_{22} & B_{26} \\ B_{16} & B_{26} & B_{66} \end{bmatrix} \\ \begin{bmatrix} B_{11} & B_{12} & B_{16} \\ B_{12} & B_{22} & B_{26} \\ B_{16} & B_{26} & B_{66} \end{bmatrix} & \begin{bmatrix} D_{11} & D_{12} & D_{16} \\ D_{12} & D_{22} & D_{26} \\ D_{16} & D_{26} & D_{66} \end{bmatrix} \end{bmatrix} \begin{Bmatrix} \begin{Bmatrix} \varepsilon_x^0 \\ \varepsilon_y^0 \\ \gamma_{xy}^0 \end{Bmatrix} \\ \begin{Bmatrix} \kappa_x^0 \\ \kappa_y^0 \\ \kappa_{xy}^0 \end{Bmatrix} \end{Bmatrix} \tag{3.109}$$

3.3.3 Laminated Beams

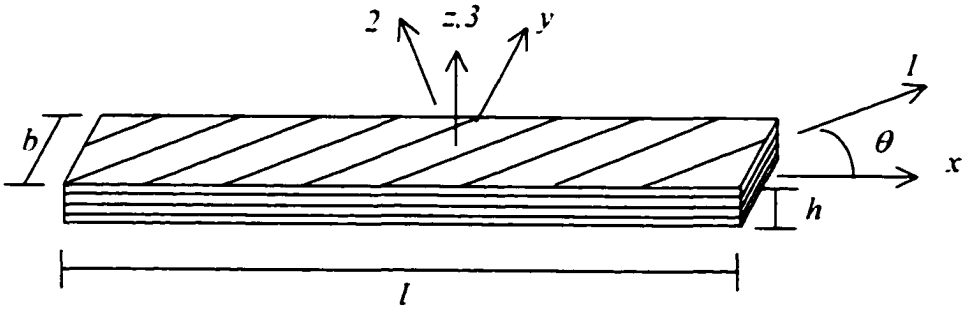

Figure 3.9 - Laminated beam with coordinate axis convention.

In the following derivation, laminated beams with symmetric stacking sequences are considered. Due to symmetry, there are no bending-stretching couplings and the bending moments are solely dependent on the curvatures. Therefore, the constitutive equations for bending reduce to the following form

$$\begin{Bmatrix} M_x \\ M_y \\ M_{xy} \end{Bmatrix} = \begin{bmatrix} D_{11} & D_{12} & D_{16} \\ D_{12} & D_{22} & D_{26} \\ D_{16} & D_{26} & D_{66} \end{bmatrix} \begin{Bmatrix} \kappa_x^0 \\ \kappa_y^0 \\ \kappa_{xy}^0 \end{Bmatrix} \tag{3.110}$$

and, the inverse relation is

$$\begin{Bmatrix} \kappa_x^0 \\ \kappa_y^0 \\ \kappa_{xy}^0 \end{Bmatrix} = \begin{bmatrix} d_{11} & d_{12} & d_{16} \\ d_{12} & d_{22} & d_{26} \\ d_{16} & d_{26} & d_{66} \end{bmatrix} \begin{Bmatrix} M_x \\ M_y \\ M_{xy} \end{Bmatrix} \tag{3.111}$$

If M_x is the only moment resultant anywhere in the beam,

$$M_y = M_{xy} = 0 \tag{3.112}$$

The curvatures calculated from equation (3.111) will determine the deflected shape of the beam. If the beam is long, *i.e.*, the beam length is very large compared to the beam width, the effects of the curvatures κ_y^0 and κ_{xy}^0 on the total transverse deflection is negligible. Thus, the transverse deflection will be only a function of x.

$$\kappa_x^0 = -\frac{\partial^2 w_0}{\partial x^2} = d_{11} M_x \tag{3.113}$$

or

$$\frac{\partial^2 w_0}{\partial x^2} = -\frac{M(x)}{E_{xx}^b I_{yy}} \tag{3.114}$$

where:

$M(x) = M_x\, b$ = bending moment;

b = beam width;

$E_{xx}^b = \dfrac{12}{h^3 d_{11}}$ = beam modulus in the x-direction;

I_{yy} = moment of inertia about the y-axis.

Considering a simply-supported beam subjected to a point load P at the mid-span,

$$\frac{\partial^2 w_0}{\partial x^2} = -\frac{1}{E_{xx}^b I_{yy}} \frac{P}{2} x \tag{3.115}$$

$$w_0 = \frac{P}{48 E_{xx}^b I_{yy}} \left(3l^2 x - 4x^3\right) \tag{3.116}$$

The maximum deflection will occur at $x = l/2$.

$$w_0 = \frac{Pl^3}{48 E_{xx}^b I_{yy}} \tag{3.117}$$

For a single layer beam,

$$d_{11} = \bar{S}_{11} \frac{12}{h^3} \tag{3.118}$$

where

$$\bar{S}_{11}(\theta) = \frac{1}{E_{xx}^{b}} = S_{11}\cos^4(\theta) + S_{22}\sin^4(\theta) + (2S_{12} + S_{66})\cos^2(\theta)\sin^2(\theta) \qquad \textbf{(3.119)}$$

Thus, for a single layered beam,

$$E_{xx}^{b} = \frac{1}{\bar{S}_{11}(\theta)} \qquad \textbf{(3.120)}$$

However, if the beam is composed of layers with different orientations, d_{11} can be obtained by computing the $[d]$ matrix as the inverse of the $[D]$ matrix. Then, $E_{xx}{}^{b}$ can be calculated as

$$E_{xx}^{b} = \frac{12}{h^3 d_{11}} \qquad \textbf{(3.121)}$$

4

Determination of the Elastic Properties of Transversely Isotropic Laminae Using Laminate Coefficients of Thermal Expansion

Information regarding engineering elastic constants of composite materials is essential for the analysis and design of structures. However, three-dimensional elastic constants for a fiber-reinforced lamina are often difficult to obtain from traditional mechanical tests. The relationships developed in this chapter enable the determination of any three of the five independent elastic constants, of a transversely isotropic lamina, from measurements of the remaining two elastic constants and the coefficients of thermal expansion (CTE's) of $[(+\theta/-\theta)_n]_s$ and of unidirectional laminates. The approach is used to predict the elastic properties of a carbon fiber reinforced epoxy material and the predicted properties are shown to be in good agreement with quoted values. Further, the developed relationships can be used to determine elastic constants over a range of temperatures and, potentially, to study the effects of manufacturing on elastic properties. Therefore, this technique constitutes an additional method for evaluating the elastic constants that characterize a transversely isotropic, fiber-reinforced lamina.

Relationships between mechanical properties and thermal expansion coefficients of composites have been successfully investigated in the past. Expressions for determining the tensor of the thermal expansion coefficients for a two-phase composite material, as a function of the mechanical properties and the thermal expansion coefficients of the constituent phases, have been developed [24]. The overall composite was assumed to be macroscopically homogeneous and each constituent phase was assumed to be homogeneous and isotropic. A further study examined the case of a unidirectional fiber composite with transversely isotropic constituent phases [25]. The equations developed related the coefficients of thermal expansion (CTE's) of the fiber reinforcement to the CTE's of the composite and to the elastic properties of the fiber, the matrix and the composite.

More recently, a relationship between the coefficients of thermal expansion of laminates and elastic constants of the component laminae was developed [26]. The final expression allowed prediction of the Poisson ratio, ν_{23}, of the individual lamina based on laminate CTE measurements and other known lamina elastic properties. A basic difference between this approach and previous micromechanics approaches is that the properties of the constituent materials, i.e., matrix and reinforcement, are not required. However, to determine ν_{23} via this approach it is still necessary to know E_1, E_2, and ν_{12} of the lamina, each of which must be measured in addition to the CTE's. Moreover, this method only results in the prediction of one of the five independent elastic constants.

Based on the concepts of the previous work [26], new relations between the CTE's of a laminate and the laminae elastic constants are developed in the following sections. However, in this present development, the constraint requiring the measured laminate to

be crossplied is relaxed. This more general approach is developed for a $[(+\theta/-\theta)_n]_s$ laminate, and results in relations between the elastic constants and the coefficients of thermal expansion, which allow the prediction of any three of the five independent elastic constants, assuming that the other two are known, or can be measured.

4.1 Lamina Elastic Constants Related to CTE's of a Laminate

The conventions used in this derivation are shown in Figure 4.1. The coordinates (1,2,3) refer to the local coordinate system for a single layer or lamina, which corresponds to the fiber direction, the in-plane direction transverse to the fiber, and the through-thickness (lamination) direction, respectively. The coordinates (x,y,z) correspond to the global or laminate directions.

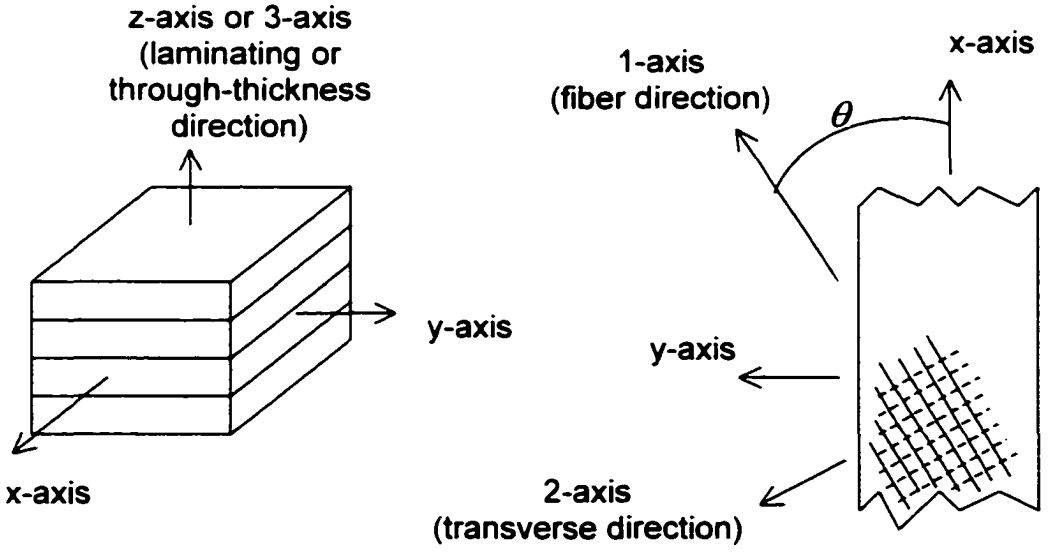

Figure 4.1 - Local or lamina (1-2-3) and global or laminate (x-y-z) reference axis.

The CTE's of a $[(+\theta/-\theta)_n]_s$ laminate are derived as a function of the engineering elastic constants of the individual lamina. To initiate the derivation it is not necessary to be restricted to a transversely isotropic material. Thus, for this derivation, a laminate composed of orthotropic layers is initially considered.

The three-dimensional thermoelastic constitutive equations for an orthotropic lamina, referred to the global coordinate system (x,y,z) may be expressed as [99]

$$\{\sigma\} = [\overline{C}]\{\{\varepsilon\} - \Delta T\{\overline{\alpha}\}\} \tag{4.1}$$

where: $\{\sigma\}$ is the stress vector in global coordinates;

$[\overline{C}]$ is the transformed stiffness matrix;

$\{\varepsilon\}$ is the strain vector in global coordinates;

ΔT is the temperature variation; and

$\{\overline{\alpha}\}$ is the vector of CTE's in global coordinates.

The CTE tensor components must transform like the tensor components of strain. Thus, for a rigid-body rotation about the 3-axis from the (1,2) coordinate system to the (x,y) coordinate system,

$$\alpha_{i'j'} = \Omega_{i'i}\Omega_{j'j}\alpha_{ij} \tag{4.2}$$

where:

$$\Omega_{ij} = \begin{bmatrix} \cos\theta & -\sin\theta & 0 \\ \sin\theta & \cos\theta & 0 \\ 0 & 0 & 1 \end{bmatrix} \tag{4.3}$$

Expressing the tensor transformation in matrix form and using engineering notation.

$$\begin{Bmatrix} \alpha_x \\ \alpha_y \\ \alpha_z \\ \alpha_{yz} \\ \alpha_{xz} \\ \alpha_{xy} \end{Bmatrix} = [R]^{-1} \begin{Bmatrix} \alpha_1 \\ \alpha_2 \\ \alpha_3 \\ 0 \\ 0 \\ 0 \end{Bmatrix} = \begin{Bmatrix} \frac{1}{2}(\alpha_1 + \alpha_2) + \frac{1}{2}(\alpha_1 - \alpha_2)\cos(2\theta) \\ \frac{1}{2}(\alpha_1 + \alpha_2) - \frac{1}{2}(\alpha_1 - \alpha_2)\cos(2\theta) \\ \alpha_3 \\ 0 \\ 0 \\ (\alpha_1 - \alpha_2)\sin(2\theta) \end{Bmatrix} \tag{4.4}$$

The resultant forces per unit length of edge along the laminate can be calculated by integrating the stresses through the laminate thickness. For an equivalent single-layer approach, this integration is performed in a layer-wise fashion since the stresses are not continuous through the laminate thickness. Hence,

$$\{N\} = \sum_{k=1}^{n_l} \int_{z_k}^{z_{k+1}} [\bar{C}]^{(k)} \left\{ \{\varepsilon\} - \Delta T \{\bar{\alpha}\}^{(k)} \right\} dz \tag{4.5}$$

where: n_l is the number of layers of the laminate.

z_k and z_{k+1} are the z coordinates of the bottom and top of the k^{th} layer, respectively.

For a $[(+\theta/-\theta)_n]_s$ laminate.

$$\{N\} = 2nh_0\left[\left[\overline{C}\right]^{(\theta)} + \left[\overline{C}\right]^{(-\theta)}\right]\{\varepsilon\} - 2nh_0\Delta T\left[\left[\overline{C}\right]^{(\theta)}\{\overline{\alpha}\}^{(\theta)} + \left[\overline{C}\right]^{(-\theta)}\{\overline{\alpha}\}^{(-\theta)}\right\} \tag{4.6}$$

where: h_0 is the layer thickness.

Thus, the CTE's of the laminate, which are equal to the strains due only to change in temperature, are determined by

$$\{\alpha\} = \frac{1}{\Delta T}\{\varepsilon\} = \left[\left[\overline{C}\right]^{(\theta)} + \left[\overline{C}\right]^{(-\theta)}\right]^{-1}\left\{\left[\overline{C}\right]^{(\theta)}\{\overline{\alpha}\}^{(\theta)} + \left[\overline{C}\right]^{(-\theta)}\{\overline{\alpha}\}^{(-\theta)}\right\} \tag{4.7}$$

Performing the matrix multiplication, the expressions for the coefficients of thermal expansion of the laminate are found to be (see Appendix 4).

$$\alpha_x(\theta) = \frac{1}{2}(\alpha_1 + \alpha_2) + \frac{1}{2}(\alpha_1 - \alpha_2)\frac{c_2(\cos(2\theta))^2 + (c_1 + c_4)\cos(2\theta) - c_2}{c_3(\cos(2\theta))^2 + c_1} \tag{4.8}$$

$$\alpha_y(\theta) = \frac{1}{2}(\alpha_1 + \alpha_2) + \frac{1}{2}(\alpha_1 - \alpha_2)\frac{c_2(\cos(2\theta))^2 - (c_1 + c_4)\cos(2\theta) - c_2}{c_3(\cos(2\theta))^2 + c_1} \tag{4.9}$$

$$\alpha_z(\theta) = \alpha_3 + (\alpha_1 - \alpha_2)\frac{c_3\left((\cos(2\theta))^2 - 1\right)}{c_3(\cos(2\theta))^2 + c_1} \tag{4.10}$$

where:

$\alpha_x(\theta)$, $\alpha_y(\theta)$ and $\alpha_z(\theta)$ are the CTE's for the $[(+\theta/-\theta)_n]_s$ laminate in x, y, and z directions, respectively;

α_1, α_2 and α_3 are the CTE's for the lamina in 1, 2, and 3 directions, respectively;

c_1, c_2, c_3, and c_4 are material constants given by

$$
\begin{aligned}
c_1 &= C_{11}C_{33} + C_{22}C_{33} + 2C_{12}C_{33} - C_{13}^2 - 2C_{13}C_{23} - C_{23}^2 \\
c_2 &= C_{22}C_{33} - C_{11}C_{33} + C_{13}^2 - C_{23}^2 \\
c_3 &= C_{11}C_{23} - C_{22}C_{13} - C_{12}C_{13} + C_{12}C_{23} \\
c_4 &= \frac{c_1(C_{11} + C_{22} - 2C_{12} - 4C_{66}) + c_2(C_{11} - C_{22}) + 2c_3(C_{13} - C_{23})}{4C_{66}}
\end{aligned}
\tag{4.11}
$$

The derivation up to this point is valid for an orthotropic material. Now, if the equations are restricted to a transversely isotropic material, where plane (2,3) coincides with the plane of isotropy, which is the typical assumption for a unidirectional fiber reinforced prepreg lamina, substitution of the engineering constants in equations (4.11) gives:

$$
\begin{aligned}
c_1 &= \frac{E_2[E_2(1+2\nu_{12}) + E_1]}{\Delta} \\
c_2 &= \frac{E_2(E_2 - E_1)}{\Delta} \\
c_3 &= \frac{E_1E_2(\nu_{23} - \nu_{21})}{\Delta} \\
c_4 &= \frac{E_2[E_1E_2 - E_1G_{12} - E_2G_{12}(1+2\nu_{12})]}{\Delta G_{12}}
\end{aligned}
\tag{4.12}
$$

where $\Delta = 1 - 2\nu_{12}\nu_{21} - \nu_{23}^2 - 2\nu_{12}\nu_{21}\nu_{23}$.

Thus, after substitution of equations (4.12) into equations (4.8), (4.9), and (4.10), three independent equations result, which include the elastic constants of a transversely isotropic material and the coefficients of thermal expansion.

4.2 Experimental Procedure for Determining the Elastic Constants

Based on the preceding derivation, and the imposition of the constraint of transverse isotropy, a procedure for determining any three lamina elastic constants, based on CTE measurements of laminates and measurements of the remaining two lamina elastic constants, can be developed. Only the three linearly independent equations, that result from substitution of equations (4.12) into equations (4.8), (4.9) and (4.10), are necessary to determine the three unknown independent elastic constants. From the CTE measurements of a $[(+\theta/-\theta)_n]_s$ laminate in all three directions (x, y, and z), and application of equations (4.8), (4.9), and (4.10), the three independent equations can be obtained. Since these equations are dependent on α_1 and α_2, CTE measurements of unidirectional laminates are also necessary to determine the elastic constants.

Theoretically, any angle θ, where $0<\theta<45°$, can be used for the manufacture of the $[(+\theta/-\theta)_n]_s$ laminate. In this work, $\theta=30°$ was chosen for the demonstration of the procedure, based on the relative ease of measurement and manufacture of this type of laminate compared to other angles. Further, this angle was found to simplify the final equations because of the numerous cos(2θ) terms. Thus, for the $[(+\theta/-\theta)_n]_s$ laminate with $\theta=30°$, equation (4.8) gives:

$$\alpha_x(30^0)=\frac{1}{2}(\alpha_1+\alpha_2)+\frac{1}{2}(\alpha_1-\alpha_2)\frac{-\frac{3}{4}c_2+\frac{1}{2}(c_1+c_4)}{\frac{1}{4}c_4+c_1} \tag{4.13}$$

If a second CTE measurement is performed in the same specimen, this time rotated 90° about the z-axis, α_y data for a $[(+\theta/-\theta)_n]_s$ laminate with θ=30° is obtained. Then, equation (4.9) gives:

$$\alpha_x(30^0) = \frac{1}{2}(\alpha_1 + \alpha_2) + \frac{1}{2}(\alpha_1 - \alpha_2)\frac{-\frac{3}{4}c_2 - \frac{1}{2}(c_1 + c_4)}{\frac{1}{4}c_4 + c_1} \tag{4.14}$$

The last measurement performed in this specimen is the CTE in the through-thickness direction. Equation (4.10), gives:

$$\alpha_z(30^0) = \alpha_2 + (\alpha_1 - \alpha_2)\frac{-\frac{3}{4}c_3}{\frac{1}{4}c_4 + c_1} \tag{4.15}$$

Equations (4.13), (4.14), and (4.15) are the three linearly independent equations for a $[(+\theta/-\theta)_n]_s$ laminate with θ=30°. Substituting c_1, c_2, c_3, and c_4 from equations (4.12) into equations (4.13), (4.14) and (4.15), and solving for ν_{12}, ν_{23}, and G_{12}, gives:

$$\nu_{12} = \frac{4(E_1\alpha_1 + E_2\alpha_2) - \alpha_x(30^0)(3E_1 + E_2) - \alpha_y(30^0)(E_1 + 3E_2)}{4E_2\left(\alpha_x(30^0) + \alpha_y(30^0) - \alpha_1 - \alpha_2\right)} \tag{4.16}$$

$$G_{12} = \frac{2E_1E_2\left[\alpha_x(30^0) + \alpha_y(30^0) - \alpha_1 - \alpha_2\right]}{3\left[\alpha_x(30^0) - \alpha_y(30^0)\right](E_1 - E_2)} \tag{4.17}$$

$$\nu_{23} = \frac{4E_1(\alpha_1 + \alpha_2) - \alpha_x(30^0)(3E_1 + E_2) - \alpha_y(30^0)(E_1 + 3E_2) + 4\alpha_z(30^0)(E_2 - E_1)}{4E_1\left[\alpha_x(30^0) + \alpha_y(30^0) - \alpha_1 - \alpha_2\right]} \tag{4.18}$$

Therefore, the procedure presented here allows the determination of ν_{12}, ν_{23}, and G_{12}, directly from equations (4.16), (4.17) and (4.18), assuming that the values of E_1 and E_2 of the lamina are known. If E_1 and ν_{12} are used as the known elastic constants, instead of E_1 and E_2, equations (4.13), (4.14) and (4.15), are solved for E_2, G_{12}, and ν_{23}, which gives:

$$E_2 = \frac{E_1\left(4\alpha_1 - 3\alpha_x(30) - \alpha_y(30)\right)}{4\nu_{12}\left(\alpha_x(30) + \alpha_y(30) - \alpha_1 - \alpha_2\right) + \alpha_x(30) + 3\alpha_y(30) - 4\alpha_2} \tag{4.19}$$

$$G_{12} = \frac{E_1\left(4\alpha_1 - 3\alpha_x(30) - \alpha_y(30)\right)}{6(\nu_{12} + 1)\left(\alpha_x(30) - \alpha_y(30)\right)} \tag{4.20}$$

$$\nu_{23} = \frac{\nu_{12}\left(4\alpha_1 + 4\alpha_2 - 3\alpha_x(30) - \alpha_y(30) - 4\alpha_z(30)\right) + 4\alpha_2 - 4\alpha_z(30)}{4\nu_{12}\left(\alpha_x(30) + \alpha_y(30) - \alpha_1 - \alpha_2\right) + \alpha_x(30) + 3\alpha_y(30) - 4\alpha_2} \tag{4.21}$$

Although the equations presented are a function of CTE measurements in a $[(+\theta/-\theta)_n]_s$ laminate with θ=30°, the same procedure can be used to derive equations for the measurements using a laminate with a different included angle θ, where $0<\theta<45°$.

4.3 Preliminary Experimental Measurements

As a preliminary evaluation of the practical aspects of this new approach, a single set of test coupons was prepared via autoclave cure. The method herein developed was used to find elastic constants of a unidirectional carbon fiber/epoxy prepreg material. Two

laminates, a 32 ply $[(+30/-30)_8]_S$, and a 32 layer unidirectional laminate, $[(0)_{32}]_T$, were produced for CTE measurements in a common autoclave cure cycle. The material used was T650-35/Cycom950-1, carbon/epoxy unidirectional prepreg tape. This prepreg was autoclave cured at a temperature of 121°C for 2 hours, at a pressure of 586 KPa, based on manufacturer cure cycle specifications.

CTE specimens were cut from the cured laminates using a diamond saw. The specimen dimensions were nominally 20x5x5 mm for the measurements of α_x and α_y, and 5x5x5 mm for the measurements of α_z. Because of the small thermal expansion expected in the fiber dominated directions the longest specimens allowed by the test equipment (20mm) were used for the measurements of α_x and α_y. The smaller dimensions of the specimens used to measure α_z were deemed acceptable because of the larger expansions expected in this through-thickness direction. Further, it did not seem prudent to produce a test laminate of 128 plies, or roughly 15mm thick, and expect the same levels of consolidation as seen in 32 ply laminates. After initial cutting, specimens were fixtured to grind and polish all faces, square and flat, using metallographic preparation techniques. Accurate dimensions of each specimen were then determined using a hand held micrometer, and these values were used for CTE determination.

The CTE's were measured using a Seiko 5200 TMA/SS 120C, Thermo Mechanical Analyzer with a quartz probe and stem (Figure 4.2), which has a manufacturer specified resolution of 0.02 μm. The measurements were performed over the temperature range of -60°C to +90°C, with a heating rate of 3.5°C/min and a constant applied load of 0.1 kgf. The CTE values, presented in this demonstration, were determined in the temperature range from 20°C to 30°C, to model room temperature performance. The developed

relationships can be used to determine elastic constants in other temperature ranges, assuming that the two measured elastic constants and the CTE's can be determined over the desired temperature range.

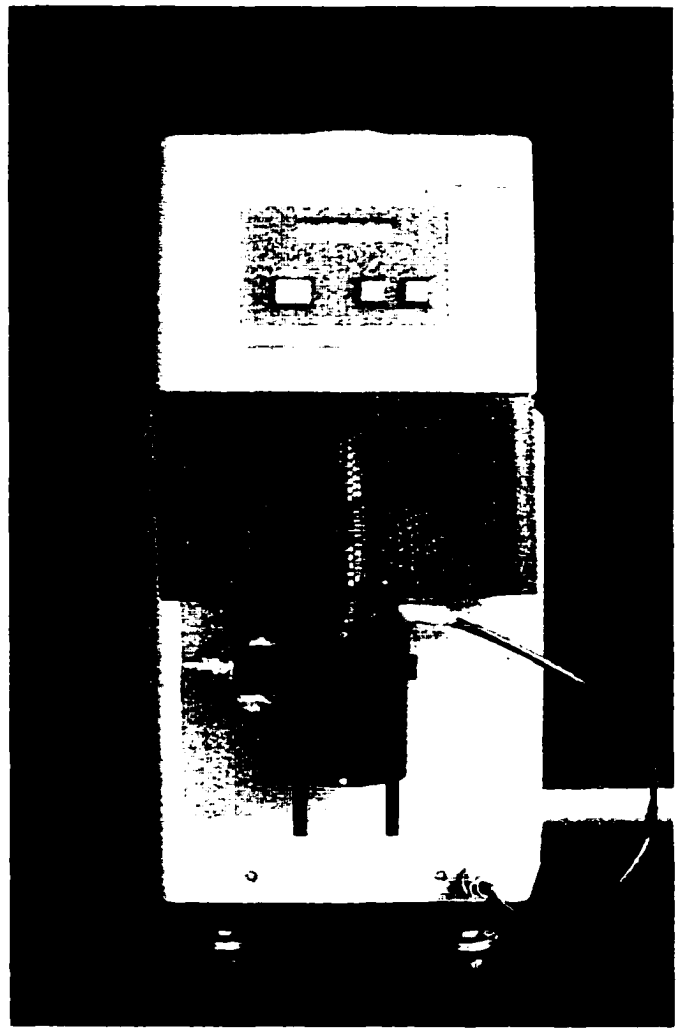

Figure 4.2 - Seiko 5200 TMA/SS 120C.

To check the consolidation quality of the cured laminate specimens and to substantiate that the cured specimens reflect the properties of a transversely isotropic material, two measurements of α_2 were performed on each unidirectional specimen. One measurement was performed in the lamination direction, $\alpha_2(0°)$, and the other in the

transverse direction, $\alpha_y(0°)$. These measurements are compared to check if the material presented $\alpha_2 = \alpha_3$, as required for a transversely isotropic material. It is noted that, while the check of $\alpha_2 = \alpha_3$ does not guarantee transverse isotropy in all cases, it is a viable test for most real unidirectional fiber reinforced materials.

4.4 Preliminary Results and Discussion

The results for the CTE measurements are presented in Table 4.1. The difference between α_y and α_z, for the unidirectional laminates, is less than 2%. This small difference was assumed to satisfy the condition of $\alpha_2 = \alpha_3$, as implied by transverse isotropy. Further, the ratio of $\alpha_z(30°)$ to $\alpha_z(0°)$ is consistent with that predicted for similar unidirectional fiber reinforced materials in previous publications [100,101].

Table 4.1 - Measured CTE data of T650-35/950-1 laminates.

θ (deg)	α_x (μm/m/°C)	α_y (μm/m/°C)	α_z (μm/m/°C)
0.0	-0.11	38.17	37.51
30.0	-5.19	22.33	47.56

Since these preliminary experiments were performed principally to demonstrate the application of the relationships developed, quoted values of the elastic constants, are used as the known values [102]. Substitution of these quoted values and the measured CTE's, into equations (4.16) - (4.21) yields the three unknown elastic constants. For comparison purposes, two approaches are used. One assumes E_1 and E_2 as the known elastic constants and the other uses E_1 and ν_{12}. The results presented in Table 4.2 show that the

engineering elastic constants determined, based on the relationships developed in Section 4.2, are in very good agreement with values indicated by the manufacturer [102]. Further, the results clearly show that the relationships are not limited to a specific pair of known elastic constants.

Table 4.2 - Elastic constants of T650/950-1 unidirectional lamina.

Elastic Constant	Quoted [102]	Computed * (from E_1 and E_2)	Computed * (from E_1 and ν_{12})
E_1 (GPa)	129.63	129.63**	129.63**
E_2 (GPa)	8.14	8.14**	8.12
G_{12}(GPa)	4.14	4.26	4.25
ν_{12}	0.33	0.33	0.33**
ν_{23}	N/A	0.49	0.49

* Results based on α_2 = 37.51 (μm/m/°C); ** Quoted data.

Obviously, since the technique requires the measurement of CTE's of the $[(+\theta/-\theta)_n]_s$ laminates, ply misorientation is a possible source of error. As a preliminary assessment of the sensitivity of the technique to ply misorientation, the CTE's for additional ply angles were estimated, based on the measured values at $[(+30/-30)_8]_s$. A nonlinear regression analysis was performed to calculate the least squares estimates for the parameters c_1, c_2, c_3, and c_4, in equations (4.8), (4.9), and (4.10), using the data from the CTE measurements (see Appendix 5).

The calculated parameters are presented in Table 4.3. Equation (4.9) was not used in the nonlinear regression analysis since it is a function of the same parameters as Equation (4.8) and the CTE data $\alpha_y(30°)$ may be entered in Equation (4.8) as $\alpha_x(60°)$. Four data points were applied for the linear regression using Equation (4.8): $\alpha_x(0°) = \alpha_1$, $\alpha_x(30°)$,

$\alpha_x(60°) = \alpha_y(30°)$, and $\alpha_x(90°) = \alpha_2$. Similarly, the data points used with Equation (4.10) are: $\alpha_z(0°) = \alpha_2$, $\alpha_z(30°)$, $\alpha_z(60°) = \alpha_z(30°)$, and $\alpha_z(90°) = \alpha_2$.

Table 4.3 shows that the nonlinear regression prediction for the parameter c_4, based on equation (4.8), matches the prediction of the same parameter based on equation (4.10). For c_1, the difference between the two predictions is only 1%. The parameters c_1, c_2, and c_4, determined from equation (4.8), are based on the laminate CTE data in x and y directions only, while the parameters c_1, c_3, and c_4, determined from equation (4.10), depend on the laminate CTE data in the z direction. Thus, the good agreement between the nonlinear regression predictions of c_1, and c_4, which appears in both equations, (4.8) and (4.10), shows that the CTE data collected in all three directions, x, y, and z, are very consistent.

Table 4.3 - Coefficients predicted by nonlinear regression.

Parameter	from Eq.(4.8)	from Eq.(4.10)
c_1	1.6178	1.6346
c_2	-1.3737	-
c_3	-	0.6874
c_4	1.1811	1.1811

After finding the parameters c_1, c_2, c_3, and c_4, equations (4.8), (4.9) and (4.10) are used to predict the CTE's in the x, y, and z directions for corresponding $[(+\theta/-\theta)_n]_s$ laminates. Figure 4.3 and Figure 4.4 show the angle dependence of α_x and α_z. The angle θ shown in these plots varies from 0° to 90°. This range of θ is intended to show the complete shape of the curves. However, due to the relation between α_x and α_y, and the symmetry of the α_z curve about $\theta = 45°$, the angle θ for the manufactured laminates

varies only from 0° to 45°. Thus, if α_x is required for a given laminate with θ larger than 45°, the measurement of α_y is performed in a laminate with $0<\theta<45°$, considering that $\alpha_x(\theta) = \alpha_y(90° - \theta)$. Therefore, the plot of α_y can be obtained as the mirror image of the plot of α_x, by reversing it about its vertical axis (Figure 4.5).

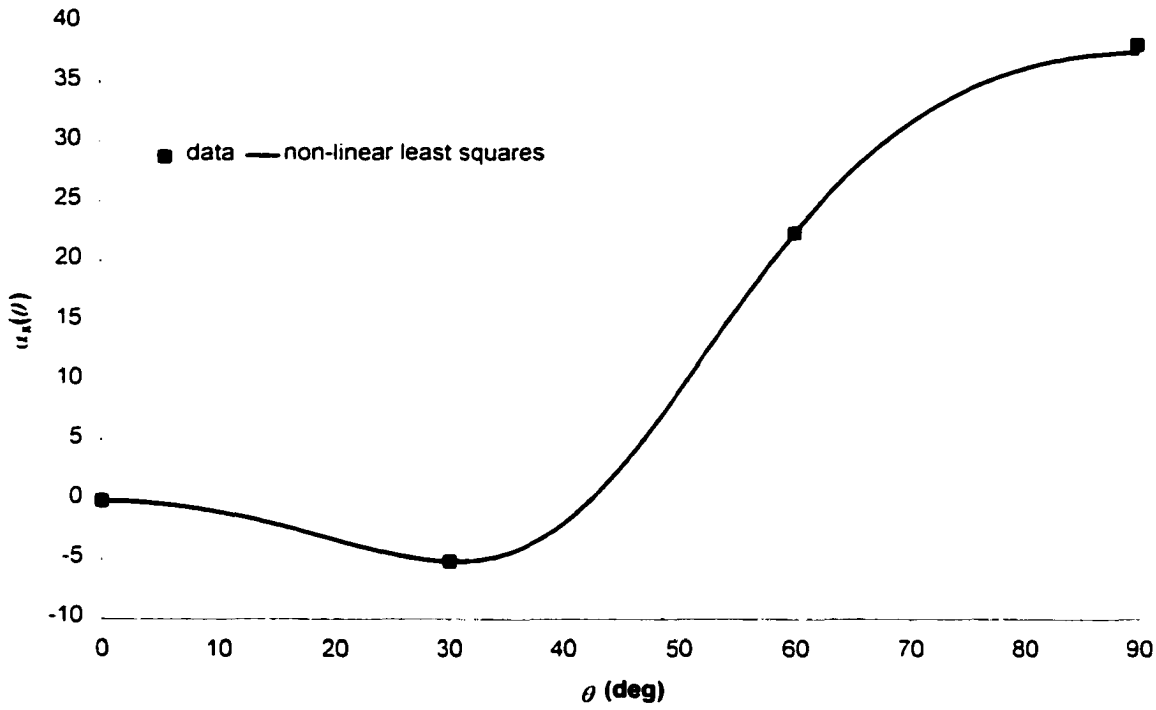

Figure 4.3 - α_x vs. θ for a $[(+\theta/-\theta)_n]_s$ T650/950-1 laminate.

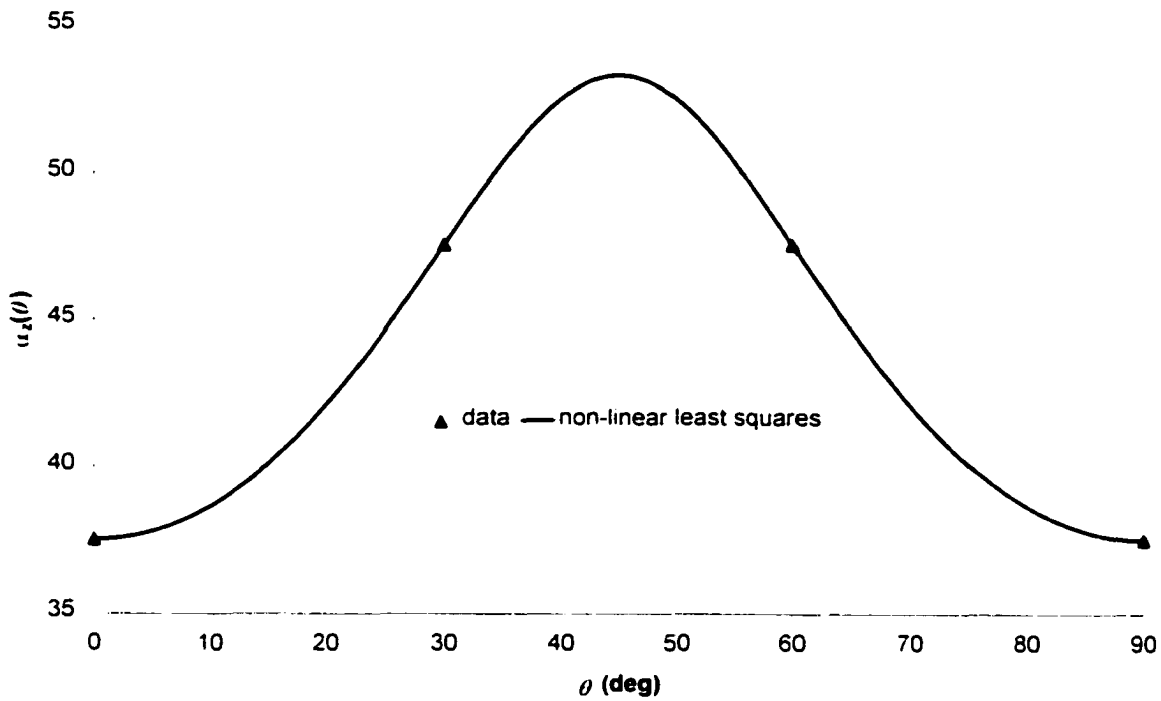

Figure 4.4 - α_z vs. θ for a $[(+\theta/-\theta)_n]$, T650/950-1 laminate.

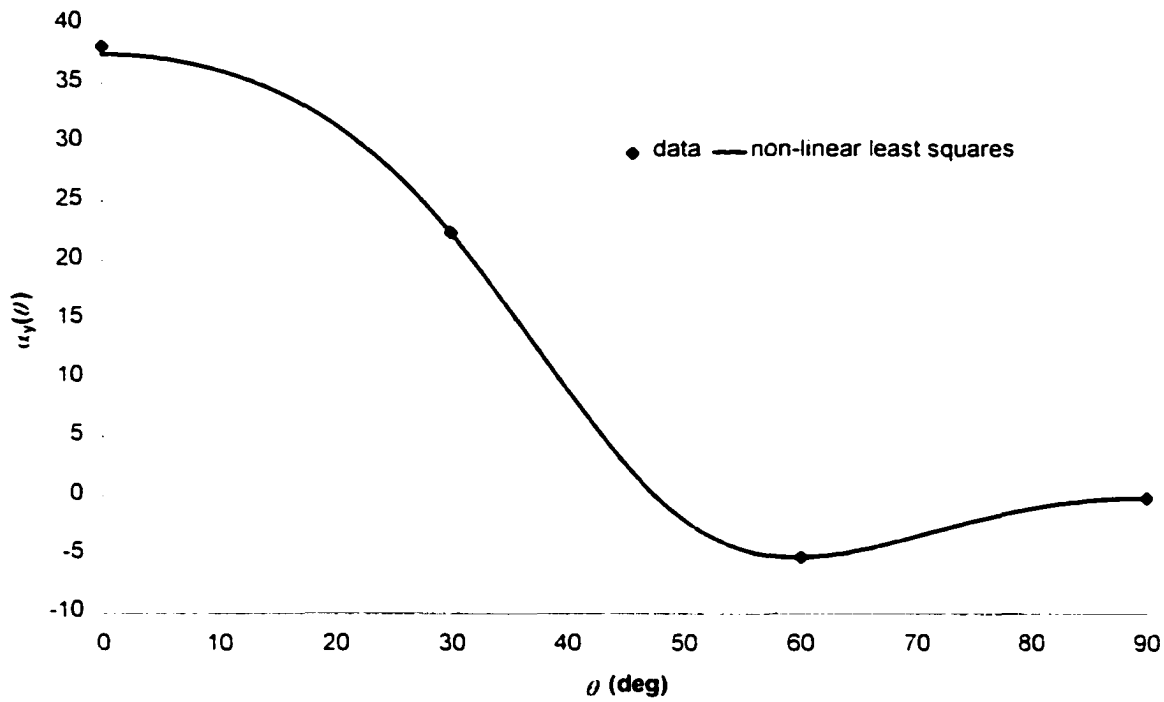

Figure 4.5 - α_y vs. θ for a $[(+\theta/-\theta)_n]_s$ T650/950-1 laminate.

The CTE's predicted by nonlinear regression for θ=30.5° and θ=31.0°, to demonstrate the differences in properties associated with ply misorientation, are presented in Table 4.4. The table also includes the measured CTE's for the $[(+30/-30)_8]_s$ laminate for comparison. It can be seen that the predicted and the measured values for the $[(+30/-30)_8]_s$ laminate are the same, indicating the quality of the regression analysis. The CTE's predicted for 30.5° and 31.0°, show the variations for 0.5° and 1.0° misorientation, respectively.

Table 4.4 - CTE data for T650/950-1 laminate predicted by nonlinear regression.

θ (deg)	α_x (μm/m/°C)	α_y (μm/m/°C)	α_z (μm/m/°C)
30.0*	-5.19	22.33	47.56
30.0	-5.19	22.33	47.56
30.5	-5.19	21.74	47.86
31.0	-5.18	21.14	48.15

* Measured values for reference from Table 4.1.

Using the CTE's for θ=30.5° and θ=31.0°, predicted by nonlinear regression (Table 4.4), the sensitivity of the calculated elastic constants to ply misorientation is assessed. The results presented in Table 4.5 indicate that the sensitivity to ply misorientation is highly dependent on the known elastic constants used, and thus, to the three unknowns to be computed. For the first case studied, when E_1 and E_2 were used as the known elastic constants, the 1.0° ply misorientation was enough to make ν_{12} unusable, and to cause variations of about 11% for G_{12} and 4% for ν_{23}. For the second case, using E_1 and ν_{12} as the known properties, the corresponding variations were about 20% for E_2 and 12% for G_{12}, while ν_{23} did not show any measurable variation. It is important to note that, in this sensitivity analysis, the ply misorientation was assumed equal in all the layers. In a real laminate, it is unlikely that all the layers will show an equal misorientation and random misorientation may ultimately result in little error. Moreover, if more than two elastic constants are known, they can be used as a redundant check of the calculated constants, thus reducing the error. Furthermore, the results for the through-thickness property, ν_{23}, which is perhaps the most difficult of the elastic constants to measure by conventional techniques, showed small sensitivity in each of the cases analyzed.

Table 4.5 - Sensitivity of the predicted elastic constants to ply misorientation.

θ (deg)	Computed (from E_1 and E_2)			Computed (from E_1 and ν_{12})		
	ν_{12}	G_{12}(GPa)	ν_{23}	E_2(GPa)	G_{12}(GPa)	ν_{23}
30.0	0.33	4.26	0.49	8.12	4.25	0.49
30.5	0.18	4.48	0.48	7.29	3.99	0.49
31.0	0.05	4.72	0.47	6.52	3.73	0.49

Note: Based on data for T650/950-1.

Relatively large specimen thicknesses (5 mm) were necessary to allow the measurement of α_x and α_y. With the TMA equipment fixture used, specimens of lesser thickness adversely affected the measurements, as the specimens would not stand without rocking, and thus showed decreased measurement repeatability. The 32 ply thickness, ultimately used for the experiments, permitted placing the probe, used to measure the change in specimen length, at the center the cross-section, away from the edges. The result was a consistent and reproducible measurement of each of the CTE's.

The CTE's measured represent a global property of the laminated specimen. The possible influence of free edge effects due to the low aspect ratio of the specimen were considered to be of higher order, and therefore, neglected. Other effects such as careful specimen preparation are expected to have a larger influence on the results.

4.5 Summary

A technique, which allows the determination of three of the five independent elastic constants of a transversely isotropic fiber reinforced lamina, has been developed. The approach uses laminate CTE measurements and two known elastic constants to predict lamina mechanical properties. The method requires CTE measurements of a

unidirectional and a $[(+\theta/-\theta)_n]_s$ laminate, assuming that at least two independent elastic constants are known. The measurement of CTE is found to be sensitive to specimen preparation requiring specimen surfaces to be polished flat, and edges trued to square to ensure reproducible results. Careful control of ply orientation is also of great importance.

The use of the mathematical relationships developed and the associated experiments performed, result in predicted elastic constants of a transversely isotropic lamina that closely match quoted values. This approach promises the ability to readily determine relationships between the elastic properties and temperature, and, potentially, to study the effects of manufacturing on elastic properties. Ultimately, this can enable improved prediction of structural performance over a range of temperatures, which could be important in designs for many applications. Further, the approach presented can be used in conjunction with more traditional elastic characterization, allowing checking of the elastic constants that are often difficult to determine using standard mechanical tests. Thus, the relationships developed present an alternative approach to the determination of the transversely isotropic lamina elastic constants, based on thermal and mechanical measurements of composite laminates.

5

Elastic Characterization of PEEK/IM7 Unidirectional Lamina

In the previous chapter, an approach for the determination of the elastic constants has been developed, for a $[(+\theta/-\theta)_n]_s$ laminate, where $0<\theta<45°$, that relates the elastic constants of a lamina and the coefficients of thermal expansion of the laminate. The method allows the computation of any three of the five independent elastic parameters that characterize a transversely isotropic material, assuming that the other two are known, or can be measured. In this chapter, the technique is applied to the determination of the elastic properties of a PEEK/IM7 unidirectional prepreg lamina.

The approach for the determination of the elastic constants allows any angle θ, where $0<\theta<45°$, to be used for the manufacture of the laminate. However, it was suggested, in the previous chapter, that a $\theta=30°$ results in easier manufacture of the laminate and also simplifies the final mathematical expressions. Moreover, although any three of the five elastic constants may be determined, if the other two are known, the sensitivity of the method to ply misorientation was shown to be highly dependent on the known elastic constants used. It was also shown that using E_1 and ν_{12} as the known properties reduces

the sensitivity to ply misorientation. Thus, for this investigation of PEEK/IM7 unidirectional prepreg, a $[(+30/-30)_8]_s$ laminate was selected for the CTE measurements, and, E_1 and ν_{12} are used as the known properties to be determined from standard mechanical tests.

First, the elastic characterization of PEEK/IM7 is performed at room temperature. The results are compared with quoted values measured by standard techniques for validation. Then, the feasibility of the use of this method to compute elastic properties over a range of temperatures is assessed.

5.1 Material

PEEK (Polyetheretherketone) is a semi-crystalline thermoplastic polymer with a superior combination of properties including high heat stability, wear resistance, low coefficient of friction, high strength, high stiffness, high impact resistance, and excellent chemical resistance (Appendix 6) [103,104]. It can be processed by many different methods, including: injection molding, extrusion, compression molding, powder coating, composite manufacturing, wire coating, compounding, foaming and solution membrane casting. When PEEK is combined with high performance carbon fibers, such as IM7 fibers, the resultant composite material exhibits properties, which meet the design requirements of many aerospace structural applications. A recent application example of PEEK/IM7 is in the Space Station Remote Manipulator System (SSRMS), known as the Canadarm2 (see Figure 1.9). The arm consists of PEEK/IM7 composite booms and was designed for construction, maintenance and repair of the Space Station [28].

The material investigated in this study was APC-2/IM7, unidirectional prepreg tape, manufactured by Cytec Fiberite Inc., with a quoted resin content of 32% and fiber areal weight of 145g/m^2. The prepreg was supplied with an average ply thickness of 0.132 mm (5.2×10^{-3} in). APC-2 (PEEK) is a semi-crystalline polymer with a quoted glass transition temperature of 142.7°C and a melting temperature of 340°C [103,104]. The elastic modulus of PEEK is about 3.6 GPa [104], while the longitudinal elastic modulus for the IM7 carbon fibers is 275.8 GPa (40 Msi) [20]. The material was chosen for this work as quoted properties data were available and because of the relatively straightforward manufacturing requirements. Further, it was expected that as a thermoplastic, mechanical property changes with temperature would be more apparent.

5.2 Tensile Test Specimen Fabrication

For the measurement of both E_1 and ν_{12}, tensile test specimens with fibers oriented at 0° with respect to the specimen length are sufficient. However, in this work, specimens for the determination of E_2 were also fabricated and tested. Although only two elastic constants need to be known, E_2 was used as a redundant check of the constants calculated using the laminate CTE-based approach.

Two unidirectional laminates were processed in a Honacomp hot press (Figure 5.1) using an aluminum tool (Figure 5.2). Both laminates were 150x200 mm and the fibers were oriented at 0° and at 90°, with respect to the largest tool dimension. The 0° laminate was used to fabricate specimens for the determination of E_1 and ν_{12}, and the 90°

laminate, for E_2. Eight prepreg layers were used for the 0° laminate and sixteen layers for the 90° laminate.

Figure 5.1 - Honacomp hot-press with computer control.

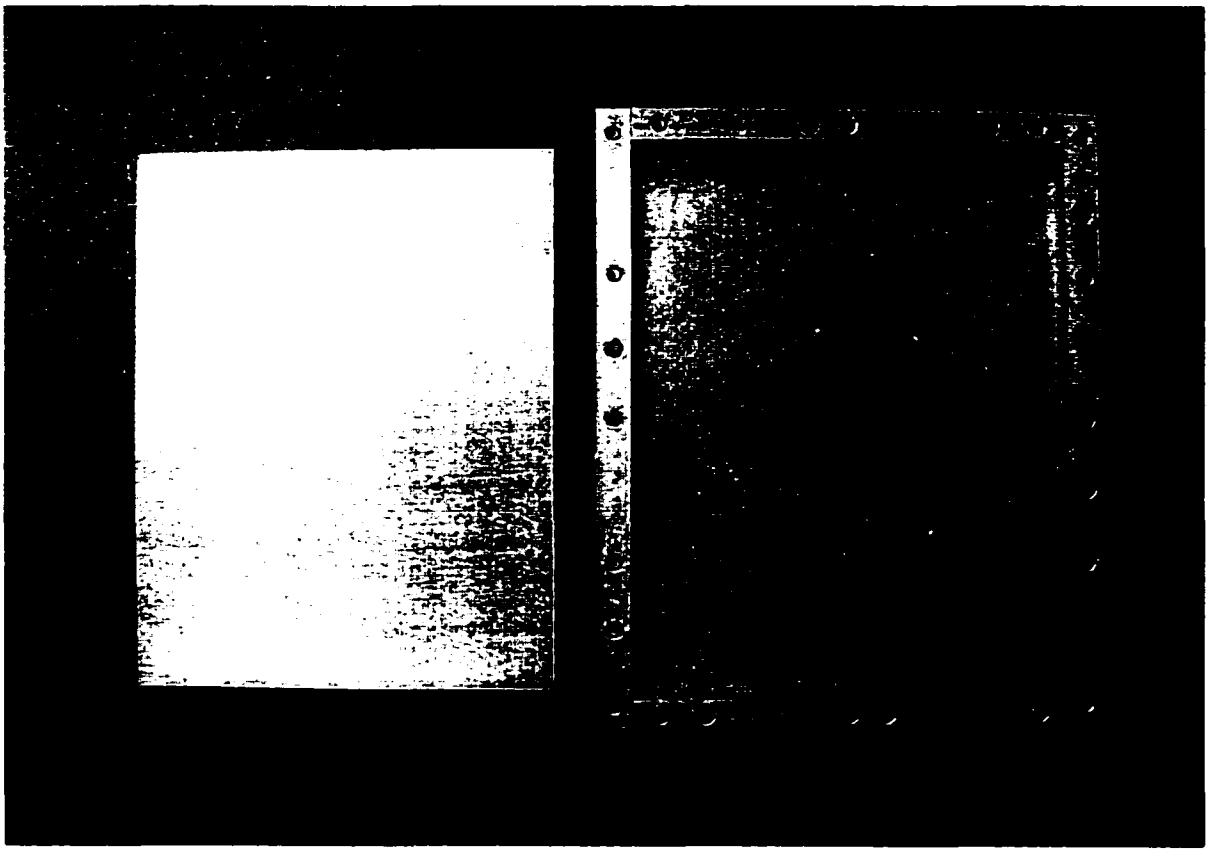

Figure 5.2 - Aluminum tool for processing laminates.

Two coats of the release agent Release All #50, from Airtech International, Inc., were applied to the aluminum tool to avoid part/tool sticking and to ensure proper release. An interval of 10 minutes was observed between the two coat applications and then the tool was baked at 125°C for 30 minutes, following the manufacturer recommendations. This mold release has a maximum use temperature of 477°C.

The laminates were processed at a temperature of 395°C for 45 minutes, under an applied pressure of 690 KPa (100 psi). First, the lay-ups were heated at a rate of 5°C/min and the pressure was gradually applied after the temperature reached 340°C. After the consolidation was complete, the laminates were cooled, under pressure, to room temperature, at a rate of 3 to 5°C/min.

The specimens were cut from the processed laminates using a diamond abrasive saw. Unidirectional laminated specimens were cut from the $[(0)_8]_T$ plate with fibers oriented at 0°, with respect to the specimen's length, for measuring E_1 and ν_{12}. From the $[(90)_{16}]_T$ laminated plate, specimens were cut for the measurement of E_2. Laminate orientation was carefully controlled during the cutting process. After the cutting procedure, the specimen edges were sanded flat for improved dimensional precision. Finally, the specimens were conditioned to reduce the effects of residual stresses and remove any moisture induced during specimen preparation. The conditioning procedure consisted of heating the specimens in an oven from room temperature to 70°C, holding for 2 hours, then heating from 70°C to 90°C followed by a hold for 2 hours, and finally, heating from 90°C to 110°C with a final hold for 2 hours. Upon cool-down, accurate dimensions of each specimen were measured using a hand-held micrometer. The final dimensions were nominally 15x200x1 mm, for the 0°, and 25x175x2 mm, for the 90° specimens (Figure 5.3). End tabs were not used since the specimens were not intended to be tested to failure [8].

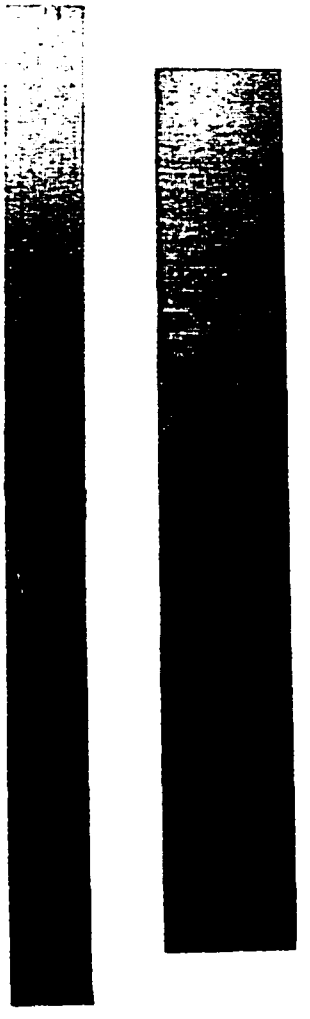

Figure 5.3 - Tensile test specimens.

5.3 CTE Specimen Fabrication

Two 64x178 mm laminates, a 32 ply $[(+30/-30)_8]_s$, and a 32 ply unidirectional, $[(0)_{32}]_T$, were produced in a hot-press using aluminum tooling. The processing conditions are the same as those described in the previous section for the tensile test specimens. Careful control of ply orientation was again practiced. Upon processing

completion, the CTE specimens were cut from the laminates using a diamond saw. The specimen dimensions were nominally 5x5x5 mm (Figure 5.4).

In the preliminary investigation presented in the previous chapter, longer specimens were used for the measurements of α_x and α_y, which are in the fiber dominated directions, because of the small thermal expansion expected in these directions. However, in this investigation, it was decided that the specimens should have the same nominal dimensions in all three directions. The dimensions selected allow the same specimen to be used for CTE measurements in all three directions, which was not possible with the specimens previously used. Also, the shorter specimens are more stable in the measuring fixture, preventing it from tilting during the measurements. Further, with the same dimensions in all directions, any possible influence of initial dimensions in the measured properties will produce the same effect in all directions.

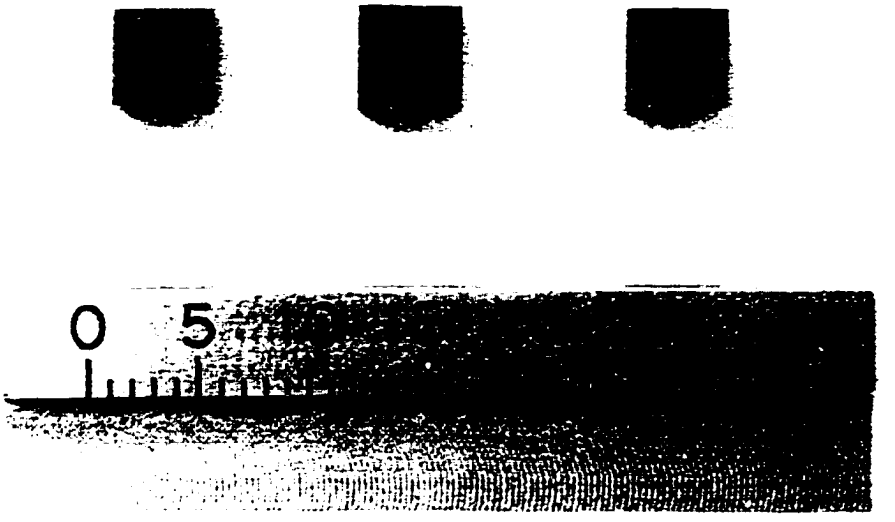

Figure 5.4 - CTE test specimens.

The study presented in the previous chapter indicated that the measurement of CTE is very sensitive to specimen preparation and ultimately to the flatness of the surfaces. Thus, after cutting, specimens were fixtured to grind and polish all faces, square and flat, using metallographic preparation techniques. An aluminum grinding/polishing fixture was designed and fabricated to allow the specimen preparation on a polishing wheel without rocking, thus assuring the perpendicularity and flatness of the specimens faces (Figure 5.5). These specimens were also submitted to the same conditioning procedure described for the tensile test specimens. Accurate dimensions of each specimen were determined using a hand held micrometer.

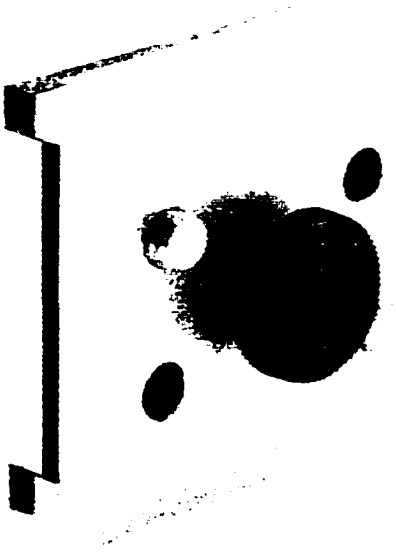

Figure 5.5 - Polishing fixture for CTE test specimens.

5.4 Verification of Resin Content of the Manufactured Specimens

A sample was taken from the laminate processed for the CTE specimens in order to verify the resin content quoted by the manufacturer. The sample was cut using a diamond saw and the edges were sanded square and flat. The specimen was then submitted to the same conditioning procedure, already described for specimen fabrication, to remove moisture. A hand held micrometer was used for the measurement of the sample dimensions, which resulted in a volume of $V=5.227cm^3$. The specimen

was weighted in a laboratory scale with 0.0001g of resolution, and the measured total mass was 8.2888g. Thus, the resulting specimen's density is 1.586g/cm^3.

The rule of mixtures is used to determine the matrix and fiber volume fractions. Hence,

$$\rho_c = \rho_m v_m + \rho_f v_f \tag{5.1}$$

where:

ρ_c = density of composite = 1.586g/cm^3

ρ_m = matrix density = 1.29g/cm^3 (see Appendix 5)

v_m = matrix volume fraction

ρ_f = fiber density = 1.78g/cm^3 [105]

v_f = fiber volume fraction = (1- v_m)

Solving the rule of mixtures equation for v_m,

$$v_m = 39.6\% \tag{5.2}$$

and, therefore,

$$v_f = 60.4\% \tag{5.3}$$

The matrix and fiber contents based on mass are

$$m_m(\%) = \frac{\rho_m v_m}{\rho_c} = 32.2\% \tag{5.4}$$

$$m_f(\%) = \frac{\rho_f v_f}{\rho_c} = 67.8\% \tag{5.5}$$

Therefore, the measured resin content by mass of 32.2% is very similar to the quoted data of 32%.

5.5 Room Temperature Elastic Characterization of PEEK/IM7

This section focuses on the elastic characterization of PEEK/IM7 at room temperature. The temperature of 20°C was defined to represent room temperature.

5.5.1 Tensile Measurements

Tensile tests were carried out in an ATS Series 910 universal testing machine (Figure 5.6), which has a load capacity of 44.5 kN (10,000 lbs). An environmental chamber was used for temperature control. All measurements were conducted at 20°C, representing room temperature. A constant cross-head displacement rate of 1.0 mm/min was used in all tests. For the 0° specimens, a maximum applied tensile load of 4.45 KN (1000 lbs) was used while the 90° specimens were loaded to 890 N (200 lbs).

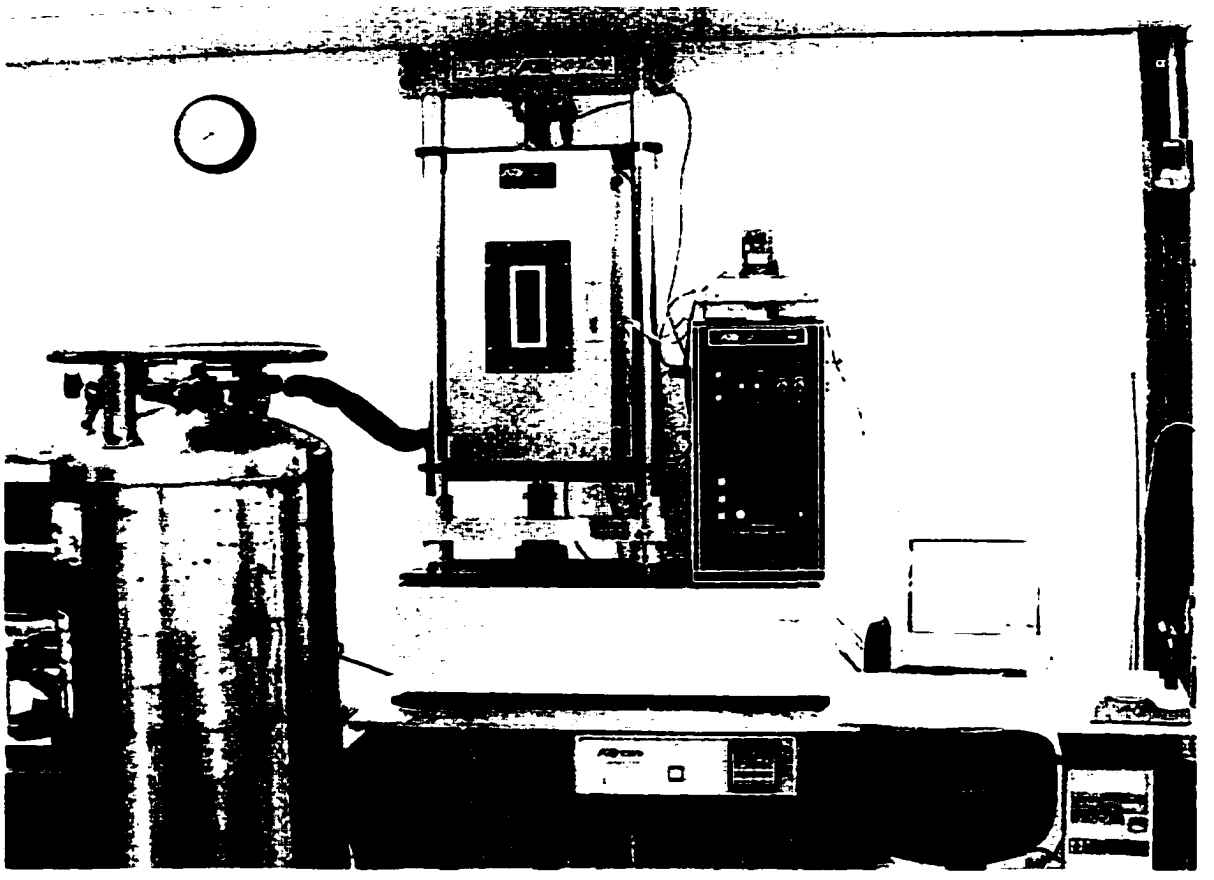

Figure 5.6 – ATS universal testing machine with temperature chamber in-place.

Strain gage rosettes were used for the strain measurements, one on each face of each specimen. 45-degree rosettes (EA-13-125RA-120) from Measurements Group, Inc., were installed with M-Bond 200 adhesive, following the manufacturer instructions. The rosettes allowed the determination of modulus and Poisson's ratio. Each rosette was connected to three CALEX Model 161 Bridgesensor Strain Gage Signal Conditioners, set to a bridge excitation voltage of 4.0 V and a gain of 500. The conditioned signal was then sent to a PC-based data acquisition system.

Direct application of strain transformation relations (see Appendix 7) allowed calculation of the principal strains at each surface of the specimen, from the rosette measurements. Then, each principal stress was averaged between the two faces of the

specimen to reduce possible bending effects from any minor grip misalignment. The modulus was determined from the slope of the stress-strain curve for a maximum strain of 0.12%. The Poisson's ratio, ν_{12}, was determined from the 0° specimen tests, using the relation between the principal strains, ($\nu_{12} = -\Delta\varepsilon_{min}/\Delta\varepsilon_{max}$).

5.5.2 CTE Measurements

The tests for the determination of the coefficients of thermal expansion (CTE's) were carried out using a Thermo Mechanical Analyzer with a quartz probe and stem (Seiko 5200 TMA/SS 120C), which has been described in the previous chapter. Average CTE's were determined using the software provided with the Seiko 5200 TMA station, over the temperature range of 10°C to 30°C, to measure room temperature performance. All CTE measurements were performed using a heating rate of 1.0°C/min and a constant applied load of 20 g.

Comparing to the preliminary measurements described in the previous chapter, the heating rate and the constant applied load were both reduced. The reduction in heating rate was intended to ensure better temperature uniformity throughout the specimen. Further, the applied compressive load, necessary to maintain the measuring probe in contact with the specimen, was reduced to 20 g without affecting the experimental precision.

To verify if the material presents $\alpha_2 = \alpha_3$, as required for a transversely isotropic material, two measurements of α_2 were performed on each unidirectional specimen: one in the lamination direction, $\alpha_z(0°)$, and the other in the transverse direction, $\alpha_y(0°)$.

5.5.3 Results and Discussion

The results of the mechanical tests are presented in Table 5.1. The data was averaged from four different samples for each of the moduli measured. Also, for each sample, two measurements were performed to check for repeatability, and the quoted individual specimen results are the average. The properties found are in good agreement with micromechanics predictions, although slightly higher than measured properties for the same material, presented in the literature [20]. However, processing conditions may account for the slight differences as the consolidation time for the laminates processed in this work was 45 minutes, while in the previous research it was only 10 minutes.

Table 5.1 - Measured elastic constants of PEEK/IM7.

Elastic constant	$\bar{x}$	s_{n-1}
E_1 (GPa)	164.4	3.0
E_2 (GPa)	9.9	0.2
ν_{12}	0.34	0.01

$\bar{x}$ = sample mean (average); s_{n-1} = sample standard deviation.

The results for the CTE measurements are presented in Table 5.2. As for the mechanical tests, each CTE presented is an average of the results based on four specimens. The measured α_1 and α_2 closely correspond to previously published data for this APC-2/IM7 material [20]. Also, the difference between α_2 and α_3, is only about 1%. This small difference is considered to satisfy the condition of $\alpha_2 = \alpha_3$, as implied by transverse isotropy. For the computation of the elastic constants, the average of α_2 and α_3 is used to represent α_2.

Table 5.2 - TMA measured CTE data of PEEK/IM7 laminates.

θ (deg)	α_x (μm/m/°C)		α_y (μm/m/°C)		α_z (μm/m/°C)	
	$\bar{x}$	s_{n-1}	$\bar{x}$	s_{n-1}	$\bar{x}$	s_{n-1}
0.0	-0.15	0.69	26.51	0.59	26.80	0.53
30.0	-2.82	0.61	13.46	0.43	34.82	0.47

$\bar{x}$ = sample mean (average); s_{n-1} = sample standard deviation.

Substitution of the measured elastic constants, E_1 and ν_{12}, and the average values of the CTE's, α_1, α_2, $\alpha_x(30)$, $\alpha_y(30)$ and $\alpha_z(30)$, into equations (4.19), (4.20), and (4.21), yields the three unknown elastic constants, E_2, G_{12} and ν_{23}. The results are presented in Table 5.3. The result of E_2 measured during tensile testing is also shown for comparison. A very good agreement between the predicted E_2 and the measured value is observed. The difference between the two values is approximately 3%.

Table 5.3 - Elastic Constants of PEEK/IM7 unidirectional lamina.

Elastic Constant	Measured	Computed (using E_1 & ν_{12})	Published [20]
E_1 (GPa)	164.4	-	153
E_2 (GPa)	9.9	10.2	9.1
G_{12}(GPa)	-	7.0	4.9
ν_{12}	0.34	-	0.33
ν_{23}	-	0.50	N/A

Comparing the mechanical properties obtained in this work with previously published data for the APC-2/IM7 material, the measured E_1 and E_2 are about 10% higher than in the former investigation [20]. For G_{12} the calculated value was significantly (about 40%) higher than the previously measured value. Therefore, even if a 10% increase is considered, as in E_1 and E_2, the computed G_{12} is still about 30% higher than that stated in

the previous research. The high prediction of G_{12} by the present approach may be related to precision in the CTE measurements, or possibly to differences in the boundary conditions imposed by the two different test approaches. No comparison was possible for ν_{23} since this value was not available in the literature, perhaps due to the difficulties involved in performing this test.

The CTE measurements presented in Table 5.2 indicate a relatively large standard deviation for α_1 and $\alpha_x(30)$, where the thermally induced displacements are very small. Improved precision of CTE results, especially in these two cases, where the absolute displacements are extremely small, could likely be attained using a dilatometer with longer specimens, rather than a TMA, which is limited to relatively short specimens. However, while longer samples could be an advantage for the in-plane measurements, for the through-thickness CTE's, if the laminate thickness is increased to generate a longer specimen, the resulting as-manufactured properties may not be a good representation of more typical laminate of lesser thickness. Thus, a thick specimen may result in improved reliability of the CTE measurement, but the measured value may ultimately be less representative of the actual lamina value than the values measured in the TMA.

The applied load of 20g, used during the measurements of thermal strains, was assumed to not affect the results. The heating rate is another important parameter for the thermal expansion measurements. A lower heating rate for the measurement of the thermal expansion may potentially increase the accuracy. However, a lower heating rate also implies longer duration tests, which can be difficult to justify.

5.6 Elastic Properties of PEEK/IM7 Related to Temperature

The present section focuses on the evaluation of the feasibility of the previously developed technique to determine the 3-D elastic constants of transversely isotropic, fiber reinforced materials, making use of CTE measurements in laminates, over a range of temperatures. It is expected that the matrix dominated elastic constants will be most affected by temperature. PEEK/IM7 exhibits properties that meet the design requirements of many aerospace structural applications. Therefore, the determination of the elastic properties of this material over a range of temperatures is of great interest.

Equations (4.19), (4.20), and (4.21), allow the determination of three elastic constants over a range of temperatures since CTE tests are conventionally carried out using a temperature sweep over a specified temperature range. Additionally, continuous CTE vs. temperature data may be produced, instead of discrete data points, which results in continuous temperature relationship for the calculated elastic constants. In contrast, standardized mechanical tests, for the determination of elastic properties, are normally carried out at a constant temperature. Thus, multiple tests are required if material elastic constants are to be determined over a range of temperatures.

5.6.1 Verification of Glass Transition Temperature of the Polymeric Matrix

The application of the proposed method for the determination of the elastic constants of polymeric matrix fiber reinforced laminae, relies on precise laminate CTE measurements. Careful specimen preparation allowed consistent and reproducible measurement of each of the CTE's. The CTE's measured represent a global property of

the laminated specimen, where the layers are assumed to be perfectly bonded. Therefore, caution must be taken if the described method is applied over a temperature range, which approaches the glass transition (T_g) region. A drop in modulus, which occurs in the T_g region, may affect the interfaces between adjoining layers and also between fiber and matrix, and therefore, the assumption of perfect bonding made may not hold anymore.

To verify the glass transition temperature of the polymeric matrix quoted by the manufacturer, a DSC analysis was conducted on a sample taken from the laminates processed for the CTE testing specimens. The measurements were performed using a Seiko 5200 DSC 220C, Differential Scanning Calorimetry analysis module, at a heating rate of 3.0°C/min. An 8.4mg resin sample, taken directly from the processed laminate, was used and the measurements were carried out in air. The DSC collected data are shown in Figure 5.7. The T_g determined by the DSC module was 148.3°C, thus very close to the quoted T_g of 142.7°C. Hence, based on this information, it was decided that the measurements could be carried out in a temperature range with an upper limit of 120.0°C without degrading the composite.

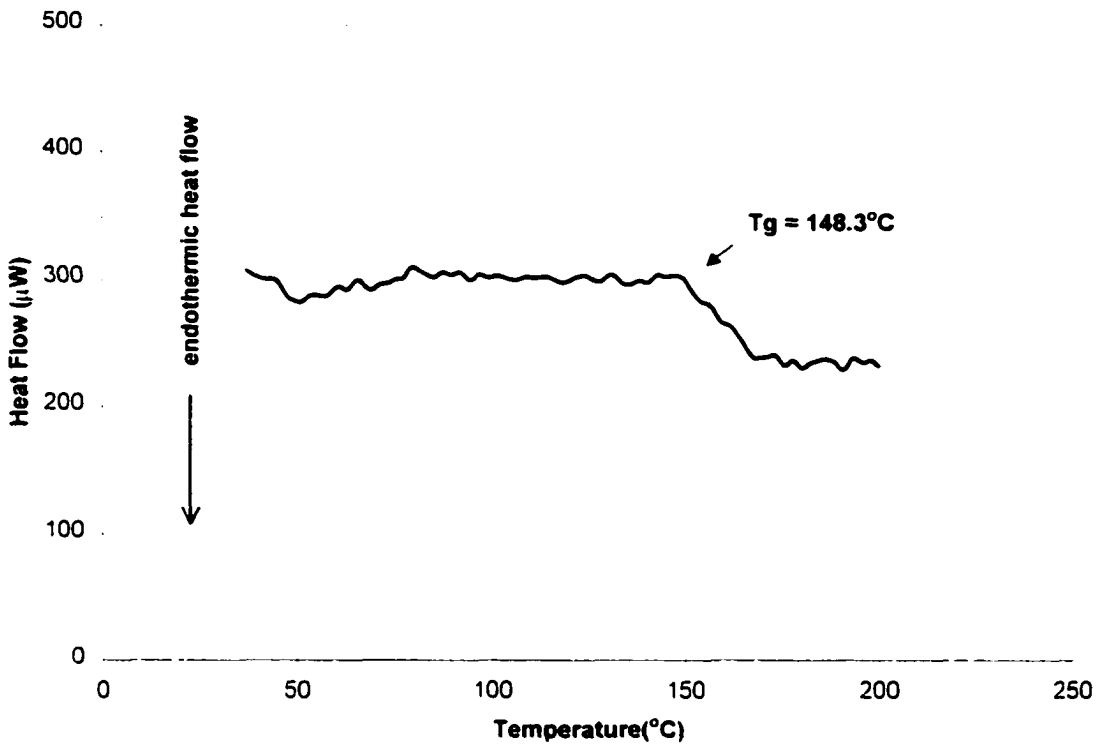

Figure 5.7 - DSC trace of APC-2.

5.6.2 Tensile Measurements

The testing equipment, cross-head displacement rate, and maximum applied load are the same as in the case of room temperature testing. The tests were conducted over the temperature range from -20°C to 120°C, with data being collected at 20°C intervals. After reaching each specified temperature, a 30 minute isothermal hold was observed, before conducting the test, to ensure uniform temperature throughout the specimen. Liquid nitrogen was used as the coolant for the sub-ambient temperature tests. Variations of the gage factor with temperature were considered in the strain calculations, according to data curve provided by the strain gage manufacturer.

5.6.3 Laminate CTE Measurements

The equipment, heating rate and applied load are the same as described in the room temperature measurements. The measurements were conducted over the temperature range of -40°C to 125°C. Strain vs. temperature data was collected by the TMA and transferred to a spreadsheet for analysis. A parabolic fit was applied to smooth the raw data, over the range of -20°C to 120°C. This type of fit was found to closely match the trends of the raw data. The smoothing procedure with a polynomial fit avoids errors induced, by electronic noise in the TMA data collection, in the raw data and also facilitates the study of the continuous change in thermal expansion with temperature.

The thermal strain is related to the coefficient of thermal expansion as,

$$\varepsilon(T) = \alpha(T) \cdot \Delta T \tag{5.6}$$

where:

$\varepsilon(T)$ is the thermal strain as a function of temperature,
$\alpha(T)$ is the coefficient of thermal expansion as a function of temperature,
ΔT is the temperature change.

The coefficient of thermal expansion changes continuously with temperature and can only be assumed constant for a particular and very small temperature range. Thus, based on equation (5.6), the "CTE vs. temperature" behavior was obtained from the first derivative of the equation determined from the "strain vs. temperature" polynomial fit, with respect to temperature (equation (5.7)).

$$\alpha(T) = \frac{d}{dT}\varepsilon(T) \tag{5.7}$$

Application of equation (5.7) results in a linear relationship between CTE and temperature, since a parabolic fit was applied to "strain vs. temperature" data.

5.6.4 Results and Discussion - Temperature Effects

The results of the mechanical tests for the determination of E_1, and ν_{12}, are presented in Figure 5.8. The data used for the computation of the elastic constants are based on the average of the four different samples for each of the measured properties. The data in Figure 5.8 shows that the longitudinal elastic modulus, E_1, does not show any measurable change with temperature, yielding an overall constant average value of 164.8 GPa. This behavior was expected, considering that E_1 is mainly controlled by the fiber properties, which are insensitive to temperature changes within the temperature range studied (-20°C to 120°C). However, the in-plane Poisson's ratio, ν_{12}, did show a small increase with temperature. A linear regression fit applied to the raw data, results in a Poisson's ratio ν_{12} of about 0.34 at -20°C, increasing with temperature, to approximately 0.35 at 120°C.

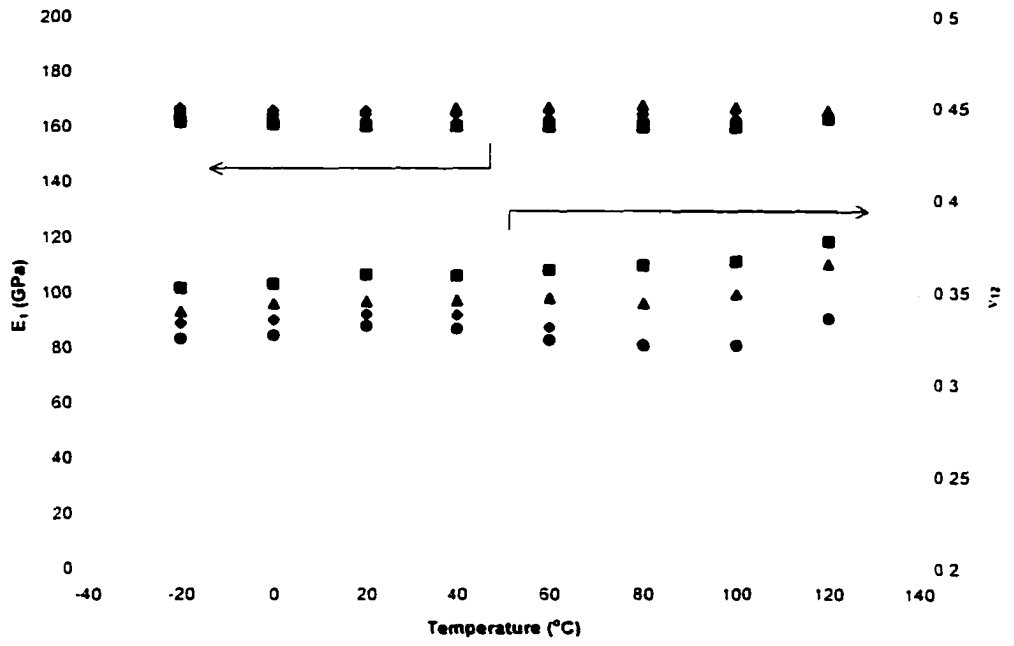

Figure 5.8 - Tensile tests data (longitudinal modulus and Poisson's ratio ν_{12}).

Figure 5.9 shows the "strain vs. temperature" behavior measured in all three directions for unidirectional (U-D) and (±30) laminate specimens. This is the raw data corresponding to the TMA measured thermal expansions. As with the mechanical tests, four different specimens were used to measure each property. However, due to the transverse isotropy, for the unidirectional (U-D) specimens, directions 2 (transverse) and 3 (lamination) produce the same thermal expansion and the curves labeled as $(U\text{-}D)_{2\&3}$, represent eight measurements. The "CTE vs. temperature" plot for each of the measurements is obtained from the first derivative of the parabolic fitting on the "strain vs. temperature" raw data. Thus, after the determination of the "CTE vs. temperature" behavior for each of the four samples, the average and standard deviation of the CTE's at any temperature is calculated for each property.

A plot of the average CTE values with the associated standard deviations, corresponding to four samples, is presented in Figure 5.10. A small percentage standard deviation for α_2 is observed, over the entire temperature range (about 2.5%). The variations between α_2 and α_3, for the same specimen, were typically smaller than the variations in α_2 or α_3 between different specimens. This satisfies the condition of $\alpha_2 = \alpha_3$, over the entire temperature range, as implied by transverse isotropy. Therefore, the average and standard deviation of α_2 presented in Figure 5.10, represent data from eight measurements: four of α_2 and four of α_3.

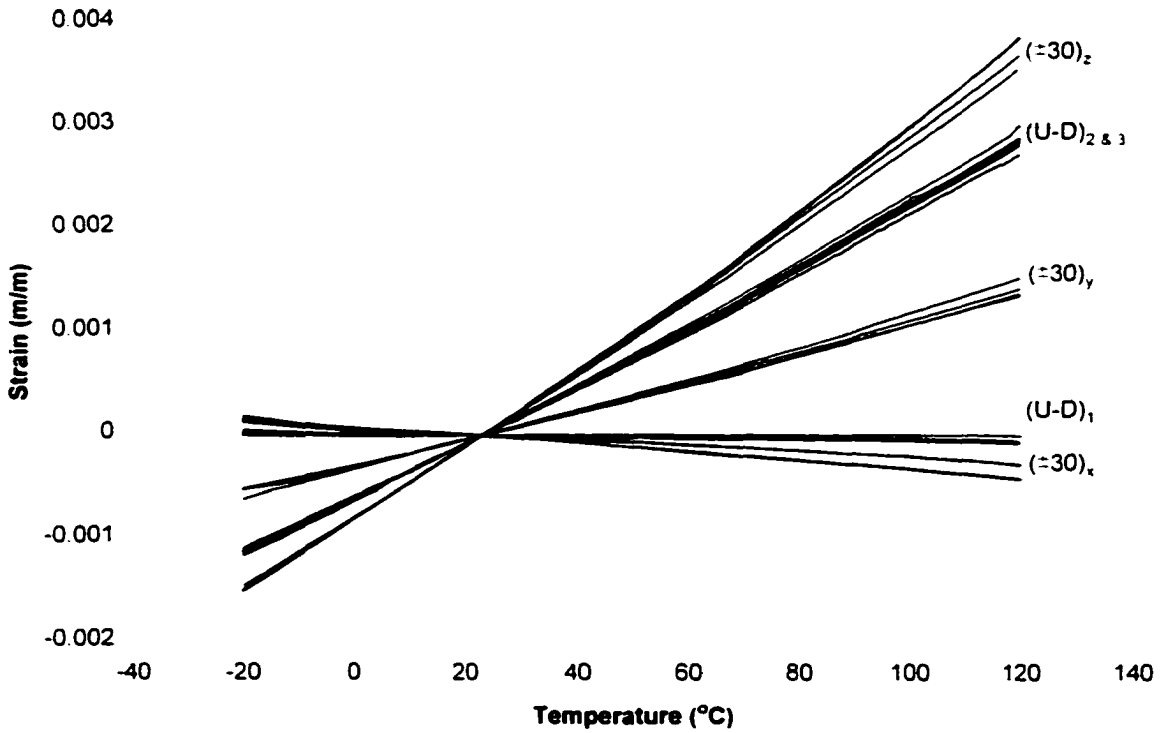

Figure 5.9 - TMA measured Strain x Temperature.

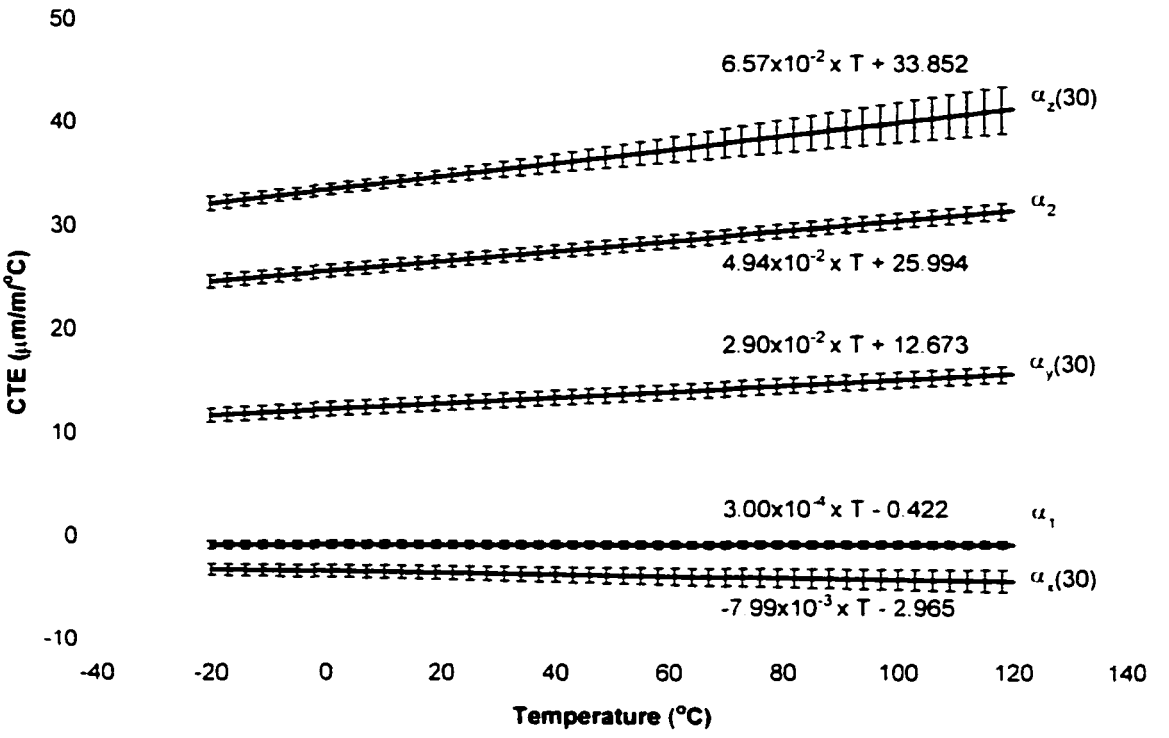

Figure 5.10 - CTEs from TMA measurements.

Small percentage standard deviations are also observed in $\alpha_y(30)$ and $\alpha_z(30)$. For the case of the $\alpha_z(30)$, although the standard deviation obtained increases with temperature reaching a maximum of 5.5% at 120°C, it is less than 5% for the majority of the temperature range. The measurements of the CTE's α_1 and $\alpha_x(30)$, result in standard deviations that are as small or smaller than any of the other orientations. However, for each of these two cases, the absolute thermally induced displacements are very small, which increases the percent error.

Substitution of the average of the measured elastic modulus, E_1, the linear regression fit for the Poisson's ratio, ν_{12}, and the average values of the CTE's, α_1, α_2, $\alpha_x(30)$, $\alpha_y(30)$ and $\alpha_z(30)$, into equations (4.19), (4.20), and (4.21), yields the three unknown elastic

constants. E_2, G_{12} and ν_{23}, over the temperature range of -20°C to 120°C. A constant, average value of 164.8 GPa was used for E_1, while for ν_{12}, the linear fit results in a ν_{12} of 0.34 at -20°C and 0.35 at 120°C. The results for the calculated elastic constants are presented in Figure 5.11 and Figure 5.12. The E_2 data measured during tensile testing are also shown in Figure 5.11, for comparison. Figure 5.12 also includes the measurements of Poisson's Ratio, ν_{12}, which are presented with the corresponding linear fit used for the calculation of the elastic constants.

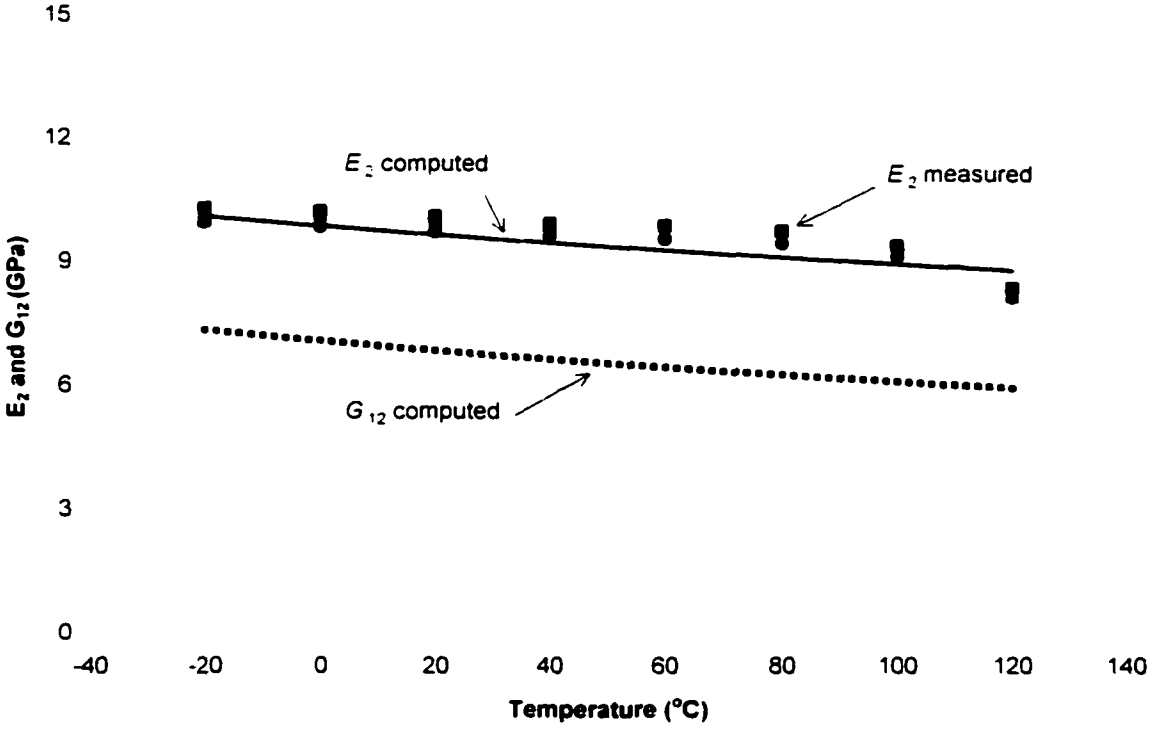

Figure 5.11 - Measured and computed elastic properties of PEEK/IM7.

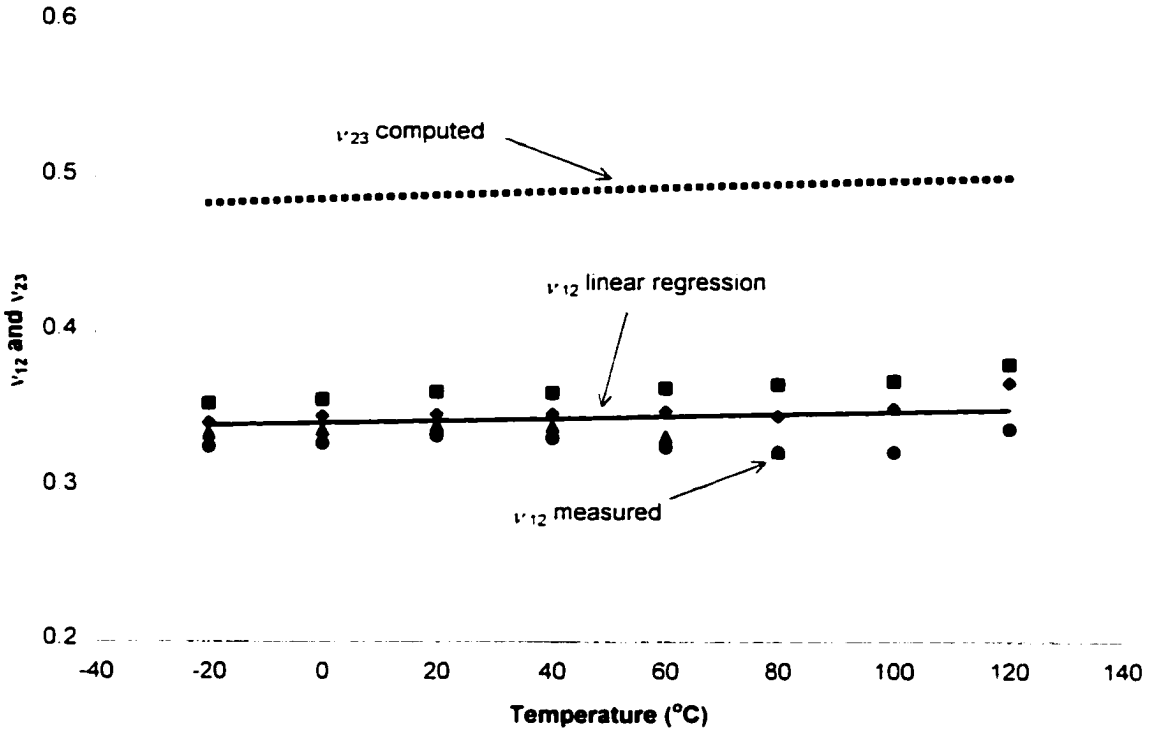

Figure 5.12 - Measured ν_{12} and computed ν_{23} vs. temperature for PEEK/IM7.

Based on the results presented in Figure 5.11, the computed transverse modulus, E_2, closely matches the linear fit of the experimentally measured E_2. Both data show a slight decrease in E_2, with increasing temperature. This decrease in E_2 may be attributed to a corresponding decrease in modulus of the polymeric material and to changes in the performance of the fiber/matrix interface. The largest difference between the measured and the calculated E_2 occurs at about 120°C where the deviation is 6.7%. For lower temperatures, the difference is smaller, and, in general, a very good agreement is

observed. For the temperature range studied, the computed shear modulus, G_{12}, shows a trend very similar to that of E_2, with the value decreasing as temperature increases.

Direct comparison of all three properties measured, E_1, ν_{12}, and E_2, at 20°C, with room temperature micromechanics predictions, shows good agreement. Nevertheless, the values are slightly higher than the room temperature measured properties for the same material, presented in the literature, as was mentioned in the room temperature study. Also, the computed room temperature value of G_{12} was notably higher than that presented in the literature. However, the trends of G_{12} with temperature, measured in the present research, are consistent with the changes noted in E_2.

The computed through-thickness Poisson's ratio, ν_{23}, shows an increase, from 0.48 to 0.50, with increasing temperature. No comparison with accepted data was possible for ν_{23} since this value was not available in the literature, even at room temperature.

The polynomial fit used for determining the relationship between thermal strain and temperature closely matches the data collected from thermal induced strain measurements. This parabolic fit implies in a linear change of CTE with temperature, which is consistent with expectations in this temperature range, and ultimately resulted in good predictions of the elastic constants. The temperature range investigated in this preliminary research was defined to remain considerably below the T_g; however, future investigations more closely approaching the T_g may yield interesting information and trends which deviate from linearity.

Future work is necessary for conclusive statements about the sensitivity of the described method to experimental parameters such as maximum testing temperature, applied load, heating rate and type of curve fit. Nevertheless, the current research

strongly supports the capability of the methodology used to study the temperature dependence of the independent elastic constants of transversely isotropic laminae.

5.7 Summary

In this chapter, the proposed approach, using coefficients of thermal expansion of laminates, is used in the three-dimensional elastic characterization of a PEEK/IM7 unidirectional prepreg tape, resulting in the determination of all the independent elastic constants. Of the five independent constants, two, E_1 and ν_{12}, were determined from standard tensile tests while the other three, E_2, G_{12}, and ν_{23}, were computed according to the relationships developed. In general, the room temperature elastic properties determined show good agreement with data available in the literature, gathered according to ASTM standards.

The technique is also applied to study the temperature dependence of the elastic properties. Three-dimensional elastic properties of PEEK/IM7 prepreg have been determined over a temperature range of -20°C to 120°C. A linear regression applied to the Poisson's ratio ν_{12} data showed a slight increase with temperature, from 0.34 to 0.35, over the temperature range studied. This increase can be observed in Figure 5.12, although the change is small, and the number of samples tested in this study may be insufficient for a more conclusive statement. E_1 showed no sensitivity to the temperature variation, with an average constant value of 164.8 GPa, as expected, since this is a fiber dominated property. All three computed independent elastic properties show sensitivity to temperature increase. E_2 decreases from 10.2 to 8.9 GPa, G_{12} decreases from 7.4 to

6.0 GPa and the through-thickness Poisson's ratio, ν_{23}, increases from 0.48 to 0.50. The computed in-plane shear modulus, G_{12}, is found to be higher than previously published data, at room temperature.

In addition to being computed according to the proposed method, the transverse modulus E_2 was also measured, over the temperature range of interest, in a standard tensile test and the data was used as a redundant check. Comparison between computed and measured data for E_2 showed a very similar trend, over the entire temperature range studied. Therefore, the results presented in this investigation confirm that the approach used, based on laminate coefficient of thermal expansions, enables the determination of the elastic properties of a transversely isotropic fiber reinforced lamina and allows investigation of the temperature dependence. Moreover, the method avoids the need to perform mechanical tests, for every property to be determined, at many different temperatures.

In summary, the results of this research demonstrate the capability of this CTE-based technique to generate elastic properties data for a transversely isotropic material, over a wide temperature range, which ultimately can be used for improved performance prediction of structural composites. The extraction of lamina properties from laminate measurements is a subtle, but important point, as it yields ply properties that incorporate effects of manufacture.

6

Determination of the 3-D Viscoelastic Properties of Transversely Isotropic Laminae and Computation of Laminate Properties

Understanding and designing for damping in composite laminates has become a topic of great interest; unfortunately, only limited viscoelastic property data is presently available. Although the knowledge of the viscoelastic material properties is of utmost importance, in existing viscoelastic models of fiber reinforced laminae, the number of independent loss factors to be determined requires experimental measurements that are not very practical [96,106]. Thus, an approach leading to the complete 3-D viscoelastic characterization using a reduced number of measured parameters is desirable. Moreover, past experimental approaches to measure the in-plane viscoelastic properties of composite laminae use a combination of bending and torsion tests [63,107]. These different boundary, and loading, conditions may affect the accuracy of the measured data.

To address the difficulties related to direct measurement of properties, a model is proposed, which allows the complete 3-D viscoelastic characterization of a transversely isotropic material, based on only five independent dynamic stiffness parameters and three

independent damping loss factors. Further, using this model, a method is developed, based on energy equations, which allows the viscoelastic parameters to be evaluated from experimental data, collected from three bend-beam oscillatory tests and two known elastic properties. Finally, after the determination of the viscoelastic parameters for transversely isotropic laminae, published models for the computation of laminate properties, based on laminae properties, are investigated.

Therefore, the goal of this chapter is to develop both a mechanics model and an experimental procedure, which, together, allow determination of the complete set of 3-D viscoelastic properties for a transversely isotropic material. The evaluation of the ability of previously published analytical models for predicting laminate viscoelastic properties, based on measured laminae properties is also undertaken in this chapter.

6.1 Viscoelastic Characteristics of Anisotropic Bodies

The typical stress-strain relationship for viscoelastic bodies can be described as (equation 3.59):

$$\sigma^{\bullet}_{ij} = C^{\bullet}_{ijkl}\varepsilon^{\bullet}_{kl} \tag{6.1}$$

where:

$\sigma^{\bullet}_{ij}$ = complex stress components.

$C^{\bullet}_{ijkl}$ = complex moduli.

$\varepsilon^{\bullet}_{ij}$ = complex strain components.

The complex moduli $C^{\bullet}_{ijkl}$ have real and imaginary components

$$C^*_{ijkl} = C'_{ijkl} + iC''_{ijkl} \tag{6.2}$$

Following similar arguments used for the elastic stiffness, due to symmetry, the number of independent parameters in storage moduli and in loss moduli tensors are reduced from 81 to 21 for the case of an anisotropic body, to 9 for an orthotropic body, and to 5 for a transversely isotropic body [60]. Thus, considering, an orthotropic body, the complex stiffness (Equation (6.2)) is expressed in matrix form as,

$$\begin{bmatrix} C^*_{11} & C^*_{12} & C^*_{13} & 0 & 0 & 0 \\ & C^*_{22} & C^*_{23} & 0 & 0 & 0 \\ & & C^*_{33} & 0 & 0 & 0 \\ & & & C^*_{44} & 0 & 0 \\ & & & & C^*_{55} & 0 \\ sym. & & & & & C^*_{66} \end{bmatrix} =$$

$$\begin{bmatrix} C'_{11} & C'_{12} & C'_{13} & 0 & 0 & 0 \\ & C'_{22} & C'_{23} & 0 & 0 & 0 \\ & & C'_{33} & 0 & 0 & 0 \\ & & & C'_{44} & 0 & 0 \\ & & & & C'_{55} & 0 \\ sym. & & & & & C'_{66} \end{bmatrix} + i \begin{bmatrix} C''_{11} & C''_{12} & C''_{13} & 0 & 0 & 0 \\ & C''_{22} & C''_{23} & 0 & 0 & 0 \\ & & C''_{33} & 0 & 0 & 0 \\ & & & C''_{44} & 0 & 0 \\ & & & & C''_{55} & 0 \\ sym. & & & & & C''_{66} \end{bmatrix} \tag{6.3}$$

Previous research with orthotropic and transversely isotropic materials, has confirmed that the Poisson's ratio can be assumed to have only a real part [96,106,108,115] and, therefore, the Poisson's coefficients determined from elastic tests can be directly applied in viscoelastic models. This implies that the off-diagonal terms of $[C'']$ do not exhibit independent viscoelastic behavior. Therefore, these terms can be expressed as a function of the diagonal terms and Poisson's ratios determined in the elastic mode.

With the assumption that Poisson's ratios have only a real component, the imaginary components of the complex stiffness matrix have been expressed as a combination of the real dynamic stiffness matrix $[C']$ and a diagonal damping matrix $[\eta]$ [96,106], to facilitate the experimental determination. Thus, the complex stiffness is written in matrix form as,

$$[C^*] = [C'] + i[C'][\eta] \tag{6.4}$$

For the case of off-axis composite layers in a laminate, the damping matrix is transformed as follows [27,96]:

$$\begin{aligned}
[C''_{\alpha\beta}] &= [C'_{\alpha\beta}][\eta_{\alpha\beta}] \\
[\eta_{\alpha\beta}] &= [C'_{\alpha\beta}]^{-1}[C''_{\alpha\beta}] \\
[\eta_{\alpha'\beta'}] &= [C'_{\alpha'\beta'}]^{-1}[C''_{\alpha'\beta'}] \\
[\eta_{\alpha'\beta'}] &= [R]^T[C'_{\alpha\beta}]^{-1}[R][R]^{-1}[C''_{\alpha\beta}][R]^{-T} \\
[\eta_{\alpha'\beta'}] &= [R]^T[C'_{\alpha\beta}]^{-1}[C''_{\alpha\beta}][R]^{-T}
\end{aligned} \tag{6.5}$$

Thus, in the global coordinates system

$$[\eta_{\alpha'\beta'}] = [R]^T[\eta_{\alpha\beta}][R]^{-T} \tag{6.6}$$

where $[R]$ is the transformation matrix (equation (3.43)).

In previous models[106], for transversely isotropic materials, the off-diagonal terms 1-3 and 2-3 of the dynamic stiffness matrix were removed, making them zero, and the corresponding damping matrix had four independent terms, *i.e.*, η_1, η_2, η_4, and η_6, considering (x_2, x_3) as the plane of isotropy. Since the dynamic stiffness matrix does not include all terms, it is referred to as $[Q']$ instead of $[C']$ [106].

$$Q' = \begin{bmatrix} Q'_{11} & Q'_{12} & 0 & 0 & 0 & 0 \\ Q'_{12} & Q'_{22} & 0 & 0 & 0 & 0 \\ 0 & 0 & Q'_{33} & 0 & 0 & 0 \\ 0 & 0 & 0 & Q'_{44} & 0 & 0 \\ 0 & 0 & 0 & 0 & Q'_{66} & 0 \\ 0 & 0 & 0 & 0 & 0 & Q'_{66} \end{bmatrix}$$

$$Q'' = \begin{bmatrix} Q'_{11} & Q'_{12} & 0 & 0 & 0 & 0 \\ Q'_{12} & Q'_{22} & 0 & 0 & 0 & 0 \\ 0 & 0 & Q'_{33} & 0 & 0 & 0 \\ 0 & 0 & 0 & Q'_{44} & 0 & 0 \\ 0 & 0 & 0 & 0 & Q'_{66} & 0 \\ 0 & 0 & 0 & 0 & 0 & Q'_{66} \end{bmatrix} \begin{bmatrix} \eta_1 & 0 & 0 & 0 & 0 & 0 \\ 0 & \eta_2 & 0 & 0 & 0 & 0 \\ 0 & 0 & \eta_2 & 0 & 0 & 0 \\ 0 & 0 & 0 & \eta_4 & 0 & 0 \\ 0 & 0 & 0 & 0 & \eta_6 & 0 \\ 0 & 0 & 0 & 0 & 0 & \eta_6 \end{bmatrix} \quad \textbf{(6.7)}$$

where:

$$Q'_{11} = \frac{E'_1}{\Delta} \qquad Q'_{12} = \frac{\nu_{12} E'_2}{\Delta}$$

$$Q'_{22} = \frac{E'_2}{\Delta} \qquad Q'_{44} = G'_{23}$$

$$Q'_{33} = E'_3 \qquad Q'_{66} = G'_{12}$$

$$\Delta = 1 - \nu_{12}\nu_{21}$$

More recently, other authors have described 3-D viscoelastic properties of orthotropic laminae as a function of a dynamic stiffness matrix [C'], in this case including the 1-3 and 2-3 terms, and a diagonal damping matrix, $[\eta]$, with six independent loss factors [96], as shown in equation (6.8).

$$C' = \begin{bmatrix} C'_{11} & C'_{12} & C'_{13} & 0 & 0 & 0 \\ C'_{12} & C'_{22} & C'_{23} & 0 & 0 & 0 \\ C'_{13} & C'_{23} & C'_{33} & 0 & 0 & 0 \\ 0 & 0 & 0 & C'_{44} & 0 & 0 \\ 0 & 0 & 0 & 0 & C'_{55} & 0 \\ 0 & 0 & 0 & 0 & 0 & C'_{66} \end{bmatrix}$$

$$C'' = \begin{bmatrix} C'_{11} & C'_{12} & C'_{13} & 0 & 0 & 0 \\ C'_{12} & C'_{22} & C'_{23} & 0 & 0 & 0 \\ C'_{13} & C'_{23} & C'_{33} & 0 & 0 & 0 \\ 0 & 0 & 0 & C'_{44} & 0 & 0 \\ 0 & 0 & 0 & 0 & C'_{55} & 0 \\ 0 & 0 & 0 & 0 & 0 & C'_{66} \end{bmatrix} \begin{bmatrix} \eta_1 & 0 & 0 & 0 & 0 & 0 \\ 0 & \eta_2 & 0 & 0 & 0 & 0 \\ 0 & 0 & \eta_3 & 0 & 0 & 0 \\ 0 & 0 & 0 & \eta_4 & 0 & 0 \\ 0 & 0 & 0 & 0 & \eta_5 & 0 \\ 0 & 0 & 0 & 0 & 0 & \eta_6 \end{bmatrix} \tag{6.8}$$

Where, the components of the damping matrix are given by:

$$\eta_1 = \tan\delta_1 = \frac{E''_1}{E'_1} \qquad \eta_4 = \tan\delta_4 = \frac{G''_{23}}{G'_{23}}$$

$$\eta_2 = \tan\delta_2 = \frac{E''_2}{E'_2} \qquad \eta_5 = \tan\delta_5 = \frac{G''_{13}}{G'_{13}}$$

$$\eta_3 = \tan\delta_3 = \frac{E''_3}{E'_3} \qquad \eta_6 = \tan\delta_6 = \frac{G''_{12}}{G'_{12}}$$

The determination, by standard techniques, of some of the independent loss factors required by this model is not straightforward. However, based on this previous model and considering the material symmetry conditions of $[C'']$ for transversely isotropic materials, a new model can be developed, with a reduced number of parameters to be determined. Thus, for a transversely isotropic body, where (x_2, x_3) is the plane of isotropy, the symmetry conditions imply,

$$C' = \begin{bmatrix} C'_{11} & C'_{12} & C'_{12} & 0 & 0 & 0 \\ C'_{12} & C'_{22} & C'_{23} & 0 & 0 & 0 \\ C'_{12} & C''_{23} & C'_{22} & 0 & 0 & 0 \\ 0 & 0 & 0 & C'_{44} & 0 & 0 \\ 0 & 0 & 0 & 0 & C'_{66} & 0 \\ 0 & 0 & 0 & 0 & 0 & C''_{66} \end{bmatrix} \tag{6.9}$$

where:

$$C''_{44} = \frac{1}{2}(C'_{22} - C''_{23})$$

or

$$C''_{44} = G'_{23} = \frac{E'_2}{2(1+\nu'_{23})} \qquad \text{and} \quad \nu'_{23} = \nu_{23}$$

Therefore, only five components of $[C']$ are independent.

If the same symmetry conditions of $[C']$ are considered for $[C'']$, then

$$C''_{44} = \frac{1}{2}(C''_{22} - C''_{23}) \tag{6.10}$$

Further, if the complex stiffness components are expressed as a dynamic stiffness matrix $[C']$, including the 1-3 and 2-3 terms (equation (6.9)), and a diagonal damping matrix, $[\eta]$, the symmetry relation (equation (6.10)) implies,

$$C''_{44} = C'_{44}\eta_4$$

or

$$C''_{44} = G''_{23} = \frac{E'_2}{2(1+\nu_{23})}\eta_4$$

but

$$G''_{23} = \frac{E''_2}{2(1+\nu_{23})} = \frac{E'_2}{2(1+\nu_{23})}\eta_2$$

Therefore,

$$\eta_4 = \eta_2 \tag{6.11}$$

Hence, considering the symmetry conditions of $[C'']$, only three loss factors, *i.e.*, η_1, η_2, and η_6 need to be determined. Thus, the matrix $[C'']$ can be expressed as

$$\begin{bmatrix} C''_{11} & C''_{12} & C''_{12} & 0 & 0 & 0 \\ C''_{21} & C''_{22} & C''_{23} & 0 & 0 & 0 \\ C''_{21} & C''_{23} & C''_{22} & 0 & 0 & 0 \\ 0 & 0 & 0 & C''_{44} & 0 & 0 \\ 0 & 0 & 0 & 0 & C''_{66} & 0 \\ 0 & 0 & 0 & 0 & 0 & C''_{66} \end{bmatrix} = \begin{bmatrix} C'_{11} & C'_{12} & C'_{12} & 0 & 0 & 0 \\ C'_{12} & C'_{22} & C'_{23} & 0 & 0 & 0 \\ C'_{12} & C'_{23} & C'_{22} & 0 & 0 & 0 \\ 0 & 0 & 0 & C'_{44} & 0 & 0 \\ 0 & 0 & 0 & 0 & C'_{66} & 0 \\ 0 & 0 & 0 & 0 & 0 & C'_{66} \end{bmatrix} \begin{bmatrix} \eta_1 & 0 & 0 & 0 & 0 & 0 \\ 0 & \eta_2 & 0 & 0 & 0 & 0 \\ 0 & 0 & \eta_2 & 0 & 0 & 0 \\ 0 & 0 & 0 & \eta_2 & 0 & 0 \\ 0 & 0 & 0 & 0 & \eta_6 & 0 \\ 0 & 0 & 0 & 0 & 0 & \eta_6 \end{bmatrix} \tag{6.12}$$

Thus, a new model is developed, using the complete dynamic stiffness matrix and applying the symmetry conditions for a transversely isotropic material, which reduces the number of independent parameters in the damping matrix to three. The previous model proposed for transversely isotropic material required knowledge of four independent loss factors η, and did not use the complete dynamic stiffness matrix [106]. Thus, this previous model did not consider the symmetry condition of equation (6.10).

For the model proposed,

$$C''_{12} = C'_{12}\eta_2 \tag{6.13}$$

and

$$C''_{21} = C'_{12}\eta_1 \tag{6.14}$$

Therefore, the form proposed implies, $C''_{12} \neq C''_{21}$. However, this asymmetry was shown not to affect the results since very good predictions for damping of composite plates can be obtained with this form [96,106]. In summary, the newly proposed mathematical model, described in equations (6.9) and (6.12), allows the complete viscoelastic characterization of a transversely isotropic material from a reduced number of independent parameters. Thus, the components of the complex stiffness matrix are determined from the five independent dynamic stiffness parameters, E'_1, E'_2, G'_{12}, $\nu'_{12} = \nu_{12}$, and $\nu'_{23} = \nu_{23}$ plus only three independent damping loss factors, η_1, η_2 and η_6.

6.2 Determination of the 3-D Viscoelastic Properties

A procedure to experimentally determine all the required parameters, according to the model described in the previous section, for the 3-D viscoelastic characterization of transversely isotropic laminae is developed. The viscoelastic properties are derived from manipulation of the relations between the dissipated energy and strain energy, resulting in equations that can be readily applied to evaluate experimental data. Specifically, this procedure focuses on bend-beam oscillatory tests alone, rather than necessitating bend

and torsion testing. However, the flexural test constraint is not inherently a limitation of the viscoelastic model presented in Section 6.1, which can, in addition to flexural tests, make use of shear data obtained from any style of oscillatory test. Nevertheless, the use of only flexural tests provides a consistent set of boundary conditions for all properties measured, and also, enables future application of DMA testing.

The relation between the energy lost and the amplitude of the elastic potential energy in one oscillatory cycle has been defined as the Specific Damping Capacity [35,61,63,96,109] (equation 3.70). Thus,

$$\psi = \frac{\Delta W}{W} \tag{6.15}$$

where: $\Delta W = \pi C''_{ijkl}\varepsilon''_{ij}\varepsilon''_{kl}$ (equation 3.75)

$W = \frac{1}{2}C''_{ijkl}\varepsilon''_{ij}\varepsilon''_{kl}$ (equation 3.14)

It has been proven experimentally that the specific damping capacity can be assumed to be independent of the amplitude of stress (or strain), if these amplitudes are small as discussed in Chapter 3.

Writing the lost energy and the strain energy equations in contracted form,

$$\Delta W = \pi\{\varepsilon\}^T[C'][\eta]\{\varepsilon\} \text{ or}$$
$$\Delta W = \pi\{\sigma\}^T[\eta][S']\{\sigma\} \tag{6.16}$$

and

$$W = \frac{1}{2}\{\sigma\}^T [S']\{\sigma\} \tag{6.17}$$

If σ_a is the only stress component applied, substitution of equations (6.16) and (6.17) into equation (6.15) gives,

$$\psi = \psi_a = \frac{\Delta W}{W} = 2\pi\eta_a \tag{6.18}$$

Considering a thin lamina of a transversely isotropic viscoelastic material, equation (6.16) can be written in reduced form as,

$$\Delta W = \pi \begin{Bmatrix} \sigma_1 \\ \sigma_2 \\ \sigma_6 \end{Bmatrix}^T \begin{bmatrix} \eta_1 & 0 & 0 \\ 0 & \eta_2 & 0 \\ 0 & 0 & \eta_6 \end{bmatrix} \begin{bmatrix} S'_{11} & S'_{12} & 0 \\ S'_{12} & S'_{22} & 0 \\ 0 & 0 & S'_{66} \end{bmatrix} \begin{Bmatrix} \sigma_1 \\ \sigma_2 \\ \sigma_6 \end{Bmatrix} \tag{6.19}$$

If off-axis plies are to be evaluated, the equations need to be transformed to global coordinates. For the case of off-axis composite layers, the damping matrix is transformed according to equation (6.6). Thus, transformation of equation (6.19) for an off-axis ply rotated by an angle, (θ), with respect to the x-axis, results in,

$$\Delta W = \pi\{\bar{\sigma}\}^T [R]^T [\eta][S'][R]\{\bar{\sigma}\} \tag{6.20}$$

For the strain energy,

$$W = \frac{1}{2}\{\bar{\sigma}\}^T [R]^T [S'][R]\{\bar{\sigma}\} \tag{6.21}$$

Thus, if σ_x is the only applied stress, and using equation (6.18),

$$\eta_x = \frac{\Delta W}{2\pi W} = \frac{1}{\bar{S}'_{11}}\left\{\frac{\eta_1}{E'_1}\cos^4(\theta) + \frac{\eta_2}{E'_2}\sin^4(\theta) + \left[\frac{\eta_6}{G'_{12}} - (\eta_1 + \eta_2)\frac{\nu_{12}}{E'_1}\right]\sin^2(\theta)\cos^2(\theta)\right\} \quad \textbf{(6.22)}$$

where

$$\bar{S}'_{11} = S'_{11}\cos^4(\theta) + S'_{22}\sin^4(\theta) + (2S'_{12} + S'_{66})\cos^2(\theta)\sin^2(\theta) \quad \textbf{(6.23)}$$

If the assumption that the damping coefficients are independent of the stress amplitude is valid, and also, if the material tensile and compressive moduli are identical, then the damping factors, equation (6.22), can be measured from dynamic flexural mechanical testing of beams. In this case, any portion of the beam cross-section can be used as a representative volume, since, according to the assumptions made, stress variations through the cross section will not affect the damping measurements.

The assumption of equal tensile and compressive moduli is valid for most fiber-reinforced composites, subjected to small strain amplitudes [98,110]. Based on this assumption, the bending mode has been used in most of the research programs, by different authors, which use mechanical testing for the study of the viscoelastic behavior of carbon fiber reinforced composites, since the high modulus, typical of these materials, makes tensile tests impractical. However, under large deformations, some fibers present a lower compressive modulus compared to the tensile modulus. This phenomenon, suggested as being related to local buckling in the fibers, is more pronounced in high modulus fibers, such as mesophase pitch-based carbon fibers [111]. Therefore, bending

tests must be carried on under very small deformations if the tensile and compressive moduli are assumed to be equal.

For a composite laminated beam, the deflection, w_0, is affected by the in-plane Poisson coupling, D_{12}, and by the shear coupling, D_{16}. Because of these couplings, the components d_{12} and d_{16} are not null (see equation (3.111), which produces the curvatures κ_y and κ_{xy}, even though M_x is the only applied moment. However, if the length-to-width of the beam is large, these effects can be neglected [99,112]. Previous research using graphite/aluminum angle-ply beams showed good prediction of experimental results, with length-to-width aspect ratio ranging from 10 to 20 [113].

A simple beam model based on the classical Bernoulli-Euler beam theory can be used if the beam is long. In the past, other authors have successfully used beam theory in viscoelastic investigations of fiber-reinforced composites [63,97,107]. Hence, using the general form of the beam equation,

$$\frac{d^2 w_0}{dx^2} = -\frac{M}{E^{*b}_{xx} I_{yy}} \tag{6.24}$$

where:

w_0 is the transverse deflection,

M is the bending moment,

E^{*b}_{xx} is the beam complex modulus in the x-direction,

I_{yy} is the moment of inertia about the y-axis.

The complex modulus for the off-axis unidirectional beam, E^{*b}_{xx}, is given by

$$E^{*b}_{xx} = E'^{b}_{xx}(1+\eta_x) \tag{6.25}$$

where,

$$E'^{b}_{xx} = \frac{1}{\bar{S}'_{11}} \tag{6.26}$$

The dynamic moduli, E'_1 and E'_2, and the damping loss factors, η_1 and η_2, can be measured directly from oscillatory bend-beam tests of unidirectional laminae with fibers oriented at 0° and at 90°, with respect to the beam length. Then, $E'^{b}_{xx} = \frac{1}{\bar{S}'_{11}}$ and η_x are measured from a bending test performed in an off-axis unidirectional beam specimen, with some intermediate angle θ, where $0° < \theta < 90°$. Subsequently, application of equation (6.23) followed by equation (6.22) allows the computation of the dynamic shear modulus, G'_{12}, and the damping coefficient, η_6, based on the measured dynamic moduli, E'_1, E'_2, and E'^{b}_{xx}, damping loss factors, η_1, η_2, and η_x, and a known value of the Poisson's ratio, ν_{12}.

Therefore, using only three oscillatory bend tests, one at 0, one at 90 and the third at an intermediate angle, and assuming that the Poisson's ratios ν_{12} and ν_{23} are also measured, or known, the procedure developed results in the complete set of 3-D independent viscoelastic properties for a transversely isotropic lamina. While E'_1, E'_2, ν_{12} and ν_{23}, and also η_1, η_2, are directly measured, the dynamic shear modulus, G'_{12}, and the damping loss factor, η_6, are computed using the procedure developed, thus avoiding the need for additional shear tests. The determination of the in-plane shear modulus, G_{12},

based on the moduli E_1, E_2, Poisson's ratio, ν_{12}, and the modulus E_{xx}, corresponding to an off-axis specimen, has been previously suggested, using tensile tests [114].

6.2.1 Numerical Examples and Discussion

To demonstrate the application of the relationships developed, published data of dynamic moduli and damping loss factors for two transversely isotropic materials are used. The materials considered are a unidirectional carbon fiber epoxy prepreg, HT-S/DX210 [107], and a glass fiber reinforced prepreg with the same epoxy matrix, Glass/DX210 [63]. These data have also been used in other published works, as a verification check of mechanics based approaches [96,115]. Bending test data gathered from many off-axis specimens are available with the published data; however, only data for a single off-axis specimen is used, with the equations developed herein, for the computation of the in-plane shear dynamic modulus and loss factor. In this case the $\theta = 30^0$ off-axis data was selected for the demonstration of the procedure, although, theoretically, any angle, where $0°<\theta<90°$, could be used. The damping coefficients of the published data are presented as specific damping capacity (SDC); however, these coefficients have been transformed to damping loss factors η, according to equation (6.18), in order to maintain consistency with the equations presented in this work. The published data for both materials are presented in Table 6.1.

Table 6.1 - Dynamic moduli and damping factors of unidirectional laminae.

Material	E'_1 (GPa)	E'_2 (GPa)	E'_{30} (GPa)	η_1 (10^{-3})	η_2 (10^{-3})	η_{30} (10^{-3})	ν_{12}
HT-S/DX210[107]	103.49 (15.01 MSI)	7.58 (1.10 MSI)	16.2 * (2.35 MSI)	0.78 (ψ_1=0.49%)	8.72 (ψ_2=5.48%)	10.03 * (ψ_{30}=6.3%)	0.3
Glass/DX210[63]	37.78	10.90	17.0 +	1.38 (ψ_1=0.87%)	8.04 (ψ_2=5.05%)	7.80 + (ψ_{30}=4.9%)	0.291

* data from Figure 2 in reference [107]; + data from Figure 4 in reference [63].

Note: data for the Poisson's ratio ν_{23} is not available.

As a verification of the capabilities of the present approach for predicting the shear properties, these bending tests data (Table 6.1) are substituted into equations (6.22), (6.23), and (6.26), to predict G'_{12} and η_6, for each of the two materials. For HT-S/DX210, the properties G'_{12} and η_6, determined from the equations and also the published shear data [107], determined directly from separate torsion tests, are presented in Table 6.2, for comparison. For G'_{12}, the difference between the predicted value and the published data was only 0.3%. For η_6, the difference was 3.8%.

Table 6.2 - Shear properties of HT-S/DX210 unidirectional lamina.

Parameter	Quoted[107]	Computed
G'_{12} (GPa)	3.83 (0.555 MSI)	3.82 (0.554 MSI)
η_6 (10^{-3})	10.74 (ψ_6 = 6.75 %)	11.15

Table 6.3 shows the quoted and computed shear properties for Glass/DX210 unidirectional lamina. Compared with the prediction for HT-S/DX210, in this case the difference between quoted and computed properties is larger. For G'_{12}, the difference

between the predicted value and the published data was about 7%, and for η_6, the difference was about 10%. In any case, the predictions are good, considering that these off-axis data are obtained from a plot, which obviously implies some error.

Table 6.3 - Shear properties of Glass/DX210 unidirectional lamina.

Parameter	Quoted [63]	Computed
G'_{12} (GPa)	4.91	4.56
η_6 (10^{-3})	11.0	9.87
	(ψ_6 = 6.91 %)	

Therefore, the method developed in the previous sections can result in shear properties, from the data of only three bend tests, which are in good agreement with published data, obtained experimentally, from torsion tests. The good predictions of in-plane shear properties, from off-axis flexure measurements, supports the assumption of negligible bending-torsion coupling effects on the measurements, if the length-to-width of the beam is large. For the examples used in this demonstration, the length-to-width ratios were 18:1 for HT-S/DX210, and 16.7:1 for Glass/DX210.

It is important to note that the torsion test is the most common approach used in published literature, for the determination of the shear properties, G'_{12} and η_6. However, in these works only the shear properties are usually determined from torsion testing, while the remaining in-plane viscoelastic parameters are determined from bend tests. In the experimental approach developed in the present work, a single test geometry, flexure, is required for all of the necessary measurements. Thus, concerns related to differing test fixture boundary conditions, as exist when multiple types of tests are combined, are negated.

After the determination of the shear modulus and loss factor, G'_{12} and η_6, these properties are applied in equations (6.22), (6.23), and (6.26), in conjunction with E'_1, E'_2, ν_{12}, η_1, and η_2, previously measured, to predict the modulus and damping for off-axis beams with any fiber orientation, where $0° \leq \theta \leq 90°$. The predicted properties for the two materials evaluated are plotted in figures 6.1 and 6.2.

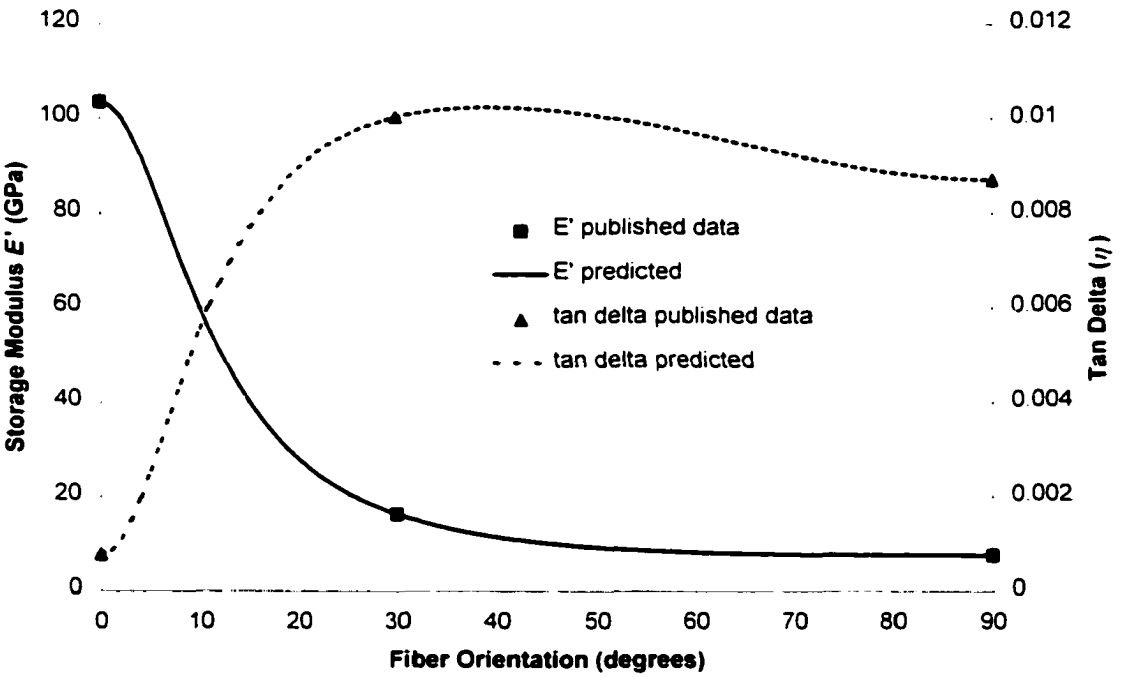

Figure 6.1 - Variation of viscoelastic properties with fiber angle for HT-S/DX210.

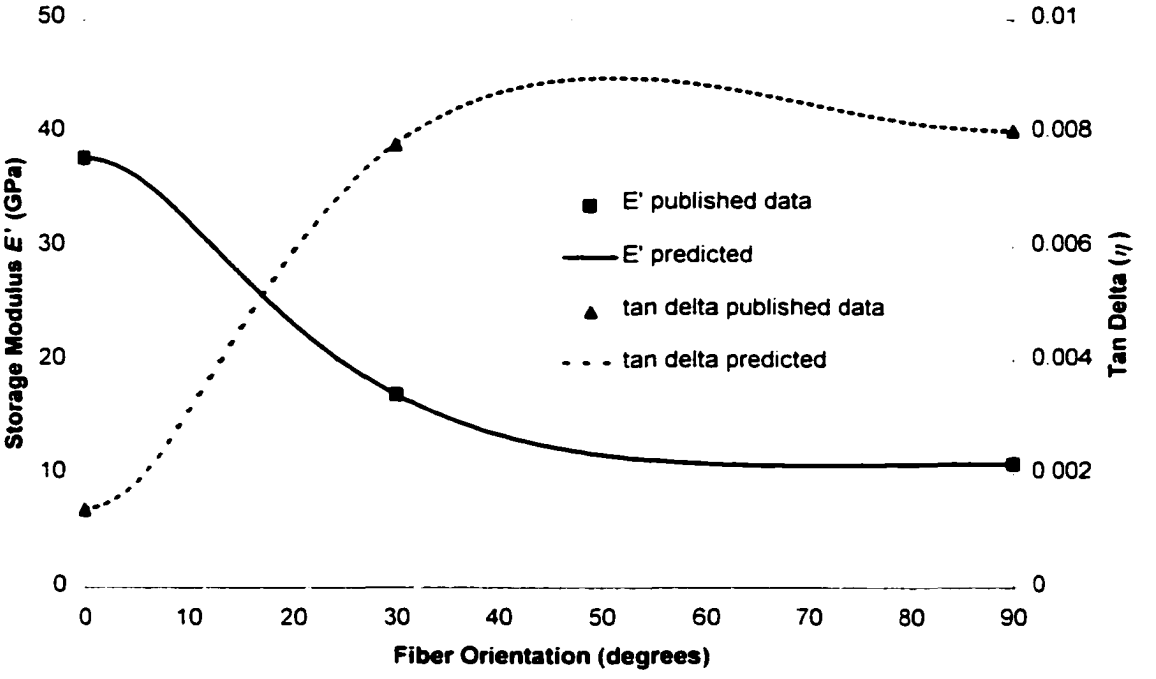

Figure 6.2 - Variation of viscoelastic properties with fiber angle for Glass/DX210.

If three-dimensional viscoelastic properties are to be determined over a range of temperatures, the Poisson's coefficients, ν_{12} and ν_{23}, need to be known over that same temperature range, in addition to the properties measured in oscillatory testing. The method presented in Chapter 4 allows the determination of all the 3-D elastic coefficients, over a temperature range, from measured data of laminate coefficients of thermal expansion, and can be used for Poisson's ratios determination. The application of this method offers the advantage of being able to conduct the measurements, elastic and viscoelastic, in the same piece of equipment. However, if equipment with combined capabilities for measuring CTE and the dynamic properties is not available, the procedure can be carried out in a separate TMA (or dilatometer) and DMA.

In summary, the approach described herein enables the determination of all the viscoelastic coefficients of a transversely isotropic layer, from oscillatory bending tests of three individual unidirectional laminae with fibers oriented at 0, 90 and some intermediate angle $0°<\theta<90°$, given that the Poisson's ratios ν_{12} and ν_{23} are known. In this demonstration, while values for G'_{12} and η_6 were readily predicted, it was not possible to complete the 3-D viscoelastic characterization since the Poisson's ratio ν_{23} was not available in the reference literature.

6.3 Expanding Lamina Properties to Laminate Properties

Investigations focusing on expanding lamina viscoelastic data to laminate viscoelastic properties have been presented in the literature [63,98,106,116]. In two of the references cited, models for predicting the dynamic properties of symmetric laminated composite beams are developed and compared with experimentally measured data [63,98]. Both the mechanics models and the experimental data presented in these published investigations form the basis for many other subsequent studies. In this section, both models will be reviewed. Laminae properties for Glass/DX210, as determined in Section 6.2, are applied to the models to predict laminate properties, and the predicted properties are compared with published experimental data.

6.3.1 Viscoelastic Properties of Laminated Beams (Model 1)

Considering a thin laminated beam composed of transversely isotropic layers (Figure 3.9), the equation for the dissipated energy (equation (6.16)) can be written in reduced form as

$$\Delta W = \int_{-\frac{h}{2}}^{\frac{h}{2}} \int_{-\frac{l}{2}}^{\frac{l}{2}} \int_{-\frac{h}{2}}^{\frac{h}{2}} \pi \{\bar{\sigma}\}^T [\bar{\eta}] \{\bar{\varepsilon}\} dz dx dy \tag{6.27}$$

where,

$\{\bar{\sigma}\}$ is the stress vector in global coordinates

$[\bar{\eta}]$ is the transformed loss factor matrix

$\{\bar{\varepsilon}\}$ is the strain vector in global coordinates

For the k^{th} layer, the strain components are given by,

$$\begin{Bmatrix} \varepsilon_x \\ \varepsilon_y \\ \gamma_{xy} \end{Bmatrix}^{(k)} = z \begin{Bmatrix} \kappa_x \\ \kappa_y \\ \kappa_{xy} \end{Bmatrix} \tag{6.28}$$

where,

z is the distance from the mid-plane of the beam, and

k_{ij} are the beam curvature components.

For symmetric laminates, the bending-stretching coupling terms are null. Thus, the beam curvatures can be written as a function of the applied bending moments only, as

$$\begin{Bmatrix} \kappa_x \\ \kappa_y \\ \kappa_{xy} \end{Bmatrix} = \begin{bmatrix} D'_{11} & D'_{12} & D'_{16} \\ D'_{12} & D'_{22} & D'_{26} \\ D'_{16} & D'_{26} & D'_{66} \end{bmatrix}^{-1} \begin{Bmatrix} M_x \\ M_y \\ M_{xy} \end{Bmatrix} \tag{6.29}$$

The bending stiffnesses, D'_{ij}, are primed to indicate that they are based on dynamic moduli.

Equation (6.29) can also be written as,

$$\begin{Bmatrix} \kappa_x \\ \kappa_y \\ \kappa_{xy} \end{Bmatrix} = \begin{bmatrix} d'_{11} & d'_{12} & d'_{16} \\ d'_{12} & d'_{22} & d'_{26} \\ d'_{16} & d'_{26} & d'_{66} \end{bmatrix} \begin{Bmatrix} M_x \\ M_y \\ M_{xy} \end{Bmatrix} \tag{6.30}$$

where $[d'] = [D']^{-1}$.

Considering a beam where $M = M_x b$ is the only applied moment,

$$\begin{Bmatrix} \kappa_x \\ \kappa_y \\ \kappa_{xy} \end{Bmatrix} = \frac{1}{b} \begin{bmatrix} d'_{11} & d'_{12} & d'_{16} \\ d'_{12} & d'_{22} & d'_{26} \\ d'_{16} & d'_{26} & d'_{66} \end{bmatrix} \begin{Bmatrix} M \\ 0 \\ 0 \end{Bmatrix} \tag{6.31}$$

Thus, equation (6.28) becomes

$$\begin{Bmatrix} \varepsilon_x \\ \varepsilon_y \\ \gamma_{xy} \end{Bmatrix}^{(k)} = \frac{zM}{b} \begin{Bmatrix} d'_{11} \\ d'_{12} \\ d'_{16} \end{Bmatrix} \tag{6.32}$$

The stress components in the k^{th} layer are related to the strain components as,

$$\{\bar{\sigma}\}^{(k)} = \left[\bar{Q}'\right]^{(k)} \{\bar{\varepsilon}\}^{(k)} \tag{6.33}$$

thus,

$$\begin{Bmatrix} \sigma_x \\ \sigma_y \\ \sigma_{xy} \end{Bmatrix}^{(k)} = \frac{zM}{b} \begin{bmatrix} \bar{Q}'_{11} & \bar{Q}'_{12} & \bar{Q}'_{16} \\ \bar{Q}'_{12} & \bar{Q}'_{22} & \bar{Q}'_{26} \\ \bar{Q}'_{16} & \bar{Q}'_{26} & \bar{Q}'_{66} \end{bmatrix}^{(k)} \begin{Bmatrix} d'_{11} \\ d'_{12} \\ d'_{16} \end{Bmatrix} \tag{6.34}$$

For a beam, where σ_y and σ_{xy} are neglected, then σ_x is the only stress considered, and

$$\{\bar{\sigma}\}^{(k)} = \begin{Bmatrix} \sigma_x \\ 0 \\ 0 \end{Bmatrix}^{(k)} \tag{6.35}$$

Where, from equation (6.34),

$$\sigma_x^{(k)} = \frac{zM}{b}\left(\bar{Q}'^{(k)}_{11} d'_{11} + \bar{Q}'^{(k)}_{12} d'_{12} + \bar{Q}'^{(k)}_{16} d'_{16}\right) \tag{6.36}$$

Hence, for the k^{th} layer,

$$\{\bar{\sigma}\}^T [\bar{\eta}]\{\bar{\varepsilon}\} = \sigma_x^{(k)}\left(\bar{\eta}_{11}^{(k)} \varepsilon_x^{(k)} + \bar{\eta}_{12}^{(k)} \varepsilon_y^{(k)} + \bar{\eta}_{16}^{(k)} \gamma_{xy}^{(k)}\right) \tag{6.37}$$

Then, considering equation (6.32),

$$\{\bar{\sigma}\}^T [\bar{\eta}]\{\bar{\varepsilon}\} = \frac{z^2 M^2}{b^2} f^{(k)} g^{(k)} \tag{6.38}$$

where,

$$f^{(k)} = \bar{Q}'^{(k)}_{11} d'_{11} + \bar{Q}'^{(k)}_{12} d'_{12} + \bar{Q}'^{(k)}_{16} d'_{16} \tag{6.39}$$

$$g^{(k)} = \bar{\eta}_{11}^{(k)} d'_{11} + \bar{\eta}_{12}^{(k)} d'_{12} + \bar{\eta}_{16}^{(k)} d'_{16} \tag{6.40}$$

Thus, substitution of equation (6.38) into equation (6.27), gives

$$\Delta W = \frac{\pi}{b^2}\int_{-\frac{b}{2}}^{\frac{b}{2}}\int_{-\frac{l}{2}}^{\frac{l}{2}}\int_{-\frac{h}{2}}^{\frac{h}{2}} f^{(k)} g^{(k)} z^2 dz M^2 dx dy \tag{6.41}$$

If the integration is performed in a layer-wise fashion, the final expression for the dissipated energy in the laminated beam is given by,

$$\Delta W = \frac{\pi}{3b}\sum_{k=1}^{n} f^{(k)} g^{(k)} \left(z_k^3 - z_{k-1}^3\right) \int_{-\frac{l}{2}}^{\frac{l}{2}} M^2 dx \tag{6.42}$$

For the determination of the loss factor of the laminated beam, the strain energy also needs to be determined. The beam strain energy can be expressed as

$$W = \frac{1}{2}\int_{-\frac{b}{2}}^{\frac{b}{2}}\int_{-\frac{l}{2}}^{\frac{l}{2}}\int_{-\frac{h}{2}}^{\frac{h}{2}} \sigma_x \varepsilon_x dx dy dz \tag{6.43}$$

Integration over the beam's width and substitution of $\sigma_x^{(k)}$ from equation (6.36) and $\varepsilon_x^{(k)}$ from equation (6.32), results in

$$W = \frac{b}{2}\int_{-\frac{l}{2}}^{\frac{l}{2}}\int_{-\frac{h}{2}}^{\frac{h}{2}} \frac{zM}{b}\left(\bar{Q}_{11}'^{(k)} d_{11}' + \bar{Q}_{12}'^{(k)} d_{12}' + \bar{Q}_{16}'^{(k)} d_{16}'\right)\frac{zM}{b} d_{11}' dx dz \tag{6.44}$$

or,

$$W = \frac{d'_{11}}{2b}\int_{-\frac{h}{2}}^{\frac{h}{2}}\left(\overline{Q}'^{(k)}_{11}d'_{11} + \overline{Q}'^{(k)}_{12}d'_{12} + \overline{Q}'^{(k)}_{16}d'_{16}\right)z^2dz\int_{-\frac{l}{2}}^{\frac{l}{2}}M^2dx \tag{6.45}$$

Next, layer-wise integration is performed, which results,

$$W = \frac{d'_{11}}{2b}\sum_{k=1}^{n}\frac{1}{3}\left(\overline{Q}'^{(k)}_{11}d'_{11} + \overline{Q}'^{(k)}_{12}d'_{12} + \overline{Q}'^{(k)}_{16}d'_{16}\right)\left(z_k^3 - z_{k-1}^3\right)\int_{-\frac{l}{2}}^{\frac{l}{2}}M^2dx \tag{6.46}$$

But,

$$\sum_{k=1}^{n}\frac{1}{3}\left(\overline{Q}'^{(k)}_{11}d'_{11} + \overline{Q}'^{(k)}_{12}d'_{12} + \overline{Q}'^{(k)}_{16}d'_{16}\right)\left(z_k^3 - z_{k-1}^3\right) = 1 \tag{6.47}$$

Thus, equation (6.46) can be simplified to,

$$W = \frac{d'_{11}}{2b}\int_{-\frac{l}{2}}^{\frac{l}{2}}M^2dx \tag{6.48}$$

Therefore, using equation (6.18), the damping factor for the laminated beam, is given by

$$\eta^h = \frac{\Delta W}{2\pi W} = \frac{\sum_{k=1}^{n} f^{(k)}g^{(k)}\left(z_k^3 - z_{k-1}^3\right)}{3d'_{11}} \tag{6.49}$$

For the determination of the beam's dynamic modulus, the beam equation is written as

$$\kappa_x = \frac{M}{E'^{b}_{xx} I} = d'_{11} M_x \tag{6.50}$$

where $M_x = \frac{M}{b}$

Thus,

$$E'^{b}_{xx} = \frac{12}{h^3 d'_{11}} \tag{6.51}$$

The model presented in equations (6.49) and (6.51), for the computation of the loss factor and storage modulus of a laminated beam, has been presented in previous research [98]. This model is consistent with the equations used, in this work, for unidirectional beams (Section 6.2). Therefore, for a beam where all layers have the same included angle θ, the equations (6.49) and (6.51) produce the same properties as equations (6.22), (6.23) and (6.26).

6.3.2 Viscoelastic Properties of Laminated Beams (Model 2)

The basic difference between the model described in equations (6.49) and (6.51), and another previously published model [63], is that, in the other model proposed, the strain component ε_y, in all layers, is considered to be much smaller than the other two components, ε_x and ε_{xy}, and therefore, it is not taken into account in equation (6.37). Thus, equation (6.37) becomes,

$$\{\bar{\sigma}\}^T [\bar{\eta}] \{\bar{\varepsilon}\} = \sigma_x \left(\bar{\eta}_{11}^{(k)} \varepsilon_x^{(k)} + \bar{\eta}_{16}^{(k)} \gamma_{xy}^{(k)} \right) \tag{6.52}$$

Hence, in the final equation for the dissipated energy (6.42), $g^{(k)}$ is given by

$$g^{(k)} = \overline{\eta}_{11}^{(k)} d'_{11} + \overline{\eta}_{16}^{(k)} d'_{16} \tag{6.53}$$

In this case, the damping factor for the laminate beam, is still given by equation (6.49), with $g^{(k)}$ given by equation (6.53), and $f^{(k)}$ given by equation (6.39). One inconsistency of this model is that the strain component ε_y is included in part of the derivation (equation (6.33)) and is only neglected afterwards (equation (6.52)). Furthermore, this model does not produce the same beam loss factor as equation (6.22) for unidirectional beams, which was used for the determination of the viscoelastic properties of an individual layer. Nevertheless, this model has been proven to produce laminate viscoelastic properties, which are in very good agreement with experimentally measured data, and therefore, it is also considered in this investigation.

6.3.3 Numerical Example

To demonstrate the application of the two laminate models presented, dynamic moduli and damping loss factors for a Glass/DX210 lamina, developed in previous section, are used to predict the dynamic properties of symmetric laminates. This material was selected due to the availability, in literature, of experimentally measured data for symmetric laminated beams [63]. The laminate stacking sequence considered, for the determination of the viscoelastic properties, was $[(0/90)_3]_s$, to allow comparison with published experimental data.

Laminae properties for Glass/DX210, determined in Section 6.2.1, from three-point bending tests, are shown in Table 6.4. Using these properties, laminate viscoelastic properties are calculated, as a function of the fiber orientation of the outer layer with respect to the beam length, in a $[(0/90)_3]_s$ laminated beam. The predictions of dynamic modulus and loss factor were carried out using two Matlab codes (Appendix 8), one for each of the two laminate models considered. The laminate properties predictions, according to the two models presented, are presented in figures 6.4 and 6.5. Experimental data for a $[(0/90)_3]_s$ Glass/DX210 cross-ply laminate, from published literature [63], are also included for comparison purposes.

Table 6.4 - Viscoelastic properties of Glass/DX210 unidirectional lamina.

E'_1 (GPa)	E'_2 (GPa)	G'_{12} (GPa)	η_1 (10^{-3})	η_2 (10^{-3})	η_6 (10^{-3})	ν_{12}
37.78	10.90	4.56	1.38	8.04	9.87	0.291

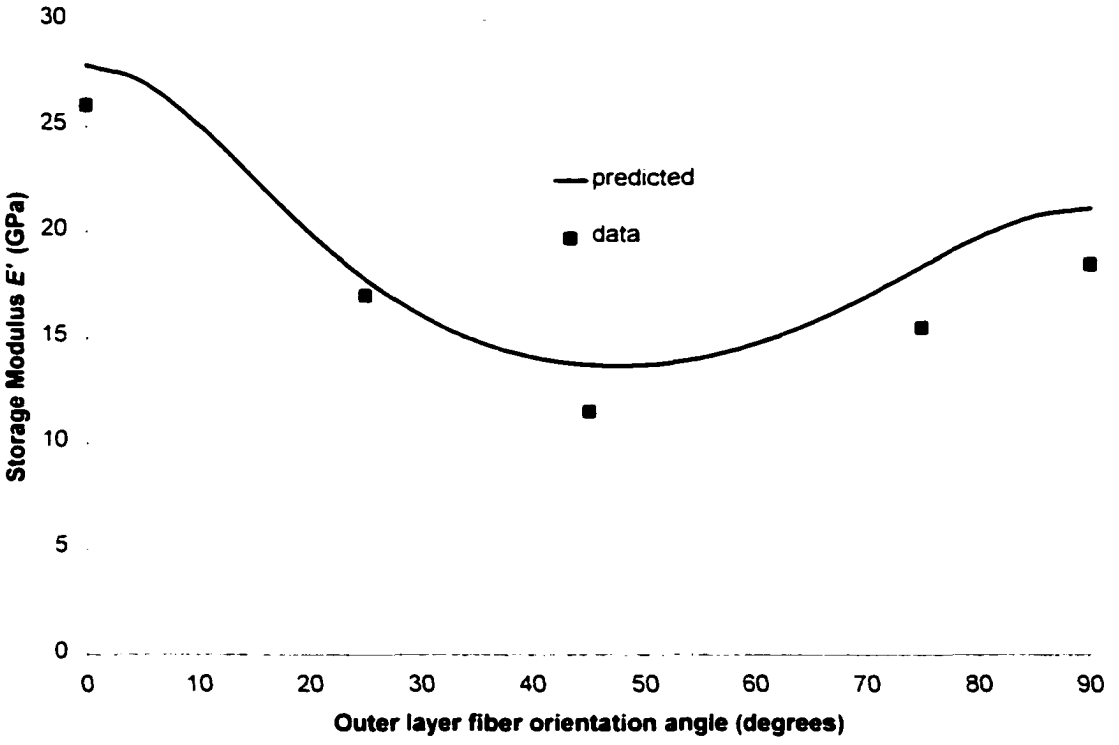

Figure 6.3 - Variation of storage modulus with outer layer fiber angle for cross-ply Glass/DX210 laminate.

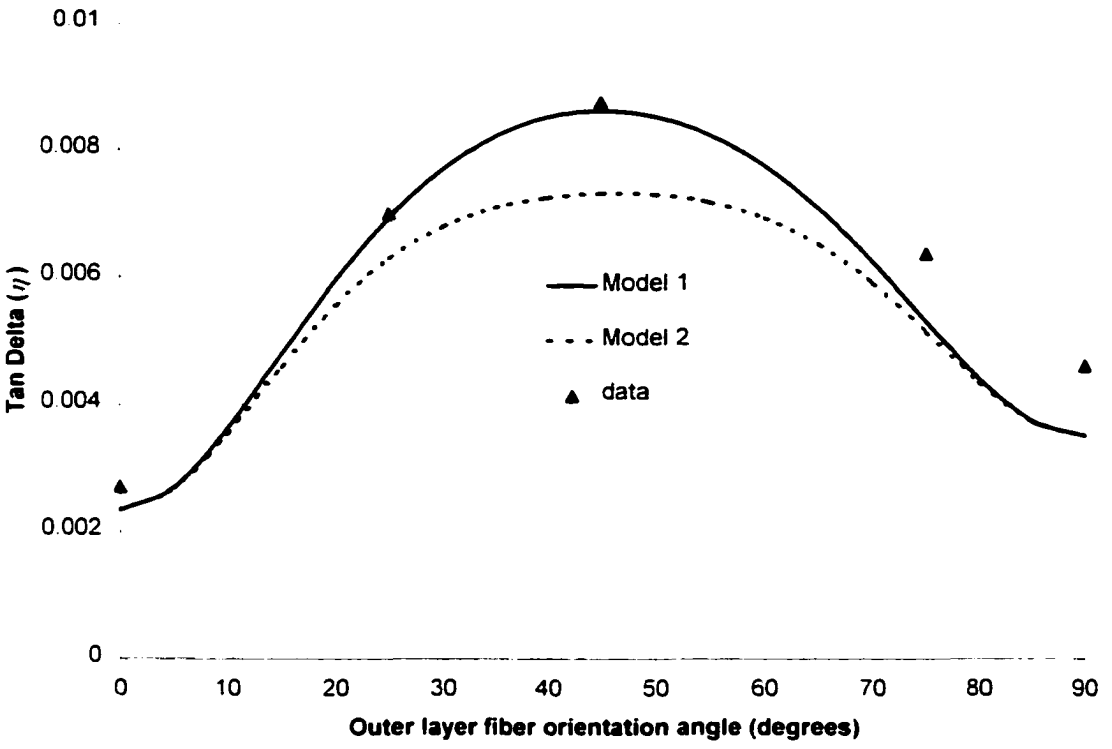

Figure 6.4 - Variation of loss factor with outer layer fiber angle for cross-ply Glass/DX210 laminate.

Figure 6.3 shows only one curve since both models result in the same predictions for the storage modulus (E'). The predicted laminate dynamic moduli were higher than the measured data. Nevertheless, the correlation of the trend is very good. For the loss factor, Figure 6.4, there is better agreement of the measured data with Model 1 than with Model 2, for this specific material and stacking sequence studied. Although, at some angles, both models underpredicted the damping loss factor, the trend correlation between the predictions and the collected data is clear.

6.4 Summary

The mechanics model proposed in this chapter reduces the number of damping coefficients to be determined, for 3-D viscoelastic characterization of a transversely isotropic material, allowing complete experimental evaluation. Further, an experimental approach was described as a practical method for the determination of all the viscoelastic parameters of a transversely isotropic material, using oscillatory bending tests of three individual unidirectional laminae with fibers oriented at 0, 90 and some intermediate angle $0°<\theta<90°$, given that the Poisson's ratios ν_{12} and ν_{23} are known. Although the procedure for the determination of the in-plane shear properties, based on off-axis beam measurements, neglects Poisson's coupling and shear coupling effects, previous research has indicated that these effects can be neglected for large length-width ratios. Moreover, with the proposed approach, based on flexure tests only, DMA equipment can be used for the complete viscoelastic characterization using sub-scale bend beams.

By extending the approach to oscillatory tests performed in a commercial dynamic mechanical analyzer (DMA), the viscoelastic properties can be evaluated over a range of temperatures and frequencies. In addition, the use of experimental measurements, in opposition to micromechanics approaches, offers the future advantage of determining, and incorporating, the effects of processing, or material degradation into the properties of the material.

Further, if the fibers offer negligible, or no, contribution to the overall composite damping, such as in carbon fiber reinforced polymers, DMA tests in reinforced and unreinforced specimens may lead to the separation of the mechanisms of damping – matrix versus interface. Since micromechanics approaches account only for the

constituent material (fiber and matrix) properties. studying the difference between the experimentally measured properties and micromechanics predictions may allow a better understanding of the individual contribution of matrix and interface to the composite damping.

The advantages related to the 3-D viscoelastic characterization of transversely isotropic laminae by the proposed method. include:

- The mechanics model presented reduces the total number of independent coefficients to be determined.
- The experimental approach described enables the determination of the complete 3-D viscoelastic material properties from only three oscillatory bending tests. providing that the two Poisson's coefficients are known.
- The method has the potential to produce laminae viscoelastic data. directly measured under the conditions required by the final application.
- Torsion tests are not necessary for the determination of the shear properties. with all properties determined by bend tests rather than through a mix of torsion and bend testing. thus overcoming any inconsistent boundary condition assumptions.

Finally. after the characterization of the transversely isotropic laminae. two published models were considered for the determination of the laminate properties. It was determined that both models can result in good predictions for laminate properties based on laminae measured properties.

7

Viscoelastic Characterization of PEEK/IM7 by Dynamic Mechanical Analysis (DMA)

A mechanics model was developed in Chapter 6, which describes the 3-D viscoelastic properties of a transversely isotropic material, based on five independent dynamic moduli and three damping loss factors. Also, it has been determined, in the same chapter, that, for the case of a transversely isotropic lamina, the computation of all 3-D viscoelastic properties can be accomplished from three bending tests, providing that two Poisson's ratios, ν_{12} and ν_{23}, are known from elastic measurements. Finally, the effectiveness of two different models for determining laminate viscoelastic performance, from lamina viscoelastic properties, was assessed.

The present chapter is intended to show the ability of the developed approach to produce viscoelastic properties of fiber reinforced composite materials from sub-scale dynamic mechanical testing. A sub-scale, Dynamic Mechanical Analysis-based (DMA) experimental approach is used to evaluate the viscoelastic properties of transversely isotropic laminae and laminates. The material used for the viscoelastic characterization

was PEEK/IM7 unidirectional prepreg, with elastic properties as determined in Chapter 5.

The DMA-based approach allows temperature and frequency effects on viscoelastic properties to be investigated, since damping is experimentally evaluated in a global sense, instead of being predicted by micromechanics. To show this ability, this study also includes measurements of viscoelastic properties of laminae and laminates over a range of temperatures and frequencies. Further, laminate properties, measured at different temperatures and frequencies, are compared with predictions, based on laminae properties, according to the two laminate models investigated in the previous chapter, for verification of both lamina properties prediction and laminate model capabilities, over a range of temperature and frequency.

Specifically, this work applies the proposed approach presented in Chapter 6, making use of DMA (Dynamic Load Mechanical Analyzer) measured parameters in unidirectional sub-scale bend beam specimens, to determine the viscoelastic material properties for a transversely isotropic, fiber reinforced material. In summary, the investigation described in this chapter consists of:

- Determination of the 3-D viscoelastic properties of a PEEK/IM7 transversely isotropic lamina by the method proposed in Chapter 6, using DMA sub-scale bending tests;
- Application of two different models, previously published in the literature, to expand lamina properties to laminate properties and comparison with experimental DMA measurements in laminates;

- Investigation of changes in viscoelastic properties, of laminae and laminates, with temperature and frequency;

7.1 Materials and Test Specimens

The material tested was APC-2/IM7, unidirectional prepreg tape, manufactured by Cytec Fiberite Inc., with a resin content of 32% and a fiber areal weight of 145g/m^2. This is the same material used in the elastic characterization described in Chapter 5. Two 150.0 x 200.0 mm laminates, were produced in a hot-press: a 8 ply unidirectional $[(0)_8]_T$ and a cross-ply $[(0/90)_2]_s$. The laminates were processed at a temperature of 395°C for 45 minutes, under an applied pressure of 690 kPa (100 psi).

Beam specimens were cut from the processed laminates using a diamond abrasive saw. Unidirectional laminated beams were cut from the $[(0)_8]_T$ plate with fibers oriented at 0°, 30°, 45°, and 90°, with respect to the beam length. In this research, the properties of these unidirectional specimens are assumed to be a true representation of the properties of one unidirectional layer. Therefore, the measured properties of the unidirectional specimens are referred to as lamina properties. From the $[(0/90)_2]_s$ cross-ply laminate, laminated beams were cut in three different angles, 0°, 45°, and 90°, resulting in specimens with stacking sequences of $[(0/90)_2]_s$, $[(+45/-45)_2]_s$, and $[(90/0)_2]_s$, respectively. Careful control of ply orientation was undertaken during the cutting process.

After the cutting procedure, the specimens' edges were sanded flat for better dimensional precision. Finally, the specimens were conditioned to reduce effects of

residual stresses and moisture induced during specimen preparation. The conditioning procedure was the same applied in tensile and CTE specimens used in the elastic characterization. It consisted of heating the specimen in an oven from room temperature to 70°C, holding for 2 hours, then heating from 70°C to 90°C followed by a hold for 2 hours, and finally, heating from 90°C to 110°C with a final hold for 2 hours. Upon cool-down, accurate dimensions of each specimen were measured using a hand-held micrometer. The specimen dimensions were nominally 50.0 x 4.0 x 1.0 mm (Figure 7.1).

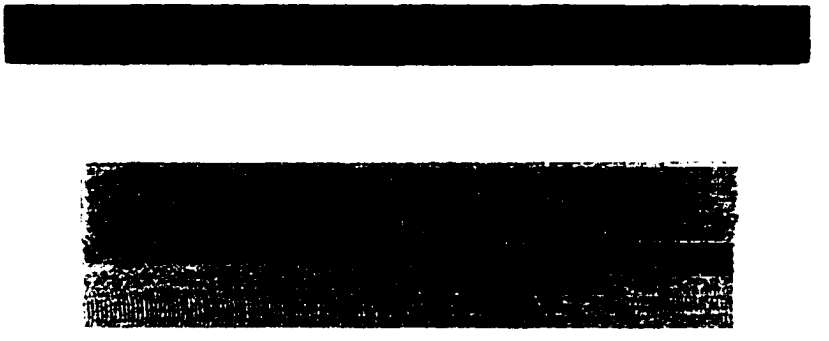

Figure 7.1 - Bend-beam specimens for viscoelastic characterization.

7.2 Testing Equipment

The dynamic mechanical tests were performed in a Rheometric Scientific DMTA-V (Figure 7.2). The DMTA-V, is a computer-controlled dynamic mechanical thermal analyzer that operates in the frequency range from 1.0×10^{-6} Hz to 200 Hz, and temperature range of -150°C to +600°C. Dynamic testing can be performed at

displacement amplitudes ranging from ±0.5 to ±128 microns, with a resolution of less than 1nm. The equipment is capable of determining material properties through tension, compression, three-point-bending, shear, and single and dual cantilever testing. The maximum applied load is 15 N, with a resolution of $1.0x10^{-3}$ N. The testing program was conducted at the Rheometric Scientific Inc. facilities, Piscataway, NJ.

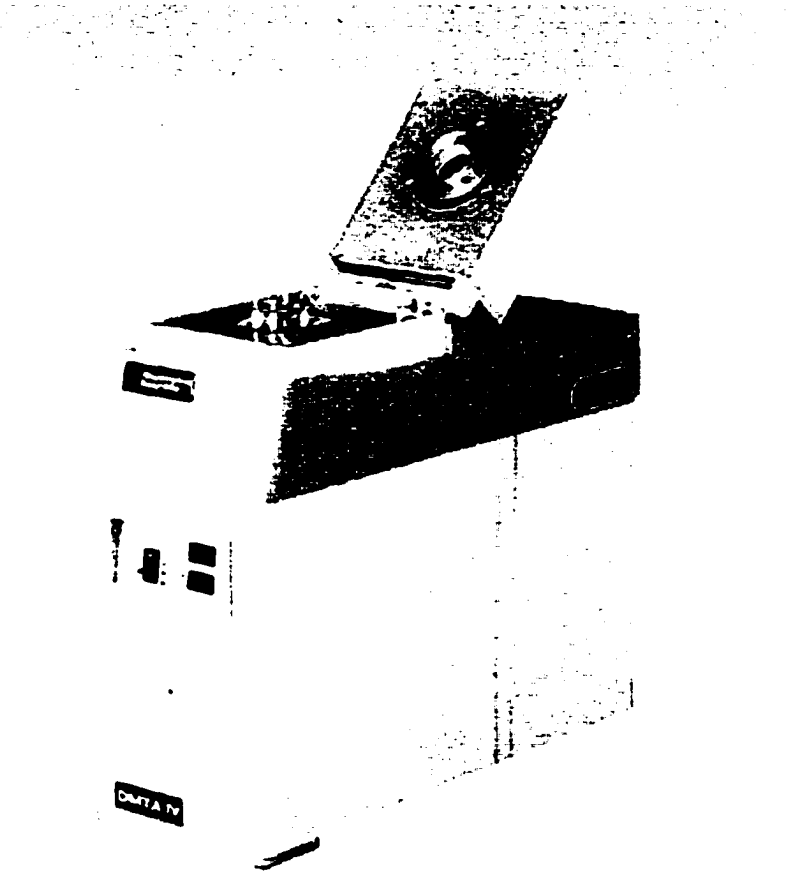

Figure 7.2 - Rheometric Scientific DMTA.

7.3 Experimental Approach

This section presents the experimental approach to study both laminae and laminates in a range of temperature and frequency. The method presented in Chapter 6. to determine the viscoelastic properties of transversely isotropic laminae. assumes that the Poisson's ratios. ν_{12} and ν_{23}. are known and that they include only the real (not imaginary) part. Therefore. these elastic properties need to first be determined. The 3-D elastic properties for PEEK/IM7 were determined in Chapter 5. over the range of temperature of -20°C to +120°C. according to a proposed approach. making use of coefficients of thermal expansion measurements.

After the determination of the two Poisson's ratios for the material studied. over a temperature range. dynamic flexural measurements in beams with three different fiber orientations. and over the same temperature range. are necessary to complete the viscoelastic characterization. Sub-scale dynamic measurements were carried out using a DMTA-V. in a 3-point bending testing mode. with a 40.0mm span between the supports. Three-point bending was selected as the preferred testing geometry since clamped boundaries are reported to affect the damping measurements. increasing the measured damping [64]. Also. if the beam is free to twist at the supports. there will be no applied torque at these locations. and therefore. there will be no stored energy associated with twisting. Moreover. if the tests are to be carried out over a range of temperatures. in-plane forces. due to the mismatch in coefficients of thermal expansion between the beam specimen and the material of the supports. will not be introduced since the beam is free to expand at the supports.

In a three-point bend-test mode, the complex modulus components are determined according to,

$$E' = \frac{P^0 L^3}{48 I v^0} \cos\delta \tag{7.1}$$

$$E'' = \frac{P^0 L^3}{48 I v^0} \sin\delta \tag{7.2}$$

where:

P^0 is the applied force amplitude,

L is the beam length between supports,

I is the moment of inertia of beam about the neutral axis,

v^0 is the mid-span displacement amplitude,

δ is the phase angle.

Two types of measurements were conducted: temperature scan and frequency scan. The temperature scan measurements were performed over the temperature range of -20°C to +120°C, with a heating rate of 3.0°C/min, and under a constant frequency of 1.0 Hz. The actual temperature sweep test was performed over a greater range - from -25°C to +125°C - to ensure that the rate of change of temperature was steady in the temperature range from -20°C to +120°C. The frequency scans were conducted at room temperature and over a frequency range from 0.1 Hz to 10 Hz, with an exponential frequency change rate using 10 data points per decade.

All dynamic tests were carried out under a sinusoidal strain-controlled mode. A very small strain amplitude (0.01%) is used throughout the measurements since the model

applied, for viscoelastic material characterization (Chapter 6), assumes that the specific damping capacity is independent of the amplitude of strain, which is a valid assumption only for very small strains. The beam specimens were pre-stressed with an applied force 10% larger than the force necessary to produce the desired strain amplitude. This procedure guarantees that the center probe is always in contact with the beam. The force necessary to pre-stress the beam is automatically calculated, through a series of static tests, by the computer control of the DMTA-V and corrected, if necessary, throughout the experimental procedure.

Sub-scale flexure tests in unidirectional beams with fibers oriented at 0°, 30°, 45° and 90°, with respect to the beam length, were conducted. Although only three different fiber orientations are necessary for the viscoelastic characterization, one of the off-axis beam tests is used as a redundant check. In this case, only the tests conducted in beams with fibers oriented at 0°, 30°, and 90°, are used for the determination of the viscoelastic parameters and test data from the 45° specimens are used as a redundant check. Even though the 45° off-axis specimens could also have been used for the computation of the shear coefficients, the properties of these specimens, storage modulus and loss factor, are very similar to the properties of the 90° specimens, which are also used in the same model, and any data scatter of these samples produce a larger effect on the predicted shear properties. The 30° off-axis specimens present properties, which are more distinct of the 90° specimens properties, and therefore they were used for the computation of the shear viscoelastic parameters. Other off-axis angles were not considered in this research due to easy of manufacture of the 30° and 45° off-axis specimens, which may ultimately help reducing the errors related to ply misalignment.

After the material characterization is complete, from the three oscillatory bending tests and the two Poisson's coefficients previously determined, equations (6.23) and (6.24) are used to predict the dynamic modulus and loss factor for an off-axis beam with any included angle, where $0° \leq \theta \leq 90°$. The measured values for a specimen with an included angle of 45° are then compared with predicted properties, for the same angle, for verification.

Following the determination of all independent viscoelastic properties for the material studied, the two previously published laminate models, which were discussed in Section 6.3, are applied to predict the behavior of three cross-ply laminates. The laminae properties determined are used in conjunction with both laminate models to predict the dynamic modulus and loss factor of laminated beam specimens with the following stacking sequences: $[(0/90)_2]_s$, $[(90/0)_2]_s$, and $[(+45/-45)_2]_s$. The properties predicted by each of the models are compared with experimental measurements.

7.3.1 General Concerns Regarding Sub-Scale Test Approaches

There are several concerns involving sub-scale test methods. These concerns are mostly related to specimen non-uniformities resulting from the manufacturing process, which may be disregarded in standard scale testing, but could have a significant influence in sub-scale testing. Unidirectional prepreg tapes are made from discrete tows of fiber and there can be variations in fiber density across the width of the tape. This can have a significant effect when the samples are only a few plies thick and very narrow. Also, precise measurement of the ply thickness is necessary because bending tests are

extremely sensitive to thickness since the moment of inertia of the beam depends on the thickness cubed. Thus, lack of thickness uniformity could potentially be a problem.

There is also a concern regarding variation of the fiber volume fraction through the ply thickness. A thin resin rich layer is sometimes observed on the outside of a sub-scale specimen, which is the surface in contact with the tool during the curing process. This non-uniformity could affect the results by making the effective thickness smaller than the measured thickness, because of the great difference between matrix and reinforcement properties. Despite all the concerns presented, preliminary testing programs proved that the technique is able to measure flexural properties with good accuracy [76,110,117].

7.4 Results and Discussion – Lamina Characterization

7.4.1 Temperature Dependence of the Viscoelastic Properties

The results of the sub-scale dynamic measurements in unidirectional flexure beams with fiber orientations of 0°, 30°, 45° and 90°, are presented in figures 7.3 to 7.6. Each figure represents temperature sweep measurements in two different specimens. The same temperature range used in the elastic characterization, -20°C to +120°C, is used in these viscoelastic measurements.

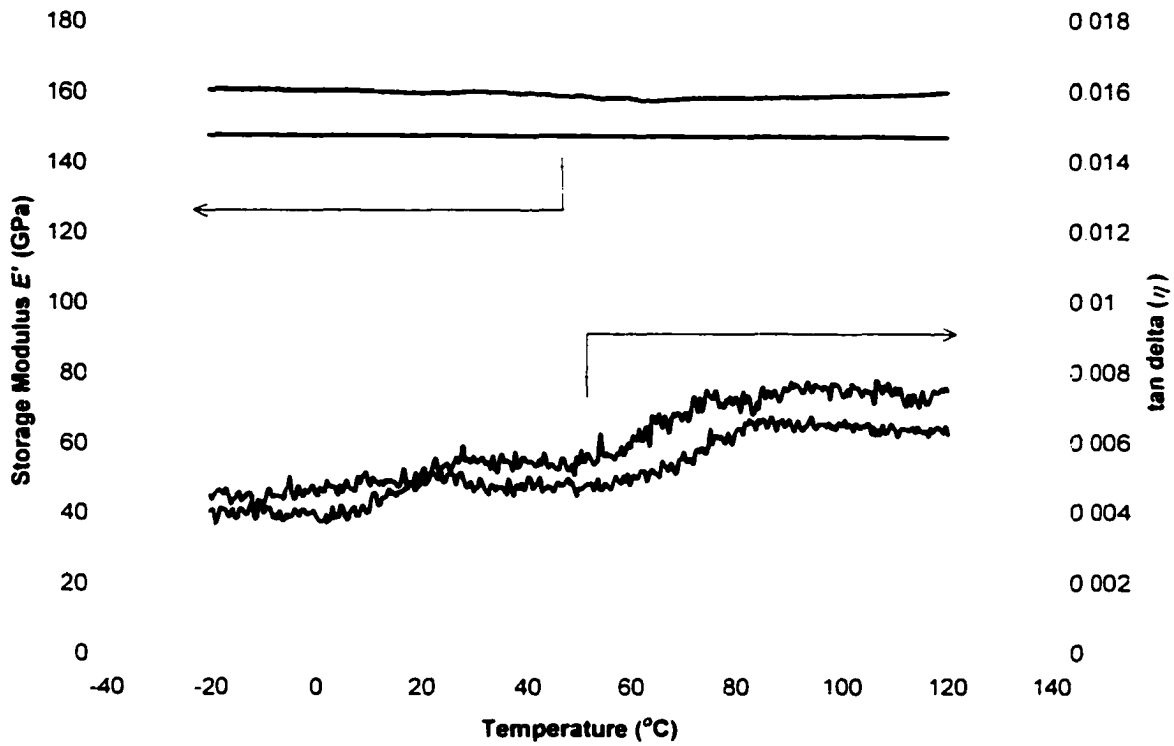

Figure 7.3 - Temperature sweep data for two unidirectional beams with fibers oriented at 0°.

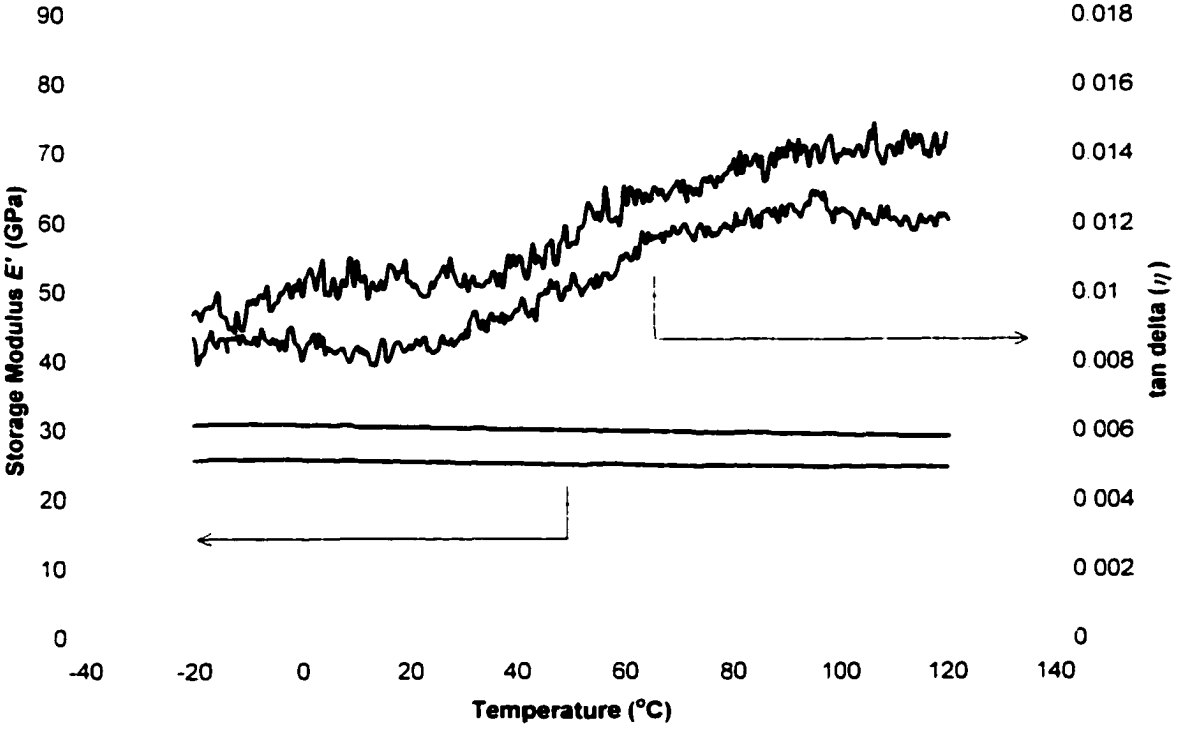

Figure 7.4 - Temperature sweep data for two unidirectional beams with fibers oriented at 30°.

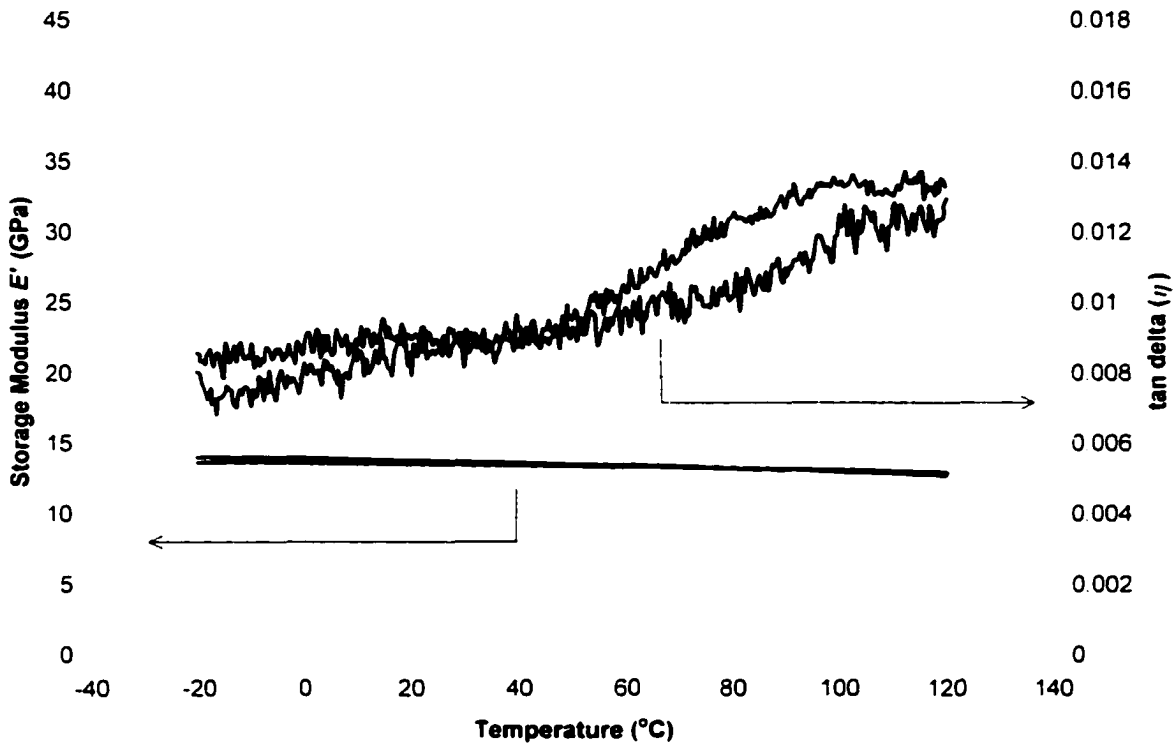

Figure 7.5 - Temperature sweep data for two unidirectional beams with fibers oriented at 45°.

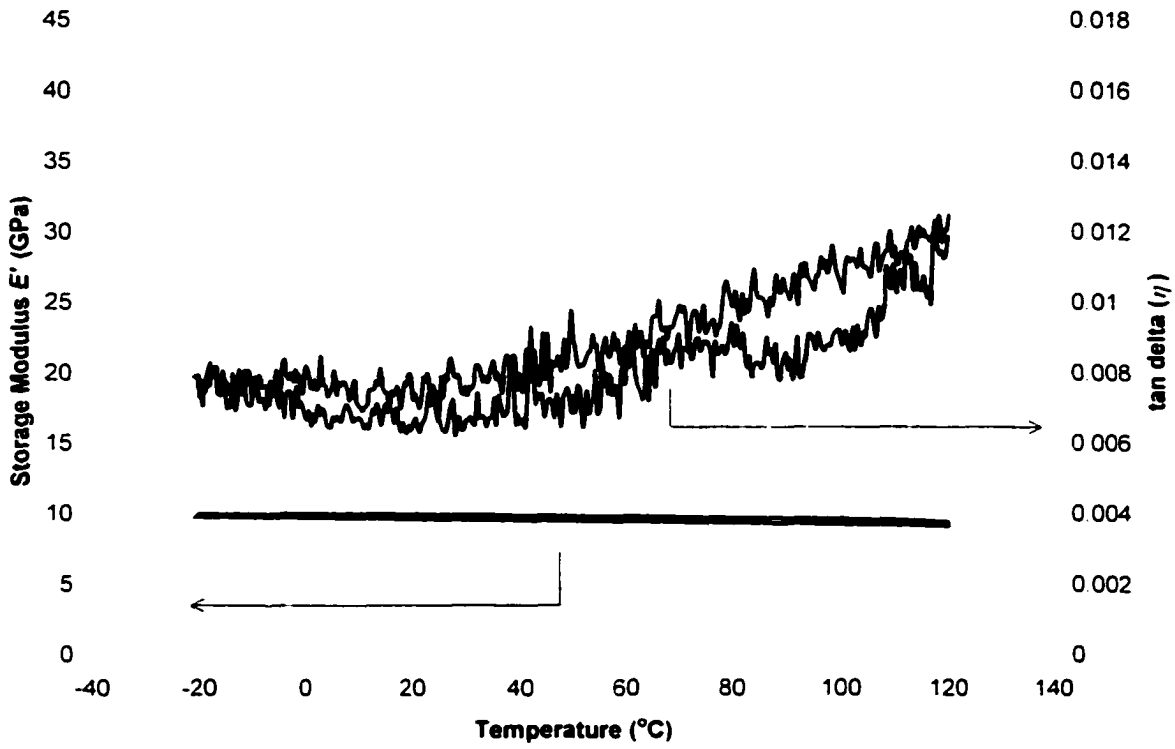

Figure 7.6 - Temperature sweep data for two unidirectional beams with fibers oriented at 90°.

The measured storage modulus and loss factor data presented in figures 7.3 to 7.6, corresponding to two beam tests in each of the four different fiber orientations tested, were averaged for the calculation of the material viscoelastic properties. For the calculation of the averages, in each fiber orientation, a sixth degree polynomial was used

to fit the loss factor data, while for the storage modulus a linear fit was applied. There is no fundamental reason in the selection of the order of fit used other than the fact that they were found to provide the best representation of the raw data collected. A high degree polynomial was applied for the curve that describes the temperature dependence of the loss factor, to allow contouring the irregular shape with peaks, which are a characteristic of these curves. Essentially, the polynomial fitting was used as a curve smoothing technique, and also as a way to generate equations of the relationships for follow-up manipulation. The average of the storage modulus and loss factor data, from two specimens tested in each fiber orientation, are presented in Figure 7.7.

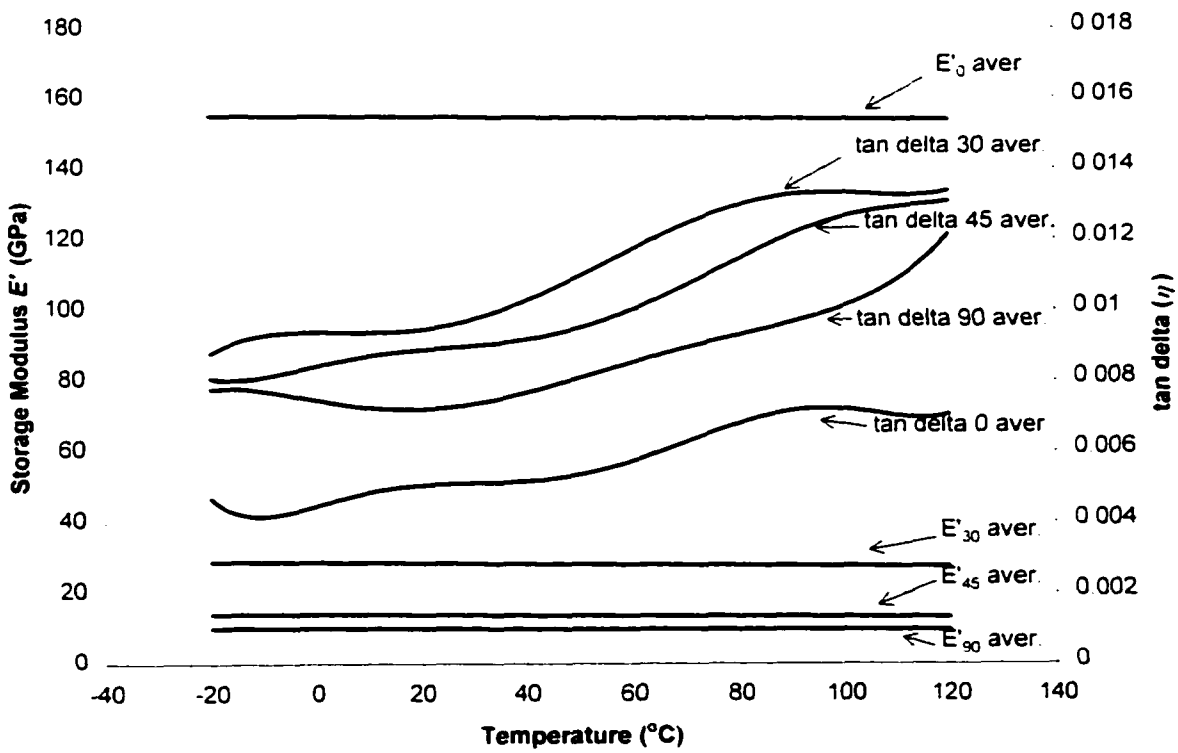

Figure 7.7 - Average storage modulus and loss factor for unidirectional beams.

Using the average of the measured viscoelastic properties for the beam specimens with fiber orientations of 0°, 30°, and 90° (Figure 7.7), and the Poisson's ratios, ν_{12} and ν_{23}, previously determined over the same temperature range, the viscoelastic properties of PEEK/IM7 were determined over the temperature range of -20°C to +120°C, using temperature increments of 20°C. The temperature dependence of the two Poisson's ratios, ν_{12} and ν_{23}, which completes the 3-D viscoelastic characterization, was previously presented in Figure 5.12, in Chapter 5. The shear storage modulus and loss factor, G'_{12} and η_6, at each temperature, were determined by application of equations (6.23) and (6.24), presented in Chapter 6. After the determination of the in-plane shear properties, at each temperature, the 3-D viscoelastic characterization of transversely isotropic PEEK/IM7 is complete. The temperature dependence of the nine independent parameters that completely characterize the material are presented in Table 7.1. The same results are also presented in graphical form in figures 7.8 and 7.9.

Table 7.1 - Temperature dependence of the viscoelastic properties of PEEK/IM7.

Temp. (°C)	E'_1 (GPa)	E'_2 (GPa)	G'_{12} (GPa)	ν_{12}	ν_{23}	η_1 (10^{-3})	η_2 (10^{-3})	η_6 (10^{-3})
-20	155.4	10.2	7.4	0.34	0.48	4.7	7.8	8.8
0	155.1	10.1	7.3	0.34	0.49	4.5	7.5	10.5
20	154.9	10.0	7.2	0.34	0.49	5.1	7.2	10.6
40	154.7	10.0	7.1	0.34	0.49	5.2	7.7	11.5
60	154.5	9.9	7.1	0.35	0.49	5.7	8.5	13.2
80	154.3	9.8	7.0	0.35	0.50	6.8	9.3	14.6
100	154.0	9.7	7.0	0.35	0.50	7.2	10.1	14.8
120	153.8	9.6	6.9	0.35	0.50	7.0	12.1	14.9

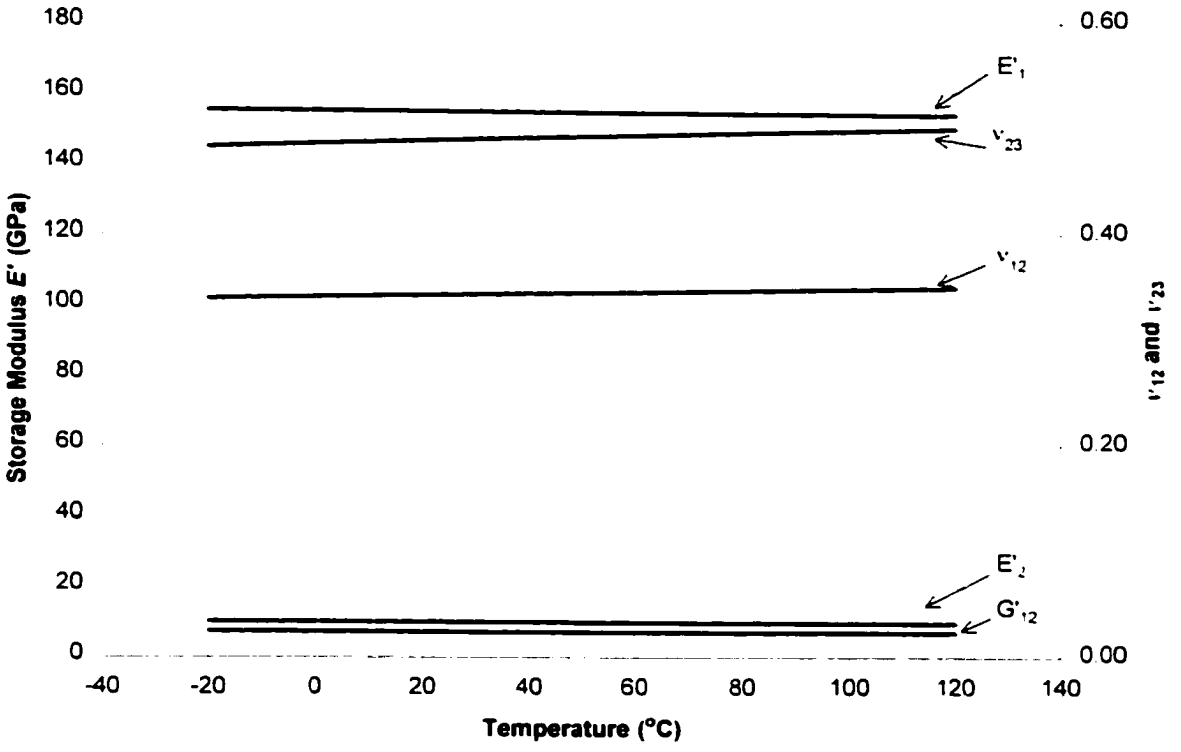

Figure 7.8 - Variation of storage moduli and Poisson's ratio with temperature for PEEK/IM7.

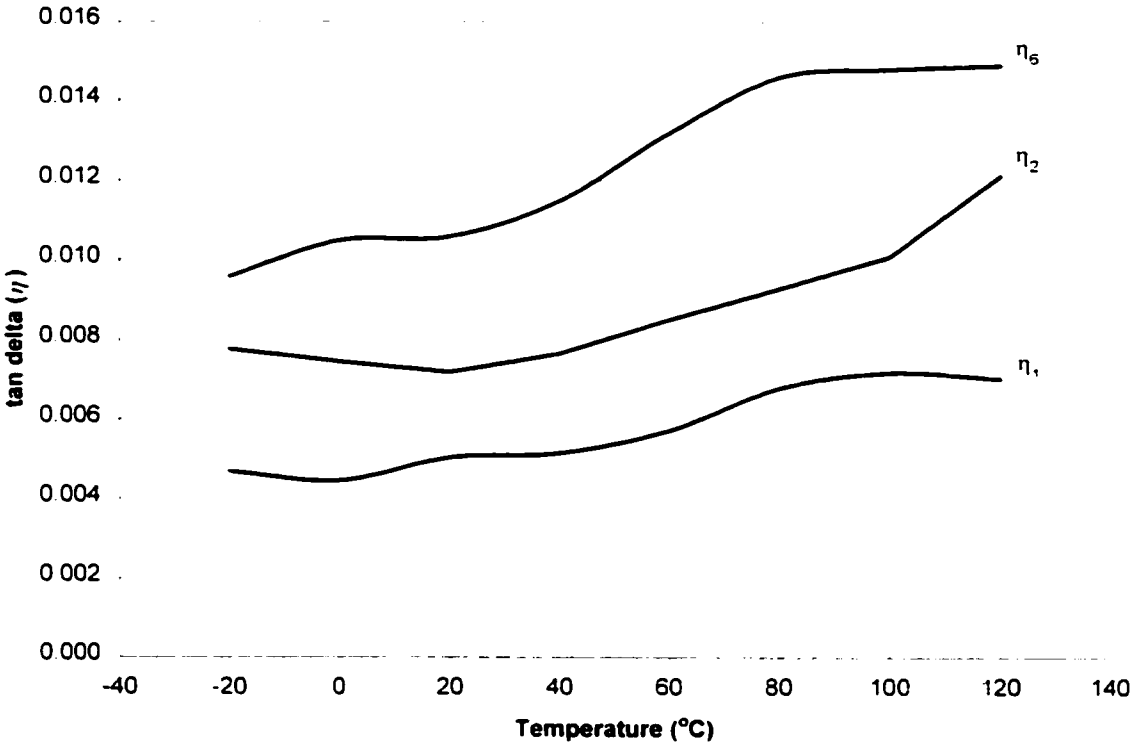

Figure 7.9 - Variation of loss factors with temperature for PEEK/IM7.

A comparison between the dynamic moduli obtained in this viscoelastic characterization at 20°C and the room temperature elastic moduli, obtained from CTE measurements, is presented in Table 7.2. It can be seen that, the agreement is very good. The shear modulus G_{12} agrees well with the value determined in the elastic characterization (Chapter 5), which was found to be higher than quoted values, and initially considered inaccurate. No comparison was made for the two Poisson's ratios because the same values obtained from the elastic measurements were used in the dynamic characterization.

Table 7.2 - Properties of PEEK/IM7 determined from elastic and dynamic tests.

Property	Elastic	Dynamic	Difference
E_1 (GPa)	164.4	154.9	6%
E_2 (GPa)	9.9	10.0	1%
G_{12}(GPa)	7.0	7.2	3%

The temperature sweep tests for all unidirectional beams (Figure 7.7) show an increase in *tan* δ and decrease in dynamic modulus with increasing temperature. However the temperature influence was different between unidirectional beam specimens with different fiber orientation, as expected. Over the temperature range studied, the carbon fiber properties are expected to show little, or no, temperature relation. In contrast, the viscoelastic properties of the PEEK thermoplastic matrix are more temperature-dependent. Therefore, the temperature effect in specimens, where the properties are more fiber-dominated, such as beams with 0° fiber orientation, the temperature effect is reduced.

According to data presented in Table 7.1, a small decrease in E_1 with temperature, is observed. E_1 decreases from 155.4 GPa, at -20°C, to 153.8 GPa, at 120°C, representing a 1% variation. The corresponding variations for E_2, over the same temperature range was from 10.2 GPa to 9.6 GPa, or 6% reduction in storage modulus. G_{12} decreased from 7.4 GPa to 6.9 GPa, representing a 7% reduction.

The modulus of the carbon fiber is very large compared to the polymeric matrix. Therefore, since the temperature effect on the carbon fibers properties is negligible, within the temperature range studied, the changes in modulus with temperature are dependent on the fiber direction. However, even in the fiber-dominated modulus, E_1, there was a trend indicating decrease with temperature. The 1% change observed in E_1

suggests changes not only in matrix properties but also changes in the fiber-matrix interface. Changes in matrix properties alone could not account for the total change in modulus, especially because the maximum temperature is considerably below the glass transition temperature. The changes in the other two modulus components, where the matrix properties are significant, such as E_2 and G_{12}, are larger due to the changes in matrix properties with temperature, combined with changes at the interface.

Contrary to the response of the modulus, the damping properties of the polymeric matrix are significantly higher compared to the carbon fiber damping. Therefore, most of the composite damping is a result of the matrix damping and the fiber-matrix interface response. Changes in damping with temperature were much larger than changes in dynamic modulus. Even in the fiber direction where the changes in modulus are very small, considerable changes in damping were detected, over the temperature range. The loss factor η_1 show the smallest temperature dependence, varying from 4.7×10^{-3}, at -20°C, to 7.0×10^{-3}, at 120°C, which represents an increase of 49%. For η_2, the loss factor corresponding to the transverse direction, the measurements varied from 7.8×10^{-3}, at -20°C, to 12.1×10^{-3}, at 120°C, thus increasing 55%. Finally, the shear loss factor, η_6, varied from 8.8×10^{-3}, at -20°C, to 14.9×10^{-3}, at 120°C, corresponding to a 69% increase.

After the determination of the shear viscoelastic properties, equations (6.23) and (6.24) can be again applied to determine the viscoelastic properties, storage modulus and loss factor, of unidirectional off-axis beams with any included angle, where $0° \leq \theta \leq 90°$. The viscoelastic properties prediction of unidirectional PEEK/IM7 beams as a function of fiber orientation, over the temperature range of -20°C to 120°C, is shown in Figure 7.10

and Figure 7.11. Figure 7.10 shows storage moduli and Figure 7.11 shows loss factor curves for every 20°C increment of temperature. Also, in both figures, the average of the measured data, from two 45° fiber orientation specimens, at each 20°C temperature increment are included for comparison with predicted properties at that angle. The reason that only the 45° experimental data is used for comparison with the predicted properties is because the other three measured orientations, 0°, 30°, and 90°, were used to generate the prediction curves, leaving the 45° as a "redundant" check.

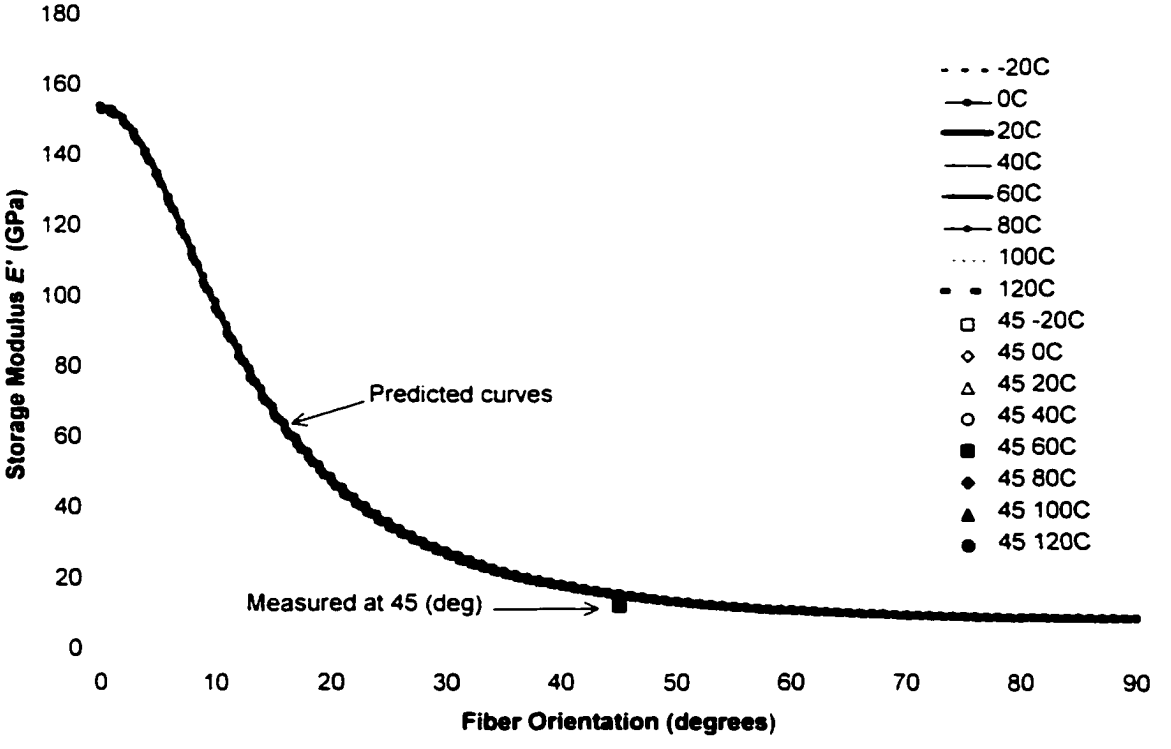

Figure 7.10 - Variation of storage modulus with fiber orientation for PEEK/IM7.

The curves for the storage modulus at different temperatures, presented in Figure 7.10, are almost indistinguishable since the variations in storage modulus components,

over the temperature range studied, were very small. Both plots show fairly good agreement between the properties predicted for a specimen with included angle of 45° and the experimental measurements at that angle. For both storage modulus and loss factor, the predicted properties were slightly higher than the measured data.

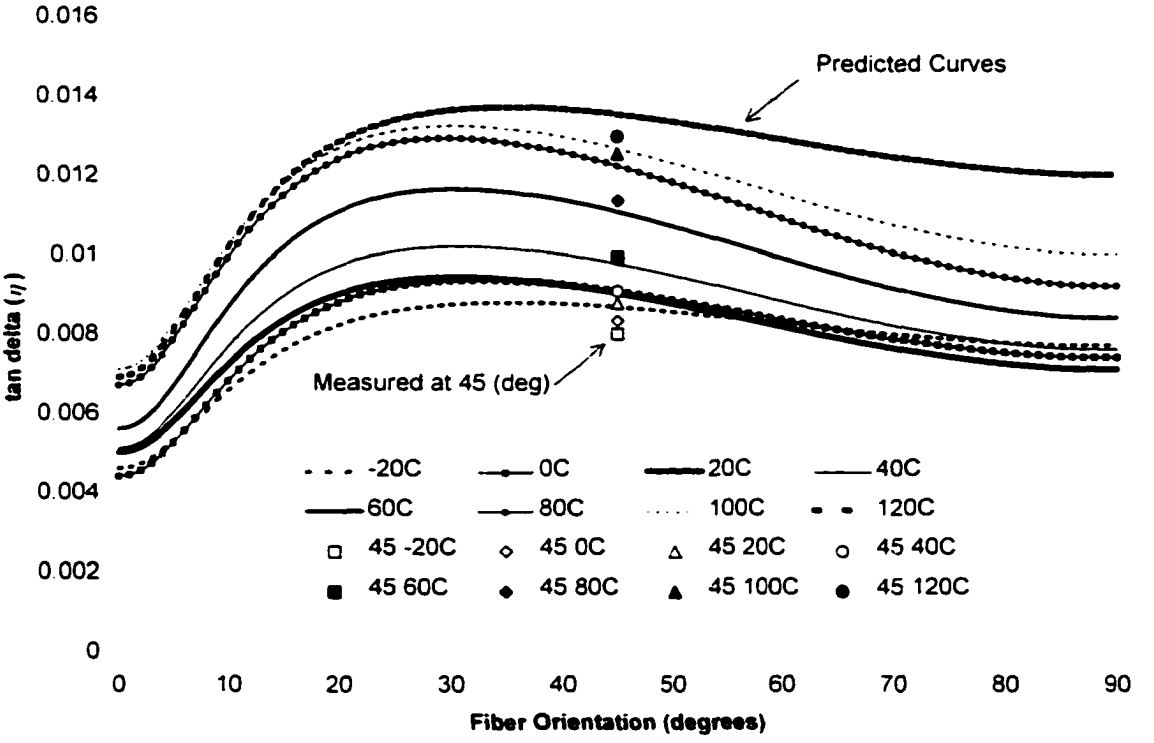

Figure 7.11 - Variation of damping factor with fiber orientation for PEEK/IM7.

Figure 7.11 shows that the largest variation in damping loss factor, *tan δ*, occurs between 40°C and 80°C. This can be an indication of a sub-T_g temperature transition of the polymer matrix in this temperature region. A DMA temperature scan of the unreinforced polymer, would be necessary to confirm this hypothesis. This test was not performed due to the unavailability of the unreinforced polymer.

7.4.2 Changes in Viscoelastic Properties with Frequency

The measurement of viscoelastic properties over a frequency range allows the determination of the material response to various shear rates. In this study, frequency effects in viscoelastic properties of PEEK/IM7 unidirectional beams with different fiber orientations were investigated by sweeping the frequency across a frequency range of two decades, from 0.1 Hz to 10 Hz, at a constant temperature of approximately 20°C (room temperature). Figures 7.12 to 7.15 show results corresponding to two specimens for each fiber orientation.

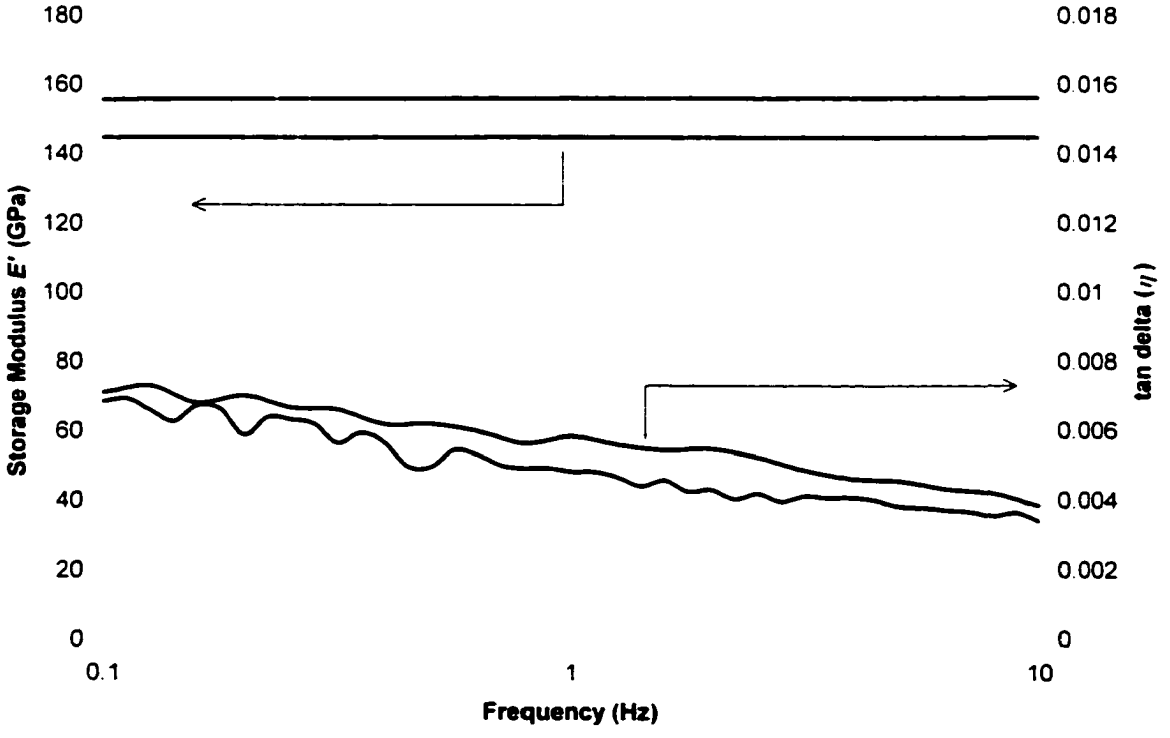

Figure 7.12 - Frequency sweep data for two unidirectional beams with fibers oriented at 0°.

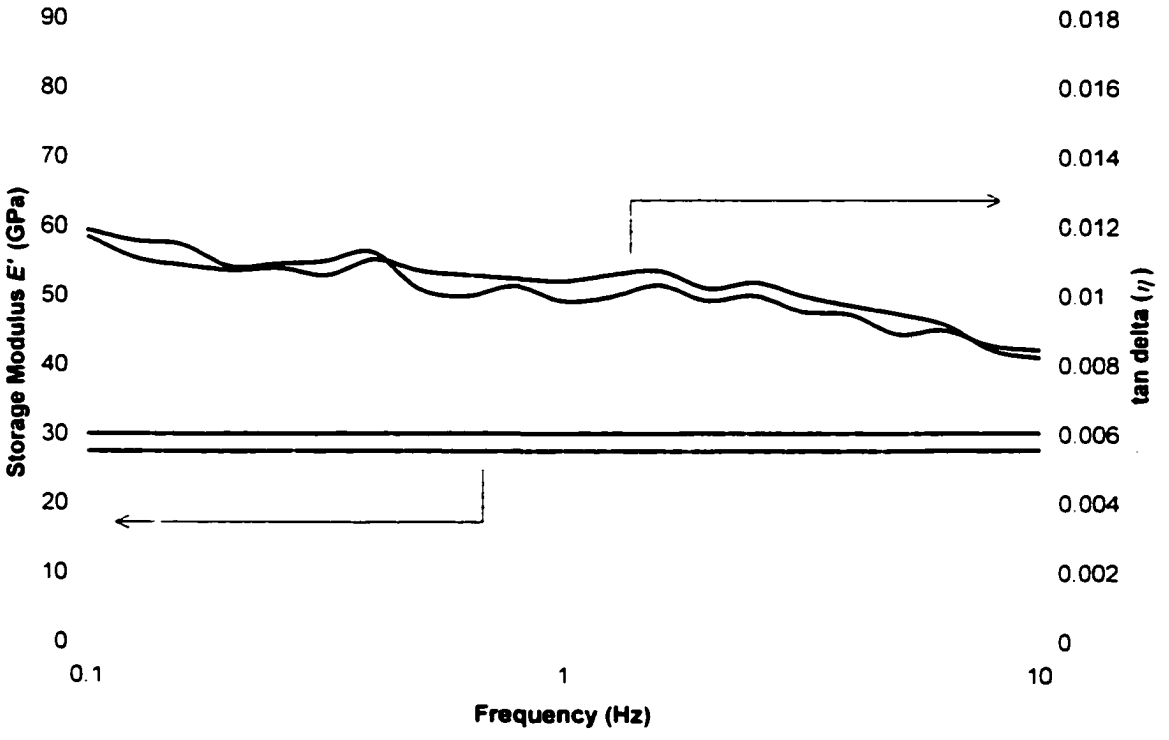

Figure 7.13 - Frequency sweep data for two unidirectional beams with fibers oriented at 30°.

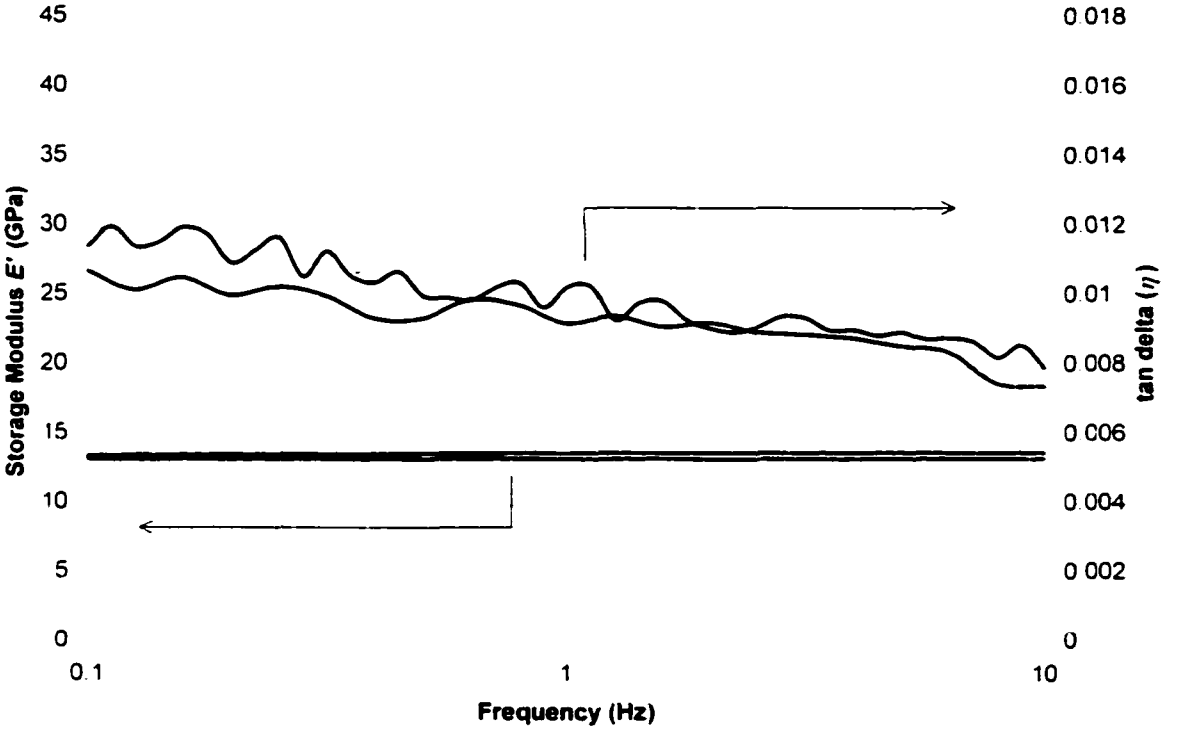

Figure 7.14 - Frequency sweep data for two unidirectional beams with fibers oriented at 45°.

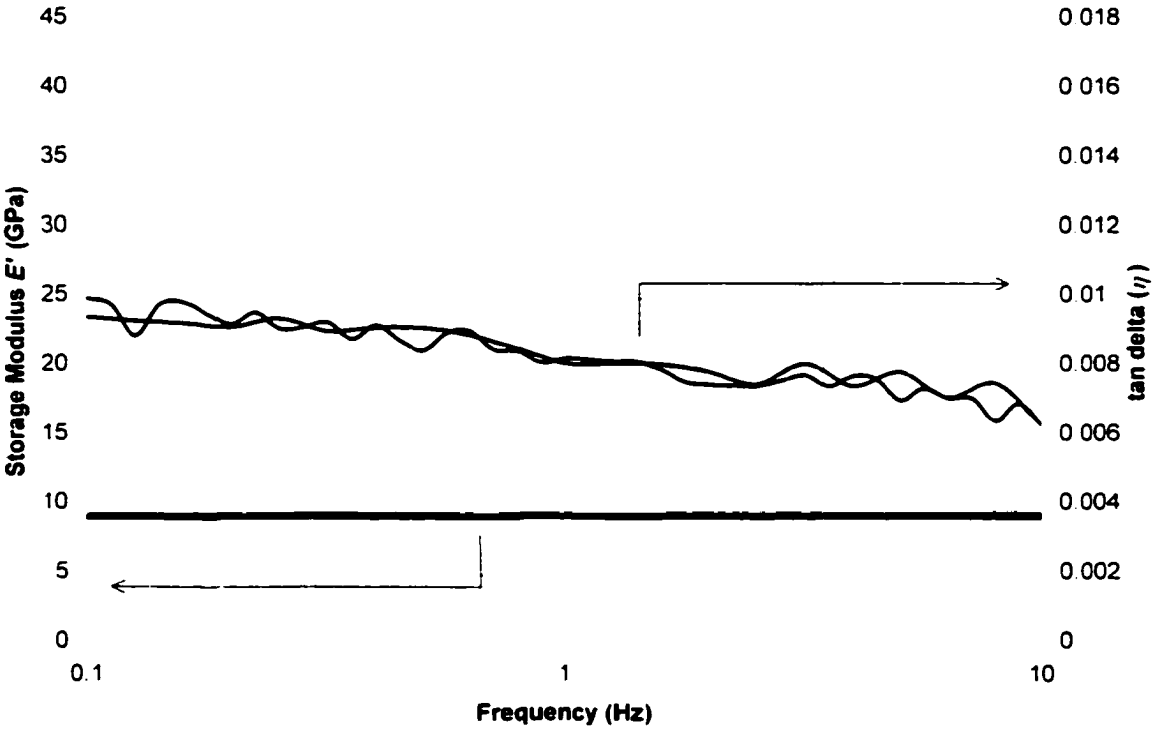

Figure 7.15 - Frequency sweep data for two unidirectional beams with fibers oriented at 90°.

The plots show that the storage modulus is relatively constant over the frequency range, while the loss factor shows a general reduction with frequency. In order to calculate the averages of measured storage modulus and loss factor data from two bend-beam specimens in each fiber orientation, (Figures 7.12 to 7.15), a linear fit was applied to the raw storage modulus data, while for the loss factors, a logarithmic fit was

used to proper represent the measured frequency dependency. The average storage modulus and loss factor data for all fiber orientations tested, are presented in Figure 7.16.

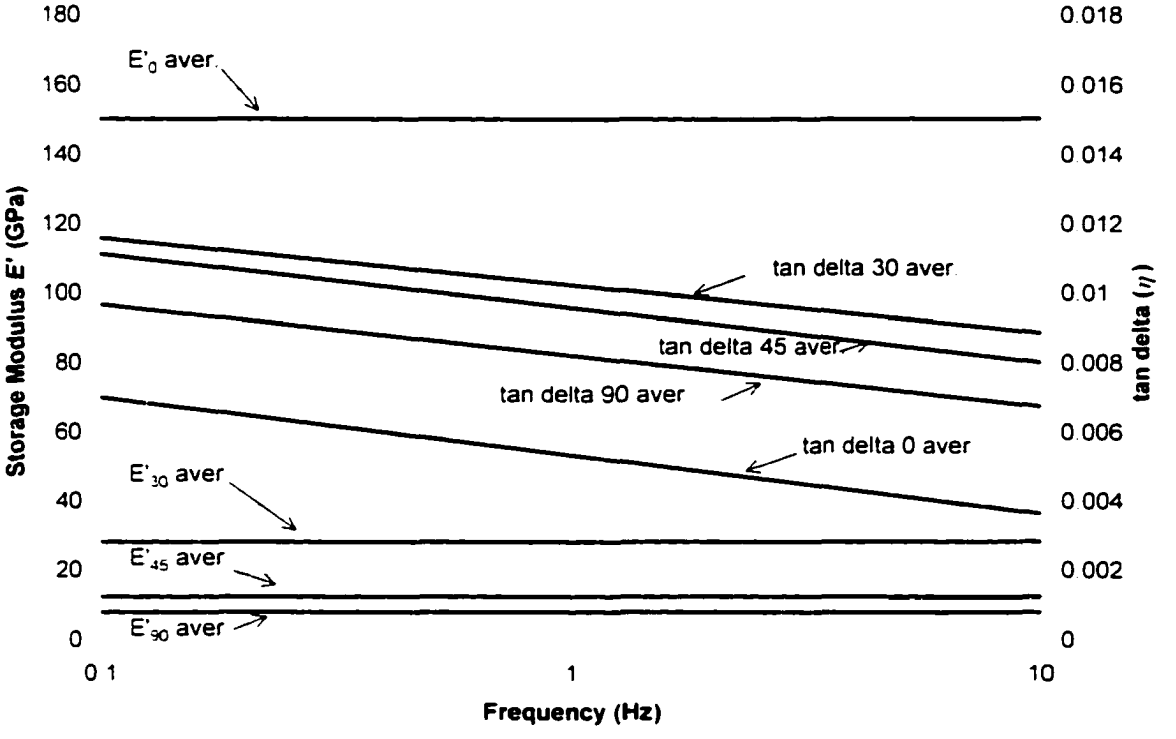

Figure 7.16 - Frequency dependence of storage modulus and loss factor for unidirectional beams. (average values)

The average of the measured viscoelastic properties for the beam specimens with fiber orientations of 0°, 30°, and 90° (Figure 7.16), and the Poisson's ratios, ν_{12} and ν_{23}, previously determined in the elastic characterization, were used for the determination of the viscoelastic properties of PEEK/IM7 at different frequencies. The properties were calculated at frequencies of 0.1, 1.0 and 10 Hz. The shear storage modulus and loss factor, G'_{12} and η_6, at each frequency, were determined through the application of equations (6.23) and (6.24), presented in Chapter 6. After calculation of the shear storage

modulus and loss factor. for the three frequencies. the frequency dependence of the nine independent parameters that completely characterize the material. is presented in Table 7.3. The same results are also presented in graphical form in Figure 7.17.

Table 7.3 - Frequency dependence of the viscoelastic properties of PEEK/IM7.

Freq. (Hz)	E'_1 (GPa)	E'_2 (GPa)	G'_{12} (GPa)	ν_{12}	ν_{23}	η_1 (10^{-3})	η_2 (10^{-3})	η_6 (10^{-3})
0.1	151.4	9.3	7.7	0.34	0.49	7.1	9.8	12.8
1.0	151.5	9.3	7.7	0.34	0.49	5.4	8.3	11.6
10.0	151.7	9.3	7.8	0.34	0.49	3.8	6.9	10.2

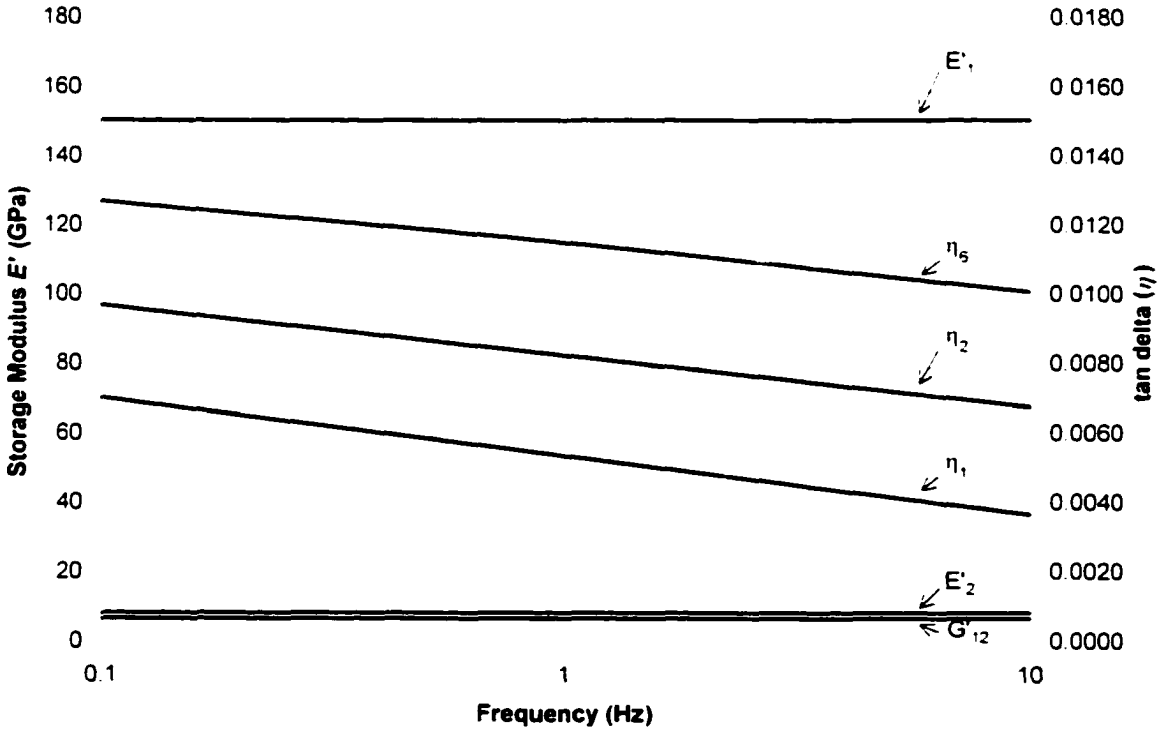

Figure 7.17 - Variation of Storage moduli and loss factors with frequency for PEEK/IM7.

The calculations assume that the Poisson's ratios, ν_{12} and ν_{23}, are not frequency dependent. The assumption of Poisson's ratios independent of frequency has been considered in the past, by other authors [115,118]. In fact, measurements of the Poisson's ratios for fiber reinforced specimens, over a frequency range of 298Hz to 18kHz, did not show any significant change with frequency [118]. In this work, the assumption of Poisson's ratios independent of frequency allows the values obtained from the elastic characterization of the material to be directly applied in these frequency dependence dynamic studies.

According to data presented in Table 7.3, the storage moduli E'_1, E'_2 and G'_{12}, were practically independent of frequency over the range studied. However, changes in damping with frequency were considerable. Even in the fiber direction (1-axis) where the changes in modulus are very small, considerable changes in damping were detected, over the frequency range. The loss factor η_1, corresponding to the fiber direction, varied from 7.1×10^{-3}, at 0.1 Hz, to 3.8×10^{-3}, at 10 Hz, which represents a 46% change. For η_2, the measurements varied from 9.8×10^{-3}, at 0.1 Hz, to 6.9×10^{-3}, at 10 Hz, thus decreasing 42%. Finally, the shear loss factor, η_6, varied from 12.8×10^{-3}, at 0.1 Hz, to 10.2×10^{-3}, at 10 Hz, corresponding to a 20% decrease. Figure 7.17 shows that the lines of frequency dependence of the three damping loss factors, η_1, η_2, and η_6, are roughly parallel to each other. However, the absolute values from Table 7.3 show a larger variation of η_1 compared to the other two loss factors. The limited data used in this research is not enough for a conclusive statement regarding this observation.

These frequency sweep measurements were performed at a temperature of approximately 20°C, and all the temperature sweep tests previously presented were

conducted at a frequency of 1.0Hz. Therefore, the properties obtained from the frequency sweep tests at 1.0Hz (Table 7.3), and those from temperature sweep tests at 20°C, (Table 7.1), is should be similar. The comparison is presented in Table 7.4. The table shows a good agreement for the three storage moduli, E'_1, E'_2, and G'_{12} obtained from the two types of measurements. However, all damping loss factors determined from frequency sweep tests were larger than those from temperature sweep tests.

Table 7.4 - Properties of PEEK/IM7 determined from temperature and frequency sweep tests.

Property	Freq. sweep	Temp. sweep	Difference
E'_1(GPa)	151.5	154.9	2%
E'_2(GPa)	9.3	10.0	7%
G'_{12}(GPa)	7.7	7.2	6%
η_1 (10^{-3})	5.4	5.1	6%
η_2 (10^{-3})	8.3	7.2	13%
η_6 (10^{-3})	11.6	10.6	8%

The smaller damping factors determined from the temperature sweep tests might be related to the rate of temperature increase used on these tests. All temperature sweep tests started at very low temperatures (-25°C) and the temperature was then increased at a constant rate of 3°C/min to the final temperature of 125°C. This procedure allowed data to be collected over the temperature range of -20°C to 120°C. The low damping loss factors obtained in these temperature tests may be an indication that the heating rate was too high and, at the time of the measurements, the specimen, or at least the internal layers of the specimen, was at a lower temperature than the equipment chamber, where the temperature is measured. The lower temperature of the specimens would explain the lower loss factors measured. The damping properties obtained at 40°C agree well with frequency sweep data, thus supporting this suggestion. Further, the largest difference

between the two tests, 13%, was observed in the damping factor η_2. In this case, in addition to the possibility of temperature gradient between the specimen and equipment chamber, Figure 7.9 shows a non-expected drop in the damping factor η_2, at 20°C, which may be an indication of inaccurate measured data at this temperature. Temperature sweep tests at a lower heating rate would confirm the suggestion of a thermal lag in the measured data. If this is verified, then a temperature shift would need to be applied to the data presented.

Using the viscoelastic properties determined at three frequencies (Table 7.3), equations (6.23) and (6.24) are applied to determine the viscoelastic properties, of unidirectional off-axis beams with any included angle, where $0° \leq \theta \leq 90°$. Storage modulus and loss factor prediction for unidirectional PEEK/IM7 beams as a function of fiber orientation, for frequencies of 0.1, 1.0, and 10.0Hz, are plotted in Figure 7.18 and Figure 7.19. Both figures also show the average of the measured data, from two 45° fiber orientation specimens, at each frequency studied, for comparison with predicted properties at that angle. Both plots show reasonably good agreement between the properties predicted for a specimen with included angle of 45° and the experimental measurements at that angle.

In Figure 7.18, only one line can be seen because of the small change in storage modulus over the frequency range studied. As in the case of temperature sweep tests, predictions of both, storage modulus and loss factor, for a specimen with included angle of 45°, were larger than measured data at that angle. For the damping loss factor, the agreement was very good for the lowest frequency measured, 0.1 Hz, with the deviation increasing for higher frequencies.

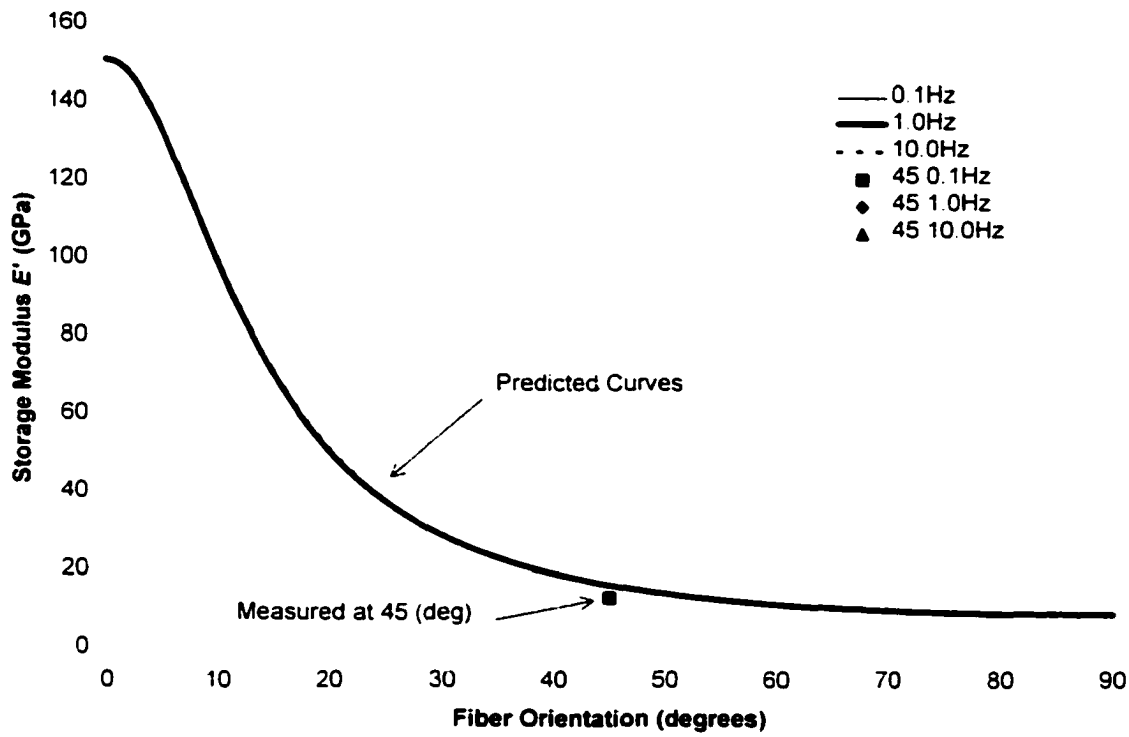

Figure 7.18 - Variation of storage moduli with fiber orientation for different frequencies.

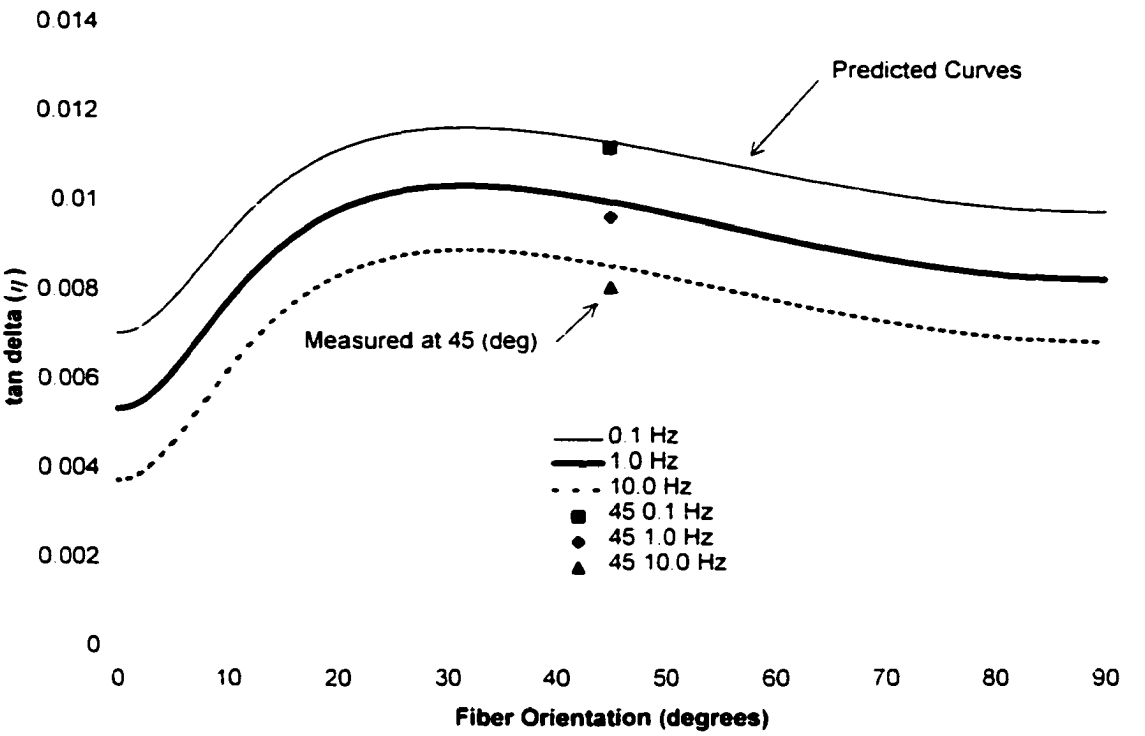

Figure 7.19 - Variation of loss factors with fiber orientation for different frequencies.

In general, at low frequencies polymeric materials flow more, acting in a similar fashion to flow at elevated temperature, thus showing a larger damping. As the frequency increases, the material behaves more elastically. Therefore, both storage modulus and loss factor vary with frequency. As mentioned in previous sections, the damping of carbon fiber reinforced polymeric composites is derived mainly from the matrix and the fiber/matrix interface response. The decrease in *tan* δ of the composite material with frequency is related to restrictions of chain motions of the polymer at

higher frequencies. The same effect is also responsible for an increase in storage modulus. The results show that the damping, *tan* δ, is considerably more sensitive to changes in frequency than the storage modulus.

The frequency dependency may be more considerable, at temperatures near the region of a transition such as the T_g, because of the temperature-frequency equivalence. For the composite material evaluated herein, the glass transition temperature of the polymeric matrix determined by Differential Scanning Calorimetry (DSC) is in the region of 150°C (see Chapter 5), and the frequency sweep tests were conducted at room temperature (approximately 20°C). In general, an increase in frequency will increase the temperature at which the transition occurs (see Figure 2.5) as less time is available for molecular rearrangement. Therefore, the frequency dependency of the viscoelastic properties is even more critical if the usage temperature is near the range where a thermal transition occurs.

7.5 Results and Discussion – Laminate Characterization

As in the study involving unidirectional beams, for the laminated beams, temperature and frequency sweep dynamic tests were conducted under sinusoidal strain-control mode. Temperature sweep tests were carried out over the range of -20°C to 120°C, with heating rate of 3°C/min. Frequency effects on the viscoelastic properties of laminates were investigated by sweeping the frequency across a frequency range of two decades, from 0.1 Hz to 10 Hz, at a constant temperature of approximately 20°C. Laminate measured properties are presented in Figures 7.20 to 7.25. The first three plots show results from

temperature sweep tests and the remaining three plots show frequency sweep results. corresponding to two specimens for each lamination tested.

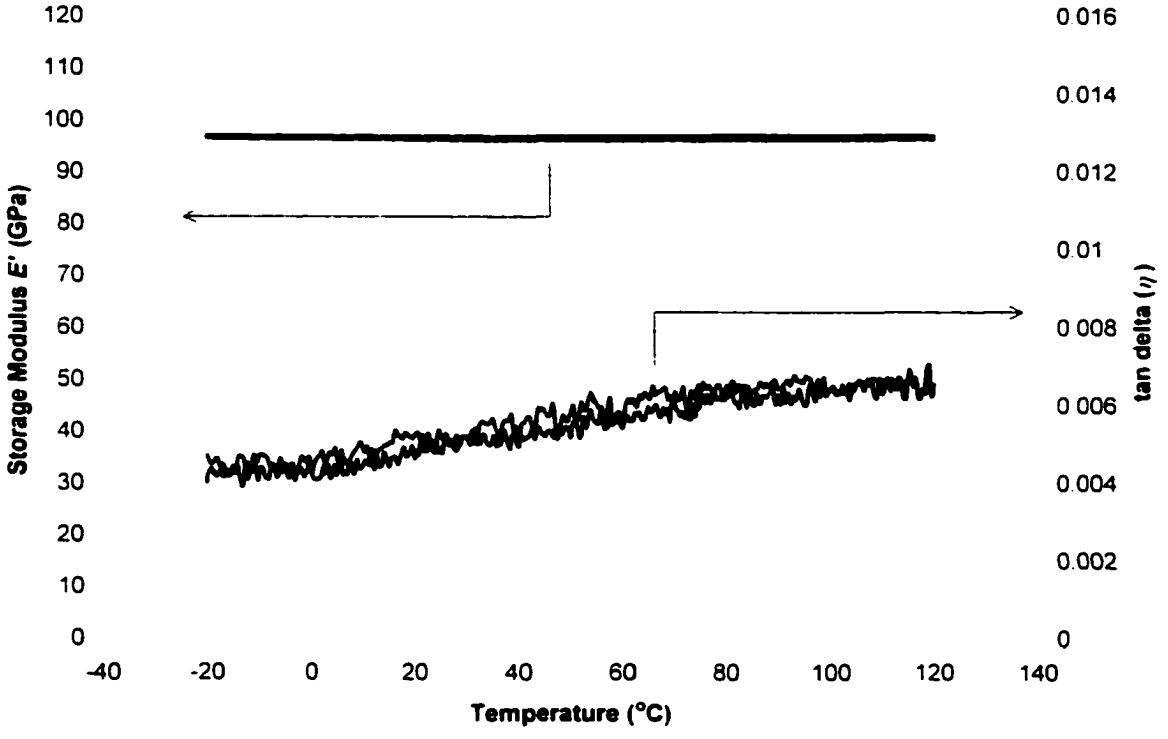

Figure 7.20 - Temperature sweep data for two $[(0/90)_2]_s$ laminated beams.

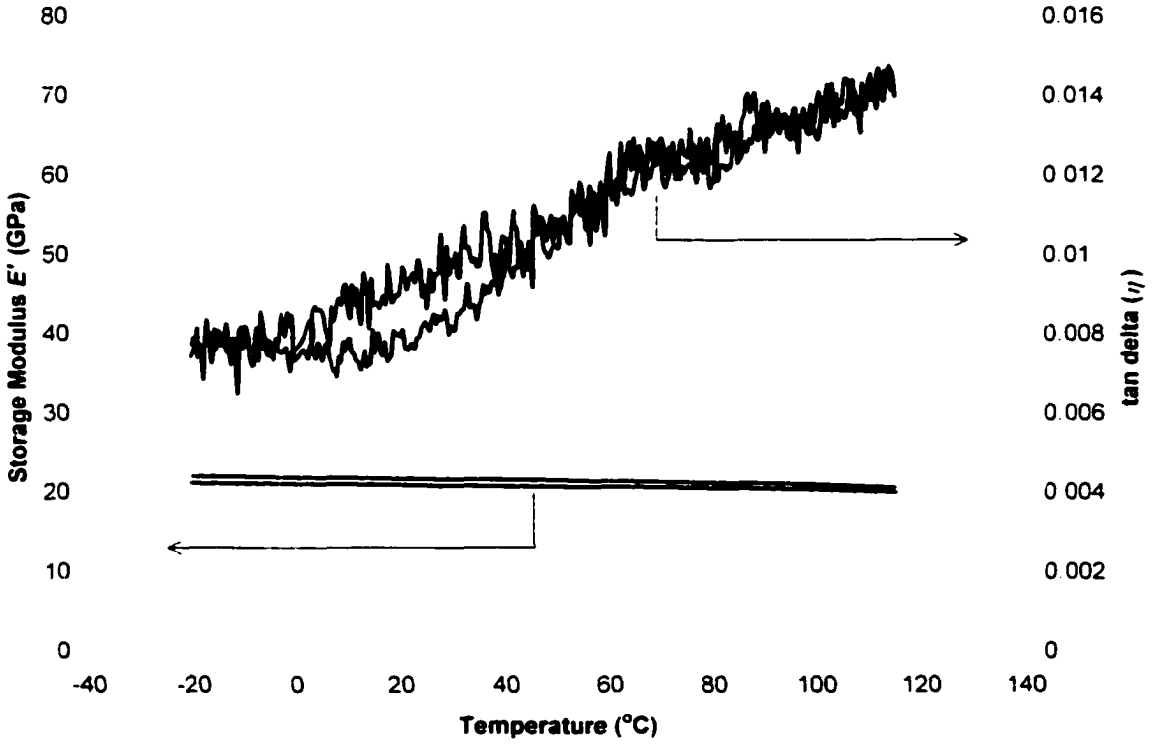

Figure 7.21 - Temperature sweep data for two $[(+45/-45)_2]$, laminated beams.

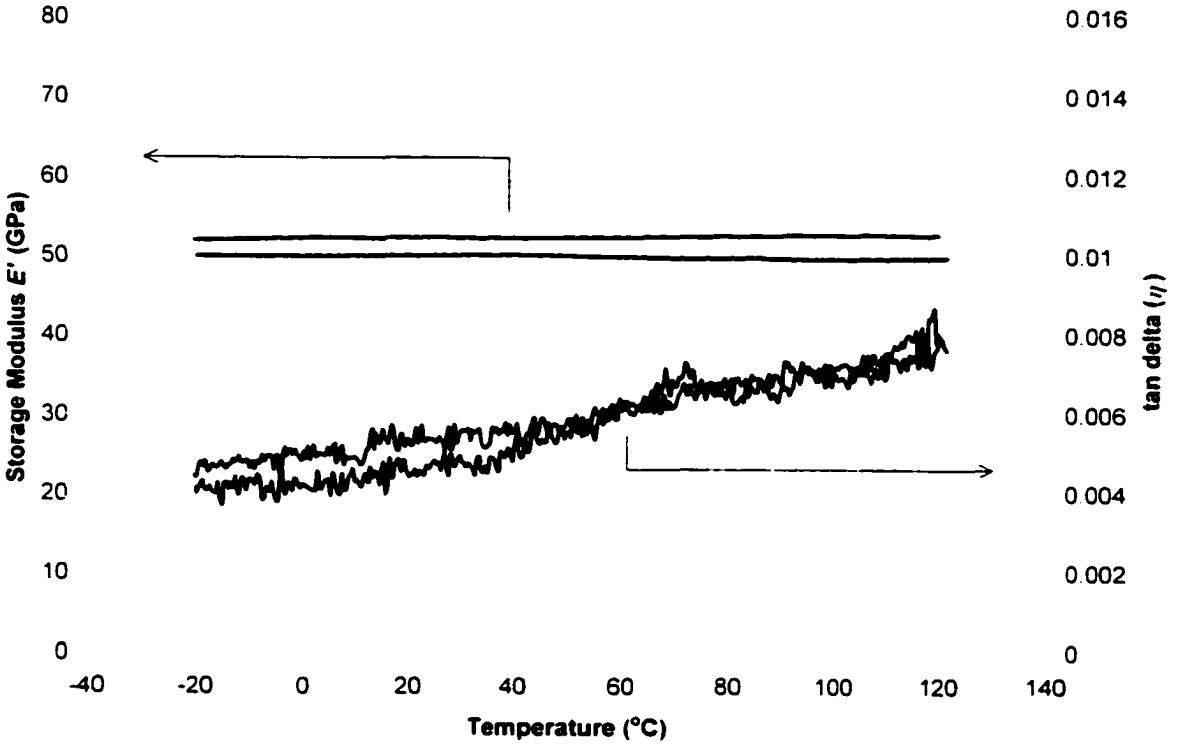

Figure 7.22 - Temperature sweep data for two $[(90/0)_2]_s$ laminated beams.

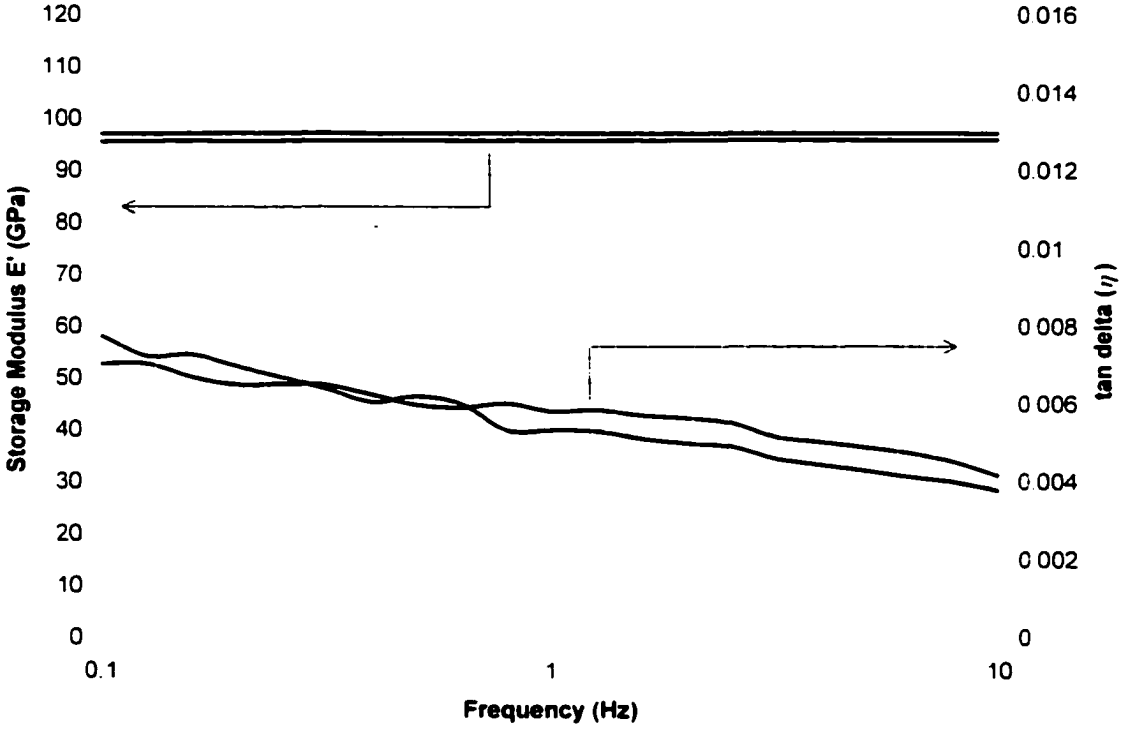

Figure 7.23 - Frequency sweep data for two $[(0/90)_2]$, laminated beams.

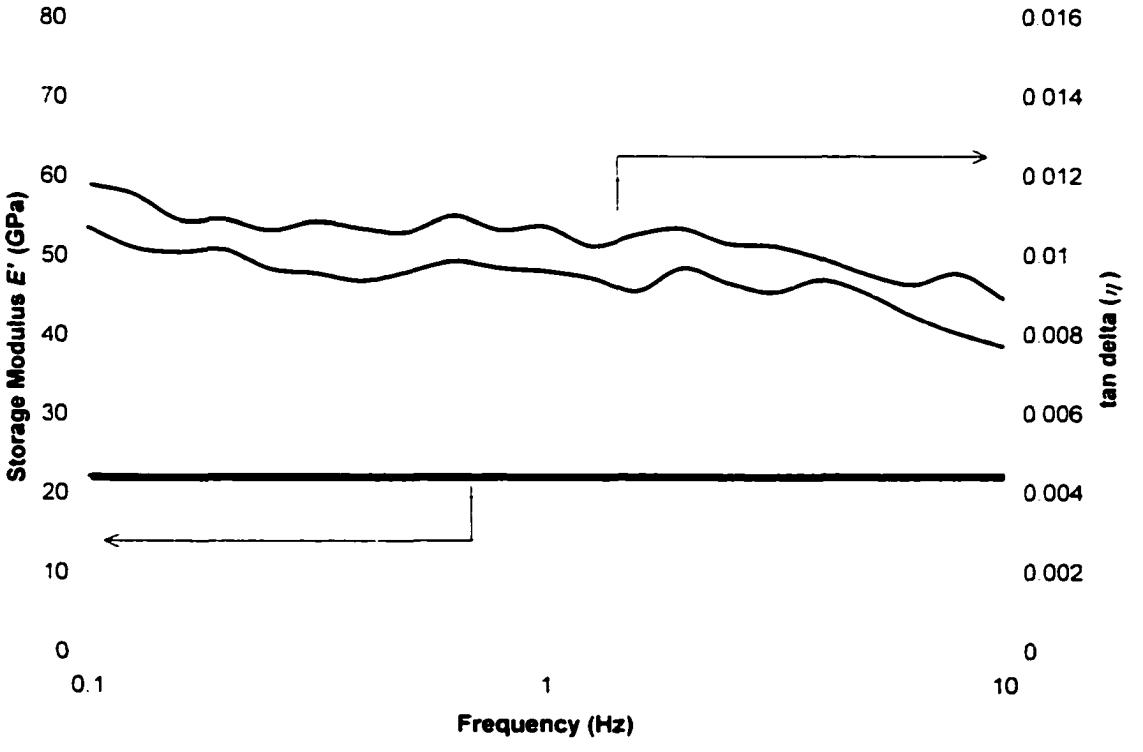

Figure 7.24 - Frequency sweep data for two $[(+45/-45)_2]_s$ laminated beams.

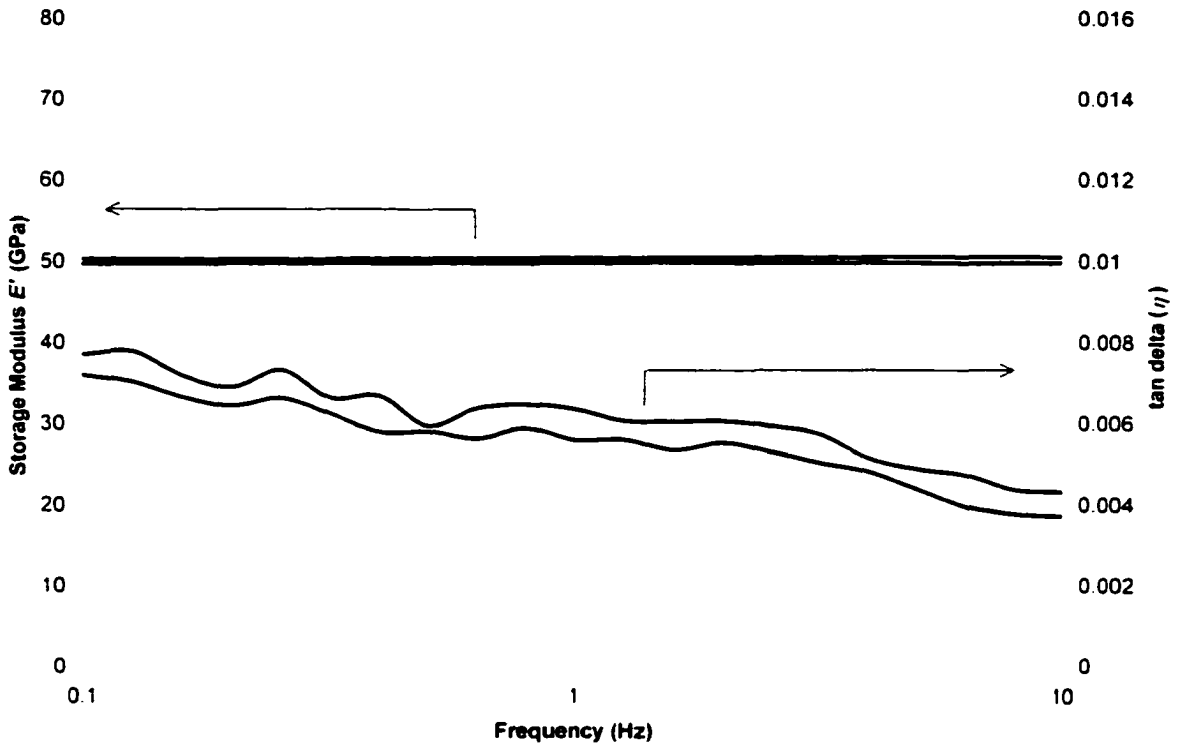

Figure 7.25 - Frequency sweep data for two $[(90/0)_2]_s$ laminated beams.

The properties measured for each laminate, through temperature sweep and frequency sweep tests, were averaged for comparison with predicted properties based on laminate models. The averaging process applied was the same used with the unidirectional beams. For the temperature dependence, a linear fit was applied to smooth the storage modulus data and a sixth degree polynomial was applied to smooth the damping loss factor. For the frequency sweep data, a linear fit was again applied to the storage modulus and, for the damping loss factor, a logarithmic fitting was used.

The two laminate models discussed in Chapter 6 are used in this research for comparison purposes. The ability of these models to accurately predict laminate viscoelastic properties, for the material studied, is evaluated. The viscoelastic properties

of the three laminates, measured over temperature and frequency ranges, are compared with the predicted values using measured laminae properties, for verification. This procedure allows verifying if the models can also produce laminate properties in ranges of frequencies and temperatures. Since it was not the goal of this research to generate new models for the prediction of laminate damping from lamina properties, but rather to generate an approach that allows the accurate determination of lamina constituent properties, it was determined that an assessment of existing models would be instructive.

The 3-D viscoelastic characterization of the PEEK/IM7 prepreg lamina, as a function of temperature and frequency, was presented in Table 7.1 and Table 7.3, respectively. The application of these properties in the two laminate models, allows the determination of the viscoelastic properties, dynamic modulus and loss factor, of laminated beams. Matlab computer codes implementing each of the two models (Appendix 8) were used for fast determination of laminated beam viscoelastic properties.

The temperature dependence results for the three laminates studied are presented in Tables 7.5, 7.7, and 7.9, while Tables 7.6, 7.8, and 7.10, show the laminate properties related to frequency. The tables present the averaged measurements and the predicted properties using models 1 and 2 (Chapter 6). In figures 7.26 to 7.31 the same data presented in tables 7.5 to 7.10 are shown in graphic form.

For the $[(0/90)_2]_s$ and $[(90/0)_2]_s$ specimens, both models, 1 and 2, result in the same predictions since the terms $\bar{\eta}_{12}$ and $\bar{\eta}_{16}$ are null for all 0° and 90° layers. Thus, the term $g^{(k)}$ given by equation (6.41) or (6.54), which is the only difference between the two models, is the same in for these two lamination sequences. For the storage modulus,

models 1 and 2, produce the same values for all symmetric stacking sequences, including $[(+45/-45)_2]_s$.

Table 7.5 - Temperature dependence of viscoelastic properties of $[(0/90)_2]_s$ PEEK/IM7 laminated beams.

	Measured		Models 1 and 2	
Temp. (°C)	E'(GPa)	η (10^{-3})	E'(GPa)	η (10^{-3})
-20	97.3	4.5	110.7	4.8
0	97.3	4.5	110.4	4.6
20	97.3	5.0	110.2	5.2
40	97.3	5.5	110.1	5.3
60	97.3	6.0	110.0	5.8
80	97.3	6.4	109.8	6.9
100	97.4	6.6	109.5	7.3
120	97.4	6.6	109.4	7.2

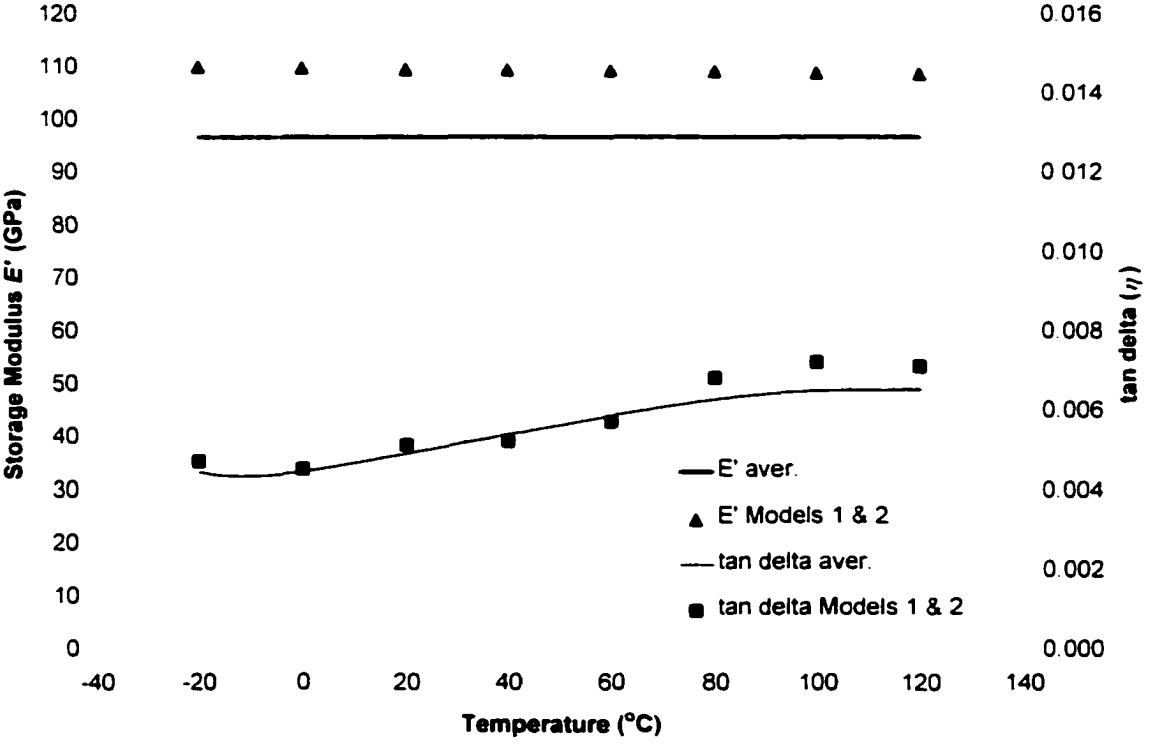

Figure 7.26 - Temperature sweep data (average values) for a $[(0/90)_2]_s$ laminated beam and the predicted properties by laminate models 1 and 2.

Table 7.6 - Frequency dependence of viscoelastic properties of $[(0/90)_2]_s$ PEEK/IM7 laminated beams.

	Measured		Models 1 and 2	
Freq. (Hz)	E'(GPa)	η (10^{-3})	E'(GPa)	η (10^{-3})
0.1	97.3	7.4	107.6	7.2
1.0	97.3	5.8	107.6	5.5
10.0	97.5	4.2	107.8	3.9

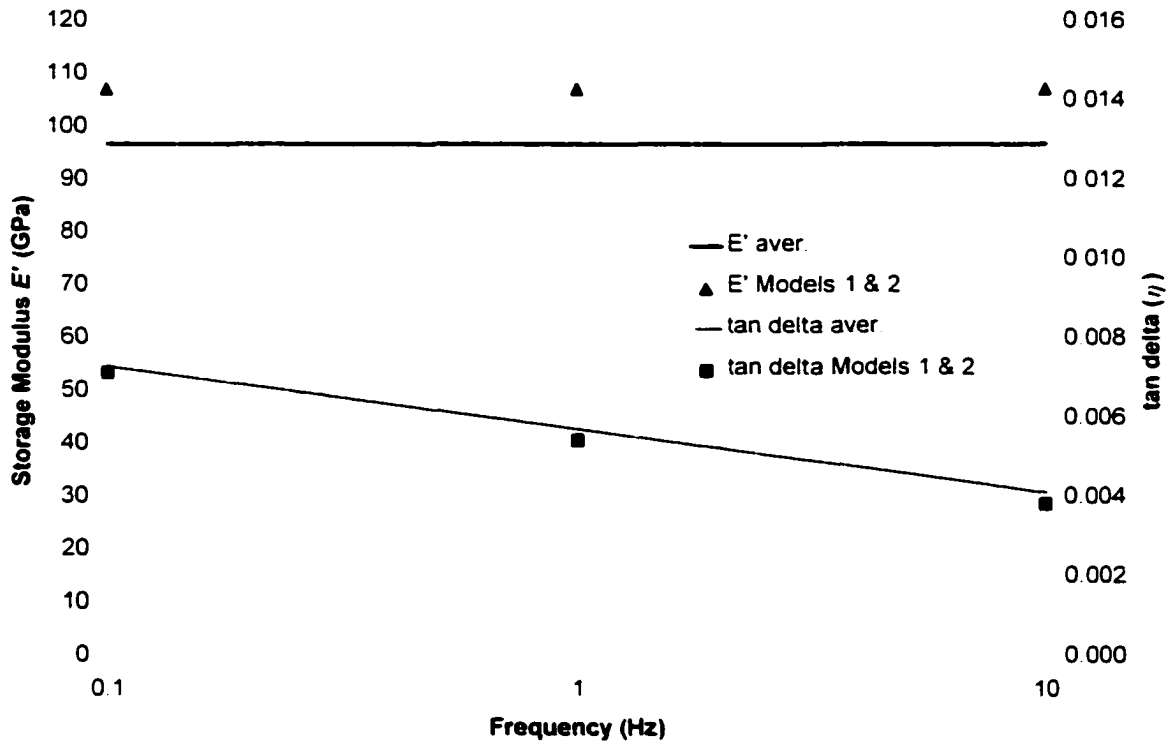

Figure 7.27 - Frequency sweep data (average values) for a $[(0/90)_2]_s$ laminated beam and the predicted properties by laminate models 1 and 2.

Table 7.7 - Temperature dependence of viscoelastic properties of $[(+45/-45)_2]_s$ PEEK/IM7 laminated beams.

	Measured		Model 1		Model 2	
Temp. (°C)	E'(GPa)	η (10^{-3})	E'(GPa)	η (10^{-3})	E'(GPa)	η (10^{-3})
-20	22.2	7.8	24.9	8.4	24.9	7.6
0	22.0	7.9	24.6	9.8	24.6	8.3
20	21.9	8.6	24.3	9.9	24.3	8.4
40	21.7	10.0	24.0	10.7	24.0	9.0
60	21.5	11.6	24.0	12.3	24.0	10.2
80	21.4	12.8	23.7	13.6	23.7	11.3
100	21.2	13.6	23.7	13.9	23.7	11 7
120	21.0	15.1	23.4	14.1	23.4	12.3

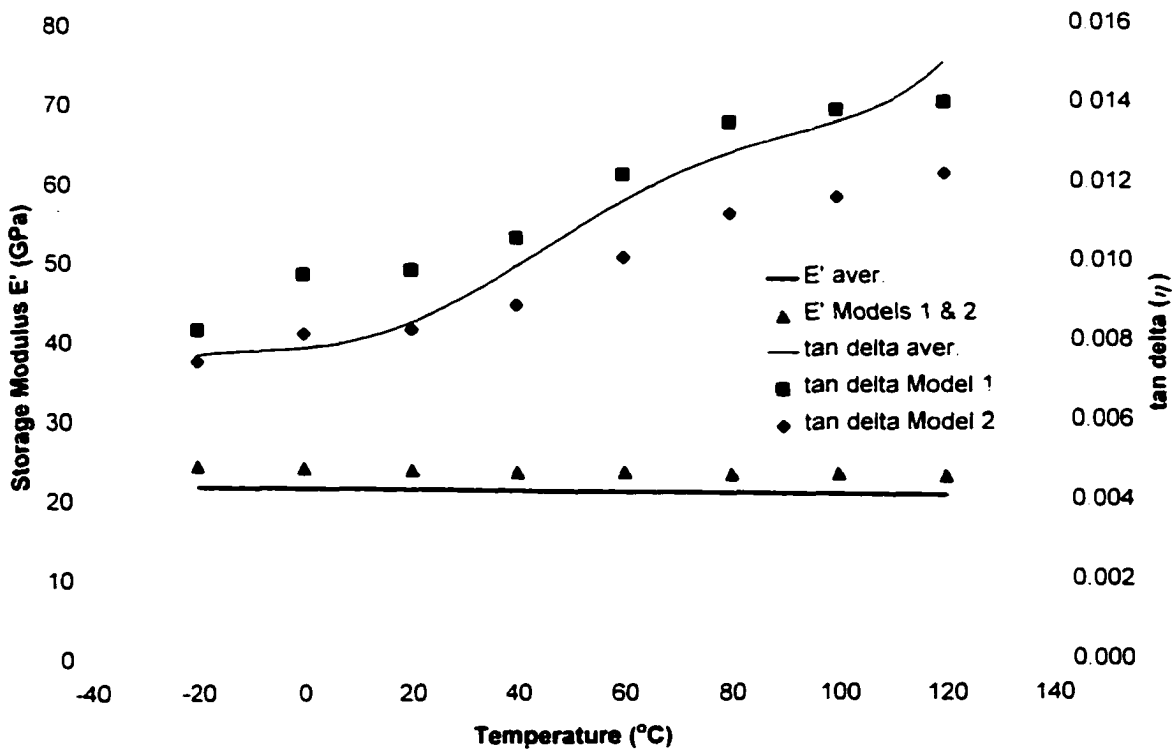

Figure 7.28 - Temperature sweep data (average values) for a $[(+45/-45)_2]_s$ laminated beam and the predicted properties by laminate models 1 and 2.

Table 7.8 - Frequency dependence of viscoelastic properties of $[(+45/-45)_2]_s$ PEEK/IM7 laminated beams.

	Measured		Model 1		Model 2	
Freq. (Hz)	E'(GPa)	η (10^{-3})	E'(GPa)	η (10^{-3})	E'(GPa)	η (10^{-3})
0.1	22.5	11.1	25.5	12.1	25.5	10.6
1.0	22.5	10.0	25.6	10.8	25.6	9.2
10.0	22.6	9.0	25.8	9.4	25.8	7.8

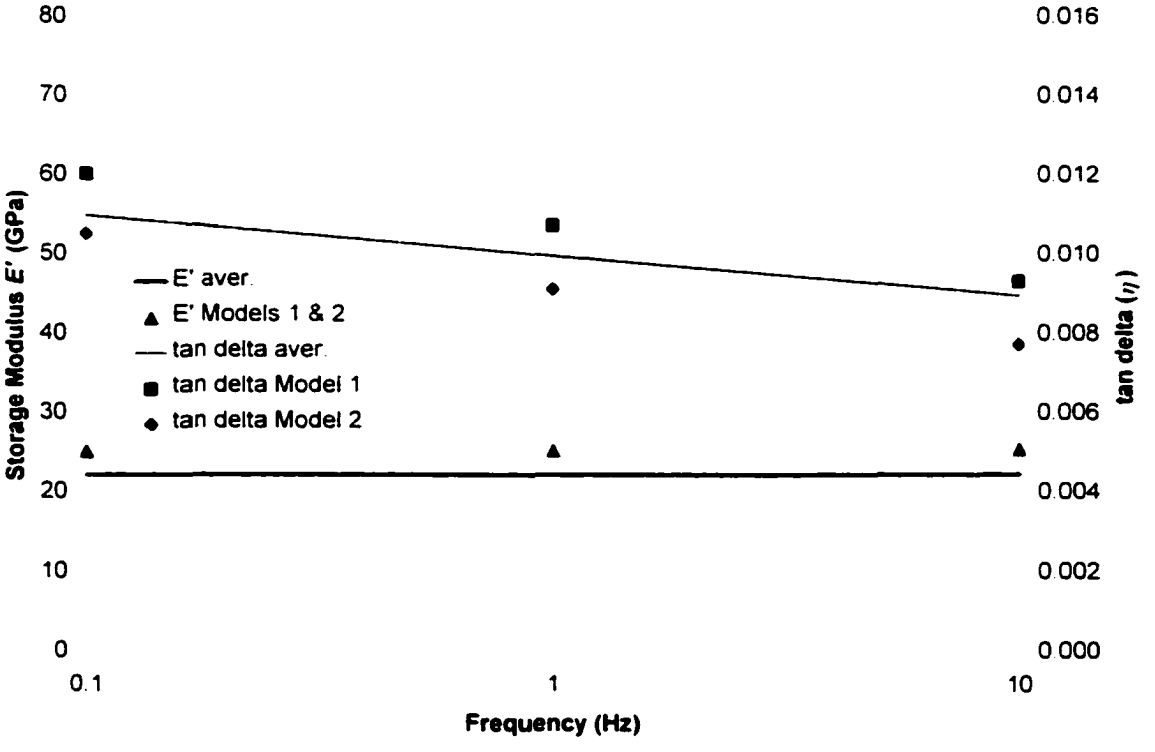

Figure 7.29 - Frequency sweep data (average values) for a $[(+45/-45)_2]_s$ laminated beam and the predicted properties by laminate models 1 and 2.

Table 7.9 - Temperature dependence of viscoelastic properties of $[(90/0)_2]_s$ PEEK/IM7 laminated beams.

	Measured		Models 1 and 2	
Temp. (°C)	E'(GPa)	η (10^{-3})	E'(GPa)	η (10^{-3})
-20	51.6	4.5	55.9	5.1
0	51.6	4.7	55.7	4.9
20	51.6	5.0	55.6	5.4
40	51.7	5.5	55.5	5.5
60	51.7	6.2	55.4	6.0
80	51.7	6.9	55.3	7.1
100	51.7	7.2	55.1	7.6
120	51.7	8.1	55.0	7.6

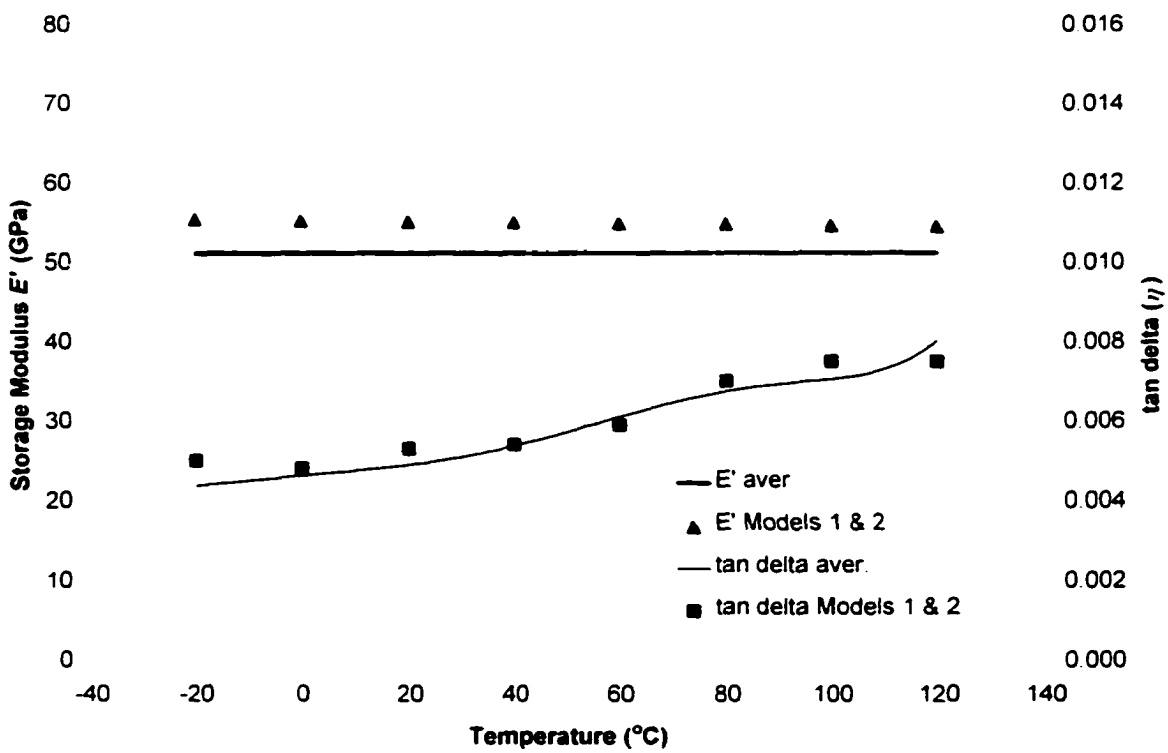

Figure 7.30 - Temperature sweep data (average values) for a $[(90/0)_2]_s$ laminated beam and the predicted properties by laminate models 1 and 2.

Table 7.10 - Frequency dependence of viscoelastic properties of $[(90/0)_2]_s$ PEEK/IM7 laminated beams.

	Measured		Models 1 and 2	
Freq. (Hz)	E'(GPa)	η (10^{-3})	E'(GPa)	η (10^{-3})
0.1	50.6	7.5	54.0	7.4
1.0	50.6	5.9	54.0	5.7
10.0	50.9	4.4	54.1	4.2

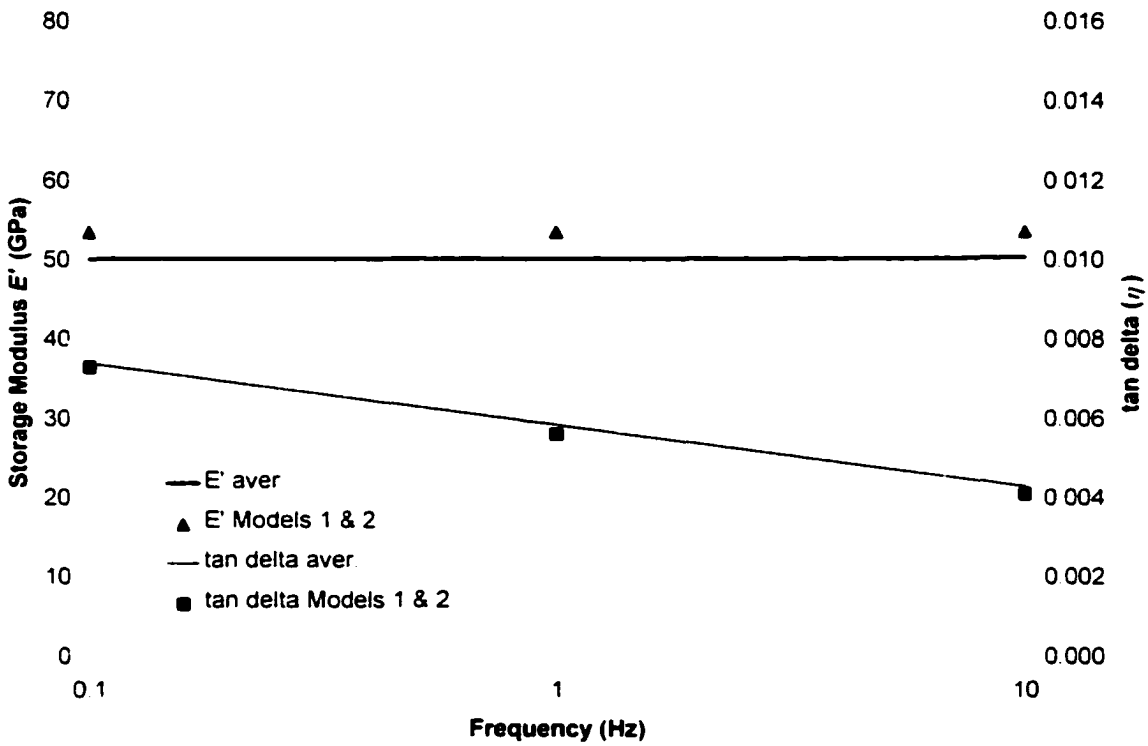

Figure 7.31 - Frequency sweep data (average values) for a $[(90/0)_2]_s$ laminated beam and the predicted properties by laminate models 1 and 2.

The data presented in Figures 7.26 to 7.31 show a very good agreement between the predicted and measured loss factors, in all three laminates tested, for both frequency and temperature dependence. For both $[(0/90)_2]_s$ and $[(0/90)_2]_s$ stacking sequences, models 1 and 2 give the same predicted loss factor, for each of the laminates, which, in both cases,

agree closely with the measurements, throughout the frequency and temperature ranges studied. Comparing the measured data for the $[(+45/-45)_2]_s$ laminate with the predictions based on the two models, it can be seen that for both, temperature sweep and frequency sweep tests, the average loss modulus measured is bounded by the two model predictions. The only discrepancy occurred at the high-temperature end of the temperature sweep test, where both models predictions shows a smaller increase of $tan\ \delta$ with temperature, compared to the average measured loss factor.

Figures 7.26 to 7.31 show that the measured laminate storage modulus were, in all cases, about 10% smaller than the properties predicted by the models. The modulus predictions for the laminates were based on laminae properties, measured by the same equipment and according to the same procedures as the measured laminate properties. A comparison between DMA measured laminae moduli and moduli obtained from elastic characterization was presented in Table 7.2. It was found that the DMA dynamic measurements resulted in smaller values only for the fiber direction modulus, E_1, with a 6% difference, while for the other two moduli, E_2 and G_{12}, the dynamic measurements were a little larger. Therefore, laminae results do not indicate smaller modulus measurements by the DMA bend-beam tests as a trend. However, both laminate models used to predict the properties of laminated beams, assume that all layers are perfectly bonded together. Thus, the lower measured values, compared to the predictions, may be an indication of debonding, or at least not perfect bonding, between layers. This hypothesis would explain why the lower modulus was only observed in cross-ply laminates and not in the unidirectional specimens.

Repeating the cross-check procedure performed with laminae measured properties, a comparison is made between viscoelastic properties obtained from temperature sweep tests at 20°C, and those from the frequency sweep tests at 1.0Hz. The comparison is presented in Table 7.11. The table shows that the storage modulus values measured in both types of test are in very good agreement. However, in all three laminates, the damping loss factor measured in the temperature sweep tests was about 15% lower than those from the frequency sweep measurements. This trend was also observed in all laminae tests and is suggested as being related to a high rate of temperature change in the temperature sweep tests leading to a thermal lag in the data.

Table 7.11 - Viscoelastic properties of PEEK/IM7 laminated beams determined from temperature and frequency sweep tests.

	$[(0/90)_2]_s$		$[(+45/-45)_2]_s$		$[(90/0)_2]_s$	
Method	E'**(GPa)**	η **(10^{-3})**	E'**(GPa)**	η **(10^{-3})**	E'**(GPa)**	η **(10^{-3})**
Temp. sweep	97.3	5.0	21.9	8.6	51.6	5.0
Freq. sweep	97.3	5.8	22.5	10.0	50.6	5.9
Difference	-	14%	3%	14%	2%	15%

In general, the data presented in this section show good agreement between the predicted and measured viscoelastic properties for all three laminates studied, over the range of frequency and temperature investigated. This agreement indicates that the laminate models from the published literature are able to predict laminate behavior, not only at room temperature, but over a range of temperature and also, a range of frequency. Further, since the predicted laminate behavior was based on laminae properties determined according to the technique developed in this work, the results also show that the approach developed for laminae viscoelastic characterization is able to produce valid ply properties. However, it is important to mention that the laminate models applied are

limited to thin laminates, and thus, do not use all of the three-dimensional laminae properties determined, since the through-thickness shear properties are not included. An investigation involving thick structures would be necessary to verify all the assumptions made for the viscoelastic model developed in Chapter 6.

7.6 Time-Temperature Superposition

A well-accepted concept in polymer behavior, is the equivalence between temperature and frequency. A particular temperature transition determined by DMA measurements, at a given applied frequency, can be observed at a lower temperature if the applied vibration frequency is decreased. Temperature and frequency produce opposite effects and the reduction in temperature can be compensated by a reduction in the frequency of measurement. Thus, according to this equivalence, the effect of reducing the applied frequency is similar to that of increasing the temperature.

Time-Temperature Superposition has been used as a way to investigate long-term behavior of materials through extrapolation of a series of short-time tests. Normally, properties are evaluated at several temperatures and within a given frequency range and, because of the equivalent effect of time (of frequency) and temperature, the data can be superposed by shifting individual curves about a given reference temperature. After shifting the data, the master curve produced covers a range much greater than each individual collected data. Master curves are generated for storage modulus and loss factor ($tan\ \delta$) [91]. This technique can be very advantageous in the prediction of the material behavior at low frequencies, without the need of performing time-consuming low frequency tests. The approach has been shown to be capable of predicting long-term

changes in strength and modulus, and as a potential prediction method of fatigue strength of fiber-reinforced plastics [119,120].

Modern DMA equipment can be programmed to perform a series of frequency scans at different temperatures. Further, the software systems that accompany such equipment offer built in functions to automatically generate time-temperature master curves based on measured data. Thus DMA's are very versatile equipment to produce time-temperature superposition curves.

In previous sections, it was demonstrated that the frequency and temperature dependence of the viscoelastic properties of transversely isotropic laminae can be determined through a combination of DMA measurements in unidirectional beams and CTE measurements in laminates. Thus, using the approach discussed in this chapter, and performing frequency scans at different temperatures, master curves can be generated for the independent viscoelastic properties. These master curves will provide essential information of material behavior, for each of the viscoelastic parameters, and outside of the available measuring range of the equipment.

7.7 Summary

In this chapter, the 3-D viscoelastic characterization of a transversely isotropic unidirectional lamina has been presented, according to the mechanics model developed in Chapter 6. The experimental procedure, which involves only three flexural tests is used to determine viscoelastic properties of PEEK/IM7. Experiments were conducted in unidirectional beams, with different fiber orientations, using the 3-point bend test mode. The procedure uses a standard piece of laboratory equipment (DTMA), which allows the

determination of the dynamic material properties over a range of temperatures and frequencies. The investigation evaluated changes in properties as related to temperature and frequency. Further, the ability of the DMTA to investigate viscoelastic properties of laminated composite materials was demonstrated.

After the viscoelastic characterization of unidirectional fiber-reinforced laminae, measurements were conducted in three different cross-ply laminates, over ranges of temperature and frequency. The measurements were compared with predicted properties, using two published models from the literature, based on measured laminae properties. The results showed a very good agreement between measured and predicted loss factors for the laminates. For the storage modulus, both models used produce the same properties and the measured data was, for all laminated beams tested, about 10% smaller than the predicted values, suggesting a presence of delaminations or imperfect bonding between adjoining layers. In general, the investigation showed that the laminate models used are capable of good predictions of viscoelastic properties, both over temperature and frequency ranges. Further, the results of laminate testing indicated that the viscoelastic model developed can produce valid lamina properties, since laminate predicted properties, that were based on laminae properties measured according to the proposed technique, closely matched the measured laminate values.

In summary, the work presented in this chapter contributes to the understanding of temperature and frequency effects on viscoelastic properties of fiber reinforced composites with polymeric matrix materials. The experimental results support the proposed approach, developed for viscoelastic characterization of transversely isotropic laminae. The investigation also proves the validity of two published laminate models for

the determination of viscoelastic properties. over ranges of frequency and temperature. Thus. the understanding of the viscoelastic properties of fiber reinforced composite plies is suggested to allow the design of laminates with tailored damping based on real. measured lamina properties.

8

Future Work

Approaches for 3-D elastic and viscoelastic characterization of transversely isotropic laminae have been developed in this work. However, the experimental results presented, for both elastic and viscoelastic characterization, are rather preliminary. In both cases, elastic and viscoelastic, the complete characterization was carried out for only one fiber reinforced material, PEEK/IM7, and even for this material only a limited number of experimental repetitions were performed. Further, through-thickness elastic and viscoelastic shear properties determined according to the approaches proposed were not verified through comparison with published data, or properties measured by other techniques, due to the lack of data available. Before these techniques can be applied in material characterization for all applications, it is necessary to use the procedures developed in this work to conduct verification measurements for other materials, including both thermoset and thermoplastic matrix composites, and compare the properties determined with those obtained according to presently accepted measuring techniques. Moreover, both the elastic and viscoelastic properties measurement techniques seem to be sensitive to factors related to specimen preparation, equipment settings and calibration, and operator experience. Thus, further experimental

investigations are necessary to provide a better insight of the influence of these testing factors on precision, repeatability, etc.

The procedure for the elastic characterization has been shown to be very sensitive to specimen preparation. A good repeatability of the CTE measurements was only achieved after a custom designed polishing tool was developed for specimen preparation, to ensure perpendicularity and parallelism of edges and surface flatness. Also, a low heating rate of 1°C/min was found necessary for the CTE measurements in an attempt to provide better temperature uniformity throughout the specimen. This heating rate must be chosen to achieve a balance between a rate low enough to minimize temperature variability within the specimen, yet sufficient to maintain a reasonable total test duration. Of course, the ideal heating rate will depend upon the type constituent materials – fiber and matrix - and also, the fiber volume fraction. Therefore, further investigation of these effects needs to be addressed in the future.

Another important issue regarding the proposed method for elastic characterization is the shear modulus, G_{12}, determined according to this technique that, for the material tested, was considerably higher - about 40% - than quoted data. In this research, it was suggested that the high prediction of G_{12} could be related to precision in the CTE measurements, or manufacturing differences, or else to differences in the boundary conditions imposed by the two different test approaches – standard method versus proposed approach. Viscoelastic characterization of the same material produced a storage shear modulus very close to the value calculated from the elastic approach. Further research is necessary to investigate this trend.

The viscoelastic characterization procedure showed considerable sensitivity to equipment settings and calibration, and to operator experience. All viscoelastic measurements presented in this research were carried out, by a very experienced technician, using the same DMA equipment. Properties measured in different equipment, but of the same manufacturer and model, and by a different operator, presented some unpredicted features and trends, which ultimately made the data unusable. For instance, in the measurements of the loss factor, *tan δ*, an unexpected peak was observed over the temperature range of 0°C to 30°C. This is the temperature range in which the temperature controller switches from cooling to heating mode. Thus, it is possible that some inconsistencies in the temperature control affected the collected data. Also, in some cases, an increase, instead of the expected decrease, in storage modulus was observed with increasing temperature (Figure 8.1). Such a change in slope had been noted previously when equipment compliance calibration parameters were mismatched. Examples of the difference between measurements used in this research and the measurements collected from the other equipment, for beams with fibers oriented at 0 and 90 degrees, are presented in Figures 8.1 and 8.2. The data with suffix "a" represent the tests where equipment inconsistency was noted.

In Figure 8.1, for the 0 degree orientation, where the viscous component is small, the repeatability of each machine is quite good; however, the consistency, machine-to-machine, is not perfect. A notable jump in the *tan δ* data occurs at ~0°C and the data otherwise seems unchanging over the complete temperature range of interest. The *tan δ* values seem comparable up to 40°C or so. For the storage modulus, the data from both machines is comparable, with only very slight differences in the trend with temperature.

However, a modulus increase with temperature, as seen in the data from the second machine, is difficult to justify based on materials fundamentals.

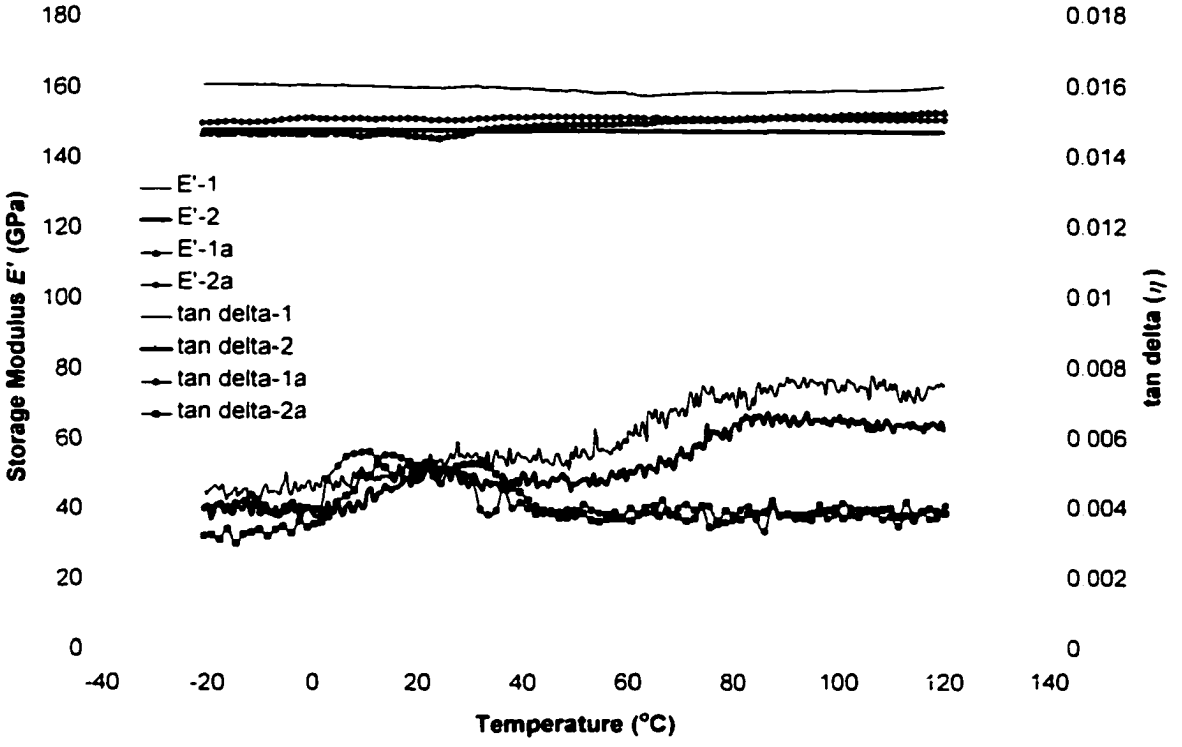

Figure 8.1 – Viscoelastic properties for 0deg beams measured by different equipment.

In Figure 8.2, for the 90 degree orientation, where the matrix component controls the material response and the *tan* δ component is expected to be appreciable, the relative magnitudes are the same for both test sets, for both the loss and storage components; however, the large excursion in the *tan* δ data between 0°C and 30°C is uncharacteristic of a material effect and seems to be equipment control related. Further, the general oscillations in *tan* δ are unacceptable. The E' data seems to correspond closely for both machines. Therefore, it seems that the oscillatory portion of the second machine is not behaving as designed and thus, the loss modulus values are being affected.

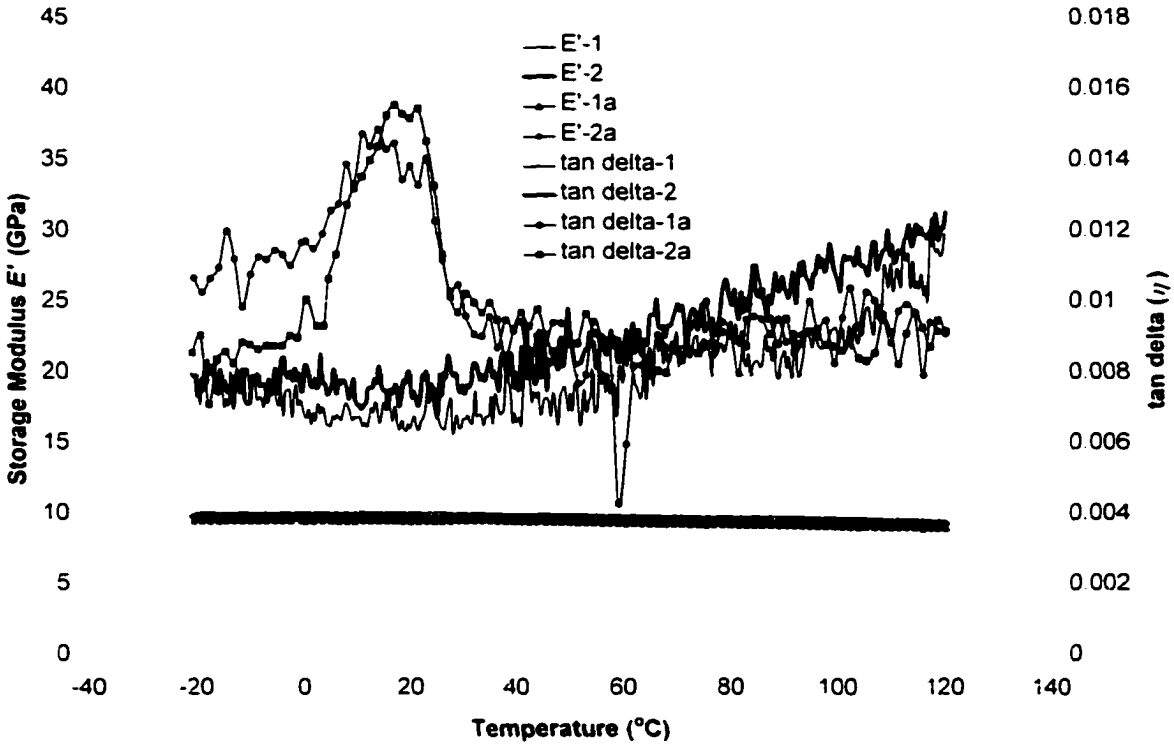

Figure 8.2 - Viscoelastic properties for 90deg beams measured by different equipment.

The experimental investigation of the viscoelastic properties of PEEK/IM7 laminae and laminated beams indicated that the approach developed in Chapter 6 for laminae viscoelastic characterization is able to produce valid ply properties. However, the laminate models applied are limited to thin laminates and use only in-plane properties. Thus, it is still necessary to develop an experimental procedure able to verify the laminae viscoelastic properties in the through-thickness direction, calculated according to the proposed model. The verification procedure may include comparison with other experimental techniques or comparison between measured properties of thick structures and predictions based on mechanics models for thick laminates.

Also, an additional topic for future research is the study of the contribution of the fiber-matrix interface on the viscoelastic material properties. In a real composite, designed for damping critical situations, the interfacial performance between the fiber and matrix is unlikely to be accurately represented by the concept of "perfect bonding". It is more likely that some combination of elastic and viscous behavior will be introduced that is related solely to the fiber-matrix interface. This contribution is also likely to be affected by temperature and frequency. If the fibers offer negligible, or no, contribution to the overall composite damping, such as in carbon fiber reinforced polymers, DMA tests in reinforced and unreinforced specimens may lead to the separation of the mechanisms of damping – matrix from interface. Since micromechanics approaches normally account only for the constituent materials (fiber and matrix) properties, studying the difference between the experimentally measured properties and micromechanics predictions may allow a better understanding of the contributions of the fiber-matrix interface to the overall composite viscoelastic performance.

Finally, the possibility of expanding the approaches developed herein to perform characterization of orthotropic materials is of great interest. The approaches developed in this investigation are limited to transversely isotropic laminae. However, studies of manufacturing effects may require orthotropic models. This is due to the fact that variations in consolidation, during manufacture, are expected to affect the properties in the laminate through-thickness direction to a higher extent than in the other directions. In this case, the assumption of transverse isotropy limits the potential to investigate the degree of consolidation since, in the transversely isotropic case, the through-thickness properties are not independent of the properties in the transverse direction. For

orthotropic materials, the number of independent parameters increases considerably, which may require additional measurements.

In summary, the suggestions for future work include the following:

- Investigate the sensitivity of the developed approach, for the determination of the elastic properties, to specimen preparation, and ultimately attempt to define optimal, standardized, preparation procedures.
- Determine if the developed technique inherently has the tendency of producing a higher prediction of the elastic shear modulus, G_{12}, and if this is the case, explore the possible causes for this deviation.
- Compare the through-thickness shear response, either G_{23} or ν_{23}, determined according to the developed method, with values measured according to ASTM standards.
- Define optimal standardized equipment calibration and testing settings, for both elastic and viscoelastic techniques to ensure reproducibility.
- Apply both approaches developed, for elastic and viscoelastic characterization, to other materials and compare results with other techniques to establish a broader database. The measurements should include composites of various polymeric matrices – thermoplastics and thermosets – and diverse types of fiber reinforcements (carbon, glass, etc).
- Define a method and conduct a verification of the through-thickness viscoelastic shear properties determined according to the approach developed in Chapter 6.

- Combine the technique for viscoelastic characterization with the principle of time-temperature superposition to generate master curves for fiber reinforced materials.
- Attempt to separate the individual contributions of the constituent materials – matrix and fiber – from the interface by comparing the composite properties measured according to the techniques proposed with micromechanics predictions.
- Study the possibilities of expanding the methods developed for characterization of transversely isotropic materials to orthotropic materials, thus allowing investigation of manufacturing effects on the material properties.

9

Conclusions

Elastic and viscoelastic material characterization has always been a topic of great interest for engineers working with design and analysis of composite material structures. Recently, the availability of powerful and inexpensive personal computers and the great advancements in software engineering for structural design and analysis have increased the expectation of the capabilities of detailed analysis and design in every facet of composites, including design for damping. However, the development of accurate model predictions for composite structures requires the determination of three-dimensional material properties to fully exploit the capabilities of the available tools. Modern structures are being designed ever more slender to become more cost and weight effective, as well as for aesthetics reasons. At the same time, these structures are being employed in more severe environmental and loading conditions, requiring knowledge of material properties - static and dynamic - over a wide range of temperatures. Current approaches commonly used, for elastic and viscoelastic characterization of materials, are not simple, often requiring specimens with complicated geometry or special testing equipment setup, which may ultimately affect the reproducibility of the measured properties. The study of new approaches with the potential to allow fast and

uncomplicated material characterization, from simplified tests and using standard laboratory equipment, are of great interest.

This research has focused on the development of techniques for 3-dimensional elastic and viscoelastic characterization of transversely isotropic laminae over a range of temperatures and frequencies. The goal was to establish theoretical relationships and corresponding experimental methods to study the properties of unidirectional fiber reinforced composite materials over a range of temperatures, using standard laboratory thermo mechanical analysis equipment. For the viscoelastic properties, the objective has included the ability to investigate frequency dependence of the measured properties.

9.1 Elastic Characterization of Laminae

A new approach for the determination of all the independent elastic properties of a transversely isotropic lamina was generated. The method uses a combination of standard tensile tests and coefficient of thermal expansion measurements in unidirectional and $[(+\theta/-\theta)_n]_s$ sub-scale laminates. This approach eliminates the need for the very thick specimens required by standard methods, for the determination of the properties in the through-thickness direction, which may not be a good representation of more common, thinner composite structures. Further, since CTE measurements are conventionally carried out using temperature sweep test methods, the approach is very advantageous for the determination of the elastic properties over a range of temperatures. Continuous CTE vs. temperature data is produced, which results in continuous temperature relationship for the calculated elastic properties. In contrast, standardized mechanical tests for the determination of elastic properties are normally carried out at a constant

temperature, thus requiring multiple tests and producing discrete data points, if material elastic properties are to be determined over a range of temperatures.

The proposed approach was experimentally verified through the three-dimensional elastic characterization of a PEEK/IM7 unidirectional prepreg tape. PEEK/IM7 exhibits properties that meet the design requirements of many aerospace structural applications, which makes the study of temperature dependence very important. CTE measurements in sub-scale specimens were carried out in a Thermo Mechanical Analyzer (TMA), over a temperature range of -20°C to 120°C. Of the five independent elastic parameters, two, E_1 and ν_{12}, were determined from standard tensile tests while the other three, E_2, G_{12}, and ν_{23}, were computed according to the relationships developed, using CTE measurements in laminates. Standard measurements of the transverse modulus, E_2, were also conducted, over the same temperature range, to compare with the values determined by the model. The measurements indicated that E_1 showed no sensitivity to the temperature variation, as expected, since this is a fiber dominated property, while the Poisson's ratio ν_{12} data showed a slight increase with temperature. All three computed independent elastic properties showed sensitivity to temperature increase. The Poisson's ratio, ν_{23}, showed an increase, while the moduli, E_2 and G_{12}, showed decrease with increasing temperature. The agreement between the transverse modulus, E_2, predicted by the model and measured according to the ASTM standard test, was very good, over the entire temperature range studied. The results support the application and accuracy of the proposed technique. Further, all properties determined at 20°C were compared to room temperature data published in the literature, for the same material, showing a good agreement. Only the computed in-plane shear modulus, G_{12}, was found to be higher than

previously published data. Although no conclusive statements could be made to explain the higher computed in-plane shear modulus, G_{12}, due to the limited data available, this effect is suggested to be related to differences in the boundary conditions imposed by the two different test approaches, or to differences in processing conditions, between the material used in this research and that used in the published literature.

The results of the experimental verification, using PEEK/IM7, demonstrate the capability of the proposed CTE-based technique to generate elastic properties data for a transversely isotropic material, over a wide temperature range. The approach also promises the ability to study the effects of manufacturing on elastic properties as it yields ply properties from laminate measurements, thus incorporating effects of manufacture. The proposed technique presents not only an alternative approach to the determination of the elastic properties of transversely isotropic laminae, but it also demonstrates the feasibility of reproducing, in sub-scale experimental measurements, the theoretical relationships between elastic and thermal properties of composite laminates.

In summary, the contributions of this study are:

- Theoretical mechanics relationships between thermal properties of laminates and elastic properties of the constituent laminae were established which allow determination of the independent elastic properties of a transversely isotropic lamina.
- An experimental procedure was developed, based on the proposed mathematical model, and applied for the determination of the three-dimensional elastic properties of a PEEK/IM7 unidirectional prepreg tape, over a temperature range from 20°C to 120°C. Room temperature results indicate

good agreement with the available quoted values measured by standard techniques.

- The proposed technique uses thinner specimens than ASTM standards, avoiding the need for manufacturing thick laminates or bonding pre-cured laminates of smaller thickness. The thinner test specimens are expected to be a better representation of common thinner composite structures.
- The experimental investigation provides insight into the practical aspects of the relationships between thermal and elastic properties of laminates, and proves the feasibility of determining elastic properties from measurements of thermal properties.

9.2 Viscoelastic Characterization of Laminae

To evaluate the viscoelastic properties of transversely isotropic fiber reinforced laminae, a mechanics model has been developed, which reduces the number of independent parameters to be determined, compared to previous models published in the literature. The model proposed allows the complete 3-D viscoelastic characterization of a transversely isotropic material, based on only five independent dynamic stiffness properties and three independent damping loss factors, rather than the more commonly accepted 4 loss factors. A direct consequence of the reduction of the number of independent parameters is the simplification of the experimental measurements required for the determination of these properties. Using the proposed model, an approach has been developed, based on energy equations, which allows the viscoelastic properties to be

evaluated from experimental data, collected from three bend-beam oscillatory tests and two known elastic properties.

The experimental procedure developed for viscoelastic characterization uses measured parameters in unidirectional bend-beam specimens, thus eliminating the need for torsion tests. With the removal of the necessity for torsion measurements, Dynamic Mechanical Analysis (DMA) equipment can be applied for the viscoelastic characterization using sub-scale flexural measurements. Extending the approach to oscillatory tests performed in a commercial DMA, avoids the need for special experimental setups normally required in dynamic characterization, and therefore, an improvement in reproducibility is expected. Further, DMA equipment allows accurate temperature and frequency control and the effects of these parameters on viscoelastic properties can be investigated in a simple and efficient way. The use of experimental measurements, in opposition to micromechanics approaches, offers the future advantage of determining, and incorporating, the effects of processing and material degradation into the properties of the material.

In the experimental approach suggested, the determination of all the viscoelastic properties of a transversely isotropic material can be accomplished using oscillatory bending tests of three individual unidirectional laminae with fibers oriented at 0°, 90° and some intermediate angle $0°<\theta<90°$, given that the Poisson's ratios ν_{12} and ν_{23} are known. The approach developed in this work, involves some simplifying assumptions, in a way similar to the development of elastic beam theories. Due to the effects of the Poisson's ratio and anisotropic shear coupling, the one-dimensional assumption, which permits using beam equations, may not be strictly correct. However, previous research has

indicated that Poisson's and shear coupling effects can be neglected for beams with large aspect ratio. Furthermore, the one-dimensional assumption allows the determination of the properties from three bending tests, only, and was applied mainly to eliminate the need of torsion tests for the determination of the shear properties. Thus, all dynamic measurements may be conducted in a commercial DMA with a consistent set of boundary conditions.

The developed approach was verified experimentally through the determination of viscoelastic properties of PEEK/IM7 prepreg tape. Experiments were conducted in unidirectional beams, with fiber orientations of 0°, 30° and 90°, with respect to the length of the beam. All measurements were performed in a commercial DMA using the 3-point bend test mode. Temperature sweep tests were conducted over a range of -20°C to 120°C, while frequency sweep tests were conducted over a range of 0.1 Hz to 10Hz. The investigation evaluated both the absolute magnitude of the viscoelastic properties as well as the changes in properties as related to temperature and frequency.

According to the mechanics model developed, the three dimensional viscoelastic properties of a fiber reinforced lamina, for a given frequency and temperature, can be described by eight independent parameters. The eight parameters determined were: E_1, E_2, G_{12}, ν_{12} and ν_{23}, and the damping loss factors η_1, η_2, and η_6. The mechanics model assumes that the Poisson's ratios, ν_{12} and ν_{23}, are real (not complex) numbers, which are time-invariant and a function of temperature, only. Thus, the Poisson's ratios considered in the viscoelastic characterization were those determined, over the same temperature range, during the elastic characterization.

The trends in temperature dependence of the storage moduli determined from DMA measurements were very similar to the trends observed in the elastic moduli. A small decrease in the fiber-dominated modulus, E'_1, with temperature, is observed. E'_1 decreased from 155.4 GPa, at -20°C, to 153.8 GPa, at 120°C, representing a 1% variation. The corresponding variations for E'_2, over the same temperature range was from 10.2 GPa to 9.6 GPa, or 6% reduction in storage modulus. G'_{12} decreased from 7.4 GPa to 6.9 GPa, representing a 7% reduction.

The 1% change observed in E'_1 may be an indication of changes in the fiber-matrix interface. Changes in matrix properties alone could not account for the this change in modulus, since the maximum testing temperature, 120°C, is considerably lower than the glass transition temperature, ~150°C. The changes in the other two modulus components, where the matrix properties are significant, such as E'_2 and G'_{12}, are larger due to the changes in matrix properties with temperature, combined with changes at the interface.

Measured changes in damping loss factors with temperature were much larger than changes in dynamic moduli. Even in the fiber direction where the changes in modulus are very small, changes in damping were considerable, over the temperature range. The loss factor η_1 showed the smallest temperature dependence, varying from 4.7×10^{-3}, at -20°C, to 7.0×10^{-3}, at 120°C, which represents an increase of 49%. For the loss factor corresponding to the transverse direction, η_2, the measurements varied from 7.8×10^{-3}, at -20°C, to 12.1×10^{-3}, at 120°C, thus increasing 55%. The shear loss factor, η_6, varied from 8.8×10^{-3}, at -20°C, to 14.9×10^{-3}, at 120°C, corresponding to a 69% increase. Most of the composite damping is a result of the matrix damping and the fiber-matrix

interface response, since the carbon fibers exhibit very low damping and negligible thermally induced variation, compared to the polymeric matrix.

In order to study the frequency dependency of the viscoelastic properties, DMA frequency scans were conducted over the range of 0.1 to 10 Hz. Since Poisson's ratios, ν_{12} and ν_{23}, are assumed independent of frequency, they were obtained from the elastic characterization of the same material. Storage moduli E'_1, E'_2 and G'_{12}, determined from the frequency sweep tests data were practically independent of frequency over the range studied. However, changes in all three independent damping loss factors, with frequency, were considerable. The loss factor η_1, corresponding to the fiber direction, varied from 7.1×10^{-3}, at 0.1 Hz, to 3.8×10^{-3}, at 10 Hz, which represents a 46% change. For η_2, the measurements varied from 9.8×10^{-3}, at 0.1 Hz, to 6.9×10^{-3}, at 10 Hz, thus decreasing 42%. Finally, the shear loss factor, η_6, varied from 12.8×10^{-3}, at 0.1 Hz, to 10.2×10^{-3}, at 10 Hz, corresponding to a 20% decrease. The decrease in damping with increasing frequency was expected since, at higher frequencies, the material has less time to flow, thus behaving more elastically. The data presented indicate that the loss factors are considerably more frequency dependent than storage moduli.

Storage moduli determined from DMA tests data were compared with elastic moduli previously determined, from CTE measurements. The results for both temperature and frequency sweep tests were in close agreement. Thus, the ability of the DMA to allow investigation of viscoelastic properties of laminated composite materials using sub-scale beam specimens was demonstrated. Further, these results indicate that the extension of the procedure to incorporate concepts of time-temperature superposition has great potential.

Thus, this research develops mechanics relationships and an experimental procedure for the determination of viscoelastic properties of transversely isotropic laminae. The approach allows the study of the effects of temperature and frequency on the measured properties. The goal is to provide a means for the measurement of the viscoelastic properties of fiber-reinforced composites, and contribute to the understanding of temperature and frequency dependence of these mechanical properties. Ultimately, this improved understanding will contribute to damping design and also, to investigate processing related problems in composites.

In summary, the contributions of this study are:

- A mechanics model for viscoelastic characterization of transversely isotropic laminae was proposed, which reduces the number of independent coefficients to be determined, compared to previous models published in the literature, and simplifies the experimental measurements required for the determination of these properties.
- An experimental approach for the measurement of the viscoelastic properties is proposed, based only on measured parameters in unidirectional bend-beam specimens, thus eliminating the need for torsion tests. All dynamic measurements may be conducted using sub-scale bend-beam oscillatory measurements in a commercial DMA, which allows a consistent set of boundary conditions.
- Viscoelastic properties of PEEK/IM7 prepreg tape were determined, according to the mechanics model and experimental approach developed, which allowed

the study of the effects of temperature and frequency on the measured properties.

- The experimental investigation, using PEEK/IM7, verified the feasibility of quantitative measurement of the viscoelastic properties of composites, using sub-scale DMA tests.

9.3 Viscoelastic Characterization of Laminates

After the viscoelastic characterization of the PEEK/IM7 transversely isotropic laminae, viscoelastic measurements were conducted on cross-ply laminated beams. Two existing approaches to predict laminate behavior, were evaluated. Layer properties determined according to the newly generated technique were used with the two models from the literature to determine laminate behavior. DMA measurements on corresponding laminates, over ranges of temperature and frequency, were also carried out and compared with the predictions, based on the two laminate models. The results show very good agreement between measured and predicted loss factors for the laminates. For the storage modulus, both models used produce the same properties and the measured data were, for all laminated beams tested, about 10% smaller than the predicted values, suggesting a presence of delaminations or imperfect bonding between adjoining layers of the laminated beams that are not accounted for in the assumptions upon which the models are based. In general, it was determined that both models result in good predictions for laminate properties based on laminae measured properties, both over temperature and frequency ranges. Further, the results indicated that the viscoelastic model developed in Chapter 6 can produce valid lamina properties, since laminate predicted properties that

were based on laminae properties, measured according to the proposed technique, closely match the measured laminate values. Thus, the measurement of laminate viscoelastic properties, and the close comparison of these measured values to the results of the model predictions for the same lamination sequences, serve as a verification of the laminae properties prediction approach developed in this work.

The main contributions of this investigation are:

- Two existing approaches to predict laminate viscoelastic behavior, were evaluated, over ranges of temperature and frequency, and it was concluded that both models provide good predictions.
- The good agreement obtained between predicted laminate properties, based on laminate models accepted in literature, and DMA measurements in laminates, indicate that the viscoelastic model developed produces valid lamina properties.
- The results obtained confirm that the sub-scale DMA testing approach can generate accurate quantitative results and thus, shows promise as a potential standardized experimental technique to measure viscoelastic properties of fiber reinforced composites.

9.4 Concluding Remarks

Three dimensional material characterization is essential for the design of many advanced composite structures. Besides the know advantages of composite materials, such as high specific stiffness and strength, design requirements may also include specified damping properties and high temperature performance.

This study has successfully developed new approaches for three-dimensional elastic and viscoelastic characterization of transversely isotropic laminae. The approaches developed enable the use of sub-scale specimens to rapidly and accurately determine material properties, over a range of temperatures and frequencies, using standard laboratory equipment. The results presented prove the feasibility of reproducing, experimentally, the theoretical relationships between elastic and thermal properties of fiber-reinforced composites. Also, a new mechanics model was developed that reduces the number of independent parameters required for viscoelastic characterization of transversely isotropic laminae, facilitating the necessary experimental measurements. It was shown in this research that thermal analysis equipment such as TMA's and DMA's offer great potential to investigate not only thermal, but also mechanical properties of composite materials.

The mechanics relationships and experimental procedures developed in this research provide a good foundation for future investigation and contribute to the understanding of temperature and frequency effects on the properties of fiber reinforced, polymeric matrix composites.

References

[1] Lee, D. G., Kim, K. S. and Kwak, Y. K., "Manufacturing of a Scara Type Direct-Drive Robot with Graphite Fiber Epoxy Composite Material." *Robotica*, 9: 219-229, 1991.

[2] Oh, H. S., Jeong, K. S. and Lee, D. G., "Design and Manufacture of the Composite Flexspline of a Harmonic Drive with Adhesive Joining." *Composite Structures*, 28: 307-314, 1994.

[3] "High Performance Composites: An Overview". *High Performance Composites 2002 Sourcebook*, 6-21, 2002.

[4] Hergenrother, P. M. " Development of Composites, Adhesives and Sealants for High-Speed Commercial Airplanes." *SAMPE Journal*, 36(1): 30-41, 2000.

[5] Facciano, A., "High-Temperature Organic Composite Applications for Supersonic Missile Airframes." *SAMPE Journal*, 36(1): 9-23, 2000.

[6] Armstrong, S. M., "High Speed Research Lessons: Report to the NASA Advisory Council," 1999. (Consulted: March 2002): http://aerospace.nasa.gov/library/hsrfinal/HSRfinal.ppt

[7] Menard, K. P., *Dynamic Mechanical Analysis: A Practical Introduction*, Boca Raton, FL, CRC Press, 1999.

[8] ASTM Standard D 3039/D 3039M – 00, Standard Test Method for Tensile Properties of Polymer Matrix Composite Materials, Annual Book of ASTM Standards, Vol 15.03, 2001.

[9] ASTM Standard D 3518/D 3518M – 94, Standard Test Method for In-Plane Shear Response of Polymer Matrix Composite Materials by Tensile Test of a ±45° Laminate, Annual Book of ASTM Standards, Vol 15.03, 2001.

[10] ASTM Standard D 4255/D 4255M – 83, Standard Guide for Testing In-Plane Shear Properties of Composite Laminates, Annual Book of ASTM Standards, Vol 15.03, 2001.

[11] ASTM Standard D 5379/D 5379M – 98. Standard Test Method for Shear Properties of Composite Materials by the V-Notched Beam Method. Annual Book of ASTM Standards. Vol 15.03. 2001.

[12] Walrath. D. E.. and Adams. D. F.. "The Iosipescu Shear Test as Applied to Composite Materials." *Experimental Mechanics*. 23 (1): 105-110. 1983.

[13] Walrath. D. E.. and Adams. D. F.. "Further Development of the Iosipescu Test Method." *Experimental Mechanics*. 27 (2): 113-119. 1987.

[14] Arcan. M.. Hashin. Z.. and Voloshin. A.. "A Method to Produce Uniform Plane-Stress States with Applications to Fiber-Reinforced Materials." *Experimental Mechanics*. 18 (4): 141-146. 1978.

[15] Iosipescu. N.. "Photoelastic Investigations on an Accurate Procedure for the Pure Shear Testing of Materials." *Revue de Mecanique Appliquée*. 8 (1). 1963.

[16] Iosipescu. N.. "New Accurate Procedure for Single Shear Testing of Metals." *Journal of Materials*. 2 (3): 537-566. 1967.

[17] Pagano. N. J.. "Shear Moduli of Orthotropic Composites." AFML-TR-79-4164. 1980.

[18] Sandorff. P. E.. "Transverse Shear Stiffness of T300/5208 Graphite-Epoxy in Simple Bending." *Journal of Reinforced Plastics and Composites*. 1: 335-352. 1982.

[19] Tsai. C. L.. and Daniel. I. M.. "Determination of In-plane and Out-of-plane Shear Moduli of Composites Materials." *Experimental Mechanics*. 5: 295-299. 1990.

[20] Silverman. E. M.. Wiacek. C. R.. and Griese. R. A.. "Characterization of IM7Graphite/Thermoplastic Polyetheretherketone (PEEK) for Spacecraft Structural Applications." *Composite Materials: Testing and Design (Tenth Volume)*. ASTM STP 1120: 118-130. 1992.

[21] Stellbrink. K. K. U.. *Micromechanics of Composites: Composite Properties of Fibre and Matrix Constituents*. Munich: New York: Hanser: Cincinnati. OH: Hanser/Gardner Publications. Inc.. 1996.

[22] Daniel. I. M.. and Ishai. O.. *Engineering Mechanics of Composite Materials*. Oxford [England]; New York: Oxford University Press. 1994.

[23] Whitney. J. M.. Daniel. I. M.. and Pipes. R. B.. *Experimental Mechanics of Fiber Reinforced Composite Materials*. Brookfield Center. Conn.: Society for Experimental Mechanics: Englewood Cliffs. NJ: Prentice-Hall. Inc.. 1984.

[24] Levin. V.M.. "Thermal Expansion Coefficients of Heterogeneous Materials." *Mechanics of Solids*. 2: 58-61. 1967.

[25] Hashin, Z., "Analysis of Properties of Fiber Composites with Anisotropic Constituents," *Journal of Applied Mechanics*, 46: 543-550, 1979.

[26] Philippidis, T.P., and Theocaris, P.S., "The Transverse Poisson's Ratio in Fiber Reinforced Laminae by Means of a Hybrid Experimental Approach," *Journal of Composite Materials*, 28(3): 252-261, 1994.

[27] Saravanos, D. A., and Pereira, J. M., "Effects of Interply Damping Layers on the Dynamic Characteristics of Composite Plates," *AIAA Journal*, 30(12): 2906-2913, 1992.

[28] Space Ref.Com (Consulted: January 2002): http://www.spaceref.com/iss/elements/mss.html#description

[29] Chattopadhyay, A., Nam, C., and Kim, Y., "Damage Detection and Vibration Control of a Delaminated Smart Composite Plate," *Proceedings of ICCM-12*, 1999.

[30] Radford, D. W., et al, "Microwave Nondestructive Investigation of Multiple Impacted Composite Laminates," *Proceedings of ICCM-10*, V 405 – V 412, 1995.

[31] Mantena, R., Place, T. A., and Gibson, R. F., "Charactherization of Matrix Cracking in Composite Laminates by the Use of Damping Capacity Measurements," *Role of Interfaces on Material Damping*, 79-93, ASM International, Materials Park, OH, 1995.

[32] Mantena, R., Gibson, R. F., and Place, T. A., "Damping Capacity Measurements of Degradation in Advanced Materials," *SAMPE Quarterly*, 17(3): 20-31, 1986.

[33] Gamstedt, E. K. and Talreja, R., "Fatigue Damage Mechanisms in Unidirectional Carbon-Fibre-Reinforced Plastics," *Journal of Materials Science*, 34: 2535-2546, 1999.

[34] Chen, A. S., Harris, B., "Fatigue-Induced Damage Mechanics in Carbon Fibre-Reinforced Plastic Composites," *Journal of Materials Science*, 28: 2013-2027, 1993.

[35] Saravanos, D. A. and Chamis, C. C., "Unified Micromechanics of Damping for Unidirectional and Off-Axis Fiber Composites," *Journal of Composites Technology and Research*, 12 (1): 31-40, 1990.

[36] Brantseva, T. V., Gorbatkina, Yu A., and Kerber, M. L., "Behavior of Polymer – Fiber Interface Under Various Loading Rates," *Proceedings of ICCM-12*, 1999.

[37] Jeng, C. and Chen, M., "Influence of Transcrystalline Interphase on Flexural Failure of Short Carbon Fiber Reinforced Peek Composites," *Proceedings of ICCM-12*, 1999.

[38] Gaertner, R., et al, "Rheological and Morphological Influences on the Viscoelastic Behaviour of Polymer Composites," *Proceedings of ICCM-12*, 1999.

[39] Gibson, R. F., *Principles of Composite Material Mechanics*, New York, NY, McGraw-Hill, 1994.

[40] Smith, R. E., "Ultrasonic Elastic Constants of Carbon Fibers and Their Composites." *Journal of Applied Physics*, 43:2555-2562, 1972.

[41] Gieske, J. H., and Allred, R. E., "Elastic Constants of B-Al Composites by Ultrasonic Velocity Measurements," *Experimental Mechanics*, 14: 158-165, 1974.

[42] Chimenti, D. E., "Guided Waves in Plates and Their Use in Materials Characterization," *Applied Mechanics Reviews*, 50 (5): 247-284, 1997.

[43] Hosten, B., "Reflection and Transmission of Acoustic Plane Waves on an Immersed Orthotropic and Viscoelastic Solid Layer," *Journal of the Acoustical Society of America*, 89 (6): 2745-2752, 1991.

[44] Rokhlin, S. I., and Wang, W., "Double Through-Transmission Bulk Wave Method for Ultrasonic Phase Velocity Measurement and Determination of Elastic Constants of Composite Materials," *Journal of the Acoustical Society of America*, 91 (6): 3303-3312, 1992.

[45] Migliori, A., Darling, T. W., Baiardo, J. P., and Freibert, F., "Resonant Ultrasound Spectroscopy," *Handbook of Elastic Properties of Solids, Liquids and Gases, Volume 1: Dynamic Methods for Measuring the Elastic Properties of Solids*, 239-262, San Diego, CA, Academic Press, 2001.

[46] Baudouin, S., and Hosten, B., "Comparison Between Prediction and measurement of Viscoelastic Moduli in Composite Materials versus Temperature Using Ultrasonic Immersion Technique With Oil," *Journal of the Acoustical Society of America*, 102 (6): 3450-3457, 1997.

[47] Van Buskirk, W. C, Cowin, S. C., and Carter Jr., R. "A Theory of Acoustic Measurement of the Elastic Constants of a General Anisotropic Solid," *Journal of Materials Science*, 21: 2759-2762, 1986.

[48] Hosten, B., "Ultrasonic Through-Transmission Method For Measuring the Complex Stiffness Moduli of Composite Materials," *Handbook of Elastic Properties of Solids, Liquids and Gases, Volume 1: Dynamic Methods for Measuring the Elastic Properties of Solids*, 67-86, San Diego, CA, Academic Press, 2001.

[49] Kelly, S P., Farlow, R., and Hayward, G., "Applications of Through-Air Ultrasound for Rapid NDE Scanning in the Aerospace Industry," *IEEE Transactions on Ultrasonics Ferroeletrics and Frequency Control*, 43 (4): 581-591, 1996.

[50] Hosten, B., Hutchins, D. A., and Schindel, D. W., "Measurement of Elastic Constants in Composite Materials Using Air-Coupled Ultrasonic Bulk Waves," *Journal of the Acoustical Society of America*, 99 (4): 2116-2123, 1996.

[51] Safaeinili, A., Lobkis, O. I., Chimenti, D. E., "Air-Coupled Ultrasonic Characterization of Composite Plates," *Materials Evaluation*, 53 (10): 1186-1190, 1995.

[52] Every, A. G., "The Elastic Properties of Solids: Static and Dynamic Principles," *Handbook of Elastic Properties of Solids, Liquids and Gases, Volume 1: Dynamic Methods for Measuring the Elastic Properties of Solids*, 3-36, San Diego, CA, Academic Press, 2001.

[53] Suarez, S. A., and Gibson, R. F., "Improved Impulse-Frequency Response Techniques for Measurement of Dynamic Mechanical Properties of Composite Materials," *Journal of Testing and Evaluation*, 15(2): 114-121, 1987.

[54] Deobald, L. R., and Gibson, R. F., "Determination of Elastic Constants of Orthotropic Plates by a Modal Analysis/Rayleigh Ritz Technique," *Journal of Sound and Vibration*, 124(2): 269-283, 1988.

[55] Suarez, S. A., Gibson, R. F., and Deobald, L. R., "Random and Impulse Techniques for Measurement of Damping in Composite Materials," *Experimental Techniques*, 8(10): 19-24, 1984.

[56] Crane, R. M., and Gillispie, J. W., Jr., "A Robust Testing Method for Determination of the Damping Loss Factor of Composites," *Journal of Composites Technology and Research*, 14(2): 70-79, 1992.

[57] DeWilde, W. P., Narmon, B., Sol, H., and Roovers, M., "Determination of the Material Constants of an Anisotropic Lamina by Free Vibration Analysis," *Proceedings of the 2nd International Modal Analysis Conference*, Orlando, FL, I, 44-49, 1984.

[58] Ayorinde, E. O., and Gibson, R. F., "Elastic Constants of Orthotropic Composite Materials Using Plate Resonance Frequencies, Classical Lamination Theory and an Optimized Three mode Rayleigh Formulation," *Composites Engineering*, 3(5): 395-407, 1993.

[59] Ayorinde, E. O., Gibson, R. F., and Wen, Y. F., "Elastic Constants of Isotropic and Orthotropic Composite Materials from Plate Vibration Test Data," *Composite Materials: Testing and Design (eleventh volume)*, ASTM STP 1206, E.T. Camponeschi, Jr., Ed., American Society for Testing and Materials, Philadelphia, 150-161, 1993.

[60] Zinoviev, P. A., Ermakov, Y. N., *Energy Dissipation in Composite Materials*, Lancaster, PA, Technomic, Inc., 1994.

[61] Zhang, P. Q., Ruan, J. H., Li, W. Z., "Influence of Some Factors on the Damping Property of Fiber-Reinforced Epoxy Composites at Low Temperature," *Cryogenics*, 41: 245-251, 2001.

[62] Jeong, K. S., Lee, D. G., and Kwak, Y. K., "Experimental Investigation of the Dynamic Characteristics of Carbon Fiber Epoxy Composite Thin Beams," *Composite Structures*, 33: 77-86, 1995.

[63] Ni, R. G., and Adams, R. D., "The Damping and Dynamic Moduli of Symmetric Laminated Composite Beams – Theoretical and Experimental Results." *Journal of Composite Materials*, 18: 104-121, 1984.

[64] Hwang, S. J., Gibson, R. F., and Singh, J., "Decomposition of Coupling Effects on Damping of Laminated Composites Under Flexural Vibration." *Composites Science and Technology*, 43: 159-169, 1992.

[65] Reed, K. E., "Dynamic Mechanical Analysis of Fiber Reinforced Composites", *Polymer Composites*, 1(1): 44-49, 1980.

[66] Hadi, A. S., and Ashton, J. N., "Measurement and Theoretical Modelling of the Damping Properties of a Uni-Directional Glass/Epoxy Composite." *Composite Structures*, 34: 381-385, 1996.

[67] Adams, R. D. and Bacon, D. G. C., "Measurement of the Flexural Damping Capacity and Dynamic Young's Modulus of Metals and Reinforced Plastics." *Journal of Physics D: Applied Physics*, 6: 27-41, 1973.

[68] Yong-Sok, O., Pillot, C., and Jourdan, C., "Modelization of Viscoelastic Behaviours of Carbon /Epoxy Unidirectional Composites." *Proceeding of the European Mechanics Colloquium 182, Mechanical Characterization of Load bearing Fibre Composite Laminates*, Brussels, Belgium, 29-31, August 1984.

[69] Gill, P. S., and Leckenby, J. N., "Dynamic Mechanical Analysis of Advanced Composites." *Composite Structures*, 2: 235-243, 1984.

[70] Yu, J. Z., and Ko, F. K., "The Effect of Fiber orientation on the Dynamic Mechanical Behavior of Kevlar Fiber Reinforced Composites." *Proceedings of ICCM-10*, 4: 431-438, August 1995.

[71] Saravanos, D. A., and Hopkins, D. A., "Effects of Delaminations on the Damped Dynamic Characteristics of Composite Laminates: Analysis and Experiments." *Journal of Sound and Vibration*, 192(5): 977-993, 1996.

[72] Kolkailah, F., Elghandour, E., Oh, T., and Bolosan, J., "The Study of Empirical Methodology to Observe Damping Characteristics of Various Laminate Composite Plates." *46th International SAMPE Symposium*, 2355-2365, May 2001.

[73] Gibson, R. F., "Sensitivity of Stiffness and Damping to Various Aspects of Material and Structural Behavior." *NCA – Vol.27, Proceedings of the ASME Noise Control and Acoustics Division – 2000, ASME 2000*: 301-318, 2000.

[74] Sichina, W. J., and Gill, P. S. "Viscoelastic Characterization of Composites." *Automotive Challenge and Plastics Response: Automotive Plastics, RETEC 87*: 205-206, 1987.

[75] Gill, P. S. "Characterization of Composites by Dynamic Mechanical Analysis." *Annual Technical Conference – Society of Plastics Engineers Conference Proceedings. ANTEC 83*: 518-521, 1983.

[76] Melo, J. D. D., and Radford, D. W., "Evaluation of Damage Initiation Using Sub-Scale Flexure Testing." *Proceedings of the SEM Annual Conference and Exposition on Experimental and Applied Mechanics*, Portland, Oregon, June 4-6, 2001.

[77] Seferis, J. C., and Buehler, F. U., "Power Issues in the Manufacturing and Characterization of Polymers and Composite Materials." *Polymer Composites*, 19 (5): 558-566, 1998.

[78] Chung, K., and Seferis, J. C., "Investigation of the Thermal Aging Behavior of Cyanate Ester/Carbon Fiber Composite." *Society for the Advancement of Material and Process Engineering, Materials and Process Affordability: Keys to the Future*, 43 (I): 387-393, 1998.

[79] Lavanga, K. L., "DMTA Immersion Study: A New Tool to Investigate Solvent Swelling and in situ Behavior." *Thermal Trends*, 5 (1), Spring 1998.

[80] Ferry, J. D., *Viscoelastic Properties of Polymers*, New York, John Wiley & Sons, Inc., 1961.

[81] Duncan, J., *Dynamic Mechanical Analysis Techniques and Complex Modulus, Mechanical Properties and Testing of Polymers, An A-Z Reference*, Ed. G. M. Swallowe, Boston, Kluwer Academic Publishers, 43-48, 1999.

[82] Browning, C. E., Husman, G. E., and Whitney, J. M., "Moisture Effects in Epoxy Matrix Composites." *Composite Materials Testing and Design, Fourth Conference, ASTM STP 617, American Society for Testing and Materials*, Philadelphia, PA, 481-496, 1977.

[83] Rehfield, L. W., Briley, R. P., and Putter, S., "Dynamic Tests of Graphite/Epoxy Composites in Extreme Environments." *Composites for Extreme Environments, ASTM STP 768, American Society for Testing and Materials*, Philadelphia, PA, 1982.

[84] Moore, G. R. and Kline, D. E., *Properties and Processing of Polymers for Engineers*, Englewood Cliffs, NJ, Prentice-Hall, Inc., 1984.

[85] Wineman, A. S., and Rajagopal, K. R., *Mechanical Response of Polymers: An Introduction*, New York, Cambridge University Press, 2000.

[86] Graesser, E. J. and Wong, C. R., "The Relationship of Traditional Damping Measures for Materials with High Damping Capacity: A Review." *M^3D: Mechanics and Mechanisms of Material Damping*, ASTM STP 1169, Kinra and A. Wolfenden, Eds., American Society for Testing and Materials, Philadelphia, 316-343, 1992.

[87] Yee, A.F., and Smith, S. A., "Molecular-Structure Effects on the Dynamic Mechanical Spectra of Polycarbonates," *Macromolecules*, 14(1): 54-64, 1981.

[88] Gordon, G. A., "Glass Transition in Nylons," *Journal of Polymer Science: Part A-2, Polymer Physics*, 9(9): 1693, 1971.

[89] Nelson, F. C., "Technical Article. A Guide to Polymers and Their use for Vibration Isolation. Part I," *Shock and Vibration Digest*, 26(2): 11, 1994.

[90] Heijboer, J., "Secondary Loss Peaks in Glassy Amorphous Polymers," *International Journal of Polymeric Materials*, 6 (1-2): 11-37, 1977.

[91] Hunt, B. J., James, M. I., *Polymer Characterisation*, New York, NY, Blackie Academic & Professional, 1993.

[92] Williams, D. J., *Polymer Science and Engineering*, Englewood Cliffs, NJ, Prentice-Hall, Inc., 1971.

[93] Lakes, R. S., *Viscoelastic Solids*, Boca Raton, FL, CRC Press, 1999.

[94] Kolsky, H., "The Measurement of the Material Damping of High Polymers Over Ten Decades of Frequency and Its Interpretation," *M³D: Mechanics and Mechanisms of Material Damping*, ASTM STP 1169, Kinra and A. Wolfenden, Eds., American Society for Testing and Materials, Philadelphia, 4-27, 1992.

[95] Ting, T. C. T., *Anisotropic Elasticity: Theory and Applications*, New York: Oxford Science Publications, 1996.

[96] Yin-Tao, W., Liang-Jin, G., and Ting-Qing, Y., "Prediction of the 3-D Effective Damping Matrix and Energy Dissipation of Viscoelastic Fiber Composites," *Composite Structures*, 54: 49-55, 2001.

[97] Gibson, R. F., "Dynamic Mechanical Behavior of Fiber-Reinforced Composites: Measurement and Analysis," *Journal of Composite Materials*, 10: 325-341, 1976.

[98] Adams, R. D., and Maheri, M. R., "Dynamic Flexural Properties of Anisotropic Fibrous Composite Beams," *Composites Science and Technology*, 50: 497-514, 1994.

[99] Reddy, J. N., *Mechanics of Laminated Composite Plates: Theory and Analysis*, Boca Raton, FL: CRC Press, Inc., 1997.

[100] Pagano, N. J. "Thickness Expansion Coefficients of Composite Laminates," *Journal of Composite Materials*, 8: 310-312, 1974.

[101] Goetschel, D. B. and Radford, D. W. "Analytical Development of Through-Thickness Properties of Composite Laminates," *Journal of Advanced Materials*, 28 (4): 37-46, 1997.

[102] Contact with Cytec Inc. 1998.

[103] *Automotive Product Guide. PEEK Polymer: A Global Player in the Automotive Industry.* (Consulted: January 2002): http://www.victrex.com/main.html.

[104] *Victrex PEEK: The High Temperature Engineering Thermoplastic – Properties and Processing.* ICI Advanced Materials. 1990.

[105] *Matweb.* (Consulted: February 2002): http://www.matweb.com

[106] Saravanos, D. A. and Pereira, J. M., "Dynamic Characteristics of Specialty Composite Structures with Embedded Damping Layers," *Journal of Vibrations and Acoustics*, 117: 62-69, 1995.

[107] Adams, R. D. and Bacon, D. G. C., "Effect of Fibre Orientation and Laminate Geometry on the Dynamic Properties of CFRP," *Journal of Composite Materials*, 7:402-428, 1973.

[108] Schultz, A. B., and Tsai, S. W., "Measurements of Complex Dynamic Moduli for Laminated Fiber-Reinforced Composites," *Journal of Composite Materials*, 3: 434-443, 1969.

[109] Saravanos, D. A. and Chamis, C. C., "Mechanics of Damping for Fiber Composite Laminates Including Hygrothermal Effects," *AIAA Journal*, 28 (10): 1813-1819, October 1990.

[110] VanGoethem, D. J., and Radford, D. W., "A Sub-Scale Flexure Test for High Modulus Composites," *Proceedings of the 31st International SAMPE Technical Conference*, Chicago, IL, 1999.

[111] Tsuji, N. and Kubomura, K., " Nonlinear Compression Stress-Strain Curve of Pitch-Based High Modulus Carbon-Fiber Composites and Structural Responses," *Journal of Material Science*, 27 (14): 3782-3788, 1992.

[112] Whitney, J. M., *Structural Analysis of Laminated Anisotropic Plates*, Lancaster, PA: Technomic Publishing Co., Inc., 1987.

[113] Wren, G. G., and Kinra, V. K., "An Experimental Study of the Complex Dynamic Modulus", *Proceedings of Damping '89*, WRDC-TR-89-3116, Vol. II, 1989.

[114] Jones, R. M., *Mechanics of Composite Materials*, Washington, D.C.: Scripta Book Company, 1975.

[115] Meunier, M., and Shenoi, R.A., "Dynamic Analysis of Composite Sandwich Plates with Damping Modelled Using High-Order Shear Deformation Theory," *Composite Structures*, 54: 243-254, 2001.

[116] Yim, J. H., "Comparison of Prediction Methods for Damping of a Symmetric Balanced Laminated Composite Beam," *KSME International Journal*, 12(4): 536-543, 1998.

[117] Suwardie, J. H., Melo, J. D., and Radford, D. W., "Measurement of Viscoelastic Properties of PEEK/IM7 by Dynamic Mechanical Thermal Analysis (DMTA)," *Proceedings of the Ninth International Conference on Composites Engineering – ICCE/9*, San Diego, CA, July 1-6, 2002.

[118] Mead, D. J., and Joannides, R. J., "Measurement of the Dynamic Moduli and Poisson's Ratios of a Transversely Isotropic Fibre-Reinforced Plastic," *Composites*, 22(1): 15-29, 1991.

[119] Nakada, M., et al, "Time and Temperature Dependence of Flexural Fatigue Strength for Pitch-based CFRP," *Proceedings of ICCM-12*, Paris, 1999.

[120] Nakada, M., et al, "Time and Temperature Dependence of Static, Creep, and Fatigue Behavior for CF/Epoxy Strands," *Proceedings of ICCM-12*, Paris, 1999.

Appendix 1

In the method of amplitude decay for the calculation of the damping loss factor, a sample is excited once and then allowed to undergo free vibrations. During the free vibrations, energy is dissipated and the loss factor, η, is related to the logarithmic decrement of vibration, Δ.

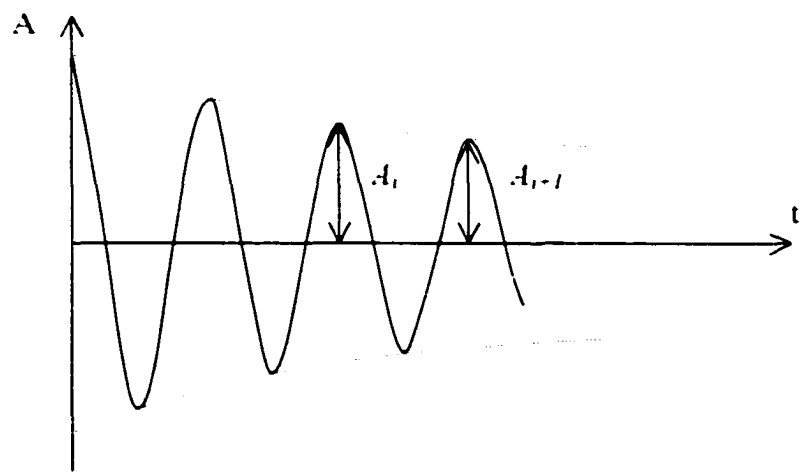

Figure A1.1 – Amplitude decay experiment.

$$\Delta = \frac{1}{n} \ln \frac{A_i}{A_{i+n}} \qquad \text{(A1.1)}$$

This logarithmic decrement is the average characteristic for n cycles since it is dependent upon the displacement amplitude. The dissipation factor, η, correspondent to n cycles, can be calculated as:

$$\Delta = \frac{\Delta W}{2\pi W_m} \tag{A1.2}$$

where:

ΔW = mean energy losses in n cycles;

W_m = mean elastic potential energy.

The mean elastic energy is calculated from the mean amplitude A_m, where,

$$A_m = \frac{A_1 + A_{1+n}}{2} \tag{A1.3}$$

Thus,

$$W_m = c\frac{(A_m)^2}{2} = c\frac{(A_1 + A_{1+n})^2}{8} \tag{A1.4}$$

where:

c = elastic stiffness.

Considering two states of maximum displacements, or displacements equal to the amplitudes, the kinetic energy is zero and therefore, all the energy in the system is in the form of potential energy. Thus, the energy loss corresponding to n cycles can be given by:

$$\Delta W = \frac{cA_1^2}{2} - \frac{cA_{1+n}^2}{2} \tag{A1.5}$$

Substitution of these into the loss factor equation gives,

$$\eta = \frac{2(A_1 - A_{1+n})}{\pi n(A_1 + A_{1+n})} \tag{A1.6}$$

The equation for the logarithmic decrement can be rewritten in series form as:

$$\Delta = \frac{1}{n}\sum_{j=0}^{\infty}\frac{2}{2j+1}\left(\frac{A_i - A_{i+n}}{A_i + A_{i+n}}\right)^{2j+1} \qquad \text{(A1.7)}$$

Previous investigations proved that the logarithmic decrement could be obtained with satisfactory accuracy by the first term of the series [1]. Thus,

$$\Delta \approx \frac{2}{n}\left(\frac{A_i - A_{i+n}}{A_i + A_{i+n}}\right) \qquad \text{(A1.8)}$$

Therefore, the dissipation factor, ψ, correspondent to n cycles, is related to the logarithmic decrement as,

$$\eta \approx \frac{\Delta}{\pi} \qquad \text{(A1.9)}$$

Reference:

[1] Zinoviev, P.A., and Ermakov, Y.N., "Energy Dissipation in Composite Materials", Lancaster, PA, Technomic, Inc., 1994

Appendix 2

Let the function f be continuous in the closed interval $[a, b]$ and let t be any number in $[a, b]$. If the function $S(t)$ is defined as.

$$S(t) = \int_a^t f(u)du \tag{A2.1}$$

then.

$$\frac{dS(t)}{dt} = f(t) \tag{A2.2}$$

Proof: Consider two points t and $t+\Delta t$ in $[a, b]$, then

$$S(t) = \int_a^t f(u)du \tag{A2.3}$$

and

$$S(t+\Delta t) = \int_a^{t+\Delta t} f(u)du \tag{A2.4}$$

Thus.

$$S(t+\Delta t) - S(t) = \int_a^{t+\Delta t} f(u)du - \int_a^t f(u)du \tag{A2.5}$$

but.

$$\int_a^{t+\Delta t} f(u)du = \int_a^t f(u)du + \int_t^{t+\Delta t} f(u)du$$
$$\int_a^{t+\Delta t} f(u)du - \int_a^t f(u)du = \int_t^{t+\Delta t} f(u)du \qquad \text{(A2.6)}$$

Hence.

$$S(t+\Delta t) - S(t) = \int_t^{t+\Delta t} f(u)du \qquad \text{(A2.7)}$$

According to the mean-value theorem, there is a number t' in the interval $[t, t+\Delta t]$ such that.

$$\int_t^{t+\Delta t} f(u)du = f(t')\Delta t \qquad \text{(A2.8)}$$

thus.

$$S(t+\Delta t) - S(t) = f(t')\Delta t \qquad \text{(A2.9)}$$

or.

$$\frac{S(t+\Delta t) - S(t)}{\Delta t} = f(t') \qquad \text{(A2.10)}$$

Taking the limit as $\Delta t \to 0$.

$$\lim_{\Delta t \to 0} \frac{S(t+\Delta t) - S(t)}{\Delta t} = \lim_{\Delta t \to 0} f(t') \qquad \text{(A2.11)}$$

The left hand-side of the equation gives.

$$\lim_{\Delta t \to 0} \frac{S(t+\Delta t) - S(t)}{\Delta t} = \frac{dS(t)}{dt} \qquad \text{(A2.12)}$$

To determine the right hand-side of the equation ($\lim_{\Delta t \to 0} f(t')$), recall that t' is a number in the interval $[t, t+\Delta t]$, so

$$\lim_{\Delta t \to 0} t' = t \tag{A2.13}$$

Thus, since f is continuous at t,

$$\lim_{\Delta t \to 0} f(t') = \lim_{t' \to t} f(t') = f(t) \tag{A2.14}$$

Therefore,

$$\frac{dS(t)}{dt} = f(t) \tag{A2.15}$$

Appendix 3

The Fourier transform of a function $f(t)$ is defined as:

$$\Im[f(t)] = F(\omega) = \int_{-\infty}^{\infty} f(t)e^{-i\omega t}\,dt \tag{A3.1}$$

The inverse Fourier transform of $F(\omega)$ is defined as:

$$\Im^{-1}[F(\omega)] = f(t) = \frac{1}{2\pi}\int_{-\infty}^{\infty} F(\omega)e^{i\omega t}\,d\omega \tag{A3.2}$$

Using the identity $e^{i\omega t} = \cos\omega t + i\sin\omega t$, the Fourier transform can also be written as:

$$\begin{aligned} F(\omega) &= \int_{-\infty}^{\infty} f(t)\cos\omega t\,dt - i\int_{-\infty}^{\infty} f(t)\sin\omega t\,dt \\ F(\omega) &= R(\omega) + iX(\omega) \end{aligned} \tag{A3.3}$$

where:

$$\begin{aligned} R(\omega) &= \int_{-\infty}^{\infty} f(t)\cos\omega t\,dt \\ X(\omega) &= -\int_{-\infty}^{\infty} f(t)\sin\omega t\,dt \end{aligned} \tag{A3.4}$$

$R(\omega)$ is an even function since $R(-\omega) = R(\omega)$ and $X(\omega)$ is odd since $X(-\omega) = -X(\omega)$.

Equation (A3.2) may be rewritten as.

$$f(t)=\frac{1}{2\pi}\int_{-\infty}^{\infty}F(\omega)e^{i\omega t}d\omega=\frac{1}{2\pi}\int_{-\infty}^{\infty}[R(\omega)+iX(\omega)][\cos\omega t+i\sin\omega t]d\omega$$
$$f(t)=\frac{1}{2\pi}\int_{-\infty}^{\infty}[R(\omega)\cos\omega t-X(\omega)\sin\omega t]d\omega+i\frac{1}{2\pi}\int_{-\infty}^{\infty}[R(\omega)\sin\omega t+X(\omega)\cos\omega t]d\omega \quad \text{(A3.5)}$$

The product of two even or two odd functions is an even function and the product of an odd and an even function is an odd function. Thus, $R(\omega)\sin\omega t+X(\omega)\cos\omega t$ is odd, and,

$$\frac{1}{2\pi}\int_{-\infty}^{\infty}[R(\omega)\sin\omega t+X(\omega)\cos\omega t]d\omega=0 \quad \text{(A3.6)}$$

since the integrand is odd.

Therefore,

$$f(t)=\frac{1}{2\pi}\int_{-\infty}^{\infty}[R(\omega)\cos\omega t-X(\omega)\sin\omega t]d\omega \quad \text{(A3.7)}$$

and $f(t)$ is real.

A3.1 Fourier cosine transform.

If $f(t)$ is given only for $0<t<\infty$, in order to find the inverse cosine transform, an extension can be defined for negative t as $f(-t)=f(t)$, or $f(t)$ is even. Since $f(t)$ is defined only for $0<t<\infty$, the final results must also be restricted for $0<t<\infty$. Given that $f(t)$ is even,

$$X(\omega)=-\int_{-\infty}^{\infty}f(t)\sin\omega t\,dt=0\text{, since the integrand is odd.}$$

In this case.

$$F(\omega) = R(\omega) + iX(\omega) = R(\omega)$$
$$F(\omega) = R(\omega) = \int_{-\infty}^{\infty} f(t)\cos\omega t\, dt \tag{A3.8}$$

or

$$F(\omega) = 2\int_{0}^{\infty} f(t)\cos\omega t\, dt \tag{A3.9}$$

and.

$$f(t) = \frac{1}{2\pi}\int_{-\infty}^{\infty}[R(\omega)\cos\omega t - X(\omega)\sin\omega t]d\omega = \frac{1}{2\pi}\int_{-\infty}^{\infty} R(\omega)\cos\omega t d\omega$$
$$f(t) = \frac{1}{\pi}\int_{0}^{\infty} R(\omega)\cos\omega t d\omega = \frac{1}{\pi}\int_{0}^{\infty} F(\omega)\cos\omega t d\omega \tag{A3.10}$$

A3.2 Fourier sine transform.

If $f(t)$ is given only for $0<t<\infty$. in order to find the inverse sine transform. an extension can be defined for negative t as $f(-t) = -f(t)$. or $f(t)$ is odd. Since $f(t)$ is defined only for $0<t<\infty$. the final results must be restricted for $0<t<\infty$. Given that $f(t)$ is odd.

$$R(\omega) = \int_{-\infty}^{\infty} f(t)\cos\omega t\, dt = 0\text{ . since the integrand is odd.}$$

In this case.

$$F(\omega) = R(\omega) + iX(\omega) = iX(\omega)$$
$$F(\omega) = iX(\omega) = -i\int_{-\infty}^{\infty} f(t)\sin\omega t\, dt \tag{A3.11}$$

or

$$F(\omega) = -2i\int_0^{\infty} f(t)\sin\omega t\, dt \tag{A3.12}$$

and.

$$\begin{aligned} f(t) &= \frac{1}{2\pi}\int_{-\infty}^{\infty}[R(\omega)\cos\omega t - X(\omega)\sin\omega t]d\omega = -\frac{1}{2\pi}\int_{-\infty}^{\infty} X(\omega)\sin\omega t d\omega \\ f(t) &= -\frac{1}{\pi}\int_0^{\infty} X(\omega)\sin\omega t d\omega = -\frac{1}{i\pi}\int_0^{\infty} F(\omega)\sin\omega t d\omega \end{aligned} \tag{A3.13}$$

A3.3 Summary:

Fourier cosine transform.

$$\begin{aligned} \Im[f(t)] &= F(\omega) = \int_0^{\infty} f(t)\cos\omega t\, dt \\ \Im^{-1}[F(\omega)] &= f(t) = \frac{2}{\pi}\int_0^{\infty} F(\omega)\cos\omega t d\omega \end{aligned} \tag{A3.14}$$

Fourier sine transform.

$$\begin{aligned} \Im[f(t)] &= F(\omega) = \int_0^{\infty} f(t)\sin\omega t\, dt \\ \Im^{-1}[F(\omega)] &= f(t) = \frac{2}{\pi}\int_0^{\infty} F(\omega)\sin\omega t d\omega \end{aligned} \tag{A3.14}$$

Reference:

[1] Hsu, Hwei P., "Fourier Analysis", Simon and Schuster, New York, 1970.

Appendix 4

The CTE's of a $[(+\theta/-\theta)_n]_s$ laminate, are determined by

$$\{\alpha\} = \frac{1}{\Delta T}\{\varepsilon\} = \left[\left[\overline{C}\right]^{(\theta)} + \left[\overline{C}\right]^{(-\theta)}\right]^{-1}\left\{\left[\overline{C}\right]^{(\theta)}\{\overline{\alpha}\}^{(\theta)} + \left[\overline{C}\right]^{(-\theta)}\{\overline{\alpha}\}^{(-\theta)}\right\} \tag{A4.1}$$

Where:

$$\left[\overline{C}\right]^{(\theta)} = \begin{bmatrix} \overline{C}_{11}^{(\theta)} & \overline{C}_{12}^{(\theta)} & \overline{C}_{13}^{(\theta)} & 0 & 0 & \overline{C}_{16}^{(\theta)} \\ \overline{C}_{12}^{(\theta)} & \overline{C}_{22}^{(\theta)} & \overline{C}_{23}^{(\theta)} & 0 & 0 & \overline{C}_{26}^{(\theta)} \\ \overline{C}_{13}^{(\theta)} & \overline{C}_{23}^{(\theta)} & \overline{C}_{33}^{(\theta)} & 0 & 0 & \overline{C}_{36}^{(\theta)} \\ 0 & 0 & 0 & \overline{C}_{44}^{(\theta)} & \overline{C}_{45}^{(\theta)} & 0 \\ 0 & 0 & 0 & \overline{C}_{45}^{(\theta)} & \overline{C}_{55}^{(\theta)} & 0 \\ \overline{C}_{16}^{(\theta)} & \overline{C}_{26}^{(\theta)} & \overline{C}_{36}^{(\theta)} & 0 & 0 & \overline{C}_{66}^{(\theta)} \end{bmatrix} \tag{A4.2}$$

and.

$$\left[\overline{C}\right]^{(-\theta)} = \begin{bmatrix} \overline{C}_{11}^{(\theta)} & \overline{C}_{12}^{(\theta)} & \overline{C}_{13}^{(\theta)} & 0 & 0 & -\overline{C}_{16}^{(\theta)} \\ \overline{C}_{12}^{(\theta)} & \overline{C}_{22}^{(\theta)} & \overline{C}_{23}^{(\theta)} & 0 & 0 & -\overline{C}_{26}^{(\theta)} \\ \overline{C}_{13}^{(\theta)} & \overline{C}_{23}^{(\theta)} & \overline{C}_{33}^{(\theta)} & 0 & 0 & -\overline{C}_{36}^{(\theta)} \\ 0 & 0 & 0 & \overline{C}_{44}^{(\theta)} & -\overline{C}_{45}^{(\theta)} & 0 \\ 0 & 0 & 0 & -\overline{C}_{45}^{(\theta)} & \overline{C}_{55}^{(\theta)} & 0 \\ -\overline{C}_{16}^{(\theta)} & -\overline{C}_{26}^{(\theta)} & -\overline{C}_{36}^{(\theta)} & 0 & 0 & \overline{C}_{66}^{(\theta)} \end{bmatrix} \tag{A4.3}$$

Thus.

$$\left[\left[\overline{C}\right]^{(\theta)}+\left[\overline{C}\right]^{(-\theta)}\right]=2\begin{bmatrix}\overline{C}_{11} & \overline{C}_{12} & \overline{C}_{13} & 0 & 0 & 0\\ \overline{C}_{12} & \overline{C}_{22} & \overline{C}_{23} & 0 & 0 & 0\\ \overline{C}_{13} & \overline{C}_{23} & \overline{C}_{33} & 0 & 0 & 0\\ 0 & 0 & 0 & \overline{C}_{44} & 0 & 0\\ 0 & 0 & 0 & 0 & \overline{C}_{55} & 0\\ 0 & 0 & 0 & 0 & 0 & \overline{C}_{66}\end{bmatrix}^{(\theta)} \tag{A4.4}$$

Then.

$$\left[\left[\overline{C}\right]^{(\theta)}+\left[\overline{C}\right]^{(-\theta)}\right]^{-1}= \tag{A4.5}$$

$$\frac{1}{2}\begin{bmatrix}\frac{\left(\overline{C}_{22}\overline{C}_{33}-\overline{C}_{23}^{2}\right)}{-\left[c_4(\cos(2\theta))^2+c_1\right]} & \frac{\left(\overline{C}_{13}\overline{C}_{23}-\overline{C}_{12}\overline{C}_{33}\right)}{-\left[c_4(\cos(2\theta))^2+c_1\right]} & \frac{\left(\overline{C}_{12}\overline{C}_{23}-\overline{C}_{13}\overline{C}_{22}\right)}{-\left[c_4(\cos(2\theta))^2+c_1\right]} & 0 & 0 & 0\\ \frac{\left(\overline{C}_{13}\overline{C}_{23}-\overline{C}_{12}\overline{C}_{33}\right)}{-\left[c_4(\cos(2\theta))^2+c_1\right]} & \frac{\left(\overline{C}_{11}\overline{C}_{33}-\overline{C}_{13}^{2}\right)}{-\left[c_4(\cos(2\theta))^2+c_1\right]} & \frac{\left(\overline{C}_{13}\overline{C}_{12}-\overline{C}_{11}\overline{C}_{23}\right)}{-\left[c_4(\cos(2\theta))^2+c_1\right]} & 0 & 0 & 0\\ \frac{\left(\overline{C}_{12}\overline{C}_{23}-\overline{C}_{13}\overline{C}_{22}\right)}{-\left[c_4(\cos(2\theta))^2+c_1\right]} & \frac{\left(\overline{C}_{13}\overline{C}_{12}-\overline{C}_{11}\overline{C}_{23}\right)}{-\left[c_4(\cos(2\theta))^2+c_1\right]} & \frac{\left(\overline{C}_{11}\overline{C}_{22}-\overline{C}_{12}^{2}\right)}{-\left[c_4(\cos(2\theta))^2+c_1\right]} & 0 & 0 & 0\\ 0 & 0 & 0 & \frac{1}{\overline{C}_{44}} & 0 & 0\\ 0 & 0 & 0 & 0 & \frac{1}{\overline{C}_{55}} & 0\\ 0 & 0 & 0 & 0 & 0 & \frac{1}{\overline{C}_{66}}\end{bmatrix}^{(\theta)}$$

Where:

$$c_1=C_{11}C_{33}+C_{22}C_{33}+2C_{12}C_{33}-C_{13}^2-2C_{13}C_{23}-C_{23}^2$$

$$c_2=C_{22}C_{33}-C_{11}C_{33}+C_{13}^2-C_{23}^2$$

$$c_3=C_{11}C_{23}-C_{22}C_{13}-C_{12}C_{13}+C_{12}C_{23} \tag{A4.6}$$

$$c_4=\frac{c_1(C_{11}+C_{22}-2C_{12}-4C_{66})+c_2(C_{11}-C_{22})+2c_3(C_{13}-C_{23})}{4C_{66}}$$

And.

$$\left\{\left[\overline{C}\right]^{(\theta)}\{\overline{\alpha}\}^{(\theta)}+\left[\overline{C}\right]^{(-\theta)}\{\overline{\alpha}\}^{(-\theta)}\right\}= \tag{A4.7}$$

$$\left[\overline{C}\right]^{(\theta)}\begin{Bmatrix}\frac{1}{2}(\alpha_1+\alpha_2)+\frac{1}{2}(\alpha_1-\alpha_2)\cos(2\theta)\\ \frac{1}{2}(\alpha_1+\alpha_2)-\frac{1}{2}(\alpha_1-\alpha_2)\cos(2\theta)\\ \alpha_3\\ 0\\ 0\\ (\alpha_1-\alpha_2)\sin(2\theta)\end{Bmatrix}+\left[\overline{C}\right]^{(-\theta)}\begin{Bmatrix}\frac{1}{2}(\alpha_1+\alpha_2)+\frac{1}{2}(\alpha_1-\alpha_2)\cos(2\theta)\\ \frac{1}{2}(\alpha_1+\alpha_2)-\frac{1}{2}(\alpha_1-\alpha_2)\cos(2\theta)\\ \alpha_3\\ 0\\ 0\\ -(\alpha_1-\alpha_2)\sin(2\theta)\end{Bmatrix}$$

or.

$$\left\{\left[\overline{C}\right]^{(\theta)}\{\overline{\alpha}\}^{(\theta)}+\left[\overline{C}\right]^{(-\theta)}\{\overline{\alpha}\}^{(-\theta)}\right\}= \tag{A4.8}$$

$$2\begin{bmatrix}\overline{C}_{11}^{(\theta)} & \overline{C}_{12}^{(\theta)} & \overline{C}_{13}^{(\theta)} & 0 & 0 & \overline{C}_{16}^{(\theta)}\\ \overline{C}_{12}^{(\theta)} & \overline{C}_{22}^{(\theta)} & \overline{C}_{23}^{(\theta)} & 0 & 0 & \overline{C}_{26}^{(\theta)}\\ \overline{C}_{13}^{(\theta)} & \overline{C}_{23}^{(\theta)} & \overline{C}_{33}^{(\theta)} & 0 & 0 & \overline{C}_{36}^{(\theta)}\\ 0 & 0 & 0 & 0 & 0 & 0\\ 0 & 0 & 0 & 0 & 0 & 0\\ 0 & 0 & 0 & 0 & 0 & 0\end{bmatrix}\begin{Bmatrix}\frac{1}{2}(\alpha_1+\alpha_2)+\frac{1}{2}(\alpha_1-\alpha_2)\cos(2\theta)\\ \frac{1}{2}(\alpha_1+\alpha_2)-\frac{1}{2}(\alpha_1-\alpha_2)\cos(2\theta)\\ \alpha_3\\ 0\\ 0\\ (\alpha_1-\alpha_2)\sin(2\theta)\end{Bmatrix}$$

Performing the matrix multiplication and substituting the values of $\overline{C}_{ij}$.

(A4.9)

$$\begin{Bmatrix}\alpha_x\\ \alpha_y\\ \alpha_{xy}\\ \alpha_{yz}\\ \alpha_{xz}\\ \alpha_{xy}\end{Bmatrix}=\begin{bmatrix}1 & 0 & 0 & 0 & 0 & \frac{1}{2}\sin(2\theta)\frac{-c_4(\cos(2\theta))+c_2}{-\left[c_4(\cos(2\theta))^2+c_1\right]}\\ 0 & 1 & 0 & 0 & 0 & \frac{1}{2}\sin(2\theta)\frac{c_4(\cos(2\theta))+c_2}{-\left[c_4(\cos(2\theta))^2+c_1\right]}\\ 0 & 0 & 1 & 0 & 0 & \sin(2\theta)\frac{c_3}{-\left[c_4(\cos(2\theta))^2+c_1\right]}\\ 0 & 0 & 0 & 0 & 0 & 0\\ 0 & 0 & 0 & 0 & 0 & 0\\ 0 & 0 & 0 & 0 & 0 & 0\end{bmatrix}\begin{Bmatrix}\frac{1}{2}(\alpha_1+\alpha_2)+\frac{1}{2}(\alpha_1-\alpha_2)\cos(2\theta)\\ \frac{1}{2}(\alpha_1+\alpha_2)-\frac{1}{2}(\alpha_1-\alpha_2)\cos(2\theta)\\ \alpha_3\\ 0\\ 0\\ (\alpha_1-\alpha_2)\sin(2\theta)\end{Bmatrix}$$

Therefore. the expressions for the coefficients of thermal expansion of the laminate are found to be.

$$\alpha_r(\theta) = \frac{1}{2}(\alpha_1 + \alpha_2) + \frac{1}{2}(\alpha_1 - \alpha_2)\frac{c_2(\cos(2\theta))^2 + (c_1 + c_4)\cos(2\theta) - c_2}{c_4(\cos(2\theta))^2 + c_1} \qquad \text{(A4.10)}$$

$$\alpha_t(\theta) = \frac{1}{2}(\alpha_1 + \alpha_2) + \frac{1}{2}(\alpha_1 - \alpha_2)\frac{c_2(\cos(2\theta))^2 - (c_1 + c_4)\cos(2\theta) - c_2}{c_4(\cos(2\theta))^2 + c_1} \qquad \text{(A4.11)}$$

$$\alpha_z(\theta) = \alpha_3 + (\alpha_1 - \alpha_2)\frac{c_3((\cos(2\theta))^2 - 1)}{c_4(\cos(2\theta))^2 + c_1} \qquad \text{(A4.12)}$$

Appendix 5

A5.1 Matlab program to calculate the least squares estimates for the parameters c_1, c_2, c_3, and c_4, (Chapter 4).

```
% Code to find c1, c2, c3 and c4 for the determination of the Elastic Constants.
% Ref.:
% http://www.mathworks.com/access/helpdesk/help/pdf_doc/stats/stats_tb.pdf
% (page 1.100)
%       ------------------------------
%           Jose Daniel D. Melo
%            August, 2001
%       ------------------------------
% This code calculates the least squares estimates for the unknown parameters
% in a series of equations.
% In other words, it finds the parameters that minimize the sum of the squared
% differences between the observed responses and their fitted values.
% The function nlinfit uses the Gauss-Newton
% algorithm with Levenberg-Marquardt modifications for global convergence.
% After the first solution, use the results as the new initial guesses
% and run the program again.

clear all;
% Specify the range for the data of guesses values of c1, c2, c3, and c4.
range = 'A3..D3';
cguess = dlmread('input.txt','',range);
% Transform the initial guesses to a column vector.
c=(cguess)';
% Specify the range for the data of theta(angle),alpha(x)and alpha(z).
data = dlmread('input.txt','',5,0);
% Note: This is a zero based specification.
% Thus, r=5, c=0, means row 6 and column 1.
theta = data(:,1); alphax = data(:,2); alphaz = data(:,3);
n = length(theta);
% Find the cosine and cosine square of theta to apply in equations.
for i=1:n
 cos2theta(i) = cos(2*theta(i)*pi/180);
 cos2theta2(i) = cos2theta(i)^2;
end
```

```
cosines = [(cos2theta)' (cos2theta2)'];
% The function nlinfit will use the cosines vector (cos and cos^2), the
% values of alpha(x), and the initial guesses of c1, c2, c3 and c4, to perform the least
% squares estimation for the values of c1, c2, c3 and c4. The first function, cs1,
% calculates the values of c1, c2, and c4 from the equation of alpha(x). The other
% function, cs2, calculates the values of c1, c3, and c4, from the equation of alpha(z).
constx=nlinfit(cosines,alphax,'cs1',c);
constz=nlinfit(cosines,alphaz,'cs2',c);
fid=fopen('output.txt','w');
fprintf(fid,'From alpha(x), c1, c2, c3, and c4 are:');
fprintf(fid,'\n  %6.4f',constx);
fprintf(fid,'\nFrom alpha(z), c1, c2, c3, and c4 are:');
fprintf(fid,'\n  %6.4f',constz);
status=fclose('all');
```

A5.2 Matlab program cs1.m with a function called by the code presented in A5.1.

```
function alphaxhat = cs(c,x)
c1 = c(1);
c2 = c(2);
c4 = c(4);

x1 = x(:,1);
x2 = x(:,2);
% where: x1 = cos (2*t) and x2 = cos^2 (2*t)

% function for alpha (x)
alphaxhat=0.5*(-0.11+37.51)+0.5*(-0.11-37.51)*((c2*x2+(c1+c4)*x1-c2)./(c4*x2+c1));
```

A5.3 Matlab program cs2.m with a function called by the code presented in A5.1.

```
function alphazhat = cs(c,x)
c1 = c(1);
c3 = c(3);
c4 = c(4);

x1 = x(:,1);
x2 = x(:,2);
% where: x1 = cos (2*t) and x2 = cos^2 (2*t)

% function for alpha (z)
alphazhat=37.51+(-0.11-37.51)*((c3*(x2-1))./(c4*x2+c1));
```

A5.4 Example of input file (input.txt) for the code presented in A5.1.

```
Enter the data for c1, c2, c3, and c4, separated by comma.
c1,c2,c3,c4
1.63,-1.36,0.70,1.18
Enter the data for theta(angle),alpha(x)and alpha(z), separated by comma.
theta,alpha(x),alpha(z)
0,-0.11,37.51
30,-5.19,47.56
60,22.33,47.56
90,37.51,37.51
```

A5.5 Example of output file (output.txt) for the code presented in A5.1.

```
From alpha(x), c1, c2, c3, and c4 are:
  1.6178
 -1.3737
  0.7000
  1.1811
From alpha(z), c1, c2, c3, and c4 are:
  1.6346
 -1.3600
  0.6874
  1.1811
```

Appendix 6

PEEK

PEEK (Polyetheretherketone) is a semi-crystalline thermoplastic polymer which holds a superior combination of properties including high heat stability, wear resistance, low coefficient of friction, high strength, high stiffness, high impact resistance, and excellent chemical resistance. PEEK can be processed by many different methods, which include: injection molding, extrusion, compression molding, powder coating, composite manufacturing, wire coating, compounding, foaming and solution membrane casting.

Due to its superior properties combined with easy processability, PEEK has been used as a substitute of other materials such as steel, aluminum, bronze, and titanium, in parts subjected to high demanding conditions. PEEK can be applied to applications with operating temperatures of 260°C. Some of the important applications for PEEK are:

Automotive

Polymers are increasingly being applied in the automotive industry, improving overall performance and reducing manufacturing costs. Figure 1 shows some potential applications for PEEK in automobiles.

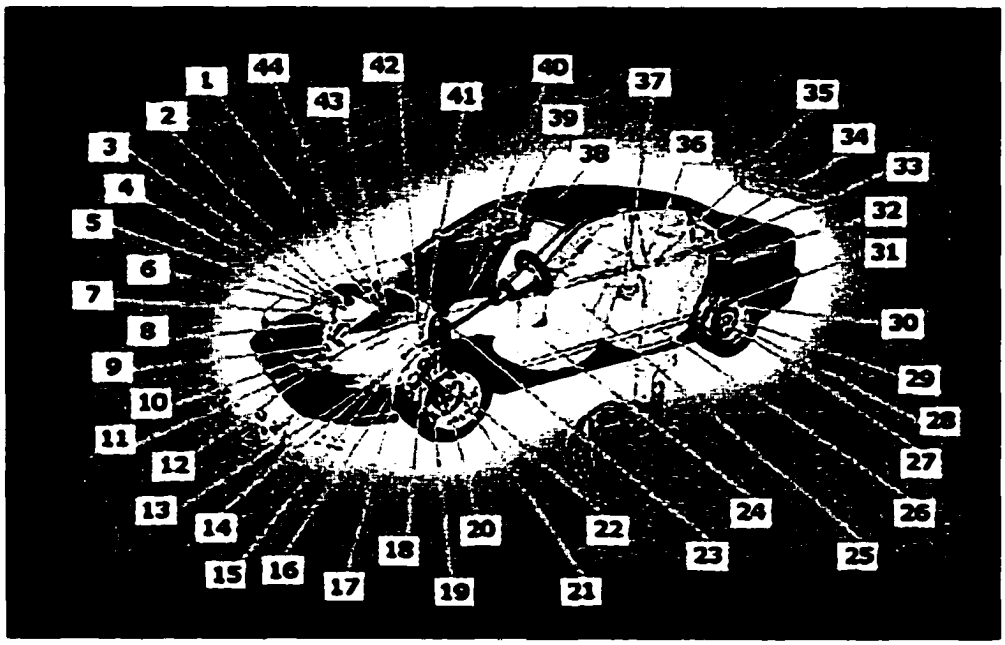

1. Throttle Body Bushings
2. Timing Chain Tensioner
3. Oil Pump Rotors
4. Oil Pump Gears
5. Oil Pump Shafts
6. Distributor Gears
7. Water Pump Impeller
8. Engine Seals
9. Turbo Charger Impellers
10. Turbo Charger Couplings
11. O2 Sensors
12. O2 Wires
13. Transmission Wear Pads
14. Transmission Thrust Washers
15. Transmission Bushings
16. Transmission Valves
17. Transmission Filter Housing
18. Transmission Seals
19. Ball Joint Liners
20. U-Joint Bearings
21. Needle Bearings
22. Tie Rod Joint Liners
23. ABS Brake Seats
24. Power Seat Components
25. Power Window Gearing
26. Fuel Line Connector
27. Brake Wear Sensors
28. Tire Studs
29. Bearing Cages
30. Wheel Sensors
31. Brake Cylinder Components
32. Shock Absorber Components
33. Fuel Pump Gears
34. Fuel Pump Motor Components
35. Fuel Pump Bushings
36. Electric Window Motor Thrust Plugs
37. Electric Motor Thrust Washers
38. Sunroof Gears
39. HVAC Gearing
40. Isolator Bolts
41. Power Steering Gears
42. Steering Shaft Isolators
43. Protective Sleeving and Braiding
44. EGR Temperature Sensor

Figure 1– Automotive application opportunities for PEEK [1].

Aerospace

The aerospace industry demands structural materials with low density, excellent physical and thermal characteristics, and fire retardant properties. PEEK is being increasingly applied in the aerospace industry as a replacement for metal components in-engine parts, and aircraft exterior and interior components [2]. In-engine applications of PEEK are in parts subjected to tribological interaction at high temperatures. For the aircraft exterior, PEEK offers a very good erosion resistance, as it is required to resist impacts from rain drops an atmosphere particles. In the aircraft interior, PEEK can be used in many applications, such as housings and brackets, offering advantages of weight reduction and easy processing.

Medical Industry

Besides providing superior mechanical properties, biomaterials have also to meet bio-compatibility and bio-stability criteria. PEEK is being applied as a substitute of more conventional materials in biomedical applications such as in spinal-fusion cages (Figure 2), replacing titanium components. Other biomedical applications include dental implants, heart valves, components for cardiac pumps, pacemaker components, elbow implants, spinal implants, artificial hips, finger implants, femoral bone replacements, and knee joints [2,3]. PEEK provides stiffness similar to bone and can withstand sterilization without affecting the physical and mechanical properties [3].

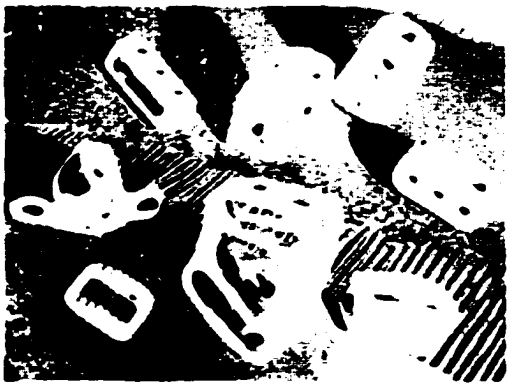

Figure 2 - PEEK spinal-fusion cages [3].

Semiconductor Industry

The semiconductor industry is currently one of the largest markets for PEEK [3]. PEEK has been used in wafer-handling devices, fixtures, pipes, etc. The increase in automation of wafer handling processes requires wafer carriers with improved tolerances, dimensional stability and abrasion resistance, to allow fast robotic operation. A recently designed wafer carrier, uses carbon filled PEEK wafer supports, providing static protection, abrasion resistance and dimensional stability (Figure 3).

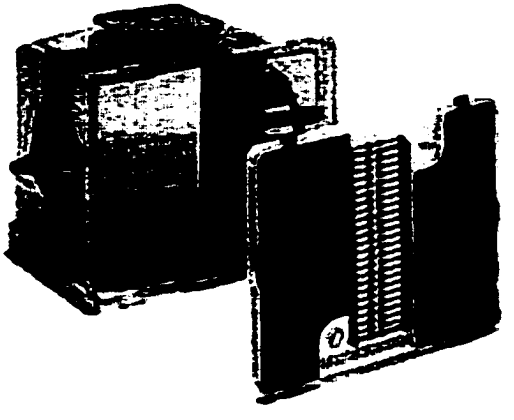

Figure 3 - F300 wafer carrier uses a static dissipative carbon fiber filled PEEK [4].

Table A6.1 - Properties of PEEK [1-5].

Property *			Method
Density (g/cm^3)	35% Crystallinity, as molded	1.29	ASTM D792
	Amorphous	1.26	ASTM D792
Tensile Strength (MPa)	23°C	100.0	ASTM D638
	250°C	12.0	ASTM D638
Tensile Modulus (GPa) Secant @ 1(%) strain	23°C	3.6	ASTM D638
Elongation @ break (%)	23°C	50.0	ASTM D638
Flexural Strength (MPa)	23°C	170.0	ASTM D790
	121°C	100.0	ASTM D790
	250°C	12.4	ASTM D790
Flexural Modulus (GPa)	23°C	4.1	ASTM D790
	121°C	4.0	ASTM D790
	250°C	0.3	ASTM D790
Shear Strength (MPa)	23°C	53.0	ASTM D3846
Shear Modulus (GPa)	23°C	1.3	
Poisson's Ratio	23°C	0.4	ASTM D638
Rockwell Hardness (R scale)		126	ASTM D785
Unnotched Izod Impact (J/m)		no break	ASTM D256
Notched Izod Impact (J/m)		7.5	ASTM D256
Glass Transition Temperature (°C) (onset value)		142.7	DSC
Melt Temperature (°C)		340.0	DSC
Thermal Conductivity (W/m/°C)		0.24	ASTM C177
Coefficient of Thermal Expansion ($10^{-6}°C^{-1}$)	Above Tg	47	ASTM D696
	Below Tg	108	ASTM D696
24-Hour Water Absorption (wt. %)		0.5	ASTM D570
Shrinkage (Molded) (%)	Flow	0.74	
	Transverse	1.18	

* Data for 450G, 150G, 381G PEEK grades.

Table A6.2 - Chemical Resistance of PEEK [1,5].

Chemical	23°C	100°C	200°C
Nitric Acid, Conc.	C	C	C
Sulfuric Acid, >40% Conc.	C	C	C
Benzyl Alcohol	A		
Ethanol	A	A	
Ethylene Glycol, 50% Conc.	A	A	A
Methanol	A	A	
Methylethylketone (MEK)	A	B	
Oils (Di-Ester and Phosphate Ester Based)	A	A	
Ethylene Oxide (ETO)	A		
Freon 113 Trichlorotrifluoroethane	A		
Freon 12, Dichloridifluoromethane	A		
Freon 134a	A		
Aviation Hydraulic Fluid	A		
Benzene	A	A	
Brake Fluid (Mineral)	A	A	A
Brake Fluid (Polyglycol)	A	A	A
Crude Oil	A		
Diesel Oil	A		
Ethane	A		
Fuel Oil	A		
Gasoline	A		
Hydraulic Fluid	A		
Iso-Octane	A		
Kerosene	A		
Lubricating Oil	A		
Methane (Gas)	A	A	A
Motor Oil	A	A	A
Oils (Petroleum)	A	A	
Petroleum Ether	A	A	
Hydraulic Fluid	A		
Transformer Oil	A	A	
Water, Sea/Salt	A	A	

Key: A – No attack, B – Slight attack, C – Severe attack.

References:

1 Automotive Product Guide. PEEK Polymer: A Global Player in the Automotive Industry. (Consulted: October 2001): http://www.victrex.com
2 Ridout Plastics. (Consulted: April 2002):http://www.ridoutplastics.com
3 Plastics Technology. (Consulted: April 2002): http://www.plasticstechnology.com
4 Entegris. (Consulted: April 2002): http://www.wafercare.com
5 Victrex Peek – The High Temperature Engineering Thermoplastic – Properties and Processing. ICI Advanced Materials. Literature Reference: VK10/0690. 1990.

Appendix 7

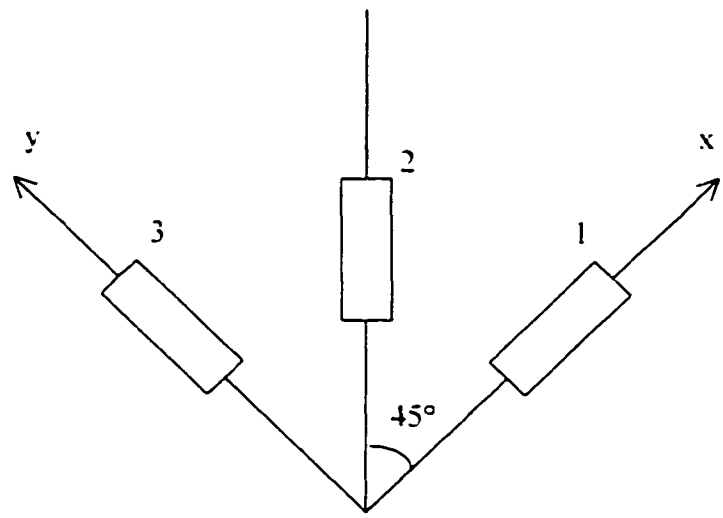

Figure A7.1 - 45° rosette.

The strain transformation equation is given by:

$$\varepsilon(\theta) = \varepsilon_x \cos^2\theta + \varepsilon_y \sin^2\theta + \gamma_{xy} \sin\theta\cos\theta \qquad \text{(A7.1)}$$

With the application of the transformation equation for each of the three gages, the strain components ε_x, ε_y, and γ_{xy}, can be determined.

$$\begin{aligned} \varepsilon_1 &= \varepsilon_x \\ \varepsilon_2 &= \frac{1}{2}\varepsilon_x + \frac{1}{2}\varepsilon_y + \frac{1}{2}\gamma_{xy} \\ \varepsilon_3 &= \varepsilon_y \end{aligned} \qquad \text{(A7.2)}$$

Solving these equations:

$$\begin{aligned} \varepsilon_x &= \varepsilon_1 \\ \varepsilon_y &= \varepsilon_3 \\ \gamma_{xy} &= 2\varepsilon_2 - (\varepsilon_1 + \varepsilon_3) \end{aligned} \tag{A7.3}$$

The principal strains are given by:

$$\varepsilon_{max,min} = \frac{\varepsilon_x + \varepsilon_y}{2} \pm \sqrt{\left(\frac{\varepsilon_x - \varepsilon_y}{2}\right)^2 + \left(\frac{\gamma_{xy}}{2}\right)^2} \tag{A7.4}$$

$$\theta = \frac{1}{2}\tan^{-1}\frac{\gamma_{xy}}{\varepsilon_x - \varepsilon_y} \tag{A7.5}$$

Thus.

$$\varepsilon_{max,min} = \frac{\varepsilon_1 + \varepsilon_3}{2} \pm \frac{1}{2}\sqrt{(\varepsilon_1 - \varepsilon_3)^2 + (2\varepsilon_2 - \varepsilon_1 - \varepsilon_3)^2} \tag{A7.6}$$

$$\theta = \frac{1}{2}\tan^{-1}\frac{2\varepsilon_2 - \varepsilon_1 - \varepsilon_3}{\varepsilon_1 - \varepsilon_3} \tag{A7.7}$$

Appendix 8

A8.1 Matlab program to calculate viscoelastic properties of a symmetric laminated beam (Model 1 – Chapter 6).

```
% This code calculates the dynamic modulus and damping factor
% (tan delta) for a symmetric laminated beam.
% Ref.: Adams. R.D.. and Maheri. M. R.. Comp. Science and Tech. 50. 497-514. (1994).
%       ------------------------------
%           Jose Daniel D. Melo
%             February. 2002
%       ------------------------------
clear all:
data = dlmread('input.txt'.'.'.3.0):
% Note: This is a zero based specification.
% Thus. r=3. c=0. means row 4 and column 1.
E1 = data(:.1): E2 = data(:.2): G12 = data(:.3): v12 = data(:.4):
eta1 = data(:.5): eta2 = data(:.6): eta6 = data(:.7):
ang = (data(:.8))*pi/180: t = data(:.9):
n=length(E1):
for layer=1:n
 S(:.:.layer)=[1/E1(layer) -v12(layer)/E1(layer) 0:
              -v12(layer)/E1(layer) 1/E2(layer) 0:
              0 0 1/G12(layer)]:
 Q(:.:.layer)=inv(S(:.:.layer)):
 ETA(:.:.layer)=[eta1(layer) 0 0:
              0 eta2(layer) 0:
              0 0 eta6(layer)]:
 c(layer)=cos(ang(layer)): s(layer)=sin(ang(layer)):
 R(:.:.layer)=[c(layer)^2 s(layer)^2 2*c(layer)*s(layer):
              s(layer)^2 c(layer)^2 -2*c(layer)*s(layer):
     -c(layer)*s(layer) c(layer)*s(layer) (c(layer)^2-s(layer)^2)]:
 QBAR(:.:.layer)=inv(R(:.:.layer))*Q(:.:.layer)*(inv(R(:.:.layer)))':
 ETABAR(:.:.layer)=(R(:.:.layer))'*ETA(:.:.layer)*(inv(R(:.:.layer)))':
end
h=sum(t):
z=-h/2:
for i=2:n+1
 z(i)=z(i-1)+t(i-1):
```

```
end
D=zeros(3):
for k=1:n
 D=D+(QBAR(:,:,k)*(z(k+1)^3-z(k)^3))/3.:
end
d=inv(D):
for layer=1:n
 f(layer)=QBAR(1,1,layer)*d(1,1)+QBAR(1,2,layer)*d(1,2)+...
        QBAR(1,3,layer)*d(1,3):
 g(layer)=ETABAR(1,1,layer)*d(1,1)+ETABAR(1,2,layer)*d(1,2)+...
        ETABAR(1,3,layer)*d(1,3):
end
etab=0:
for k=1:n
 etab=etab+(f(k)*g(k)*(z(k+1)^3-z(k)^3))/(3*d(1,1)):
end
Exb = 12/(h^3*d(1,1)):
fid=fopen('output.txt','w'):
fprintf(fid,'The properties for this laminated beam are:'):
fprintf(fid,'\n  Total number of layers n= %2d',n):
fprintf(fid,'\n  Dynamic modulus Exb= %5.4e',Exb):
fprintf(fid,'\n  Damping factor eta= %5.2e\n',etab):
status=fclose('all'):
```

A8.2 Matlab program to calculate viscoelastic properties of a symmetric laminated beam (Model 2 – Chapter 6).

```
% This code calculates the dynamic modulus and damping factor
% (tan delta) for a symmetric laminated beam.
% Ref.: Ni. R.G. and Adams. R.D.. J. Comp. Mat.. 18. 104-121. (1984).
%       ------------------------------
%          Jose Daniel D. Melo
%            February. 2002
%       ------------------------------
clear all:
data = dlmread('input.txt'.'.'.3.0):
% Note: This is a zero based specification.
% Thus. r=3. c=0. means row 4 and column 1.
E1 = data(:.1): E2 = data(:.2): G12 = data(:.3): v12 = data(:.4):
eta1 = data(:.5): eta2 = data(:.6): eta6 = data(:.7):
ang = (data(:.8))*pi/180: t = data(:.9):
n=length(E1):
for layer=1:n
 S(:.:.layer)=[1/E1(layer) -v12(layer)/E1(layer) 0:
              -v12(layer)/E1(layer) 1/E2(layer) 0:
              0 0 1/G12(layer)]:
 Q(:.:.layer)=inv(S(:.:.layer)):
 ETA(:.:.layer)=[eta1(layer) 0 0:
              0 eta2(layer) 0:
              0 0 eta6(layer)]:
 c(layer)=cos(ang(layer)): s(layer)=sin(ang(layer)):
 R(:.:.layer)=[c(layer)^2 s(layer)^2 2*c(layer)*s(layer):
              s(layer)^2 c(layer)^2 -2*c(layer)*s(layer):
    -c(layer)*s(layer) c(layer)*s(layer) (c(layer)^2-s(layer)^2)]:
 SBAR(:.:.layer)=(R(:.:.layer))'*S(:.:.layer)*R(:.:.layer):
 QBAR(:.:.layer)=inv(R(:.:.layer))*Q(:.:.layer)*(inv(R(:.:.layer)))':
 ETABAR(:.:.layer)=(R(:.:.layer))'*ETA(:.:.layer)*(inv(R(:.:.layer)))':
end
h=sum(t):
z=-h/2:
for i=2:n+1
 z(i)=z(i-1)+t(i-1):
end
D=zeros(3):
for k=1:n
 D=D+(QBAR(:.:.k)*(z(k+1)^3-z(k)^3))/3.:
end
  d=inv(D):
for layer=1:n
 f(layer)=QBAR(1.1.layer)*d(1.1)+QBAR(1.2.layer)*d(1.2)+...
```

```
        QBAR(1,3,layer)*d(1,3);
  g(layer)=(ETABAR(1,1,layer)*d(1,1)+ETABAR(1,3,layer)*d(1,3));
end
etab=0;
for k=1:n
 etab=etab+(f(k)*g(k)*(z(k+1)^3-z(k)^3))/(3*d(1,1));
end
Exb = 12/(h^3*d(1,1));
fid=fopen('output.txt','w');
fprintf(fid,'The properties for this laminated beam are:');
fprintf(fid,'\n  Total number of layers n= %2d',n);
fprintf(fid,'\n  Dynamic modulus Exb= %5.4e',Exb);
fprintf(fid,'\n  Damping factor eta= %5.2e\n',etab);
status=fclose('all');
```

A8.3 Example of input file (input.txt) for codes presented in A8.1 and A8.2 .

Enter the data for all layers of the laminated beam. in the following
order. and separated by comma.

E1 E2 G12 v12 n1 n2 n6 theta(deg) thickness

151.7.9.3.7.8.0.34.0.0038.0.0069.0.0102.90.0.0.1
151.7.9.3.7.8.0.34.0.0038.0.0069.0.0102.0.0.0.1
151.7.9.3.7.8.0.34.0.0038.0.0069.0.0102.90.0.0.1
151.7.9.3.7.8.0.34.0.0038.0.0069.0.0102.0.0.0.1
151.7.9.3.7.8.0.34.0.0038.0.0069.0.0102.0.0.0.1
151.7.9.3.7.8.0.34.0.0038.0.0069.0.0102.90.0.0.1
151.7.9.3.7.8.0.34.0.0038.0.0069.0.0102.0.0.0.1
151.7.9.3.7.8.0.34.0.0038.0.0069.0.0102.90.0.0.1

A8.4 Example of output file (output.txt) for codes presented in A8.1 and A8.2 .

The properties for this laminated beam are:
Total number of layers n= 8
Dynamic modulus Exb= 5.4090e+001
Damping factor eta= 4.17e-003